

Technical Report

TR-09-04

Climate conditions in Sweden in a 100,000-year time perspective

Erik Kjellström, Gustav Strandberg

Rossby Centre, SMHI

Jenny Brandefelt, Department of Mechanics, KTH

Jens-Ove Näslund, Svensk Kärnbränslehantering AB

Ben Smith, Dept of Physical Geography
and Ecosystems Analysis, Lund University

Barbara Wohlfarth, Department of Geology
and Geochemistry, Stockholm University

April 2009

Svensk Kärnbränslehantering AB
Swedish Nuclear Fuel
and Waste Management Co

Box 250, SE-101 24 Stockholm
Phone +46 8 459 84 00



Climate conditions in Sweden in a 100,000-year time perspective

Erik Kjellström, Gustav Strandberg
Rossby Centre, SMHI

Jenny Brandefelt, Department of Mechanics, KTH

Jens-Ove Näslund, Svensk Kärnbränslehantering AB

Ben Smith, Dept of Physical Geography
and Ecosystems Analysis, Lund University

Barbara Wohlfarth, Department of Geology
and Geochemistry, Stockholm University

April 2009

Preface

This document contains information on possible future climate extremes in Fennoscandia. The information is relevant for the analysis of long-term repository safety in e.g. SKB's safety assessment SR-Site. In particular, the information will be used by SKB in the report "Climate and climate-related issues for the safety assessment SR-Site".

Stockholm, April 2009

Jens-Ove Näslund

Person in charge of the SKB climate programme

Summary

This report presents results from a project devoted to describing the climatic extremes within which the climate in Fennoscandia may vary over a 100,000 year time span. Based on forcing conditions which have yielded extreme conditions during the last glacial-interglacial cycle, as well as possible future conditions following continued anthropogenic emissions, projections of climate conditions have been made with climate models. Three different periods have been studied; i) a stadial within Marine Isotope Stage 3 (MIS 3) during the last glacial cycle, representing a cold period with a relatively small ice sheet covering parts of Fennoscandia, ii) the Last Glacial Maximum (LGM), with an extensive ice sheet covering large parts of northern Europe and iii) a possible future period in a climate warmer than today. The future case is characterised by high greenhouse gas concentrations in the atmosphere and a complete loss of the Greenland ice sheet.

The climate modelling involved the use of a global climate model (GCM) for producing boundary conditions that were used by a regional climate model (RCM). The regional model produced detailed information on climate variables like near-surface air temperature and precipitation over Europe. These climate variables were subsequently used to force a vegetation model that produced a vegetation cover over Europe, consistent with the simulated regional climate. In a final step, the new vegetation cover from the vegetation model was used in the regional climate model to produce the final regional climate. For the studied periods, data on relevant climate parameters have been extracted from the regional model for the Forsmark and Oskarshamn areas on the Swedish east coast and the Olkiluoto region on the west coast of Finland. Due to computational constraints, the modelling efforts include only one forcing scenario per time period. As there is a large degree of uncertainty in the choice of an appropriate forcing scenario, we perform some additional sensitivity studies, and also compare our scenarios to other existing model scenarios when possible.

In addition to the modelling activities, an effort has been made to collect palaeoclimatic information by compiling various MIS 3 and LGM proxy data from different sources. An attempt to use part of this palaeoclimatic information to constrain the forcing conditions used in the climate models has been made. Other proxy data were used for model evaluation purposes. We have compared results from the global climate model with proxy records of sea-surface temperatures and with terrestrial records. The regional climate model results have been compared with existing terrestrial palaeoclimate records from Europe.

The results show that the climate models produce climates for the three periods that are in broad agreement with proxy data and other climate model simulations. The resulting climates are also in qualitative agreement with the imposed extent of ice sheets and types of vegetation. In particular, we show that the results for the MIS 3 stadial are consistent with ice-free conditions in south-central Fennoscandia and that this climate is suitable for permafrost growth. The simulations show that there is a large range in possible climates for the Fennoscandian region in a 100,000 year time perspective. Excluding the glacial situation, annual mean temperatures for the Forsmark, Oskarshamn and Olkiluoto sites differ from MIS 3 to the future warm climate by 12–15°C. Correspondingly, annual mean precipitation is almost a factor two higher in the future warm climate compared to MIS 3 at these sites.

This report documents forcing conditions and model results, both from the global and regional climate models as well as from the vegetation model. Results from the project in the form of modelled climate and vegetation data for different climatic extremes are available for further impact studies in other projects. In addition to this report, other publications have also resulted from the project, summarised in Appendix A.

Contents

1	Introduction	9
1.1	Background and objectives	9
2	Methodology	11
2.1	Selection of time periods	11
2.2	Climate modelling	12
2.2.1	The global climate model	14
2.2.2	The regional climate model	16
2.2.3	Vegetation modelling at the regional scale	18
2.3	Identification of forcing and initial conditions for the model simulations	19
2.3.1	Astronomical and solar forcing	21
2.3.2	Greenhouse gases and aerosols	22
2.3.3	Ice sheets	23
2.3.4	Freshwater forcing of the oceans	25
2.3.5	Sea level, coastlines, topography and bathymetry	25
2.3.6	Vegetation	27
2.4	Climate proxy data for model evaluation purposes	30
3	Results and discussion	35
3.1	The warm case	36
3.1.1	Global climate model simulations	36
3.1.2	Regional climate model simulations	41
3.1.3	Regional vegetation model simulations	47
3.1.4	Synthesis of the <i>warm case</i>	48
3.2	The glacial case	50
3.2.1	Global climate model simulations	50
3.2.2	Regional climate model simulations	63
3.2.3	Regional vegetation model simulations	72
3.2.4	Synthesis of the <i>glacial case</i>	73
3.3	The permafrost case	75
3.3.1	Global climate model simulations	75
3.3.2	Regional climate model simulations	81
3.3.3	Regional vegetation model simulations	87
3.3.4	Synthesis of the <i>permafrost case</i>	89
4	Extreme climate conditions in Sweden and Finland – synthesis	91
4.1	General features of the simulated climate for the different cases	91
4.2	Climate conditions at three sites in Sweden and Finland	96
4.2.1	Forsmark	97
4.2.2	Oskarshamn	100
4.2.3	Olkiluoto	102
4.2.4	Summary and comparison of the climate at the three sites	104
5	Summary and conclusions	107
5.1	Summary of limitations and uncertainties in the methodology	107
5.2	Summary of results and conclusions	108
Acknowledgements		113
References		115
Erratum February 2010		123

Appendix A	Publications resulting from the project	135
Appendix B	Deliverables and data format for input- and output data stored in data base at SKB	137
Appendix C	Glossary	141
Appendix D	Terrestrial proxy data for the glacial case (LGM)	143
Appendix E	Terrestrial proxy data for the permafrost case (MIS 3)	145
Appendix F	SST proxy data for the permafrost case (MIS 3)	151

1 Introduction

1.1 Background and objectives

Svensk Kärnbränslehantering AB (SKB) is responsible for the management of spent nuclear fuel and radioactive waste generated within Sweden. Site investigations for a deep geological repository for spent nuclear fuel have been performed at two sites (Oskarshamn and Forsmark) located along the Baltic Sea coast in eastern Sweden. In the near-future, SKB plan to submit an application to build a deep geological repository at one of these sites. An important document in the application is an assessment of long-term repository safety. In this assessment, a range of climate evolutions form the basis for a number of safety assessment scenarios. In Finland, Posiva Oy is responsible for the final disposal of spent nuclear fuel of the power plant units. One single location, Olkiluoto on the coast of the Baltic Sea in western Finland, was selected for the deep geological repository in the decision-in-principle ratified by the Finnish Parliament in 2001. Within a few years, Posiva will submit an application for the nuclear construction licence, including a long-term safety assessment.

These deep geological repositories are intended to keep radiotoxic material separated from man and environment for at least 100 kyrs (100,000 years). Over the last 800 kyrs, ~100 kyr long glacial-interglacial cycles have dominated climate variation. The time span of such a glacial-interglacial cycle is similar to the time it takes for the radioactivity of the spent nuclear fuel to decay to levels comparable to the activity in the uranium ore that was used to manufacture the fuel. Therefore, 100 kyrs is one of the main time scales appropriate to analysing the safety of a repository for spent nuclear fuel.

It is not possible to predict climate evolution in a 100 kyr time perspective. However, the extremes within which the climate of Sweden and Finland may vary can be estimated with reasonable confidence. The main objective of this project is to support the work on climate development that is conducted within in the Swedish and Finnish safety assessments by identifying and describing the extremes within which the climate conditions may vary in a 100,000-year time perspective. Considering the factors of importance for repository safety, this can be specified as identifying the extreme combinations of:

- a) air temperatures,
- b) precipitation,
- c) surface water balance,
- d) length of vegetation periods and type of vegetation.

The identification of extreme temperatures, precipitation and evaporation, including their annual variation and the related alterations of vegetation (factors a–d), is the first step in identifying and describing the extremes within which the climate conditions in Sweden and Finland may vary.

A second objective of the study is to make a rudimentary validation of the climate model results for the investigated periods by comparisons with corresponding quantitative information from available palaeoclimate proxy data.

Based on the extreme combinations of the climatic parameters (a–c), and corresponding estimations of vegetation types (d), also derived in this project, subsequent analyses can be made of e.g. the following properties:

- e) occurrence and depth of permafrost,
- f) thickness and extent of ice sheets.

This project focuses on identification and description of extremes regarding factors a–d above for three cases representing significantly different climate conditions. At SKB, the results of the project will primarily be used to assess and specify climate characteristics to be used in the SR-Site safety assessment.

2 Methodology

In the present study, the identification and description of extreme climate conditions is based on numerical modelling with climate models. In a first step we choose which periods to study. In the long run, future changes in insolation due to variations in Earth's orbit around the sun will lead to a transition from today's interglacial to a new glacial /e.g. Berger and Loutre 2002/. However, the timing of this event is uncertain, partly due to uncertainties regarding the effects of human emissions of greenhouse gases to the atmosphere. From simulations with an Earth system Model of Intermediate Complexity (EMIC) /Cochelin et al. 2006/ shows that glacial inception could be imminent if CO₂ concentrations were to stay at levels of 280 ppm (i.e. pre-industrial levels). Higher levels, with CO₂ concentrations at 280–290 ppm and also including a peak in CO₂ in the first 1,200 years, delays the inception to about 50 kyr from now, a result also supported by /Berger and Loutre 2002/. Even higher concentrations of CO₂ (300 ppm) might push the next glacial inception outside of the next 100 kyr. Also the BIOCLIM studies suggest that a full glacial episode comparable to the last glacial cycle may not occur within the next 300 kyr given certain emission scenarios /BIOCLIM 2001, Texier et al. 2003/. For very high emissions of CO₂ (i.e. 5,000 Gt C) /Archer and Ganopolski 2005/ report of simulations placing the next glacial inception 500 kyr from now. Given the large uncertainties in estimates like these, one can conclude that the timing of the next glacial onset is also indeed uncertain.

By selecting appropriate time periods from the last glacial-interglacial cycle, periods with extreme climate conditions can be studied. After such a selection of time periods, we set up the climate models and decide upon the configuration of external forcing that should be applied for the various cases. The setup of forcing conditions for the model simulations is based on separate periods during the Weichselian (i.e. the last glacial period in northern Europe, occurring approximately 115–10 kyr before present (BP)), the Holocene (i.e. the present interglacial starting about 10 kyr BP) and a future hypothetical case with higher levels of greenhouse gases in the atmosphere than today. Steady-state simulations of equilibrium climates for the different periods are then compared to the pre-industrial climate and the climate at the end of the 20th century. The simulated climate for the different periods is also compared with proxy data for climate variables when applicable. In a last step, selected climate data are extracted for the Oskarshamn, Forsmark and Olkiluoto regions.

2.1 Selection of time periods

Typical climate cases during a full glacial-interglacial cycle at mid-latitudes include, in a general sense, warm temperate climates, cold permafrost climates and cold glacial climates. In this project we focus on the following three periods or cases, introduced here and described in more detail in Section 2.3:

1. *Warm case* – a period a few thousand years into the future with increased greenhouse gas concentrations.
2. *Glacial case* – a period during the Last Glacial Maximum, 21 kyr BP.
3. *Permafrost case* – a period during Greenland Stadial (GS) 12 during Marine Isotope Stage (MIS) 3, 44 kyr BP.

The *warm case* describes a situation with a temperate climate with increased greenhouse gas concentrations in the atmosphere. Furthermore, a complete loss of the Greenland ice sheet is assumed. Since this deglaciation is a process that may take up to a couple of thousand years, we can only speculate as to what other climate-related conditions may be prevailing at that time. According to climate-change scenarios from simulations with global climate models (GCMs), melting of the Greenland ice sheet may start at a time when the global mean temperature has increased by about 1.9–5.1°C above today's conditions and the temperature over Greenland has increased by about 3–6.5°C /Gregory et al. 2004, Gregory and Huybrechts 2006/. Such increases in temperature are projected by GCMs within the 21st century for some emission scenarios and resulting increases in atmospheric CO₂ levels /Meehl et al. 2007/. If such high temperatures persist for a long enough time (several

hundreds to a couple of thousand years depending on the degree of warming) the Greenland ice sheet will eventually disappear. In this time perspective, CO₂ levels will start to decrease again (if/when emissions cease). Nevertheless, at one thousand years from now, the atmospheric CO₂ concentrations will remain considerably higher than today /Lenton et al. 2006/. Here, we choose the time period for the *warm case* as a compromise between a high level of CO₂ (needed to simulate a warm climate that melts the Greenland ice sheet) and a not too high level (that remains in the atmosphere a long time after the emissions have ceased). Thus, the *warm case* can be considered as representative of the climate a few thousand years into the future after a complete melting of the Greenland ice sheet and a partial recovery towards lower background CO₂ concentrations.

The *glacial case* has been set up to resemble conditions at the time of the Last Glacial Maximum (LGM) in a way as similar as possible to what was done in the Palaeoclimate Modelling Intercomparison Project /PMIP1; Joussaume and Taylor 2000, PMIP2; Harrison et al. 2002/. This choice facilitates comparisons with other GCM results. It also allows the use of pre-existing long simulations with the general circulation model CCSM3 performed at the National Centre for Atmospheric Research (NCAR) in the USA /Otto-Bliesner et al. 2006a/, reducing the model spin-up time needed for this study. Further, as the LGM is part of the most recent Weichselian glacial period, there is a better possibility of finding climate proxy data than for earlier cold stadials during the Weichselian. In addition, LGM is also associated with temperatures that are among the lowest of the last glacial cycle /Jouzel et al. 2007/.

For the *permafrost case* we chose the orbital year 44 kyr BP, which corresponds to a stadial interval (Greenland stadial GS 12) during MIS 3. The choice for this interval follows from a workshop on MIS 3 organised by SKB in September 2007 /Näslund et al. 2008/. Only limited and in cases controversial, palaeo-information is available to reconstruct the extent of the Fennoscandian ice sheet during the different warm and cold intervals of MIS 3. We here assume, in line with several recent results from glacial geological studies /Näslund et al. 2008/, that the southern part of Fennoscandia was ice free during some of the MIS 3 stadials.

2.2 Climate modelling

Experimental setup

The modelling activities included the use of; i) a fully coupled Atmosphere-Ocean General Circulation Model (AOGCM), ii) a Regional Climate Model (RCM), and iii) a dynamic vegetation model (DVM). The AOGCM was used to simulate the global climate in steady-state simulations for the selected cases. As these numerical models use descriptions of the physical processes governing the climate system, they can be applied not only for the present-day climate but also for different climates in the past and future. Even though AOGCMs are powerful models they are relatively coarse in their resolution due to computational limitations. Therefore, we use output from the AOGCM as input to the RCM that provides output at a relatively high horizontal resolution for Europe. Both global and regional climate models hold descriptions of the land surface, including vegetation. In the regional model, it is important to describe the vegetation cover with a high degree of regional detail. Such details are missing in available global fields (see Section 2.3.6 below) and details of the vegetation cover have to be estimated, based on the global fields and consideration of among other things land-sea distribution. In order to improve the representation of the regional vegetation, we use a DVM to simulate the European vegetation resulting from the RCM-simulated climate. In a subsequent step, the new vegetation is used in a new RCM simulation that provides the final output. Figure 2-1 outlines the chain of models and simulations.

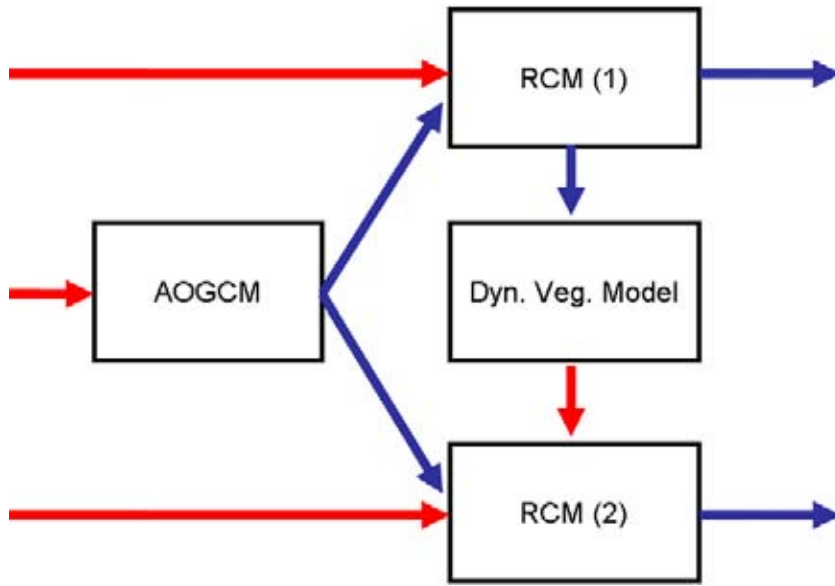


Figure 2-1. The model chain used in the present study. Red arrows symbolize climate forcing conditions and blue arrows simulated climate.

Uncertainties and limitations in climate modelling

There are a number of uncertainties related to climate simulations. These include; uncertainties in forcing conditions, model formulation and natural variability of the climate system. Preferably, all these uncertainties should be addressed. One way of doing this is to use an ensemble of simulations with different forcings, different models and different initial conditions for the simulations. Due to computational constraints, this is not feasible with fully coupled global climate models such as the one used in this study. As an alternative to our single scenario approach, one could use simpler global climate models running at low resolution or with less complexity. Such Earth system Models of Intermediate Complexity (EMICs) can be run for long periods alternatively in multiple simulations with much lower computational demands than fully coupled global climate models. However, as these models do not represent the full climate system as well as a fully coupled climate model, we have chosen a fully coupled AOGCM. To account for some of the uncertainty in the forcing conditions as described below we conducted a number of sensitivity experiments. In addition to the actual simulations undertaken in this project, we compared the results to other simulations with other models described in the literature. In this way, parts of the uncertainties related to model formulation is treated. Additionally, we strive for a high degree of detail in the regional climate. The current setup, with a fully coupled AOGCM feeding boundary conditions into a regional climate model (RCM), as described in more detail below, is more favourable for this purpose, as a larger jump in horizontal resolution, which would be the case when going from an EMIC to a RCM, would degrade the results /Antic et al. 2004/.

In modelling studies of past climates, the models can be used to supplement the limited observational picture of the climate system. The lack of observations however, remains a major problem, since observations are needed also for model evaluation. Here we rely on models that have been extensively tested in simulations of the climate in the second half of the 20th century when observations are available and, based on those tests, judged to be reliable. We compare model results from the AOGCM with global palaeo-data and from the RCM with European palaeo-data. The palaeo-data are described in Section 2.4. We also compare results for the different cases to simulations or observations valid for the recent past (roughly the time period 1961–2000) or to simulations of the pre-industrial climate (i.e. with forcing conditions set at levels consistent with those preceding the 18th century. Finally, when applicable, model results are also compared with previous modelling studies of the climates of the studied periods.

In addition to forcing conditions, we need initial conditions to set up the simulations. Since the purpose of this project is to study equilibrium climates and not transitions between different climates, we ran all simulations until a global equilibrium in the simulated climate was reached. The simulations were started from other existing long-term simulations made with the CCSM3, and were continued for 400–900 years until equilibrium was reached. To reduce the computation time for our simulations, we choose to start them when the original simulation has reached a stable or quasi-stable equilibrium if such data were available. The model simulations were performed as steady-state experiments, in which the annual mean forcing conditions are held constant over time. In this way, we could check for any long-term spurious drift in the simulations. Such drift is generally caused by an imbalance in the initial model state. To decide when a simulated climate had stopped drifting and reached a quasi-stable equilibrium, we needed to set up criteria for the simulated climate evolution. There is no common practice for these criteria in the literature, probably due to the fact that only few state-of-the-art climate model simulations of climates substantially different from the recent past climate have been performed so far. We have chosen to set up criteria on the evolution of the annual global mean surface temperature. Based on the results from our simulation of the *glacial case* (see Section 3.2) we require that the linear trend in the annual global mean surface temperature is less than 0.2°C per century for the last 100 years of the simulation. In the following, this criterion is the basis for using the term quasi-equilibrium.

This approach is in contrast to the real climate system in which there are always transient changes in forcing leading to changes in climate. However, our assumption about steady-state conditions may be justified as relatively long (~1,000 years) periods of stable forcing and climate conditions did occur for periods of extreme climate conditions during the Weichselian /Krogh-Andersen et al. 2006, Jouzel et al. 2007/. Also, steady-state simulations may be used in SKB's and Posiva's safety assessments for other studies of hypothetical stable periods longer than those during the Weichselian. The selected time periods for the three cases are separate in time and can be thought of as three independent climate scenarios exemplifying possible climatic conditions during the three situations.

Our approach, based on use of global and regional climate models, has to some degree been applied for a glacial climate by /Jost et al. 2005/ and for a permafrost climate for Europe by /Barron and Pollard 2002/ and /van Huissteden et al. 2003/. However, in these studies, the simulations were relatively short, of the order of a few years to a decade at most. Also the BIOCLIM project (<http://www.andra.fr/bioclim/>), aiming at assessing the possible long term impacts on the safety of radioactive waste repositories due to climate and environmental change, has used a similar approach. They used an EMIC to simulate a possible climate evolution for the coming one million years and a GCM and a RCM to go more into detail for some chosen periods during this time, focussing on five locations in central and southern Europe.

2.2.1 The global climate model

In the present study, we used the Community Climate System Model version 3 (CCSM3) /Collins et al. 2006/. CCSM3, which is a coupled atmosphere-ocean model, has been tested for the recent past climate (1960–2000) and also in simulations of a pre-industrial climate (around AD 1800) /Otto-Bliesner et al. 2006b/, the Last-Glacial Maximum (21 kyrs BP) and the Mid-Holocene warm period (6 kyrs BP), /Otto-Bliesner et al. 2006a/. The equilibrium climate sensitivity of CCSM3 is 2.7°C for a doubling of CO₂. The corresponding number for a transient response occurring at a rate of 1% increase per year is 1.5°C. These numbers could be compared to those by the other AOGCMs participating in the Climate Modelling Intercomparison Project 3 (CMIP3), e.g. 2.1–4.4°C and 1.3–2.6°C for equilibrium and transient climate sensitivities respectively /Meehl et al. 2007/.

The simulations performed within the present study are compared to two other simulations with CCSM3 of i) the recent past climate, in which all forcings (greenhouse gases, solar forcing, aerosols, etc) are set to values representing the year 1990 /Collins et al. 2006/ and ii) the pre-industrial climate (around AD 1800) with forcings set to pre-industrial values /Otto-Bliesner et al. 2006b/. In the following, these two simulations are denoted RP and PI respectively. The climate in these simulations is taken to represent the recent past and pre-industrial climate, respectively, but it should be noted that there are differences between the simulated and observed climate. By taking the difference between two simulations with the same model we assume that systematic errors in the simulated climate are canceled. However, it is important to note that the processes in the model are coupled, implying that errors in the description of specific processes in the model may influence the simulated climate differently depending on the climate.

For the recent past climate, we have performed a continuation of the simulation with CCSM3 run at NCAR /Collins et al. 2006/. Our simulation starts after 600 years of simulation at NCAR and we use the first 50 years of our simulation to describe the recent past climate (henceforth this simulation is referred to as RP). The simulation was run at the same resolution in all model components as the other simulations performed within this project. For the simulations performed and analyzed within this project, atmospheric and land components of the CCSM3 share a horizontal resolution of T42, that is equivalent to a grid spacing of approximately 2.8° in latitude and longitude. The ocean and sea-ice components share a horizontal grid of 320 x 384 points with poles located in Greenland and Antarctica. The vertical resolution is 26 levels in the atmosphere and 40 levels extending to 5.5-km depth in the ocean.

The simulated climate of the recent past is compared with the National Centre for Environmental Protection (NCEP) re-analysis /Kalnay et al. 1996/ of surface temperature (T_s) for summer (June–August) and winter (December–February). The re-analysis data set consists of data from a numerical weather prediction model that is forced by a very large number of observations of the state of the atmosphere. This implies that the re-analysis closely follows the actual evolution of the climate system and that it is a physically consistent data set. The simulated climate shows a reasonable agreement to observations although regionally large differences of up to 10°C occur (Figure 2-2). The simulated summer near-surface temperature is 1°C too warm in western Fennoscandia and 4°C too cold in eastern Fennoscandia. Fennoscandian winter near-surface temperature is $1\text{--}4^{\circ}\text{C}$ too warm as compared with the re-analysis. The simulated present-day total surface precipitation is shown in comparison to observed precipitation in Figure 2-3. Rather large errors are found in the tropics similar to the results reported by /Collins et al. 2006/ for their simulation with CCSM3 of the recent past climate with higher atmospheric resolution. The simulated climate is 20–30% too dry in southern Fennoscandia and 20–30% too wet in northern Fennoscandia in summer. The simulated climate is 50–60% too dry at the Norwegian west coast and up to 50% too wet in eastern Fennoscandia in winter. This west to east distribution of the error across the Scandinavian mountain range is mainly explained by the coarse resolution of the Scandinavian mountain range in the CCSM3 simulation. Taken together, the biases

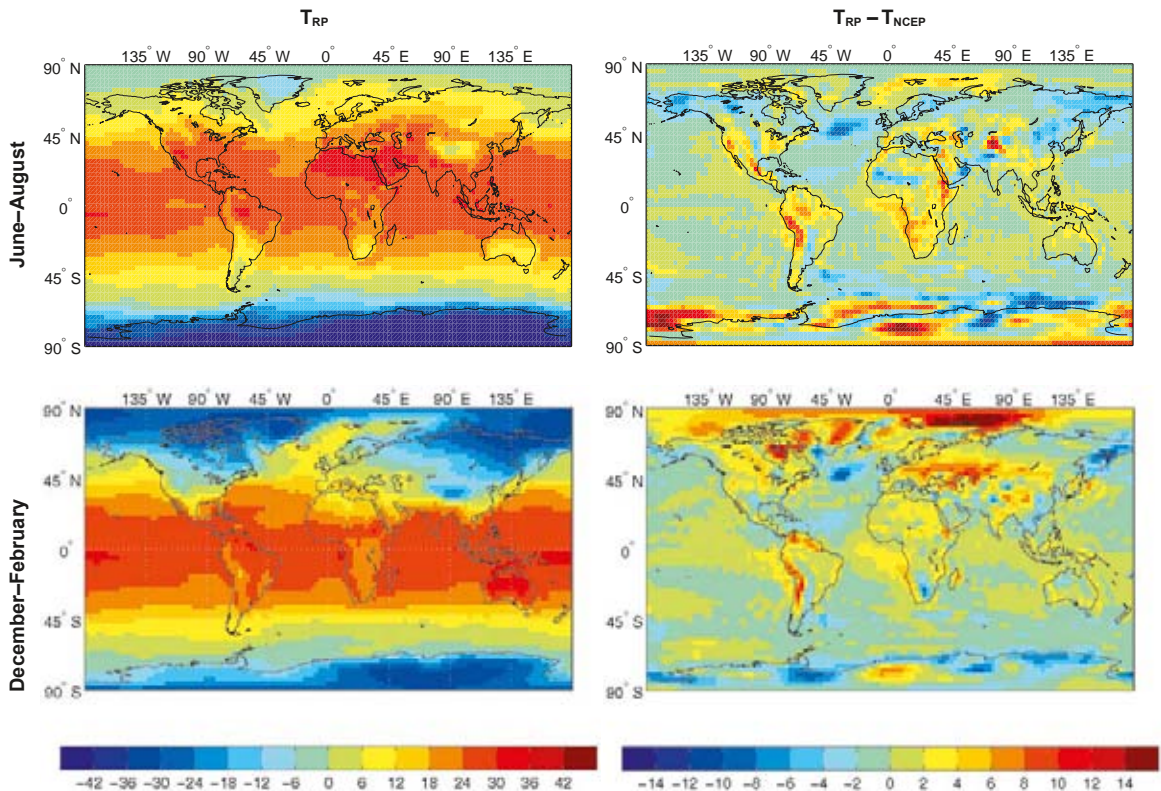


Figure 2-2. The simulated recent past (RP) near-surface temperature (T_{RP}) and the difference between the simulated recent past climate and the NCEP re-analysis (T_{NCEP}). Units are $^{\circ}\text{C}$.

in the seasonal mean precipitation in the eastern parts of Fennoscandia leads to an erroneous seasonal cycle. In those areas, CCSM3 simulates maximum precipitation in winter, whereas observations show a maximum in summer. Part of the overestimate in precipitation during winter over Fennoscandia may also be related to undersampling and thus errors in the observational records /Rubel and Hantel 2001/.

Deviations from the observed climate can also be attributed to the coarse horizontal resolution of the global model and to errors introduced by the parameterization of processes that can not be resolved in the global model such as cloud processes and small-scale motions. In addition, the natural variability in the climate system sometimes leads to large differences between a model and the observed climate. This is a result of the fact that these models do simulate the “natural” variability. Hence, a model simulation may include both warm and cold (or wet and dry) periods that may or may not coincide with the observed climate. Furthermore, parts of the differences may be due to the fact that the real recent past climate was not in equilibrium as was the case in the simulation. Similar deviations of the simulated climate from observed climate exist in all simulations with state-of-the-art climate models /Randall et al. 2007/. When these models are used to study the future response of the Earth’s climate to an increased greenhouse gas forcing, the large-scale spatial patterns and sign of the simulated response is similar among the models. The spatial patterns of T_s in the simulated recent past climate and the re-analysis are also quite similar. These results form the basis for the present study to simulate the response of the climate system to changes in the forcing and boundary conditions of the Earth’s climate. We must, however, always bear in mind that these models have errors and therefore it is important to compare the simulated climate to observations or proxy data when available, as done in the present study.

2.2.2 The regional climate model

The Rossby Centre regional climate model RCA3 /e.g. Kjellström et al. 2005/ was applied for the downscaling of results from CCSM3 to a higher resolution for Europe. RCA3 and its predecessors RCA1 and RCA2 have been extensively used for downscaling experiments for the recent past climate and future climate change scenarios /Rummukainen et al. 1998, 2001, Jones et al. 2004,

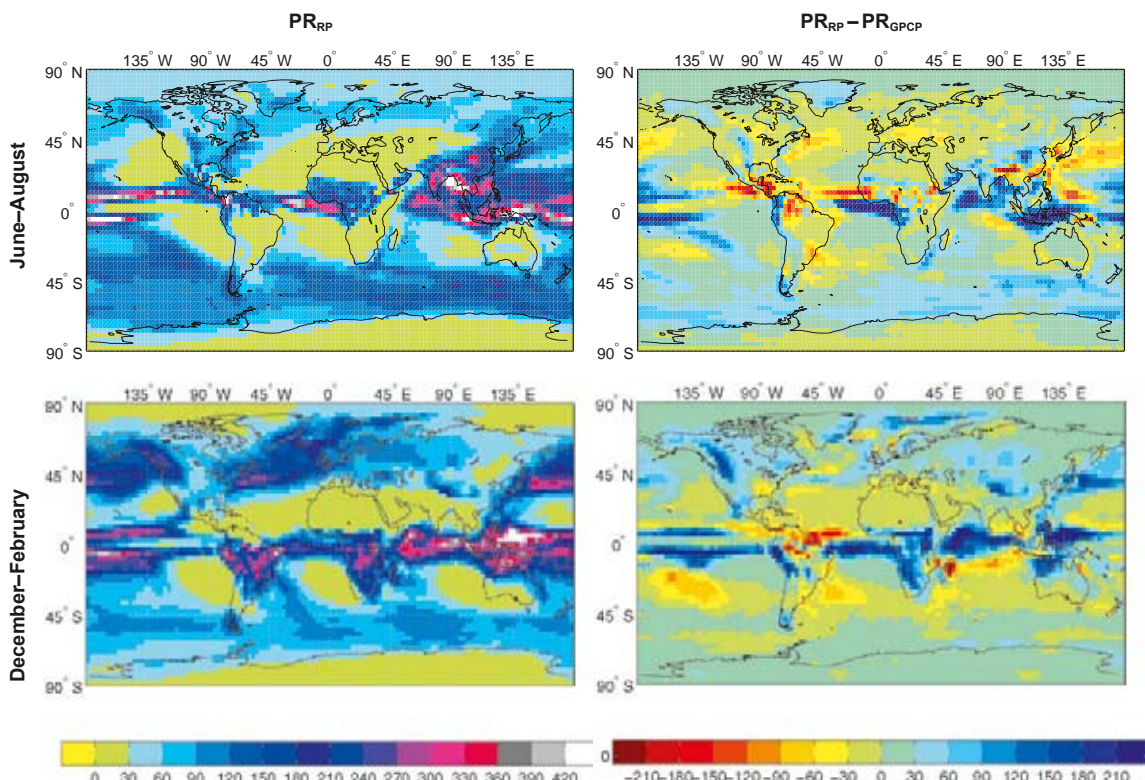


Figure 2-3. The simulated recent past (RP) precipitation (PR_{RP}) and the difference between simulated recent past climate and observed data as shown by the GPCP dataset (PR_{GPCP} /Adler et al. 2003/. Units are mm/month.

Räisänen et al. 2003, 2004/. Also, in a previous SKB project, RCA3 has been used in a palaeoclimatological application for downscaling global model data for parts of the last millennium /Moberg et al. 2006/. In the present study, RCA3 was run over Europe with a spatial resolution of 50 km and time resolution of 30 minutes. When initialising RCA3, data were taken from CCSM3. After that, CCSM3 data were used only to account for what is happening outside the model domain and at the sea surface. Every 6 hours of the simulations, RCA3 reads sea ice concentration, pressure, humidity, air temperature, winds and sea surface temperature along the boundaries of the model domain. All simulations have been run with one year spin-up time, after that time the atmosphere/land surface system is assumed to have forgotten its initial state. Inside the model domain, RCA3 produces its own climate. Nevertheless, the ability of the regional model is strongly dependent on the realism of the driving global model simulation.

Previous studies with initial conditions and lateral boundary conditions from reanalysis products (so-called perfect-boundary condition simulations), have shown that RCA is capable of simulating the climate in Europe in a realistic way /Jones et al. 2004, Kjellström et al. 2005/. This applies both for annual and seasonal mean conditions as well as for extremes and daily variability of, for instance, temperature. If instead boundary conditions are from a global climate model simulation (as, in this case, from CCSM3), a somewhat poorer agreement with the observed climate is typically obtained. Here, a simulation of the recent past climate with RCA3 forced by boundary conditions from CCSM3 (henceforth this simulation is labelled RP-r) is discussed. It should be noted that the forcing fields from CCSM3 are not identical to those discussed in Section 2.2.1, as these are taken from another experiment with the same model. We used a climate change simulation performed at the Rossby Centre with the same version of CCSM3 that was used to produce boundary conditions to RCA3. This simulation is a transient simulation covering the time period 1870–2000 with prescribed forcing for the 20th century /Forster et al. 2007/. The differences in forcing conditions (i.e. transient change 1961–1990 versus 1990 conditions) leads to some differences between the two for the 1961–1990 period. Typically, seasonal mean temperature differences between the two global simulations are within $\pm 1^{\circ}\text{C}$ for most European regions in winter while larger differences of up to 3°C are present in southern Europe in summer (not shown). Corresponding differences in precipitation are within $\pm 15\text{--}20\%$.

Figure 2-4 shows a comparison between the RP-r simulation and climatological data from observations from the Climatic Research Centre (CRU, version TS2.1) /Mitchell and Jones 2005/ for the years 1961–1990. The CRU gridded data are interpolated into the RCA3 grid without any adjustment of altitude. In locations where the altitude of the model grid and the CRU grid differs significantly this can result in biases as there is a strong altitude dependence in temperature (6.5°C per 1,000 m in the standard atmosphere). As large differences in altitude are restricted to a few grid boxes in mountainous areas this will only have a local effect and even there it does not introduce any large-scale systematic differences. The comparison between RCA3 and CRU is made for monthly mean conditions for July and January. These specific months are the coldest and warmest in Europe in the *glacial case* and are consequently used for the RCM comparison to proxy data (see Section 3.2.2). Large-scale features inherited from CCSM3 are seen also in RCA3. Examples of this are; a warm bias in winter particularly over eastern Europe (Figure 2-4, upper right panel), and a cold bias in most of northern Europe in summer (Figure 2-4, upper left), implying too weak a seasonal cycle in large areas. Likewise, for precipitation, large-scale features from CCSM3 can also be identified, like a dry bias in summer in south-eastern central Europe (Figure 2-4, lower left) and a wet bias in parts of western Europe in winter (Figure 2-4, lower right). Also notable differences between RCA3 and CCSM3 can be seen. Due to the higher horizontal resolution, RCA3 shows, as expected, more details in many areas including mountainous areas and coastal regions. The geographical distribution of precipitation across the Scandinavian mountain range is in better agreement with observations in RCA3 than in CCSM3 during winter (i.e. a smaller dry bias along the Norwegian west coast and a smaller wet bias in Sweden) (Figure 2-4, lower right). Most of the improvements in precipitation in this area are related to the higher horizontal resolution in the regional model. Some biases still exist, these may include excessive precipitation in mountainous regions, although part of this potential bias may in fact be related to the observations, as there are known problems with under-catch of precipitation /Rubel and Hantel 2001/. Some more results showing how RCA3 simulates the recent past climate are given when we present results for the *warm case* (Section 3.1.2). A limited comparison with observations for the combination RCA3 and CCSM3 for the recent past climate can be found in Chapter 4, where we present results for a few specific locations in Sweden and Finland.

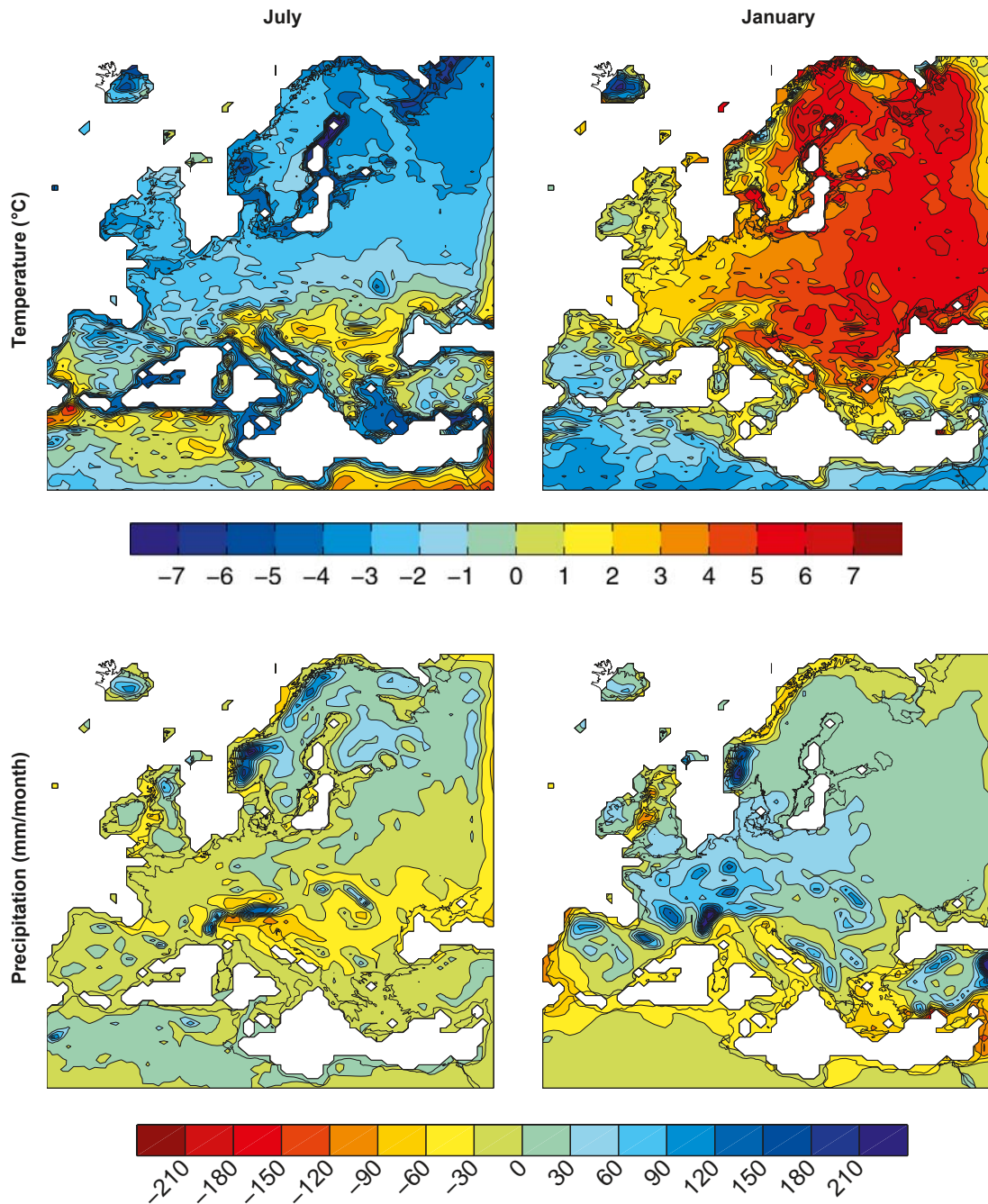


Figure 2-4. Difference between RCA3 forced by a simulation of the recent climate with CCSM3 (RP-r) and the observed climatology from CRU of near-surface temperature and precipitation.

2.2.3 Vegetation modelling at the regional scale

For each of the three climate cases simulated within the study, we used the dynamic vegetation model (DVM) LPJ-GUESS /Smith et al. 2001/ to generate fields of potential vegetation (i.e. the vegetation that would exist if it were not for human intervention) for land areas covered by the RCM domain (Europe and northern Africa). LPJ-GUESS is a process-oriented model optimised for application across a regional grid. The model shares a common plant physiological and biogeochemical core with the global model LPJ-DGVM /Smith et al. 2001, Sitch et al. 2003/, widely used in studies of the global carbon cycle and biosphere-atmosphere coupling /e.g. Cramer et al. 2001, Sitch et al. 2005, 2008/, but is more detailed and mechanistic in its representation of vegetation structure and dynamics, distinguishing plant populations, age classes, vertical stand structure and patch-scale heterogeneity. This level of detail is arguably necessary to correctly characterise the transient vegeta-

tion dynamics under periods of rapid climatic change, such as the present day, which are controlled by population processes operating on similar time scales to the climate change itself. LPJ-GUESS has been validated by comparison with observed vegetation patterns and dynamics /Smith et al. 2001, 2008, Hickler et al. 2004, Zaehle et al. 2006, Miller et al. 2008/ as well as ecosystem carbon exchange /Morales et al. 2005, Yurova and Lankreijer 2007, Smith et al. 2008, Wramneby et al. 2008/ and has been used to model climate change impacts on European vegetation and ecosystems in a variety of studies /Gritti et al. 2006, Koca et al. 2006, Morales et al. 2007, Wolf et al. 2008/. The model has also been applied to Africa /Hély et al. 2006/ and other regions /e.g. Hickler et al. 2004/.

The input data required by LPJ-GUESS are inter-annually varying monthly mean values of surface air temperature, precipitation and incoming shortwave radiation, as well as atmospheric CO₂ concentration and a soil texture class from which thermal and hydrological properties can be derived /Smith et al. 2001/. To generate vegetation maps for each time period, LPJ-GUESS was run driven by climate data from the RCM when it was forced by the “first-guess” vegetation as described in Section 2.3.6. CO₂ concentrations of 185, 200 and 750 ppm were used for the glacial, permafrost and *warm case* time periods, respectively (Section 2.3.2). Soil texture classes within each grid cell followed the scheme given by /Sitch et al. 2003/, based on texture classes from the FAO global soil data set /Zobler 1986, FAO 1991/. Grid cells falling over extant ocean areas were assigned a medium-coarse texture /Sitch et al. 2003/. Patch-destroying disturbances, which are implemented as a stochastic process, were prescribed to occur with a mean, expected, interval of 100 years in each patch /Koca et al. 2006/.

A spinup of 300 simulation years /Smith et al. 2001/ was performed to bring the simulated vegetation and soil state into approximate steady state with the average climate simulated by the RCM. The first 30 years of RCM-generated climate data, cycled repeatedly and with any temperature trend removed, were used to force the vegetation model during the spinup phase of the simulation. The spinup phase was followed by an experimental phase, in which the model was forced with the full 50 (for the *permafrost case*) or 100 (other cases) year time series of RCM-generated data for each grid point. All presented results from the vegetation model, as well as the land-cover fractions returned to the RCM for a second set of simulations (see below), were averages across all years of the experimental phase.

A new RCM run was then performed, replacing the first-guess vegetation with that simulated by LPJ-GUESS. This had the advantage that the simulated new regional climate was more consistent with the forcing conditions (i.e. the vegetation), potentially resulting in a more realistic climate description. The sensitivity of the local/regional climate to changes in vegetation was also investigated by comparing outcomes of the initial (“first-guess”) and final RCM runs.

In addition to the application described above, the output from the performed vegetation model simulations can be used in other studies that include future vegetation in e.g. the SKB and Posiva safety assessments, as well as in studies of palaeovegetation over Europe.

Input- and output data from the climate and vegetation simulation made within the project are stored at a database at SKB. These data are described in Appendix B.

2.3 Identification of forcing and initial conditions for the model simulations

Once the time periods had been established (see Section 2.1) the first step of the modelling work consisted of identifying plausible global forcing conditions generating the sought extreme conditions in Sweden and Finland. The climate conditions on long time scales (100 kyrs) are affected by:

- Astronomical and solar forcing (insolation).
- Concentrations of greenhouse gases (GHG) and aerosols in the atmosphere.
- Extent of ice sheets.
- Distribution of land and sea.
- Topography.
- Vegetation.

Only insolation is entirely external to the climate system, whereas the other parameters are more or less influenced by the climate. However, in this study, we were not interested in the transient climate change signal, so we used climate models that took land-sea distribution, topography and extent of ice sheets as constants. Also vegetation is treated as a constant in the standard simulations albeit with a seasonal cycle. As previously described, at the regional scale we performed additional simulations in which the vegetation, in an iterative way, could influence the regional climate (see Sections 2.2.3 and 2.3.6). The identification of plausible combinations of forcing factors is based on a combination of information from palaeodata and information from supporting models.

In this chapter, we present and discuss the forcing conditions used for the three different cases studied in the project. Table 2-1 summarizes the prescribed forcing conditions used in CCSM3. In addition to the standard set of forcing conditions for the *warm* and *glacial cases* we also conducted a number of sensitivity experiments with CCSM3, with changes in vegetation and atmospheric dust loads as indicated in the table.

As mentioned above, we were not seeking transient climate change signals going from one climate state to another but rather quasi-equilibrium conditions. Consequently, we did not prescribe changing forcing conditions in our simulations. Rather, we used the numbers from Table 2-1 as constants over time for the three selected time periods.

As CCSM3 does not include a model for continental ice sheets, these ice sheets were prescribed as indicated in Table 2-1. In addition, melting of ice sheets will influence the fresh water content of the upper oceans and thereby the ocean circulation. In Section 2.3.4, we describe how we dealt with large fresh water fluxes arising due to the melting of the Greenland ice sheet in the *warm case*.

Differences in the description of forcing conditions in RCA3 compared to CCSM3

We tried to use consistent forcing conditions in CCSM3 and RCA3, but there are some differences. These differences are partly related to the finer resolution of RCA3 and thus the possibility to include more detailed regional information. Also differences in model formulation play a role. A few differences are indicated in Table 2-1 and at the end of the following sections we devote a paragraph to more explicitly describing differences between RCA3 and CCSM3.

Table 2-1. Forcing conditions in CCSM3 for the three cases. BP, PI and RP denote “before present”, “pre-industrial” and “recent past (AD 1961–2000)”, see also Appendix A for a glossary. Additional sensitivity experiments undertaken in CCSM3 are marked in italics. Square brackets indicate when different forcing conditions were used in RCA3. For full references see text.

	Warm	Glacial	Permafrost
Insolation	1,365 Wm ⁻²	1,365 Wm ⁻²	1,365 Wm ⁻²
Orbital year	AD 1990	21 kyrs BP	44 kyrs BP
CO ₂	750 ppm	185 ppm	200 ppm
CH ₄	RP (1,714 ppb)	350 ppb	420 ppb
N ₂ O	RP (311 ppb)	200 ppb	225 ppb
Ozone	PI	PI	PI
Sulphate	PI	PI	PI
Dust, sea salt	PI	PI/PI x 3	PI
Ice sheets	RP (Excluding Greenland ice sheet)	ICE-5G	SKB, 2006 CLIMBER2, ICE-5G
Land-sea distribution	RP	ICE-5G	ICE-5G [SKB, 2006], RP
Sea level	RP [+7 m]	−120 m	−120 m [−70 m]
Topography, bathymetry	RP (Excluding Greenland ice sheet)	ICE-5G, RP	ICE-5G [SKB, 2006]
Vegetation	RP/GHG	RP/LGM	RP

2.3.1 Astronomical and solar forcing

The astronomical forcing of the radiation balance from changes in Earth's orbit around the sun is calculated explicitly in CCSM3 according to /Berger 1978/ and represents conditions like the inclination of the Earth's axis and the eccentricity of the Earth's orbit around the Sun for the chosen years specified in Table 2-1. The changes in the astronomical forcing are large over long time spans. Over high latitudes, /Berger and Loutre 2002/ present calculated numbers varying by 50–100 W/m² in roughly 10 kyrs time. Here, we simulate periods of a few hundred to a thousand years for each of the selected cases, making the influence of changing long-term astronomical forcing within each simulation small. We use a single astronomical year and hence a constant forcing for each simulated case.

For the *warm case* we note that the astronomical forcing will not change much in the next few thousands of years /Berger and Loutre 2002/. This relates to the fact that the eccentricity of the orbit is close to its minimum at present, implying that changes in the precession (controlling the distance between the Sun and Earth during summer and winter) are not as important as when the eccentricity is large. Consequently, we used the orbital year 1990 for these simulations. For the *glacial case* we used the PMIP2 set up /Harrison et al. 2002/. We choose the orbital year 44 kyrs BP representing a stadial during MIS 3 for the *permafrost case*. The variations in solar insolation due to changes in the Earth's orbit are relatively minor through much of MIS 3 although a strong decrease started around 35 kyrs BP /Berger and Loutre 2002/.

As we have no information about changes in the intensity of the solar radiation for the three cases, we assume that the present-day value 1,365 W/m² applies for all cases. The combined astronomical and solar forcing is illustrated by showing the insolation at all latitudes as a function of month for the three time periods in Figure 2-5. The differences compared with the present day conditions are largest at high northern latitudes and imply colder summers for the *glacial case* and warmer summers in the *permafrost case*. The differences compared with present day conditions are generally less than 2%.

Differences in the treatment of astronomical forcing in RCA3 compared with CCSM3

RCA3 does not include a description of the astronomical forcing and its variation over time. Therefore, we conducted a number of sensitivity tests in which we changed the solar constant to mimic the most extreme changes in astronomical forcing in CCSM3 for the three cases. As indicated by Figure 2-5, differences in insolation compared with the *warm case* (viz. today's conditions) were generally below 2–3%. The tests that were conducted included reductions in the solar constant by 2, 4 and 6%, respectively. The difference between the reference simulation and a sensitivity test with the reduction amounting to 6% in an eight-year long simulation is shown in Figure 2-6. The result

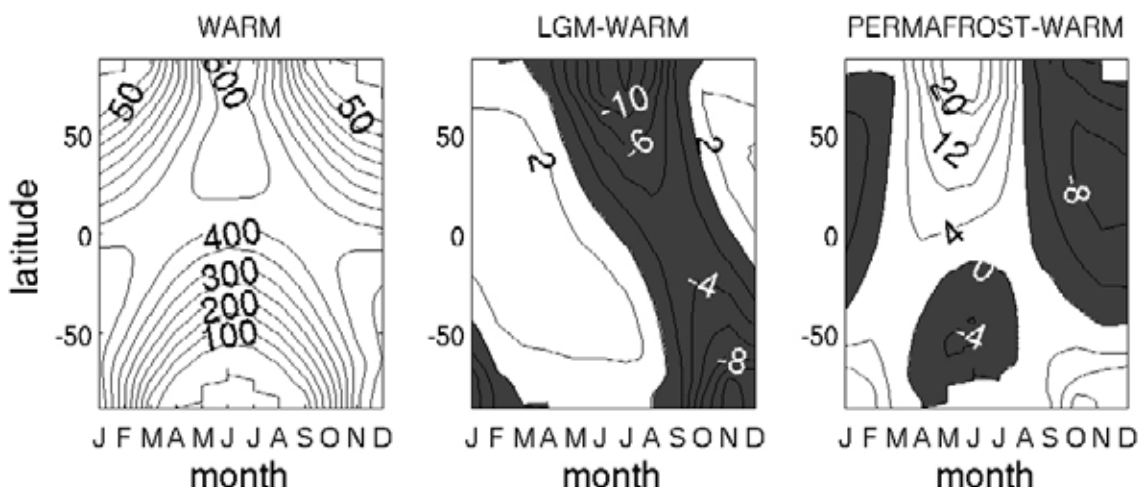


Figure 2-5. Insolation as a function of month of the year and latitude. The warm case (here according to 1990 conditions) insolation (left) and the difference between the glacial/permafrost case and the warm case insolation are shown (middle/right panel). Units are (W/m²). Differences compared with the warm case are generally below 2–3%.

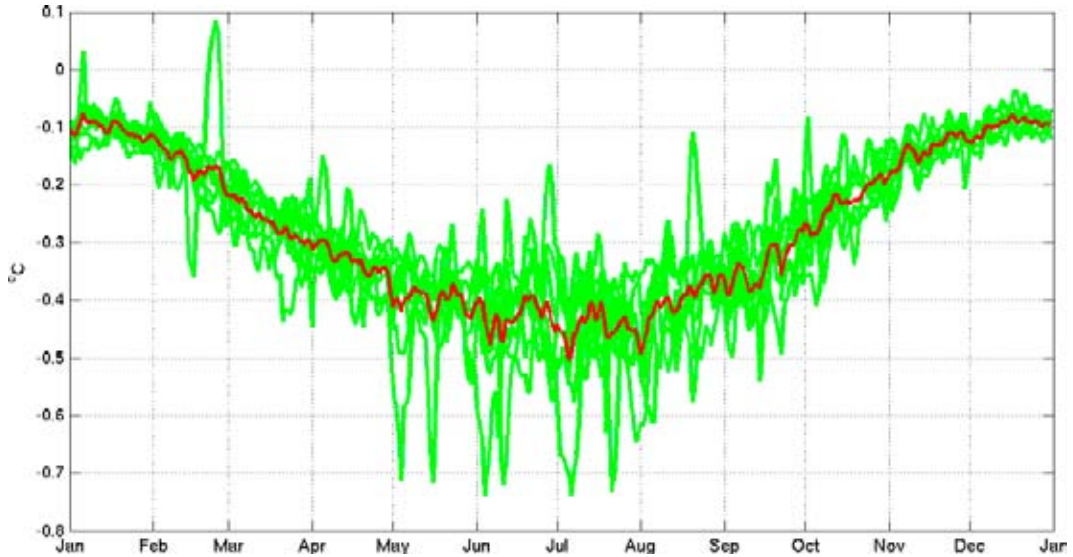


Figure 2-6. Difference in temperature over Europe when the solar constant in RCA3 is reduced by 6% (green) The red line shows an average over the eight individual years.

from this sensitivity tests shows that RCA3 is not very sensitive to local changes in radiation as the temperature differences generally stays below 0.3–0.4°C in all months with maximum differences in summer. And, for smaller changes in the solar constant (i.e. less than 2%), the temperature differences between the sensitivity simulation and the reference are at most a few tenths of a degree (not shown). This low sensitivity to the insolation may sound counter intuitive as it is the difference in insolation that is the main underlying forcing factors of the long-term changes in climate between interglacial and glacial conditions. However, the climate in a relatively small region, like the RCA3 domain, is to a very strong degree governed by the large-scale climatic features related to the general circulation which is imposed on RCA3 from the global model. Also, other locally stronger forcing factors like changes in ice sheet extent play a major role. Based on these findings we have chosen not to change the astronomical forcing conditions in RCA3 as in CCSM3. Instead we use constant forcing conditions reflecting the end of the 20th century in all three cases.

2.3.2 Greenhouse gases and aerosols

Greenhouse-gas concentrations were inferred from ice-core records spanning the last 800 kyr /EPICA members 2004, Siegenthaler et al. 2005, Spahni et al. 2005, Lüthi et al. 2008/. As discussed above, we chose the CO₂ level for the *warm case* as a compromise between a high level (needed to simulate a warm climate that melts the Greenland ice sheet) and a not too high level (that remains in the atmosphere a long time after emissions have ceased). According to /Lenton et al. 2006/, a 750 ppm level still means that all “conventional” fossil fuel resources (including coal, oil and gas) need not have been used. There are many uncertainties on how the biosphere and oceans will respond to an increased warming. This makes it difficult to estimate the concentrations of CH₄, N₂O, and CO₂ for this case at a time period in the distant future. Just as for CO₂, the abundances of CH₄ and N₂O will peak and then subsequently drop to lower levels if emissions decrease. In the IPCC Fourth Assessment Report (AR4) there are some estimates of concentrations for the year 2100 /Meehl et al. 2007/. Here, we assume that these are close to the peak levels and that the concentrations will then decrease to levels close to those observed today. Therefore, we set the concentrations of CH₄ and N₂O at present-day levels.

We set concentrations of ozone, mineral dust, sea salt and other aerosols to their pre-industrial concentrations in all three cases. We realize that setting mineral dust at pre-industrial concentrations is probably a gross underestimate for past cold climates, in particular for the LGM case, as ice-core records indicate much higher concentrations for the glaciated time periods. Therefore, we conducted a sensitivity experiment in which we changed the aerosol content by increasing the mineral dust load by a factor of 3 to simulate LGM conditions. Henceforth, this simulation is termed LGM-vd. The

“d” denotes dust, and the “v” relates to the fact that the vegetation is also altered compared with the reference case, see Section 2.3.6 for details. This is of course also a rather crude simplification as the increase in dust concentration is inferred as a constant in time and space. An alternative would have been to use data from reconstructed/simulated mineral dust concentrations /e.g. Mahowald et al. 2006a/. However, this would have forced us to set up and use a different version of the global model, which was not feasible within the present project. The selected approach, with a dedicated sensitivity experiment, is considered appropriate for the purpose of the study.

Differences in the treatment of greenhouse gases and aerosols in RCA3 compared with CCSM3

In RCA3 we could easily vary only CO₂, whereas in CCSM3 other forcing agents are also explicitly treated in the radiation code. These are greenhouse gases like CH₄, N₂O and ozone and also aerosols like sulphate, mineral dust and sea salt. To make the radiative forcing consistent between the models we expressed the concentrations of the other forcing agents (Table 2-1) in RCA3 in terms of CO₂-concentrations (i.e. so-called CO₂-equivalents). The radiative forcings from all greenhouse gases and aerosols were added into one term, ΔF. The amount of CO₂ corresponding to that forcing was calculated using the equation $\Delta F = 5.35 \ln(CO_2/CO_{2\text{ref}})/\text{IPCC } 2001$. The resulting equivalent CO₂ concentrations obtained in this way and used in RCA3 were 841 ppm in the *warm case*, 168 ppm in the *glacial case* (109 ppm in the three times dust sensitivity experiment) and 187 ppm in the *permafrost case*. As a comparison, we use 333 ppm in the control climate representing the conditions in the period 1961–1990. These imposed changes in radiative forcing have been applied without taking regional heterogeneity in aerosols into account in order to keep the change in forcing as similar to that in the global model as possible. As the radiative forcing of the mineral dust aerosols during LGM was higher at high northern latitudes than in the corresponding global mean /Mahowald et al. 2006b/ this implies that the regional cooling may be underestimated in our simulations.

2.3.3 Ice sheets

For the *warm case* we assumed that there are no ice sheets in the Northern Hemisphere. For the Antarctic, an increased surface mass balance in a warmer climate as indicated by for instance AOGCMs and ice sheet modelling could be offset by an increased discharge due to reduction in the major West Antarctic ice shelves /Meehl et al. 2007/. However, as the uncertainties are large we make the assumptions that the Antarctic ice sheet remains identical to that in today’s conditions. As this is a hypothetical case for the future, there are, of course, no proxy data to be used for restricting forcing conditions. However, we can make parallels to earlier warm periods like the Eemian (i.e. the previous interglacial period that occurred ca 130–115 kyrs BP, MIS 5e). During that period, large parts of Greenland were deglaciated and the global mean sea level was 4–6 metres higher than today /e.g. Overpeck et al. 2006/.

For the *glacial case* we used the same ice sheet setup as in the PMIP-2 project /Harrison et al. 2002/, see Figure 2-7. This is based on the ICE-5G data /Peltier 2004/ which has been shown to improve the simulated climate in western Siberia compared with previous estimates /Kageyama et al. 2006/.

The extent of the Northern Hemisphere ice sheets at the LGM is rather well constrained, but is much more uncertain for preceding time intervals during the Weichselian. For the *permafrost case*, selected as a period during MIS 3, we sought for an ice sheet configuration with restricted ice sheet cover over Fennoscandia so that the three sites, Forsmark and Oskarshamn in Sweden, and Olkiluoto in Finland, were ice free. This ice sheet set up was based on the output from a workshop on palaeoenvironment and ice sheet dynamics during MIS 3 held in Stockholm during 2007 /Näslund et al. 2008/. One of the conclusions of the workshop was that a restricted ice sheet configuration in Fennoscandia during parts of MIS 3 is supported by glaciological inferences, ¹⁴C dates on mammoth remains and plant material, and palaeobotanical proxies, see /Näslund et al. 2008/. In addition to a relatively small Fennoscandian ice sheet, we assumed a fairly large (but smaller than for the LGM) Laurentide ice sheet. With this set up, it is possible to test if the climate models yield a climate that is in agreement with the prescribed restricted ice sheet extent or not. If they do support such an ice sheet it is also possible to test if the models simulate a cold and dry climate favourable for permafrost growth in the suggested ice-free parts of Fennoscandia. For the Northern Hemisphere, the ice sheets were taken as a combination of a Fennoscandian MIS 3 ice sheet from an earlier SKB project /SKB 2006/ and

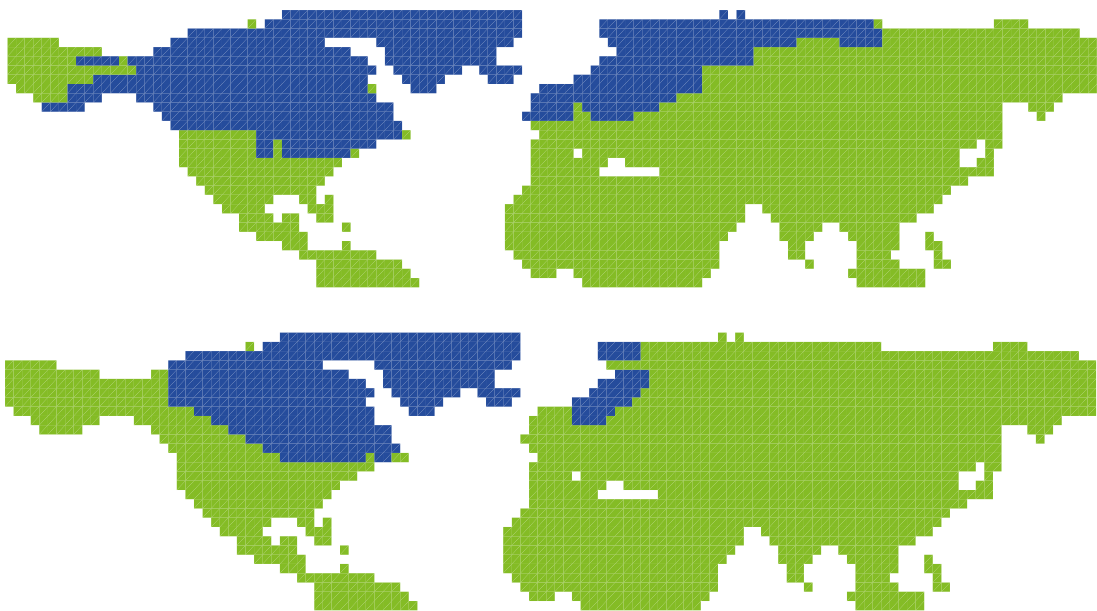


Figure 2-7. Land (green) and ice extent (blue) in CCSM3 in the northern hemisphere in the glacial case (LGM) (top) and permafrost case (MIS 3) (bottom). Grid boxes with a land fraction lower than 20% are not filled.

the Laurentide ice sheet from a simulation with CLIMBER-2 /Calov et al. 2005/. The Laurentide ice sheet was adjusted in its westernmost part according to the results of the workshop on MIS 3 by a complete removal of the ice sheet in Alaska /Näslund et al. 2008/. For the Southern Hemisphere we used the ICE-5G data /Peltier 2004/ for the Antarctic ice sheet for 14 kyrs BP as a proxy for ice sheet extent and thickness at 44 kyrs BP (Figure 2-7).

Differences in ice sheets in RCA3 compared with CCSM3

In the regional climate model, the ice sheets in northern Europe were taken to be identical to those used in the global model, albeit with a higher horizontal resolution. As in CCSM3, there is no module in RCA3 that explicitly calculates properties of glaciers and/or ice sheets. Therefore, we simulated the presence of an ice sheet by: i) assigning all grid points within the ice sheet area (Figure 2-8) with a thick layer of snow and ii) changing the topography so that the elevation of the surface corresponds to the assumed elevation of the ice sheet (see Section 2.3.5). With this approach, RCA3 has a crude representation of the ice sheets in terms of both elevation and surface properties. However, the setup does not allow for any refined calculations of the mass balance or runoff from the ice sheet.

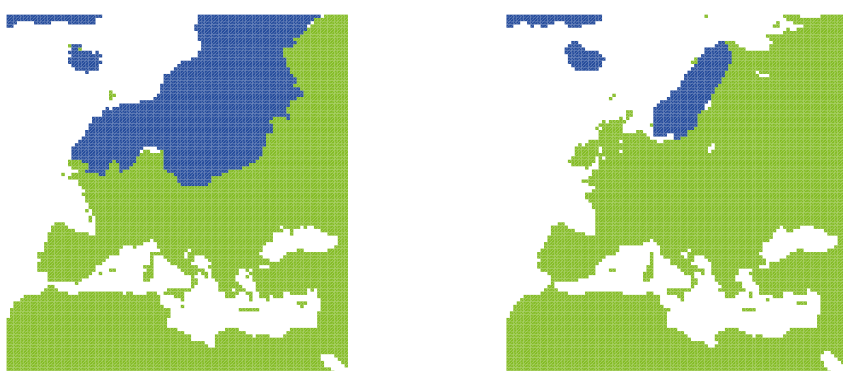


Figure 2-8. Land (green) and ice extent (blue) in RCA3 in Europe in the glacial case (LGM) (left) and the permafrost case (MIS 3) (right). Grid boxes with a land fraction lower than 20% are not filled.

2.3.4 Freshwater forcing of the oceans

Our assumption of a complete loss of the Greenland ice sheet for the *warm case* (Section 2.3.3) implies that a large amount of fresh water is added to the North Atlantic. The influence of a freshwater perturbation on the Atlantic Meridional Overturning Circulation (AMOC) has been investigated by several groups /e.g. Ridley et al. 2005, Stouffer et al. 2006, Bitz et al. 2007/. These studies show that for a disturbance in terms of a freshwater flux of 0.1 Sv (Sverdrups; 1 Sv=10⁶ m³s⁻¹) the AMOC recovers within a few centuries, depending on the duration of the freshwater flux and the background climate. /Ridley et al. 2005/ simulated the response of the climate system to a stabilization of the atmospheric CO₂ concentration at about four times pre-industrial levels (1,130 ppm) with an AOGCM coupled to a dynamical ice sheet model of the Greenland ice sheet. In their simulation, the Greenland ice sheet has almost completely melted after 3,000 years. The strongest freshwater fluxes from the ice sheet occurred during the first 350 years of the simulation and amounted to 0.1–0.15 Sv. The AMOC weakened in response to the freshwater flux, but the circulation recovered after 400 of the 3,000 years of the simulation.

If the Greenland ice sheet were to melt in a couple of centuries, the mean freshwater perturbation would amount to 0.5 Sv or more and available studies do not tell us what to expect from the AMOC. However, estimates of the rate of melting of the Greenland ice sheet indicate that the melting may take more than 1,000 years /e.g. Ridley et al. 2005/ or at least more than 300 years /Lenton et al. 2008/. If the ice sheet melts in 1,000 years, the mean freshwater flux will be approximately 0.1 Sv, and the corresponding value for a 300 year melting time is slightly more than 0.3 Sv.

Based on the above results, we assume in the *warm case* that the AMOC has had time to recover, which depicts a situation a few thousand of years into the future. The freshwater from the melted ice is assumed to be well mixed with the ocean water without changing the salinity. The primary effect of the weakening of the AMOC in the aforementioned studies is a cooling of the North Atlantic region. Thus if the AMOC was more permanently weakened by the melting of the Greenland ice sheet, we would expect colder conditions in this region than we get in our simulation. This conclusion rests on the assumption that the response of the climate system to the changes in greenhouse gas concentrations and topography imposed in our simulation is, to first order, independent of the state of the AMOC. It was not possible to test this assumption within the current project due to the time needed for each simulation. The purpose of the simulations performed within this project was to investigate three climates with extreme conditions for Fennoscandia. In this respect, the simulation we performed for the *warm case* is likely to give a warmer climate in Fennoscandia than if there was a more sustained weakening of the AMOC. Nevertheless, it is important to note that there are uncertainties in the results.

2.3.5 Sea level, coastlines, topography and bathymetry

For the *warm case* the complete melting of the Greenland ice sheet results in an increase in the sea level by 7 m /IPCC 2001/. Additional contributions from thermal expansion of sea water could add another 0.5–2 m and a complete removal of the West Antarctic ice shelves would contribute an additional 5 m /Meehl et al. 2007/. Albeit dramatic, a sea-level rise of 7–14 m will have only marginal effects on the coarse land-sea distribution in the global model and was therefore neglected. More important are effects of isostatic recovery due to land uplift. We use topography from a Global Isostatic Adjustment (GIA) model, simulating conditions after a removal of the Greenland ice sheet /SKB 2006/. The topography of the continents in the *warm case* is taken as that of today, albeit with a marked reduction in altitude in Greenland due to loss of the ice sheet (Figure 2-9). However, the assumed topography of Greenland includes partial isostatic recovery thereby lifting the surface up to about 400 m above sea.

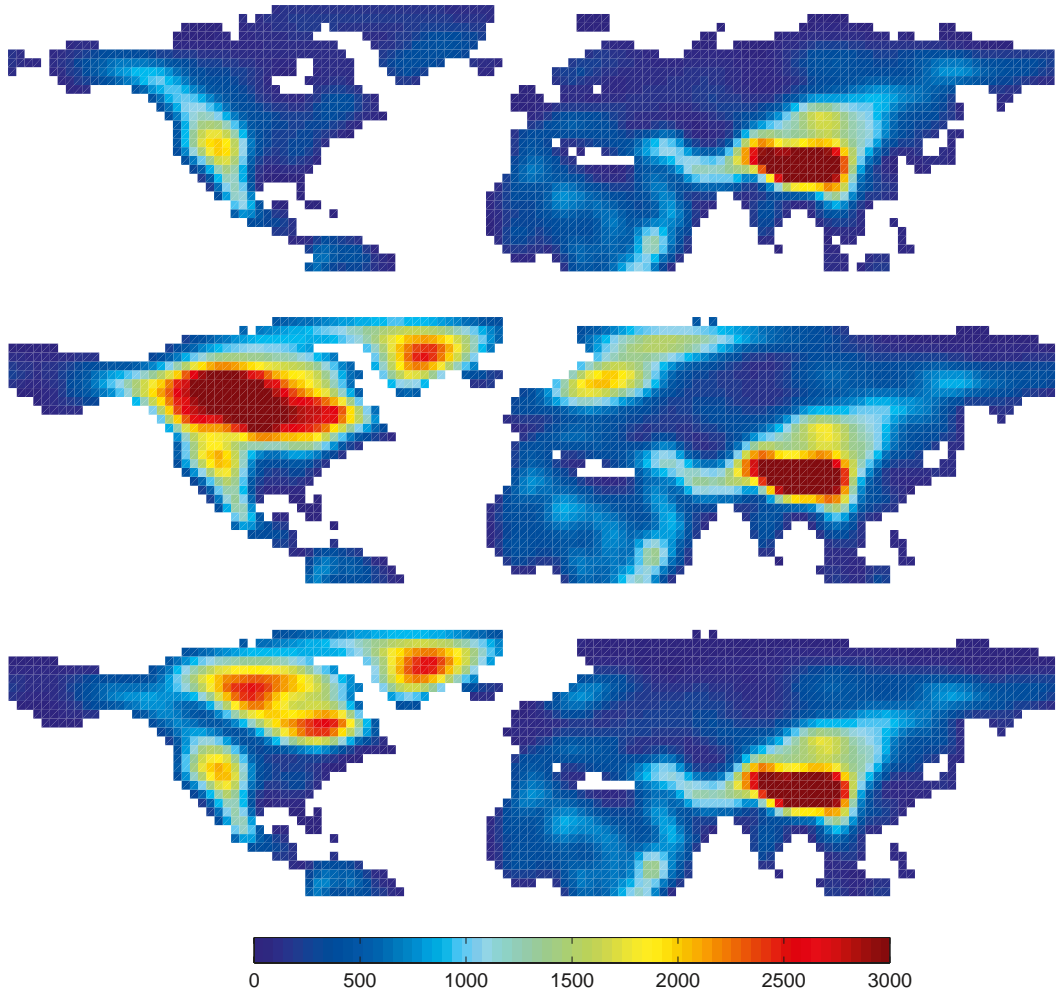


Figure 2-9. Distribution of land areas and elevation (m) in CCSM3 for the warm (top), glacial (middle) and permafrost (bottom) cases. Grid boxes with a land fraction lower than 20% are not filled.

The topography for the *glacial case* was taken as the LGM conditions from ICE5G /Peltier 2004/. Present day bathymetry was used with the coastline moved according to a 120 m sea-level lowering /Lambeck 2004/. The topography for the *permafrost case* was taken as a combination of LGM topography (including the 120 m sea-level lowering, but excluding the LGM ice sheets) and the ice sheets for the *permafrost case* as described in Section 2.3.3. A major difference in the glacial and permafrost simulations compared with present conditions is that the Bering Strait is closed due to the 120 m sea-level lowering. The 120 m lowering is an overestimate for the *permafrost case*, for which ~70 m could be more appropriate /Lambeck 2004/. But, the impact of this difference is modest at the coarse scale of the global model justifying our choice to use the LGM value.

Differences in coastline and topography in RCA3 compared with CCSM3

For the *warm case* we included the effect of melting the Greenland ice sheet by adding 7 m to the sea level. This leads to a change in the land-sea mask of RCA3 as low-lying areas get submerged by the ocean. But, as there is still land uplift due to isostatic recovery after the last glaciation, slightly larger land areas than today emerge from the Baltic Sea (Figure 2-10). These areas that today are the Baltic Sea are given a land-lake fraction of 80–20% in RCA3 in the time periods when they emerge out of the sea due to land uplift. Data on coastlines and topography are taken from model studies with the GIA model /SKB 2006/. The GIA model results were also used in RCA3 for the land/sea distribution, topography and bathymetry for the *glacial* and *permafrost cases*. The sea level was lowered by 120 m in the *glacial case*. As it is important to have the regional details adequately represented in the regional model, we used a 70 m lowering in the *permafrost case*.

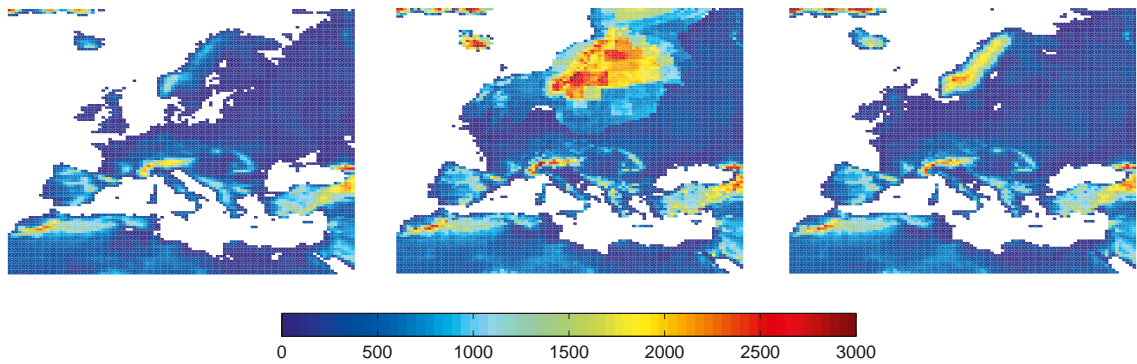


Figure 2-10. The distribution of land areas and elevation (m) in RCA3 for the warm (left), glacial (middle) and permafrost (right) cases. Grid boxes with a land fraction lower than 20% are not filled.

2.3.6 Vegetation

For the land-surface fields applied in the GCM simulations, we should ideally use a dynamic vegetation model coupled to CCSM3 that simulates vegetation consistent with the climate. But, since such a model was not available, we instead used prescribed vegetation covers in the global experiments.

For the *warm case* we took as a starting point vegetation data consistent with the recent past climate, referred to as RP in Table 2-1 /Bonan et al. 2002, Bonan and Levis 2006/. In addition, we used vegetation from a future climate scenario representative of the year 2300 /Scholze et al. 2006/ (GHG in Table 2-1). These latter conditions are from an experiment in which atmospheric concentrations of greenhouse gases were held constant for 200 years at the level obtained in the SRES A1B emission scenario /Nakićenović and Swartz 2000/ by the year 2100. This includes a CO₂ concentration at 730 ppm. The two sets of vegetation used in the global model for the *warm case* are shown in Figure 2-11. Each gridpoint of the land surface in CCSM has a maximum of four different plant functional types (PFTs, see explanation in Appendix C); the dominating PFT (with the highest percentage) is shown in the figure. The overall difference between the two is the increase in trees relative to grass and shrub in Canada, northern and south eastern Eurasia, Europe and South and North America in the greenhouse-gas (GHG) case. The arid regions of today, e.g. the Saharan desert, also increase in size.

In PMIP-2, vegetation was prescribed and today's conditions were applied for all ice-free regions for the LGM. This is our reference case, but as this is not a realistic vegetation cover for the LGM we performed a sensitivity study (henceforth LGM-v) with vegetation from /Mahowald et al. 2006a/ who forced a biome model with the LGM climate simulated in NCAR's PMIP-2 simulation with CCSM3. The vegetation in the global model for the LGM simulation and the LGM-v simulation is shown in Figure 2-12. The overall difference between the LGM-v and LGM vegetation is the smaller amount of forests and shrublands relative to grass and tundra areas in the LGM-v simulation.

For the *permafrost case*, we use the same vegetation as in the LGM simulation (i.e. the recent past vegetation). Again, this should be considered as a coarse simplification. No sensitivity studies were performed for this case.

Differences in vegetation in RCA3 compared with CCSM3

In the regional model, the recent past vegetation is, as previously mentioned, used as “first-guess vegetation” in all three cases. This may imply inconsistencies between the climate and the vegetation type. To investigate this in more detail, vegetation consistent with the climate generated by the initial RCM run based on the ‘first-guess’ vegetation was simulated by the vegetation model LPJ-GUESS (Section 2.2.3) and used to force a subsequent RCM simulation. The climate from the latter experiment was used in all subsequent analyses. The vegetation model provides fractional vegetation cover in the classes broadleaf and coniferous forests, open land and bare ground. In RCA3, broadleaf and coniferous forests are lumped together for calculation of the forest fraction. However, information about the two classes is kept separately when calculating seasonally varying leaf area index. Open land and bare ground are lumped together into an open land fraction.

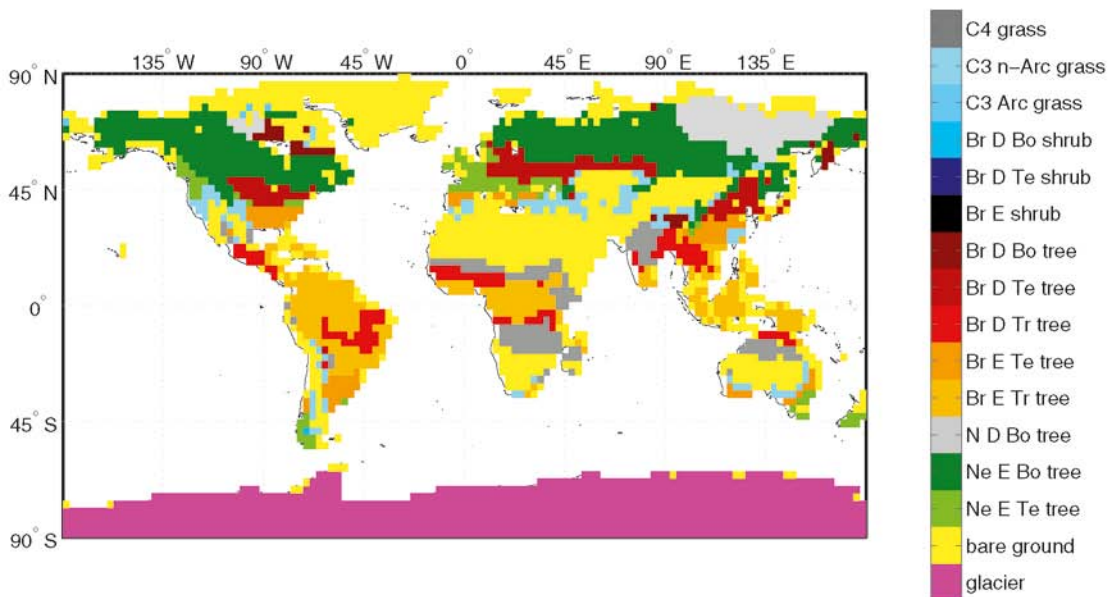
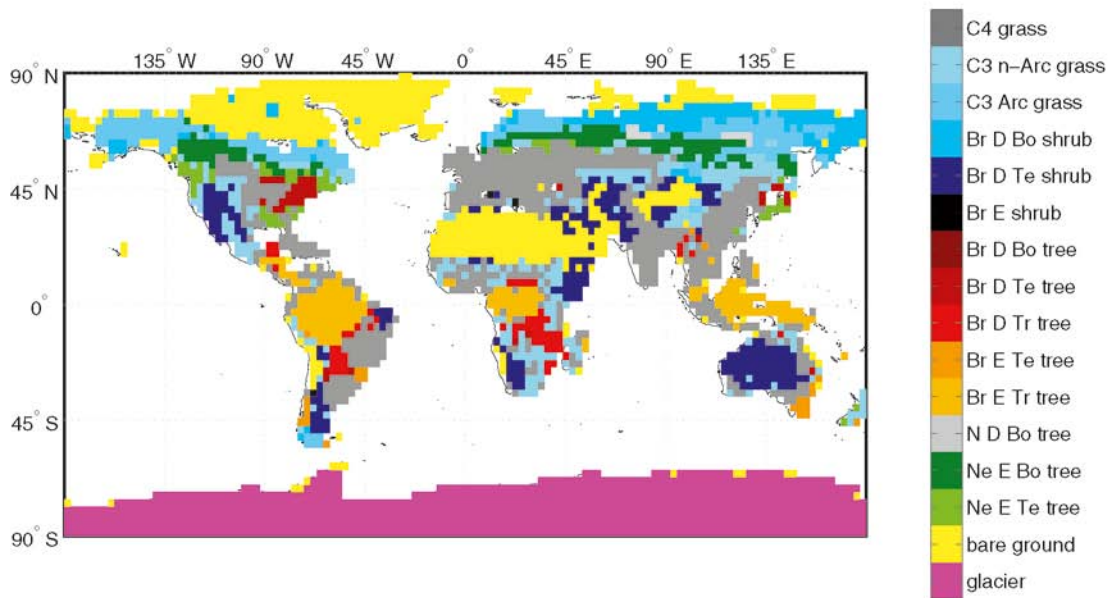


Figure 2-11. The vegetation in the CCSM3 for the warm case. The vegetation from the recent past situation (top) and the future greenhouse warming experiment (bottom) are shown. The dominating plant functional type (PFT) is shown for each gridpoint. Explanation: n-Arc=non-Arctic, Arc=Arctic, Br=Broad-leaved, D=Deciduous, Bo=Boreal, Te=Temperate, E=Evergreen, Tr=Tropical, Ne=Needle-leaved.

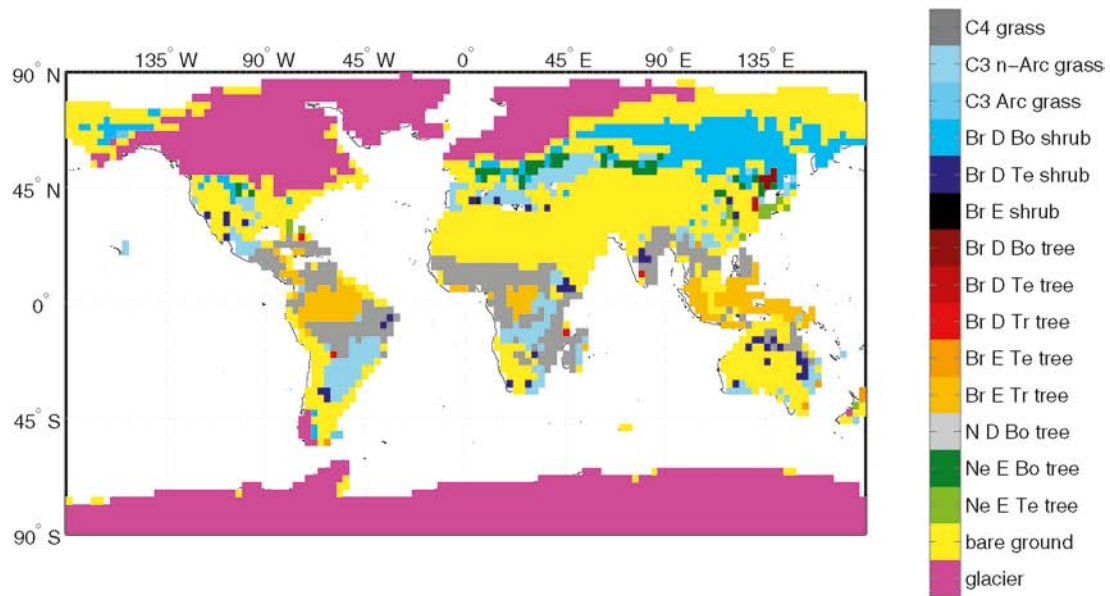
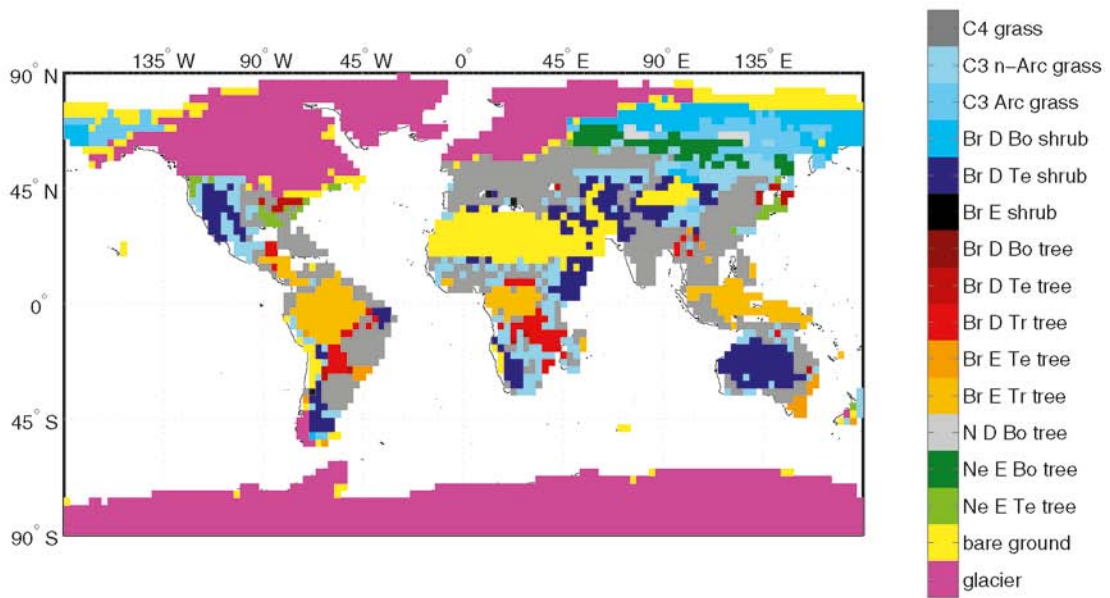


Figure 2-12. The vegetation in CCSM3 for the glacial case as used in the LGM (top) and the LGM-v and LGM-vd (bottom) simulations. The dominating plant functional type (PFT) is shown for each gridpoint. Explanation: n-Arc=non-Arctic, Arc=Arctic, Br=Broad-leaved, D=Deciduous, Bo=Boreal, Te=Temperate, E=Evergreen, Tr=Tropical, Ne=Needle-leaved.

2.4 Climate proxy data for model evaluation purposes

Climate proxy data are quantitative and qualitative estimates of, for example, temperature and precipitation derived from marine records, ice-core archives and terrestrial records, such as speleothems, lake sediments, or glacial deposits. Each of these geological archives contains biological, physical and/or chemical information which can be interpreted qualitatively and, based on certain transfer functions, also be translated into quantitative climate information. In the present report, proxy data are used for two purposes: i) to support estimates of forcing conditions for the climate models (see Section 2.3) and ii) for model evaluation as discussed in this section. We make use of both marine and terrestrial proxy records for the latter purpose.

Proxy records from marine archives include sea-surface temperature reconstructions based on transfer functions for counts of planktonic foraminifera, diatoms, radiolaria and dinoflagellate cysts, $\delta^{18}\text{O}$ measurements on planktonic foraminifera (representing the upper 100 m in the ocean), $\text{U}^{238}_{\text{K}}$ index based on unsaturated alkenones derived from phytoplankton (coccolithophorids) (representing the upper 30–50 m in the ocean), and Mg/Ca ratios of planktonic foraminifera. For the *glacial case* we used the data compilation in the MARGO (Multiproxy Approach for the Reconstruction of the Glacial Ocean surface) database, which is available at www.pangaea.de /Kucera et al. 2005/, whereas we relied on a palaeoclimate data compilation for the *permafrost case* (Antje Voelker, personal communication). This compilation is based on data from the database presented in /Voelker et al. 2002/. The availability of data differs between the *glacial* and the *permafrost case*, with 446 sites with annual mean, summer and winter data for the LGM and only 13–24 sites with data, depending on season, for the chosen MIS 3 time period for the *permafrost case*. The uncertainties in the methods used to transfer the proxy data to water temperature leads to an uncertainty in the temperature reconstructions of $\pm 2\text{--}3^\circ\text{C}$ (Antje Voelker, personal communication).

Palaeo-records assembled from terrestrial archives are based on a variety of sedimentological, chemical and biological proxies. Most of these are qualitative and thus indicate only relative information such as warm/cold and wet/dry conditions, whereas others, such as pollen, plant macrofossils, chironomids (non-biting midges), beetles and diatoms provide quantitative temperature estimates. For the *glacial case* we used reconstructed LGM winter and summer temperatures /Tarasov et al. 1999, Wu et al. 2007/. There is no general uncertainty range for these pollen-based temperature reconstructions. Rather they are presented with intervals of 10–20°C for winter and of 3–5°C for summer temperatures /Tarasov et al. 1999/. Pollen assemblages can be used to classify vegetation types. Using a vegetation model and an inverse technique it is possible to reconstruct the bioclimatic variables that constrain vegetation and therefore pollen assemblages. In that way precipitation for the LGM was also reconstructed /Wu et al. 2007 and references therein/. The errors for proxy-based estimates of precipitation are $\pm 60 \text{ mm/month}$. The LGM data that were used for the comparisons with the RCA3 regional climate model results are presented in Appendix C.

For the *permafrost case*, we used the global compilation described above for the global model and a regional data compilation for Europe /Wohlfarth 2009/. To compare the regional RCA3 run for the *permafrost case* with palaeoclimate data sets, we compiled published records of reconstructed temperature and precipitation estimates and of vegetation reconstructions (Figure 2-13 and Appendix E).

Since most records are published on a radiocarbon (^{14}C) time scale, these age estimates need to be transferred to an absolute time scale to be comparable to the interstadial (GIS) and stadial (GS) events identified in the Greenland isotope record during MIS 3 /NGRIP Members 2004/. Interstadial and stadial events in Greenland ice cores are generally defined by variations in oxygen isotope values ($\delta^{18}\text{O}$), whereas interstadials and stadials on land are traditionally defined as biostratigraphic zones, which are mainly based on pollen stratigraphic zones and reconstructed changes in vegetation /Behre 1989/. Depending on the region where these zones have been recognized, they have been named differently (Figure 2-14). A first attempt to correlate land-based interstadials recognized in northern Europe with those of the Greenland ice core project (GRIP) was made by /Dansgaard et al. 1993/. Later, when the first high-resolution and continuous terrestrial lake sediment sequence of Lago Grande di Monticchio in Italy was published /Allen et al. 1999, Allen and Huntley 2000/, the pollen zones were tentatively correlated with the GISP2 (Greenland Ice Sheet Project 2) ice core from Greenland. The tentative correlation between interstadial and stadial events recognized in European land archives and the Greenland ice core record shown in Figure 2-14 is based on translating published ^{14}C ages into absolute ages through a comparison with the curve of /Hughen

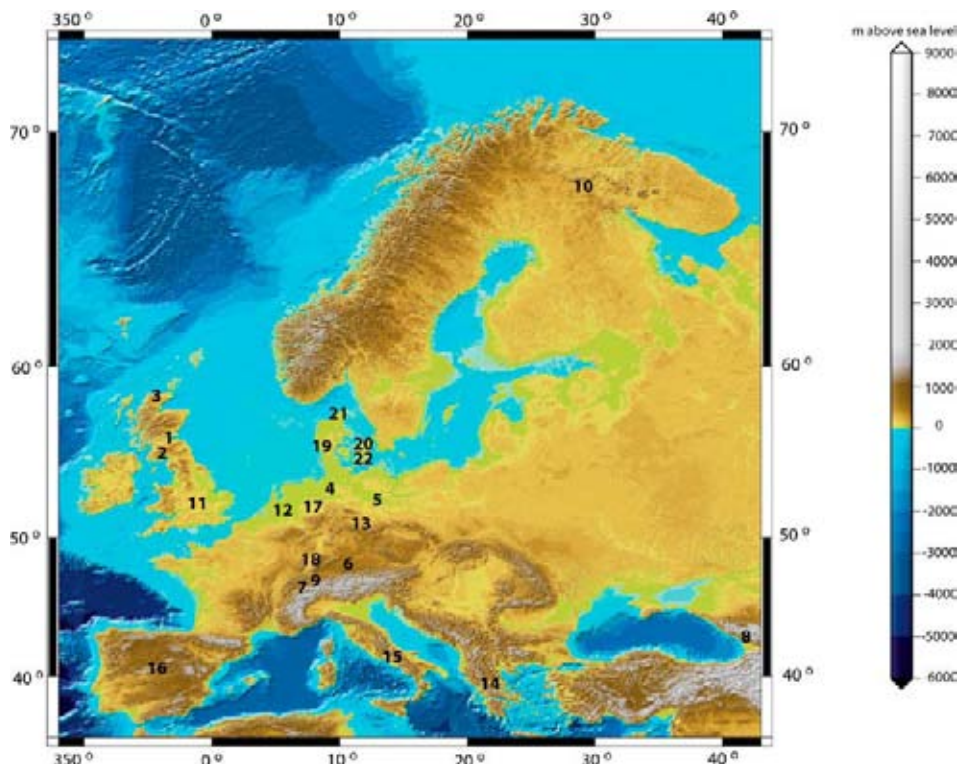


Figure 2-13. Location of the sites used in the MIS 3 data set compilation. Numbers 1–22 refer to Figure 2-15 and the Table E1 in Appendix E.

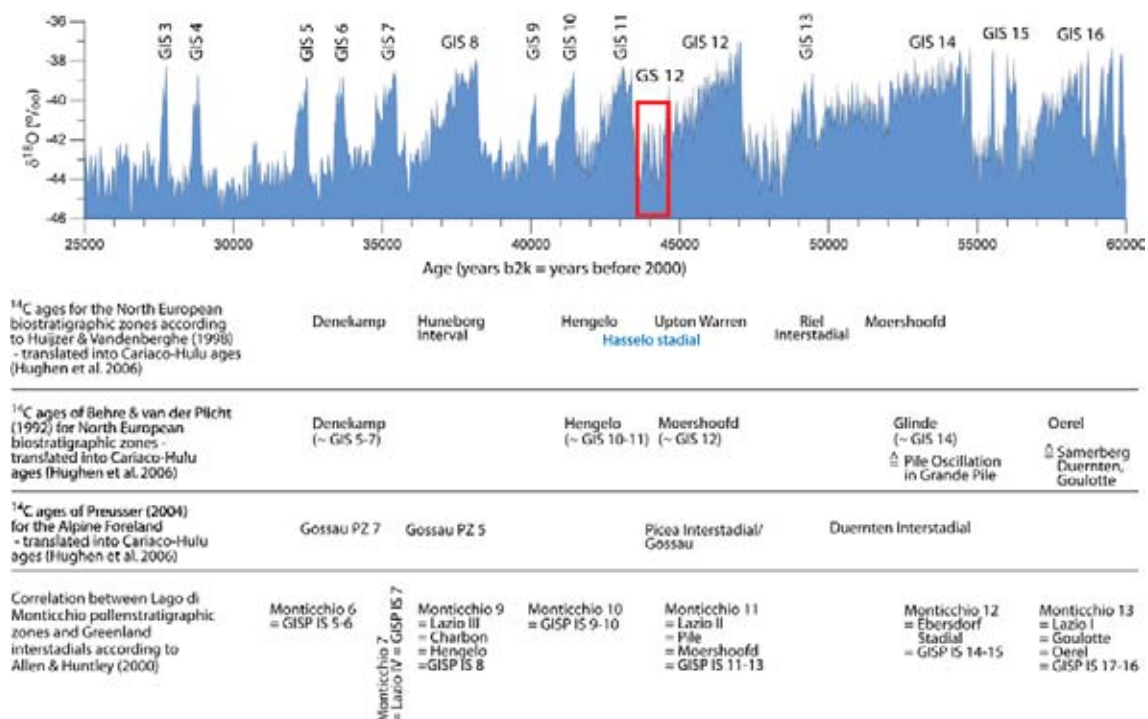


Figure 2-14. Tentative correlation of European interstadials and stadials with the Greenland ($\delta^{18}\text{O}$) curve /NGRIP Members 2004/. The ^{14}C ages published by Huijzer and Vandenbergh 1998, Behre and van der Plicht 1992, Preusser 2004/ for interstadial events were translated into absolute ages (“Cariaco-Hulu ages”) using the curve given in Hughen et al. 2006/, while the correlation between Lago di Monticchio, European pollen-stratigraphic and Greenland interstadials is after Allen and Huntley 2000/. GIS = Greenland Interstadial, GS = Greenland stadial. PZ = pollenstratigraphic zone; GISP = Greenland ice sheet project. GS 12, for which the models were run, is marked in red.

et al. 2006/. The discrepancy between age estimates for the land-based interstadials is related to chronological uncertainties and to the fact that most records are discontinuous. It is, however, obvious that the interstadials recognized on land extend over several of the shorter GIS, while some of the long GIS seem to have clear counterparts on land. In contrast, stadial events are rarely seen in land records.

Most terrestrial palaeoclimate reconstructions are based on biological proxies, such as for example pollen, plant macrofossils, coleoptera (beetles), diatoms (algae) and chironomids (midges). Temperature estimates are therefore mainly estimates for the mean temperature of the warmest month (MTWM), i.e. the time interval when the species were living, although some proxies also allow the mean temperature of the coldest month (MTCM) or the mean annual temperature (MAAT) to be reconstructed. As shown in Figure 2-15 only limited information is available from biological proxies for MIS 3 stadials. The climatic regime of the stadials has instead been inferred based on the occurrence of ice-wedge casts /Huijzer and Vandenbergh 1998/.

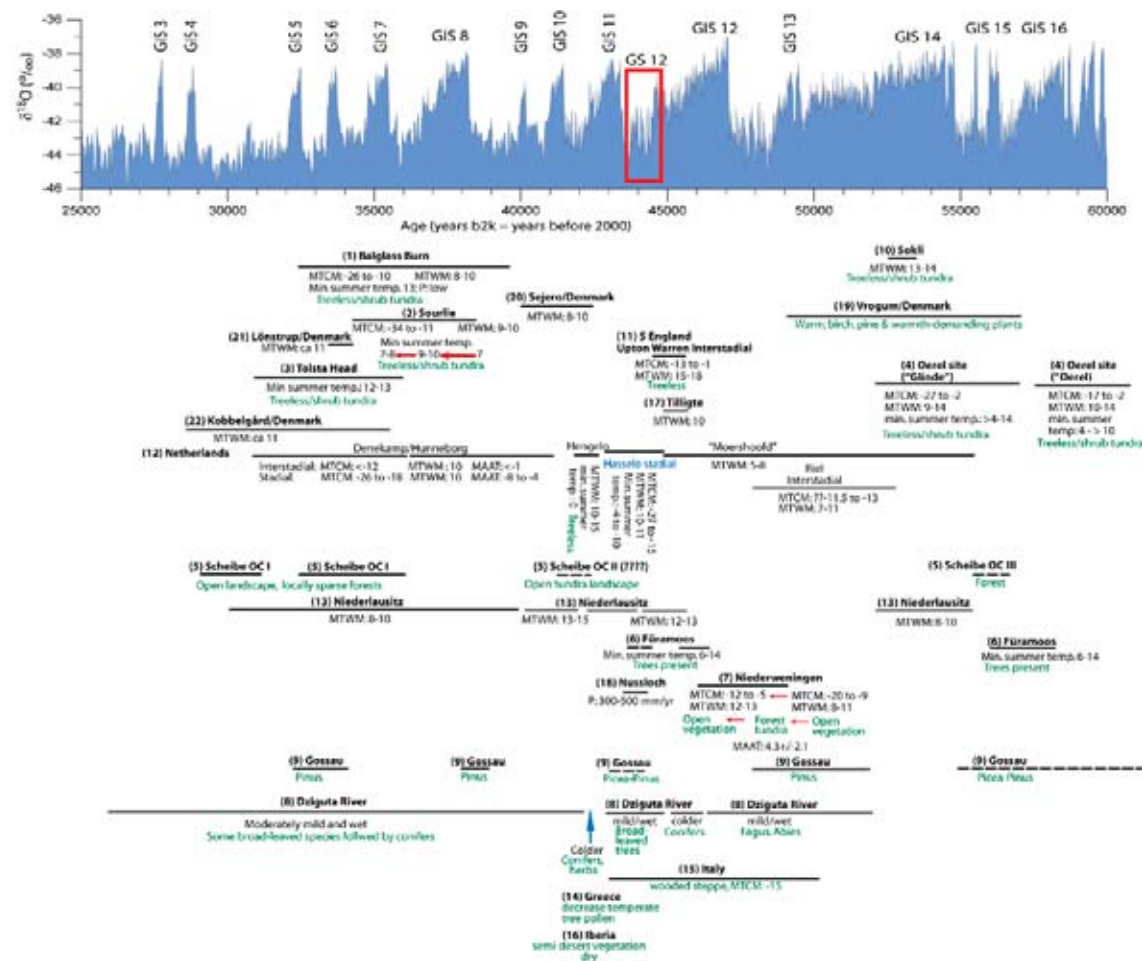


Figure 2-15. Compilation of estimates for temperature (°C), precipitation (mm/yr) and vegetation for selected sites in Europe during MIS 3 and their comparison to the Greenland $\delta^{18}\text{O}$ curve (NGRIP Members 2004). The age assignment for the terrestrial records is based on published ^{14}C ages which were transformed into absolute ages using the curve given by /Hughen et al. 2006/. Most records are short and discontinuous and cover only parts of MIS 3 or parts of a MIS 3 interstadial and some records have very uncertain chronologies. See Figure 2-13 for the location of the sites and Table E1 in Appendix E for details on each record. MTWM = mean temperature of the warmest month, MTCM = mean temperature of the coldest month, MAAT = mean annual temperature, P = precipitation, GIS = Greenland interstadial, GS = Greenland stadial. GS 12, for which the models were run, is marked in red.

Limitations in usefulness of proxy records for model evaluation purposes

Geological archives and their proxy records are the only “real” data at hand to reconstruct past climatic and environmental conditions. Nevertheless, they suffer from a number of limitations. Lakes fill in over time and lakes with deposits reaching far back in time are scarce. In formerly glaciated areas, older deposits have often been eroded and, therefore, the longest continuous records are found outside areas that have been glaciated. In formerly glaciated areas or areas with permafrost, lake records are discontinuous. Moreover precise dating of lake sediments is hampered by the fact that radiocarbon dating is only possible back to *ca* 40 kyr. Other dating methods, such as optically stimulated luminescence, have large error margins, preventing precise age determinations for a sequence. The same holds true for marine sediments, where age models are often established by wiggle-matching to ice core chronologies. Speleothems are in contrast often precisely dated, but the interpretation of a climate signal in these deposits is not straightforward.

Transfer functions used to estimate climate parameters are based on the assumption that organisms live under specific climatic conditions and that today’s climate-organism relationship was also valid in the past. Different types of data sets and transfer functions have been developed over the years for e.g. foraminifera, diatoms, chironomids, pollen, plant macrofossils, and beetles. Each data set has its own limitations which need to be taken into consideration when these proxies are used to infer climatic conditions. Reconstructed temperatures or precipitation are often regarded as correct values. However, each value depends on the data set used to develop the transfer function, has its specific assumptions and inherent errors. Most biological proxies moreover only provide information on summer conditions.

Proxy data can be used to describe the conditions only at the specific location where the sample was taken. This implies that they are not necessarily representative of the large-scale, or even regional, features of the climate. This also means that points close to each other can show rather different values. It is important to keep these uncertainties and the error estimates in mind when using proxy data for model evaluation purposes. There is an analogue to this problem in the present climate when it sometimes can be difficult to interpret and use even high-quality meteorological observations from single observational sites as these may not be representative for larger scales, such as a grid box in a climate model.

The uncertainty of proxy-derived climate reconstructions, combined with uncertain chronological constraints on marine and lake sediments, and the scarcity of records covering the time intervals of the LGM and particularly MIS 3, limit their use for detailed data-model comparisons. In the following comparisons between available proxy data and model results it is important to keep this limitation in mind.

3 Results and discussion

As described in Chapter 1, the main objective of this project has been to study three extreme climates within a 100 kyr year time perspective, for periods that are thought to be relatively stable on the timescale of a thousand years. This was accomplished by performing integrations with climate models given constant forcing conditions over long time periods (Chapter 2). The goal with these long-term integrations is that the global climate model should reach quasi-equilibrium within given boundary conditions and forcings. These quasi-equilibria can then be seen as representatives of the extreme climates sought here. Due to the thermal inertia of the global ocean, a complete equilibration of the climate system may take more than 1,000 years to accomplish. The time for equilibration in case of *glacial* and *warm case* conditions was estimated as 400–500 years in an earlier study with the CCSM3 for the LGM and the relatively warm mid-Holocene period /Otto-Bliesner et al. 2006a/. We found this to be an underestimate. The simulations for the *glacial* and *permafrost cases* needed approximately 800 years to reach quasi-equilibrium (as defined in Chapter 2.2), even though our *glacial case* simulation is a direct continuation of a LGM simulation performed by Otto-Bliesner et al. Furthermore, we find that the equilibration of the simulated climate is an important aspect of the results and discuss that aspect for each simulation in the following sections.

In this chapter we first present and discuss, separately for each case, the resulting climate from the global and regional models as well as the simulated regional vegetation. We compare results from the experiments for all three cases with either the recent past (RP) climate simulation (reference period 1961–1990) or the pre-industrial (PI) simulation. The various simulations are denoted as outlined in Table 3-1. Finally, we give a synthesis for each case, in which we compare our results with available proxy data and other modelling efforts from the literature.

The simulations with the global climate model generally cover several hundred years as mentioned above. From these long-term simulations, we used 50-year periods for the subsequent downscaling with the regional model. The choice of 50 years allowed us to investigate inter-annual, and to some degree also inter-decadal, variability in the simulations. The model years given in subsequent diagrams and text represents the number of years since the start of a particular simulation. It has no bearing on calendar years and is given merely as a reference to keep track of exactly which time periods are being discussed.

Table 3-1. Summary of all simulations referred to in this report. Simulations in italics are not from this project but were obtained from the literature and used for comparison with our results. Abbreviations in the forcing column refer to Table 2-1 (REF = reference forcing, GHG and LGM denotes different vegetation in the respective sensitivity experiments, Plx3 denotes three times pre-industrial concentrations of atmospheric mineral dust). *) This simulation is analyzed in two parts referred to as LGM1 and LGM2 (see Section 3.2.1). (-r) denotes the regional model and (-veg) denotes that new vegetation from LPJ-GUESS has been used. (-vd) means that both vegetation and dust are changed according to Table 2-1.

Case	Simulations		Regional model	Vegetation
	Global model	Forcing		
Warm	WARM	REF	WARM-r WARM-r-veg	RP LPJ-GUESS
	WARM-v	GHG	—	—
Recent past	RP		RP-r	
Pre-industrial	PI		—	—
Permafrost	PERMAFROST	REF	PERMAFROST-r	RP
			PERMAFROST-r-veg	LPJ-GUESS
Glacial	LGM*	REF	LGM2-r LGM2-r-veg	RP LPJ-GUESS
	LGM-v	LGM	—	—
	LGM-vd	LGM + Plx3	LGM-r-vd	LGM + Plx3

In the present analysis, we focus on the same 50-year periods in the global and regional models. We focus on the large-scale circulation, mean temperature and precipitation as these three variables summarize many important aspects of the climate. For the global model, we present results from the oceanic part of the simulations with a focus on sea-surface temperature (SST), sea-ice conditions and the Atlantic Meridional Overturning Circulation (AMOC), which is of vital importance for the North Atlantic and European climate. We present results both for long-term (i.e. on a 50-year timescale) mean conditions and to some extent also for inter-annual variability. We do not explicitly discuss variability on shorter time scales, like synoptic or diurnal variability. Results are presented both for annual and/or seasonal mean conditions. Seasonal means are calculated for December–February and June–August respectively. Sometimes we present results for the warmest and coldest months of the year to facilitate comparisons with proxy data. In this case, July is considered the warmest month of the year in both the global and regional model. For the coldest month we take February conditions in the global model and January in the regional model. The difference is motivated as we compare with different proxy data for the two models. CCSM3 results are compared with SST proxies while RCA3 is compared with proxies for near-surface temperatures over land. The seasonal cycle in temperature over the oceans is shifted later by one to two months compared with that over the continents. Figure 3-1 shows the domain of the regional model and some regions for which we present averages from both the global and regional models. A close-up look at the climate in the Fennoscandian region for the three cases is presented in Chapter 4.

3.1 The warm case

3.1.1 Global climate model simulations

Stability of the simulated global climate

The global warm case simulation (WARM, Table 3-1) was started from a simulation with CCSM3.0 performed at the Earth Simulator in Japan. That simulation in turn was started from a simulation of the recent past climate run at NCAR with an increase in the atmospheric CO₂ concentration of 1% per year until a doubling of the atmospheric CO₂ concentration at 730 ppm after 70 years /Kiehl et al. 2006/. It was continued for another 310 years with a constant atmospheric CO₂ concentration of 730 ppm. The WARM simulation is a continuation of this simulation. The atmospheric CO₂ concentration was increased to 750 ppm and the atmospheric ozone and aerosol concentrations were decreased from



Figure 3-1. The RCA3 model domain. The areas marked with red are Sweden (A), West Continental Europe (B) and the Iberian Peninsula (C) respectively. Also shown are the three sites for which we discuss the simulated climate in more detail in Chapter 4. The sites are Forsmark (1), Oskarshamn (2) and Olkiluoto (3).

present-day to pre-industrial concentrations and then the simulation was run for another 457 years. The annual global mean surface temperature (T_{agm}) is displayed in Figure 3-2 (upper panel) as a function of time, and is used as one indicator of the balance of the simulated climate. The linear trend in T_{agm} over the last 100 years of the simulation is 0.064°C per century, thus indicating that the simulated climate is in quasi-equilibrium according to our definition (Section 2.2).

As described in Section 2.3.6 we have tested the sensitivity of the simulated global climate to a change in the vegetation from present-day vegetation to vegetation simulated with a biome model which is forced by a warm climate similar to that in our WARM simulation. This sensitivity experiment (henceforth WARM-v) was initialised after 320 years of integration in the WARM simulation and was run for another 139 years (green line in Figure 3-2). T_{agm} for this case is also displayed in Figure 3-2 and the linear trend in T_{agm} over the last 100 years of the simulation is 0.013°C per century, thus also indicating that the simulated climate is in quasi-equilibrium. The mean T_{agm} in the WARM-v simulation is 17.2°C as compared with 16.9°C in the WARM simulation with present-day vegetation. A plausible explanation for the WARM-v simulation being warmer is that there are more extensive forests instead of grass lands in high northern latitudes which lead to higher temperatures due to the decrease in surface albedo. As a comparison T_{agm} is 14.8°C in the simulation of the recent past (RP).

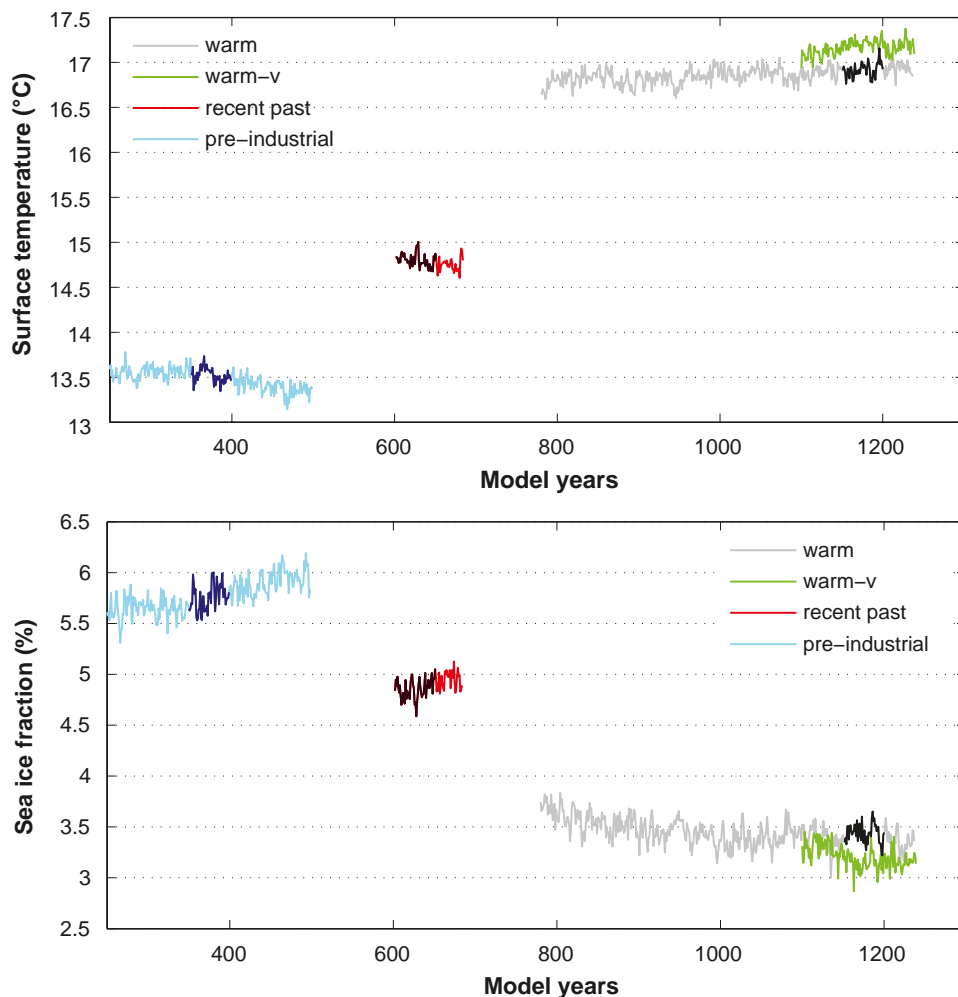


Figure 3-2. Annual mean global mean surface temperature (upper panel) and sea ice fraction (lower panel) in the pre-industrial (PI) simulation (blue), recent past (RP) simulation (red), WARM simulation (grey) and the WARM-v simulation (green). Darker parts of the curves mark the 50-year periods analysed here and used for downscaling by RCA3 (Section 3.2.1). Units are $^{\circ}\text{C}$ and % of the surface covered by sea ice.

The increase in T_{agm} is accompanied by a decrease in the percentage of the Earth's surface that is covered by sea ice (Figure 3-2, lower panel). During the last 100 years of the simulations, the fraction of sea-ice covered area stabilizes around new quasi-equilibrium values in both the WARM and the WARM-v simulations, giving a further indication that the simulated climate is close to quasi-equilibrium.

Temperature and sea ice

Seasonal mean changes in temperature in the WARM simulation as compared with the simulation of the recent past (RP) climate are shown in Figure 3-3. The sea-ice edge in the WARM simulation and in the simulation of the recent past is also indicated. The removal of the Greenland ice sheet produces a strong heating of up to 17°C over Greenland in both summer and winter. This heating is primarily due to a combination of i) the lowering of the surface by up to 3,000 m and ii) the decrease in surface albedo and changes in heat fluxes between the atmosphere and the ground produced by the replacement of the glacier ice surface by tundra. Similar to all greenhouse warming scenarios presented in the IPCC AR4 report /Meehl et al. 2007/, the Arctic region exhibits strong heating by up to 15°C in winter (due to a substantial decrease in the Arctic sea-ice cover and a decrease in the snow cover). The seasonal mean temperature is up to 5°C warmer in summer and up to 7.5°C warmer in

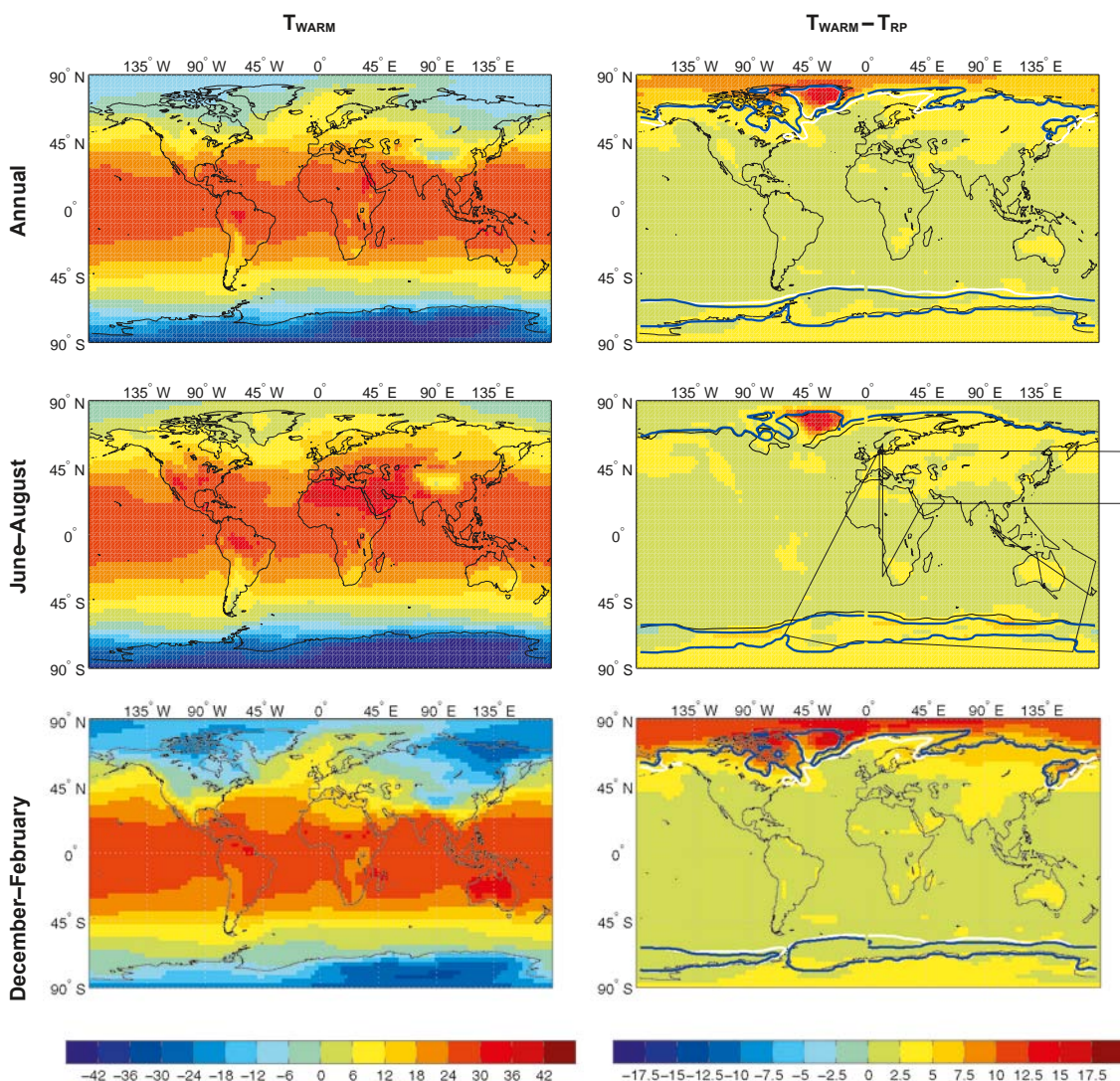


Figure 3-3. The simulated near-surface temperature in the WARM simulation (T_{WARM}) and the difference compared with the simulated recent past climate (T_{RP}). Units are $^{\circ}\text{C}$. Also show by isolines in the rightmost panels is the extent of sea-ice in the simulation of the recent past climate (white) and in the WARM simulation (blue).

winter over Fennoscandia in the WARM simulation as compared with the simulation of the recent past. The resulting summer and winter temperatures are also shown in Figure 3-3. Seasonal mean summer temperatures in Sweden vary in the range 12–18°C and winter temperatures vary in the range 0–6°C.

The decrease in sea-ice cover is evident (Figure 3-3, right panels), with a complete loss of winter sea-ice cover in the North Pacific and a substantial decrease in the North Atlantic and Barents Sea in both summer and winter.

Precipitation

The change in precipitation in the WARM simulation as compared with the simulation of the recent past climate (RP) is shown in Figure 3-4. The removal of the Greenland ice sheet leads to a 25% decrease in precipitation in particular over south-eastern Greenland in both summer and winter, indicating that much of the precipitation in that area in today's climate is triggered by the steep ice sheet topography. Similar to all greenhouse warming scenarios presented in the IPCC AR4 report /Meehl et al. 2007/, precipitation is increased over mid-latitude Northern Hemisphere continents and the Arctic. For Fennoscandia there is an increase in precipitation, most notably in the north. Also similar to other greenhouse warming scenarios, precipitation is shifted towards the equator over the equatorial Pacific and decreased in the subtropics in summer and winter.

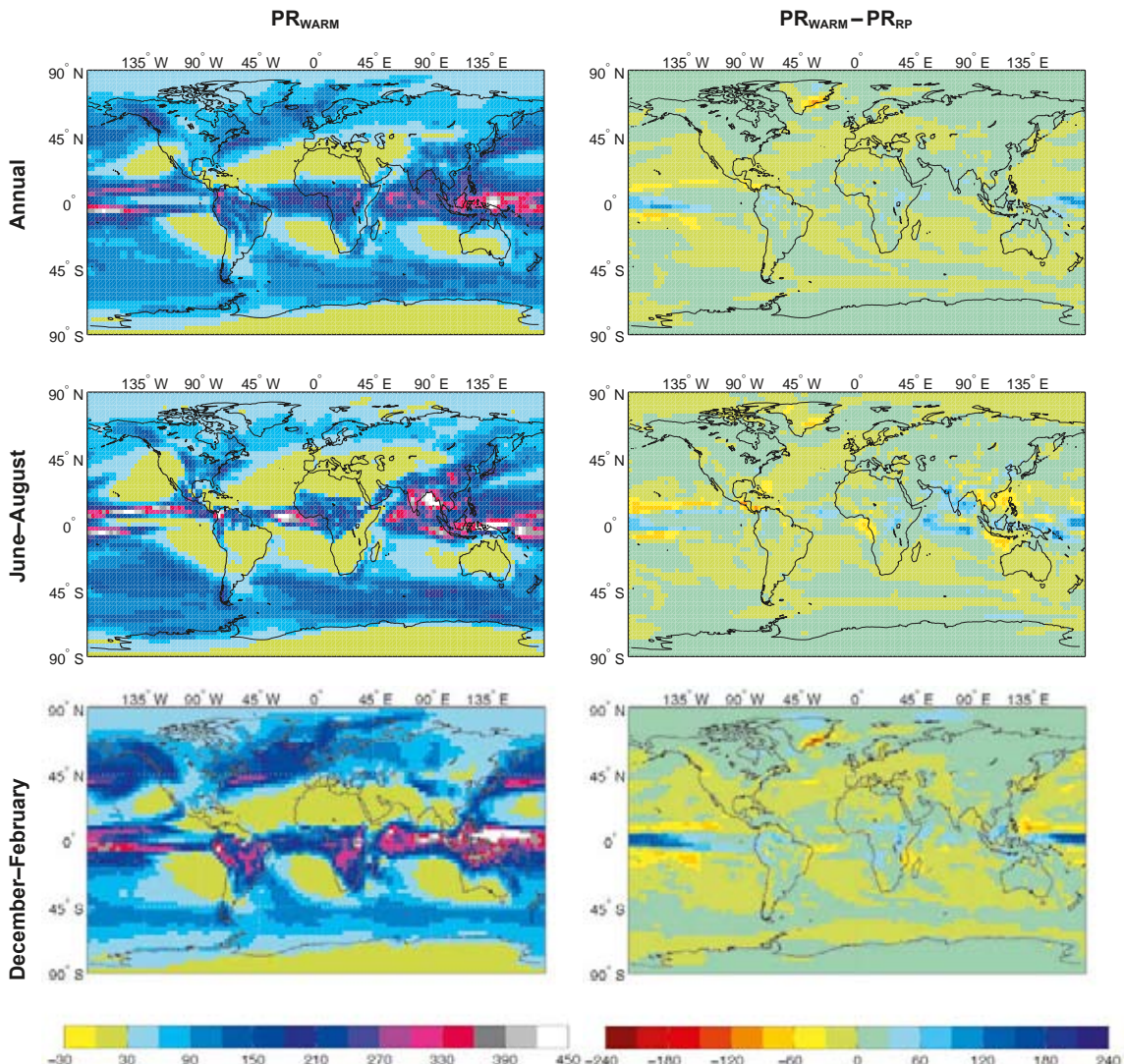


Figure 3-4. The simulated precipitation in the WARM simulation (PR_{WARM}) and the difference compared with the simulated recent past climate (PR_{RP}). Units are mm/month.

Atmospheric circulation

Differences in surface temperature and precipitation between any two simulated climates can be explained both by changes in external forcing (such as greenhouse gas content, aerosols, etc), local effects (such as changes in surface albedo and topographic height) and by effects of differences in the atmospheric circulation (such as wind directions and frequency and intensity of mid-latitude cyclones). The mean sea level pressure (MSLP) gives a picture of the circulation close to the Earth's surface. However, in the diagnosis of the global model we only make limited use of this variable since MSLP is influenced by the changes in the topographic height over the ice sheets between the different cases (cf. Figure 2-9). MSLP is derived from the pressure at the surface under assumptions regarding the atmospheric lapse rate (decrease in temperature as function of height above the surface) between the surface and the mean sea level. Instead, we use the geopotential height at 300hPa (Z300). This variable gives a good picture of the winds in the upper troposphere (the wind basically follows the contour lines of Z300 with high Z300 to the right (in the Northern hemisphere) and the wind speed is proportional to the gradient in Z300). Further, mid-latitude cyclones are connected to the strongest winds at this level, the so called jet stream.

The change in Z300 in the WARM simulation as compared to the simulation of the recent past climate is shown in Figure 3-5. The north-south gradient in Z300 over the North Atlantic is strengthened, in particular in winter. This change is in agreement with a strengthening of the jet stream which is strongly connected to the traverse of mid-latitude cyclones over the Atlantic to Europe.

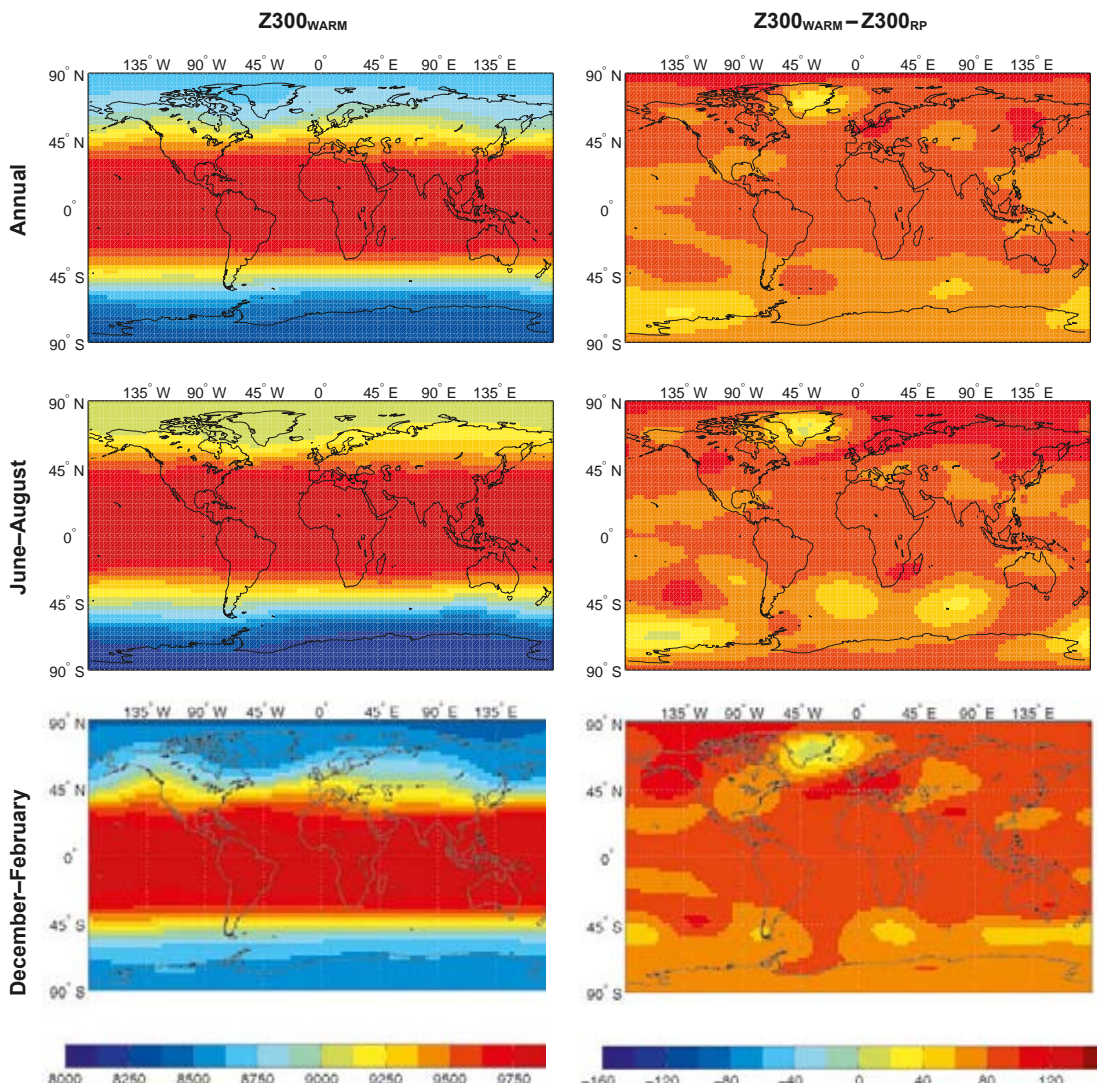


Figure 3-5. The simulated geopotential height at 300 hPa in the WARM simulation ($Z300_{WARM}$) and the difference compared with the simulated recent past climate ($Z300_{RP}$). Units are geopotential metres.

Sensitivity to changes in vegetation

As expected, the regional changes in temperature caused by the change to new vegetation (i.e. from WARM to WARM-v) are largest in the regions where the vegetation cover has changed. The high latitude regions where grass has been replaced by trees (cf. Figure 2-11) are heated by up to 4°C in summer (not shown). In North America there is also a larger heating in WARM-v than in WARM in winter as could be expected. For Fennoscandia and north-western Siberia there is instead a cooling of up to 2°C. The reason for this is not clear, but it may be a result of a large-scale change in the atmospheric circulation in this area as the lower atmosphere over the Nordic seas is also cooler in this simulation, indicating that the difference is not caused by terrestrial changes. Further, the winter heating of the Arctic is even stronger in the WARM-v simulation than in the WARM simulation.

The changes in precipitation caused by the change to new vegetation are small, with increased amounts of precipitation in summer over Fennoscandia paralleling increasing temperatures in summer. In winter, the reverse is true, with a smaller temperature increase in WARM-v compared with WARM and therefore also a decrease in precipitation in WARM-v relative to WARM.

The change in Z300 in the WARM-v simulation as compared with the WARM simulation partly cancels the strengthening of the North Atlantic Z300 gradient that occurs from the recent past climate to the WARM simulation. This change is associated with a decrease in the zonal mean wind. The decrease in winter temperatures over the Nordic seas, Fennoscandia and north-western Siberia is consistent with these changes in the large-scale circulation which gives more high-pressure situations in the region.

The mean temperature of the oceans is increased by 1–2°C in all basins with the strongest heating in the upper ocean in the WARM simulation as compared with the recent past simulation. The salinity is increased by less than 0.1 psu (practical salinity units; measures the conductivity ratio of a sea water sample to a standard solution) in the upper 1,000 m and decreased by less than 0.05 psu below 1,000 m. The salinity is decreased in the upper 50–100 m in the North Atlantic. This change, in combination with the increased temperature, makes the surface waters less dense. The freshening and heating of the surface waters in the North Atlantic is even stronger in the WARM-v simulation. These changes are accompanied by a decrease in strength of the upper branch of the mean Atlantic Meridional Overturning Circulation (AMOC). Measured as the maximum of the AMOC stream function in the North Atlantic the AMOC is 19.4 Sv in the simulation of the recent past climate, 18.2 Sv in the WARM simulation and 15.1 Sv in the WARM-v simulation. The latter case thus shows a reduction of the AMOC by 22% compared with the recent past climate (1961–2000). These changes can be compared with the 0–50% reductions as simulated by the CMIP3 models for the 21st century under a range of given emission scenarios /Meehl et al. 2007/.

Variability

The amplitude of the variability in annual global mean temperature T_{agm} (Figure 3-2) is decreased from the simulation of the pre-industrial (PI) to the recent past climates (RP) and even further to the simulation of the *warm case* (WARM). Expressed as the standard deviation of the inter-annual variability in T_{agm} it changes from 0.08 in PI, to 0.07 in RP and to 0.05 in WARM and WARM-v.

3.1.2 Regional climate model simulations

In this section we discuss the downscaling of the model years 1150–1200 in the WARM simulation. RCA3 was first run to produce an initial climate (WARM-r). This climate was then used to produce a new vegetation distribution, as outlined in Section 2.2.3 and presented below in Section 3.1.3. Finally, a repeated run with RCA3 forced also by the new vegetation was completed to produce the final climate (WARM-r-veg) discussed here. We also present differences between the WARM-r-veg and WARM-r simulations to indicate sensitivity to regional changes in vegetation. Comparisons are also made with the simulation of the recent past climate (RP-r) as reference.

Temperature

In the WARM-r-veg simulation, the warming compared with the recent past climate (RP-r) is strongest over northern Europe in winter. The simulated temperature increase for the coldest month is more than 5°C in northern Fennoscandia (Figure 3-6, second row, middle panel). In southern Europe the warming is stronger in summer, where the temperature of the warmest month increases with more than 4°C in large areas (Figure 3-6, second row, left panel). The stronger warming in the areas of the Bothnian Bay, Bothnian Sea and in the Gulf of Finland in summer in this experiment is due to the land uplift converting sea to land in those areas. The same phenomenon is also responsible for the weaker warming in these areas in winter.

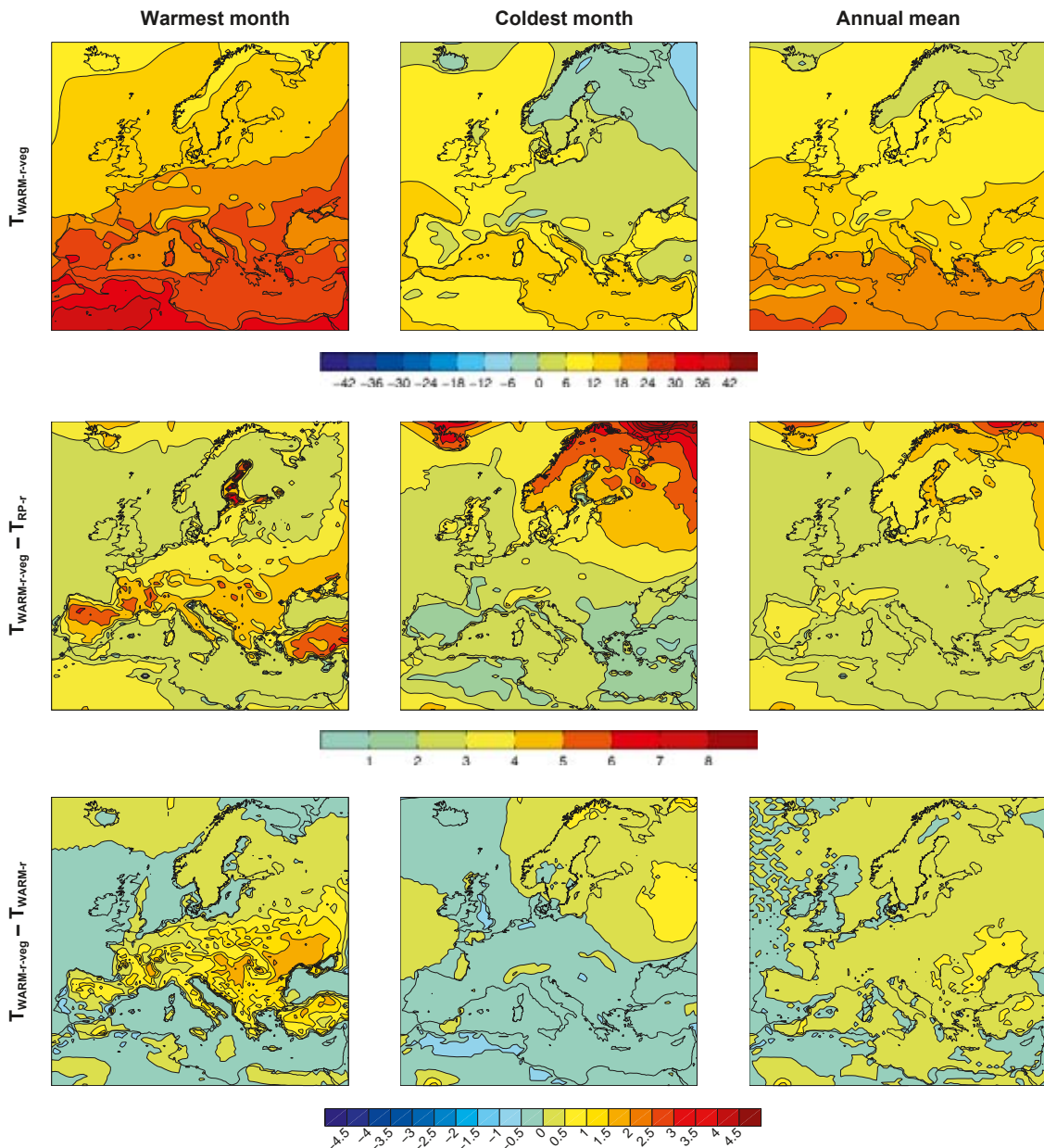


Figure 3-6. Mean near-surface temperatures of the warmest month, coldest month and annual mean in the WARM-r-veg simulation. Also shown are differences between WARM-r-veg and the simulations of the recent past climate (RP-r), and the simulation with the initial vegetation (WARM-r). Units are °C.

The addition of a new vegetation distribution from the vegetation model, more consistent with the climate, generally leads to larger differences when compared with the recent past climate (Figure 3-6, lowermost panels). The differences between WARM-r-veg and WARM-r are largest in south-eastern Europe during summer where WARM-r-veg is up to 2°C warmer. A larger forest fraction in WARM-r-veg in this area compared with that in WARM-r leads to higher temperatures as the night time temperatures does not drop as much as over an open land surface. This is also the area where the climate change signal, i.e. between WARM-r-veg and RP-r, is largest. This difference between the two simulations (WARM-r-veg and WARM-r) indicates that the climate is sensitive to local surface properties in south-eastern Europe. In winter, the differences are fairly small in all of Europe, with a maximum of up to 1°C warmer in the northeast. Again, this is an area where the increase in the forest fraction leads to higher temperatures as forests are warmer than open land during winter in snow covered areas.

Comparing the WARM-r-veg simulation with the simulated climate of the recent past (RP-r) we note that the amplitude of the seasonal cycle in temperature increases in the south and decreases in the north. This is a result of the larger temperature increase in the north in winter and in the south in summer (Figure 3-7). From the figure we can again note that the strength of the seasonal cycle in temperature in parts of Europe (including Sweden and West Continental Europe) is slightly underestimated for the recent past climate (cf. Section 2.2.1 and 2.2.2).

Seasonal mean temperatures for the *warm case* in RCA3 are in general similar to those in CCSM3, at least on a regional scale. However, local differences of up to 1–2°C exist in some regions and seasons. Notably, the winter temperatures in RCA3 are on average 1.5°C colder than in CCSM3 in Sweden (Figure 3-8), but up to 1°C warmer in north-eastern Europe (not shown). In central and eastern Europe, RCA3 simulates similar temperatures as CCSM3 (not shown), whereas on the Iberian Peninsula RCA3 is 2°C colder than CCSM3 (Figure 3-8). The large systematic differences in the Iberian Peninsula are partly due to differences in topography as the average elevation of the Iberian Peninsula is higher at the higher resolution in RCA3 leading to lower, more realistic, temperatures. The average difference in elevation between the models is about 300 m (in the standard atmosphere with a temperature decrease of 6.5°C/1,000 m this would correspond to about 2°C). Summer temperatures are similar in RCA3 and CCSM3 in Sweden and west continental Europe. In central and southern Europe, RCA3 is up to 2°C colder (not shown). As can be seen in Figure 3-8 the temporal correlation between RCA3 and CCSM3 is, as expected, often high in all regions. The correlation coefficient is larger than 0.9.

Precipitation

In winter there is a clear line between increasing precipitation in northern Europe and decreasing precipitation in southern Europe compared with the recent past climate (Figure 3-9, lower middle panel). The differences are relatively small (mostly below 30 mm/month). The largest differences are increasing precipitation on the west coast of Fennoscandia and the British Isles and over Iceland, and decreasing precipitation over parts of the Iberian Peninsula and France. In these regions, changes are up to 90 mm/month, most notably in winter. The changes in annual precipitation are similar to

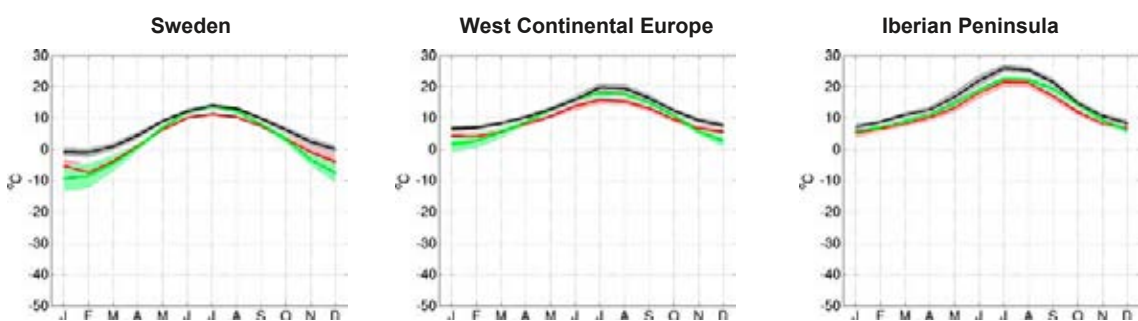


Figure 3-7. Annual cycle of temperature for the WARM-r-veg (black) and RP-r (red) simulations. Also shown is the CRU observational data from 1961–1990 (green). Shaded areas in corresponding colours indicate the ± 1 standard deviation calculated for the range of individual monthly averages in the three data sets.

the changes in winter precipitation, but with slightly lower amplitudes (Figure 3-9, lower right). The precipitation change in summer is small with mostly decreased precipitation except for the North Atlantic and northern Fennoscandia that receive more precipitation in this scenario (Figure 3-9, lower left). Changes in precipitation are not influenced by the change in vegetation in any systematic way and the differences between the two simulations (WARM-r-veg and WARM-r) that do occur are everywhere small (not shown).

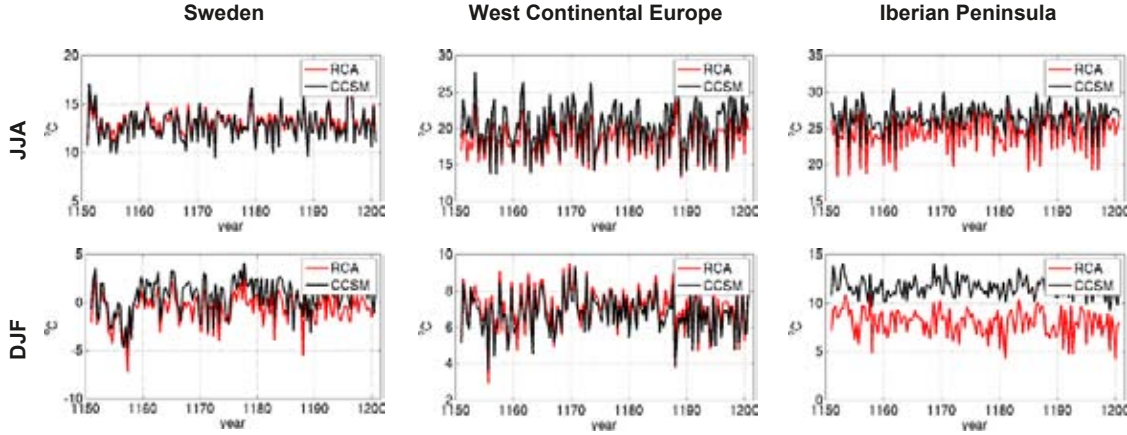


Figure 3-8. Summer (JJA) and winter (DJF) temperatures for the warm case in RCA3 (WARM-r-veg, red) and CCSM3 (WARM, black). Units are °C.

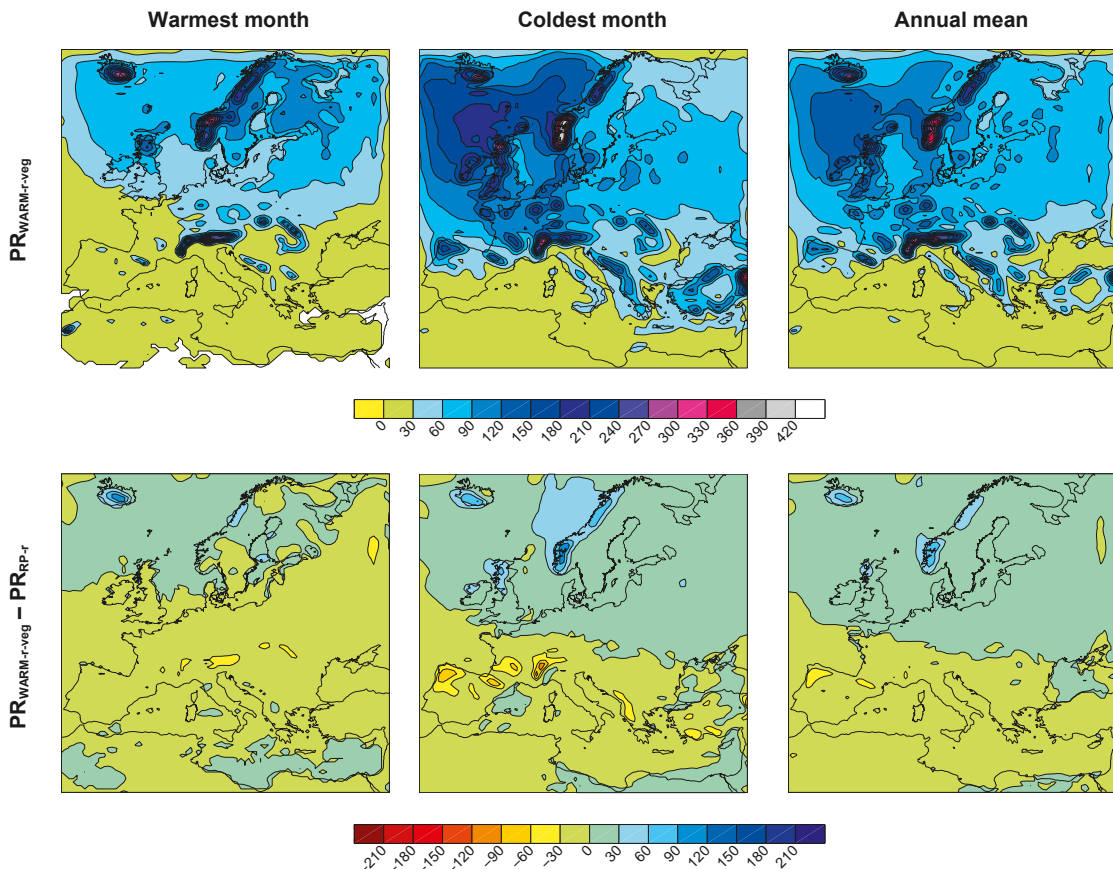


Figure 3-9. Mean precipitation of the warmest month, coldest month and annual mean in the WARM-r-veg simulation. Also shown are differences between WARM-r-veg and the simulation of the recent past climate (RP-r). Units are mm/month.

Common to Sweden and the Iberian Peninsula, the above-mentioned changes in winter and summer precipitation lead to a weaker seasonal cycle (Figure 3-10). On an annual basis, however, there are clear differences between the north becoming wetter and the south becoming drier. However, compared with the simulation of the recent past climate the changes are small, as exemplified for west continental Europe in Figure 3-10.

Winter precipitation is around 20% higher in RCA3 (WARM-r-veg) in Sweden and west continental Europe compared with CCSM3 (WARM). In the rest of Europe, the models give approximately the same amounts (Figure 3-11). In summer, RCA3 gives almost twice as much precipitation in Sweden as CCSM3 and half as much as CCSM3 on the Iberian Peninsula. The higher precipitation over Sweden in the regional model compared to the corresponding global model is seen also in other simulations /Kjellström and Lind 2009/. They noted that some of the discrepancies between RCA3 and the global models are related to the higher resolution and better representation of land-sea contrasts and topography in the Baltic Sea runoff area. In central and eastern Europe, RCA3 and CCSM3 give about the same amounts of precipitation. As for temperature, the temporal correlation of precipitation between the models is high (>0.8) during winter. In summer the correlation is lower, a result of the weaker westerlies during that season implying that the regional model is freer to develop its own climate within the interior of its domain. This is a feature typically seen also for today's climate.

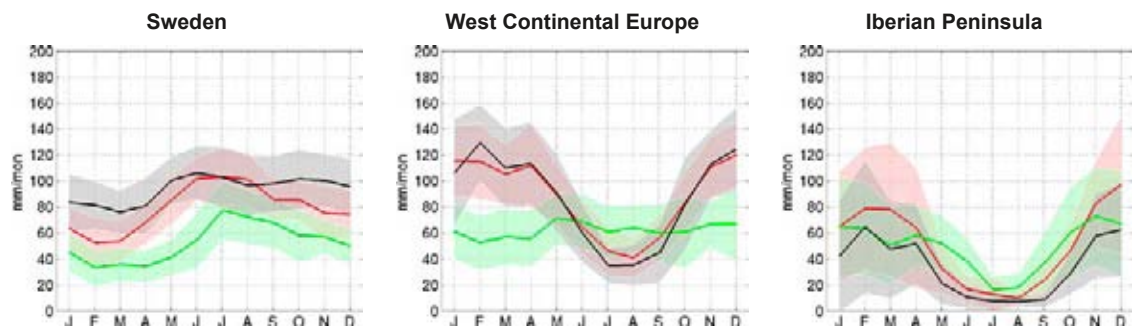


Figure 3-10. Annual cycle of precipitation for the RCA3 simulations WARM-r-veg (black) and the RP-r (red). Also shown is the CRU observational estimate for the time period 1961–1990 (green). Shaded areas in corresponding colours indicate the ± 1 standard deviation range of individual monthly averages in the three data sets.

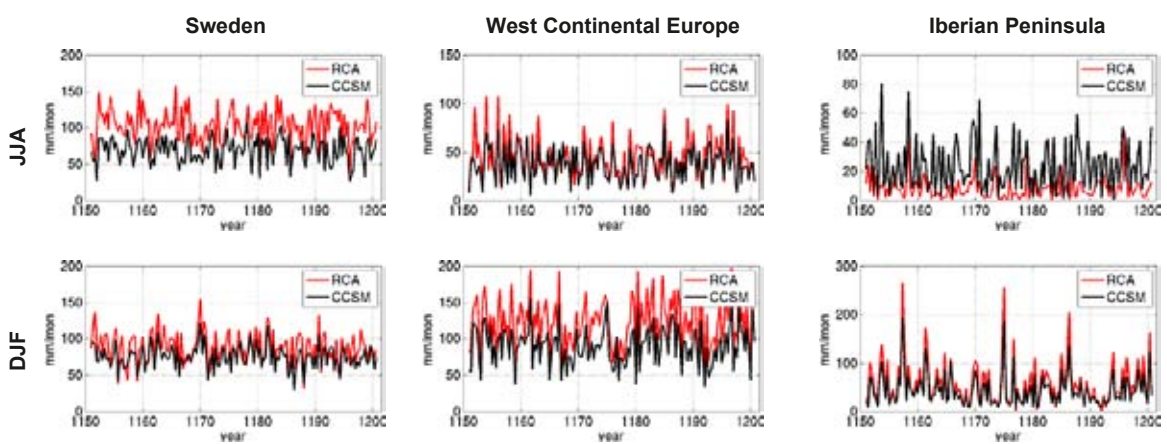


Figure 3-11. Summer (JJA) and Winter (DJF) precipitation for the warm case in RCA3 (WARM-r-veg, red) and CCSM3 (WARM, black). Units are mm/month.

Mean sea level pressure

The changes in the pattern of mean sea level pressure presented here are inherited from the global model and can be compared with the strengthened gradient in Z300 as shown in Figure 3-5. The pressure patterns are similar to the late 20th century, but with a more pronounced westerly flow over the North Atlantic and Fennoscandia in winter and in the north-western parts of the domain also in summer (Figure 3-12). In winter, the average north-south pressure gradient over the North Atlantic (measured from Portugal to Iceland) increases from around 30 in RP-r to almost 38 hPa in WARM-r-veg. The pressure gradient between these regions varies, which is known as the North Atlantic Oscillation (NAO).

Here, we present a time series of a normalised NAO-index /Hurrell 1995/ to illustrate the inter-annual variability of the westerlies (Figure 3-12, lower left). There is a strong connection between the NAO-index and the temperature climate of parts of Europe in winter. In Sweden, there is a statistically significant positive correlation coefficient (0.43) for the winter implying that a high-index situation with strong westerlies leads to a mild winter. Statistically significant here means that the correlation coefficient is above 0.28 which is the limit given by a two-sided Student t-test for a sample size of 50. At the same time there is a negative correlation coefficient for the Iberian Peninsula in both temperature (-0.37) and precipitation (-0.63) implying that strong westerlies over the Atlantic leads to a relatively cold and dry winter in that region. All the correlation coefficients are lower than in the corresponding simulation of the recent past. As in the RP-r simulation, there is a relatively large inter-annual variability with both high- and low-index years. In the WARM-r-veg simulation there is a slight shift towards lower absolute values of the normalised index at both ends of the distribution (i.e. high- and low-index years). This indicates that the inter-annual variability in the strength of the wintertime westerlies tends to be slightly weaker compared with that in the late 20th century.

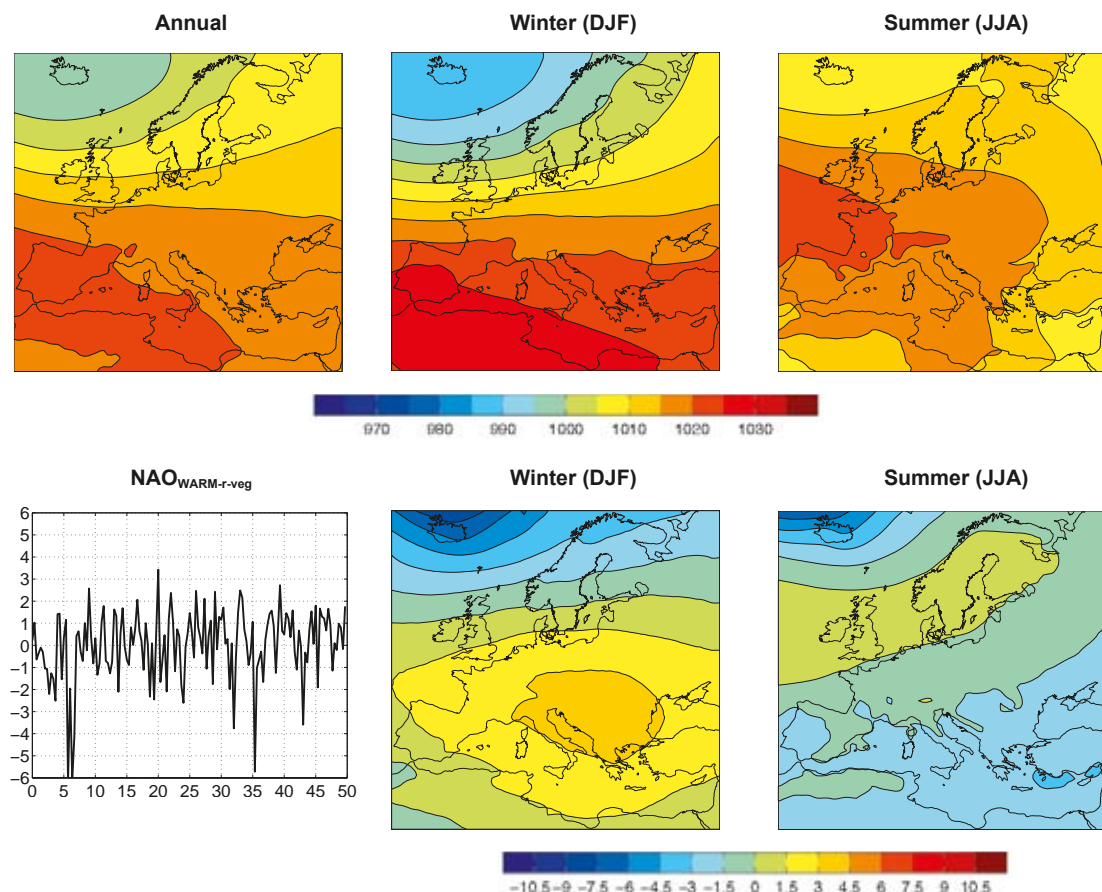


Figure 3-12. Annual and seasonal mean MSLP (top panels). Lower panels show winter (DJF) normalised NAO index in WARM-r-veg (left) and MSLP anomalies for WARM-r-veg compared with the simulation of the recent past climate (right), units are hPa.

3.1.3 Regional vegetation model simulations

For the *warm case*, the vegetation model shows a dominance of winter deciduous and evergreen broadleaved trees over central and western Europe (Figure 3-13). Boreal needle-leaved forests shift northward relative to their extant distribution due to warm winters that prohibit regeneration in southern parts of the actual range /Sykes and Prentice 1995/, while dry summers with enhanced evapo-transpiration relative to recent past conditions limit tree growth in Mediterranean areas. Simulated vegetation biomass, leaf area index and net primary productivity were not used to force RCA3 in the WARM-r-veg simulation, but are shown as a reference in Figure 3-14.

The vegetation cover over Europe and northern Africa simulated by LPJ-GUESS for the *warm case* shows little resemblance to the vegetation map (Figure 2-11, upper panel) for the same region assumed in the *warm case* simulation by CCSM3. In the latter case, the vegetation over most of central and eastern Europe appears to comprise mainly grasses, C₃ grasses in the Fennoscandian north, and C₄ grasses in central, southern and eastern Europe. Forest cover is restricted to a narrow band of boreal needle-leaved trees, approximately in southern Fennoscandia, and a few pixels dominated by temperate needle-leaved trees further south. The explanation for this apparently quite unrepresentative vegetation map presumably lies in the weighting applied to agricultural areas, which in Europe consist largely of C₃ (wheat, rye, barley) and C₄ (maize) cereals and which, at the grid resolution of the GCM, apparently cover a larger proportion of the landscape than forests in most parts of Europe. Conifer forests that are characterized by the boreal species Norway spruce (*Picea abies* (L.) Karst) and Scots pine (*Pinus sylvestris* L.) nevertheless dominate extensive parts of Scandinavia and north-east Europe, and it is striking that these are largely missed by the vegetation map adopted by CCSM3.

A comparison of the /Scholze et al. 2006/ vegetation map used in the WARM-v simulation with CCSM (Figure 2-11, lower panel) with that generated by LPJ-GUESS and shown in Figure 3-13 does show some similar spatial patterns, including a corresponding boundary between needle-leaved and broadleaved forest striking NW-SE through northern Europe, and forests petering out into grassland in southern Europe/northern Africa. As the Scholze et al. vegetation map was generated by a version of the LPJ vegetation model, a global-scale relative of LPJ-GUESS /Smith et al. 2001/, the existence of some agreement in the vegetation maps is to be expected.

In comparison with the present-day land cover map used to prescribe land surface physiography for the future in the WARM-r simulation with RCA3, the LPJ-GUESS-generated vegetation represents more extensive forest cover over present-day cropland areas, and a more north-easterly boundary between temperate broadleaved and boreal needle-leaved forest, as outlined above.

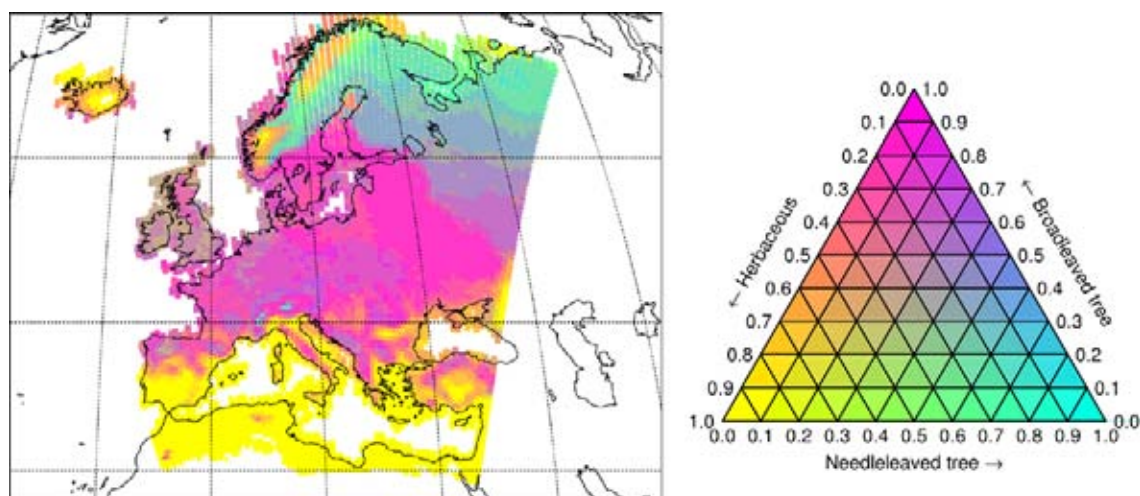


Figure 3-13. Vegetation map resulting from the LPJ-GUESS simulation forced by the initial RCA3 climate for the warm case (WARM-r).

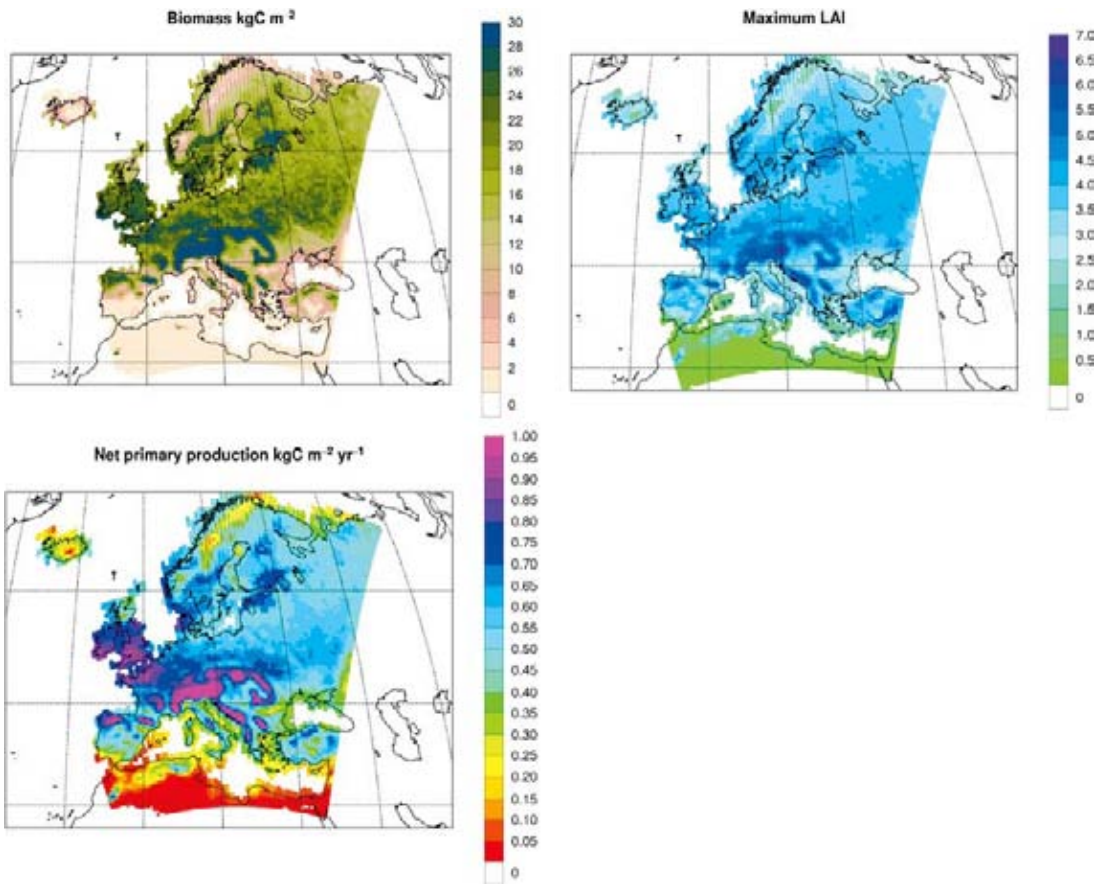


Figure 3-14. Vegetation biomass (kgC m^{-2}), maximal growing season leaf area index (LAI; projective foliar area/ground area) and net primary productivity (NPP, $\text{kgC m}^{-2} \text{yr}^{-1}$) as simulated by LPJ-GUESS forced by the initial RCA3 climate for the warm case (WARM-r).

3.1.4 Synthesis of the warm case

Comparison to other model simulations

As expected, the simulated climate of the *warm case* clearly resembles many of the scenarios for the 21st century from the climate model intercomparison project (CMIP3) as presented by the Intergovernmental Panel on Climate Change /Meehl et al. 2007/. Seasonal mean changes in precipitation and temperature from a large number of the CMIP3 scenarios have been analysed for Sweden by /Lind and Kjellström 2008/. They report increased temperatures of 4–6°C by the end of the 21st century in northern Sweden and about 3°C in southern Sweden relative to the 1961–1990 period. The corresponding increases in precipitation are about 25% in the north and only a small average increase in the south albeit with a large spread between the models. These changes are annual averages over a range of different emission scenarios. As noted in Section 2.3.2, the uncertainties related to the future forcing in our *warm case* are large and we can not rule out either substantially lower or higher greenhouse-gas concentrations than the one we have used. Considering the large spread between the emission scenarios and the uncertainty related to the climate models we can not rule out that a future warmer climate can be warmer than the one simulated here. However, the high-end emission scenarios (A1FI and A2) /Nakićenović and Swart 2000/ may have CO₂ concentrations that are too high to be sustained over the long period that it takes to melt the Greenland ice sheet, which was a requisite here (Section 2.1). But, even so, the CO₂ concentrations may very well reach levels high enough to sustain long-term (i.e. multi-century) temperature anomalies exceeding those simulated here.

Part of the uncertainty is related to the emission scenario but another part is dependent on the model formulation. Given identical forcing, different models will simulate different responses. The fact that the responses are different in different models depends not only on the climate sensitivity of

the models (i.e. change in global mean temperature as a result of a change in radiative forcing) but also on how the models simulate regional aspects of the climate in different seasons. As an example of different responses, changes in monthly mean temperature and precipitation as simulated for the southern half of Sweden in a number of the CMIP3 Atmosphere-Ocean General Circulation Models (AOGCMs) are shown in Figure 3-15. In this case, the AOGCMs have been forced by the A1B emission scenario /Nakićenović and Swart 2000/ which close to the end of the 21st century has a greenhouse-gas forcing of about the same level that we used for our *warm case* simulations (Table 2-1). Although there is a very large spread between the different models, some general features are common to most of them. These include a weakening of the seasonal cycle in temperature and increased precipitation during winter. Many models also show decreased precipitation over the southern half of Sweden during summer, but this is not general to all of them.

Clearly, our WARM and WARM-v case simulations fall within the range of climate change signals given by this set of global models. Consequently, also the regional climate model gives a climate change signal that is within the range defined by the global models in Figure 3-15. The climate change signal for Sweden is +4°C in winter and +3.5°C in summer in the WARM-r-veg simulation and the corresponding numbers for precipitation are +37% in winter and no change ($\pm 0\%$) in summer. A similar climate change signal in a RCM and the forcing AOGCM has previously been shown for the 21st century for various areas in Europe /e.g. Déqué et al. 2005/, the Baltic Sea runoff region /Graham et al. 2008/ and Sweden /Lind and Kjellström 2008/. We recall here that the climate sensitivity of CCSM3 is 2.7°C for an equilibrium response and 1.5°C for a transient response. This sensitivity is lower than average but still in the range of the climate sensitivities of the CMIP3 AOGCMs (2.1–4.4°C and 1.3–2.6°C respectively). Another model with higher climate sensitivity may therefore have a stronger response than CCSM3 in this area. Given the ranges in temperature and precipitation changes in Figure 3-15, a regional response in a high-sensitivity model twice that simulated by CCSM3 does not seem unlikely for the Fennoscandian region. In Chapter 4 we give some examples from other climate change simulations with RCA3 for a few locations in Sweden and Finland.

Our WARM and WARM-v simulations differ from the CMIP3 simulations since we have removed the Greenland ice sheet. Another difference is that the CMIP3 simulations are not in any kind of quasi-equilibrium as they show transient response to changes in external forcing. A comparison of our WARM simulation and the CCSM3 CMIP3 simulations for the end of the 21st century under different emission scenarios shows large differences in seasonal mean temperatures over Greenland and parts of the high Arctic. At lower latitudes, including Fennoscandia, regional differences between the simulations are in general less than 2–4°C (not shown). Based on these relatively small differences and the fact that our simulated climate in Fennoscandia falls within the range of climate change signals given by the CMIP3 set, we conclude that the topography of Greenland is of secondary importance for the future climate in Fennoscandia as compared with other factors generating the variation seen in Figure 3-15.

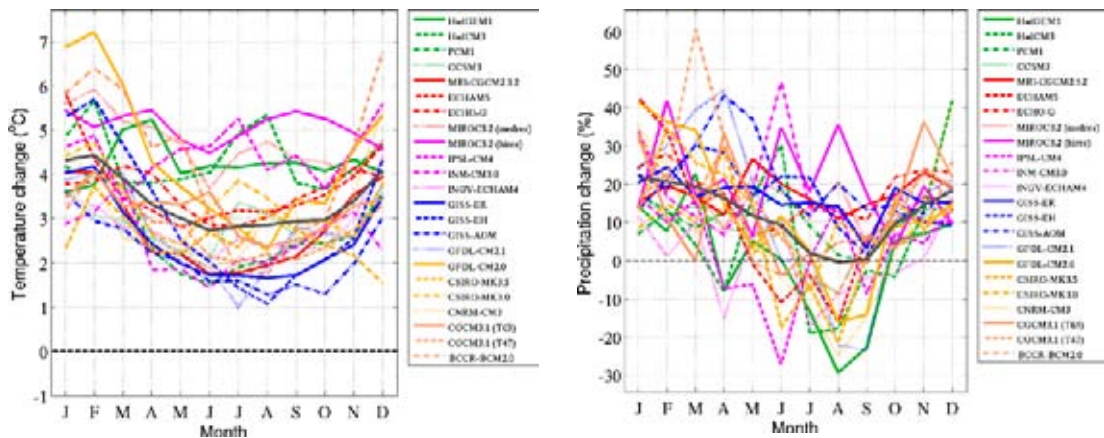


Figure 3-15. Simulated climate-change signal in the southern half of Sweden in 24 AOGCMs in CMIP3, from /Lind and Kjellström 2008/. All models are forced by the A1B emission scenario /Nakićenović and Swart 2000/. Differences are shown for the period 2071–2100 compared with 1961–1990. The grey line is the multi-model mean. For details see /Lind and Kjellström 2008/.

It is also worth noting that the lowering of the annual mean Atlantic Meridional Overturning Circulation (AMOC) in the WARM and WARM-v simulations, by 6 and 22% compared with the recent past climate respectively, are not large enough to cause regional cooling over Fennoscandia. This is in general agreement with the AOGCM simulations of the 21st century as presented by /Meehl et al. 2007/. They show that the AOGCMs project a decreased intensity of the AMOC in the 21st century in the range from 0 to 50%. As in our simulations, none of these AOGCM simulations indicates a cooling over Fennoscandia.

Finally we note that the Greenland summer temperatures are well above 0°C, clearly indicating that there is no chance of ice sheet regeneration under these circumstances once the ice has been removed. A similar result was obtained previously for the pre-industrial climate when the Greenland ice sheet was removed in the Hadley Centre HadCM3 coupled model /Tonietto et al. 2004/. The climate in Greenland in the present WARM-v case resembles that in Alaska, as simulated for the recent past climate (cf. Figures 2-2 and 3-3).

Implications of the sensitivity studies

Differences between our WARM and WARM-v simulations are largest in regions where the vegetation cover has changed. For the Fennoscandian region the WARM-v simulation is colder by up to 2°C. As this difference is also seen over the Nordic Seas we believe that the difference is not caused by terrestrial changes in the area but instead a result of large-scale changes in atmospheric circulation. We also note that these differences between WARM and WARM-v in the Fennoscandian region are relatively small when compared with the spread between different AOGCMs and emission scenarios. Taken together this indicates that the role of vegetation is not the dominating source of uncertainty in this area.

3.2 The glacial case

3.2.1 Global climate model simulations

Stability of the simulated global climate

The LGM simulation is a continuation of a LGM simulation performed at NCAR, USA /Otto-Bliesner et al. 2006a/. The simulation was originally initiated from a simulation of pre-industrial climate, except for the ocean which was initiated by adding three-dimensional anomalies of ocean temperature and salinity derived from a LGM simulation with the Climate System Model version 1.4 (CSM1.4) /Shin et al. 2003/ to the CCSM3 pre-industrial simulation. The simulation was first run for 400 years at NCAR, and was then continued for another 856 years within the present study. The annual global mean surface temperature (T_{agm}), displayed in Figure 3-16 (grey line), reaches a quasi-equilibrium after 100–150 years, then it continues to cool and reaches a new quasi-equilibrium after a total of 750–800 years. This second quasi-equilibrium extends until the simulation is ended at model year 1256. The mean T_{agm} is 9.0°C in the first quasi-equilibrium (years 150–300; henceforth LGM1) and 7.9°C in the second (model years 800–1256; henceforth LGM2), i.e. 4.5°C and 5.6°C colder than the simulated pre-industrial T_{agm} . The linear trend in T_{agm} over the last 100 years of the NCAR simulation is –0.36°C per century and –0.17°C per century over the last 100 years of the LGM case simulation. Thus, although the linear trend at the end of our simulation is only half of what it is at the end of NCAR's simulation, it is more than ten times the linear trend at the end of the WARM simulation. From these results, we cannot be certain that the simulated climate would not continue to undergo significant change if the simulation was to be continued. Due to the requirements in both time and computing resources, we were not able to run the LGM case simulation for another 500 years (the current simulation took nine calendar months running parallel on 32 computer processors at the National Centre for Supercomputing). We therefore analyse the simulated LGM climate in the two quasi-equilibria and compare them with the available proxy data for the LGM. /Brandefelt and Otto-Bliesner in prep./ discuss the equilibration of this simulation in more detail.

As described in Sections 2.3.2 and 2.3.6, we tested the sensitivity of the simulated climate to a change in the atmospheric mineral dust concentration and the vegetation. The vegetation was changed from present-day vegetation to vegetation simulated with a biome model forced with the

simulated LGM climate of the first quasi-equilibrium /Mahowald et al. 2006a/. This sensitivity experiment (LGM-v) was initialised after a total of 900 years simulation in the LGM simulation and was run for another 531 years. T_{agm} for this case is also displayed in Figure 3-16 (green line) and the linear trend in T_{agm} over the last 100 years of the simulation is 0.081°C per century, indicating that the simulated climate is close to quasi-equilibrium. The mean T_{agm} is 7.3°C as compared with 7.9°C in the LGM simulation with present-day vegetation.

To further test the sensitivity of the results to our assumptions, the atmospheric mineral dust concentrations were tripled as compared to the pre-industrial (PI) concentrations used in the LGM simulation. This sensitivity experiment (LGM-vd) was initialised after a total of 308 years of integration in the LGM-v simulation (utilising also the same vegetation as in LGM-v) and was run for another 452 years. T_{agm} for this case is also displayed in Figure 3-16 (blue line) and the linear trend in T_{agm} over the last 100 years of the simulation is 0.074°C per century. The mean T_{agm} is 6.5°C as compared with 7.9°C in the LGM simulation with present day vegetation and pre-industrial mineral dust concentrations and 7.3°C in LGM-v.

The sea-ice covered percentage of the Earth's surface is also shown for the LGM, LGM-v and LGM-vd simulations in Figure 3-16. The inter-centennial evolution in T_{agm} is anti-correlated to the evolution of the sea-ice cover in all three simulations. The correlation coefficient is -0.98 for the annual mean time series of sea ice fraction and T_{agm} .

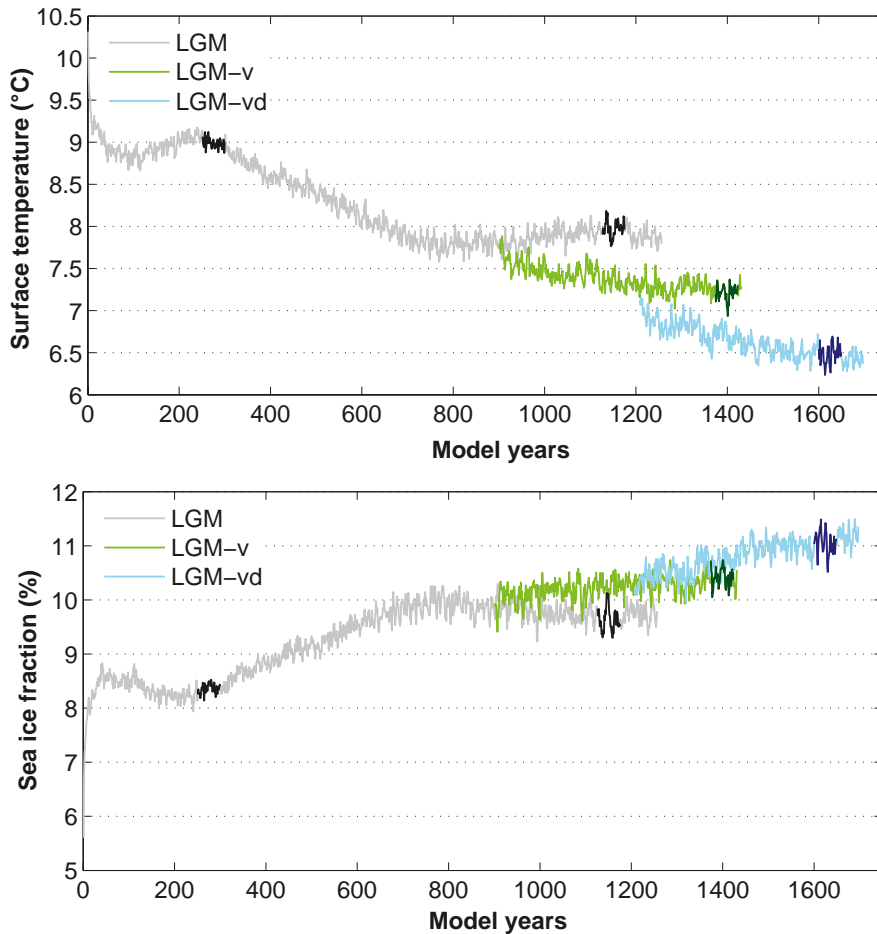


Figure 3-16. Annual global mean near-surface temperature (upper panel) and sea-ice fraction (lower panel) for the glacial case in the LGM (grey), LGM-v (green) and the LGM-vd simulation (blue). Darker parts of the curves mark the 50-year periods analysed here (in the LGM simulation the first 50-year period is referred to as LGM-1 in the text and the second as LGM-2). Units are $^{\circ}\text{C}$ and % of the surface covered by sea ice.

In the following, we discuss 50-year time series from the different simulations. The time periods are model years 250–299 for LGM1, 1125–1174 for LGM2, 1382–1431 for LGM-v and 1600–1649 for LGM-vd. These periods coincide with the periods chosen for the subsequent regional simulations (Section 3.2.2).

Temperature and sea ice

To further analyse the climate of the LGM simulation, we compared the simulated climate with that of the pre-industrial (PI) simulation described in Section 2.2.1. The annual mean surface cooling in the LGM1 simulation as compared with the PI climate is most pronounced over the Laurentide and the Fennoscandian ice sheets, with a maximum cooling of 35°C, and over high latitudes (Figure 3-17). The cooling over the ice sheets is, to a large degree, an effect of the increased surface elevation. It is also a result of the permanent snow and ice cover leading to a high albedo and also acts to suppress ground heat flux. The cooling amounts to 5–15°C north of 40°N in the Atlantic Ocean, the Arctic Ocean and over Antarctica and the Southern Ocean. The annual mean surface cooling in the LGM2 simulation as compared with that in LGM1 is most pronounced over the Greenland-Iceland-Norwegian Seas with 10–14°C cooling and north of 40°N in the Atlantic Ocean, the Arctic Ocean and the Labrador Sea with 4–8°C. The spatial patterns of the cooling from the PI simulation to LGM1 and from LGM1 to LGM2 differ substantially with atmospheric surface albedo effects dominating the PI to LGM1 cooling and sea ice – ocean circulation processes dominating the LGM1 to LGM2 cooling. The year-to-year evolution of the sea-ice covered fraction of the Earth's surface is anti-correlated to T_{agm} . This coupling can also be seen in the difference in the sea-ice extent between LGM2 and LGM1 (Figure 3-17). The sea-ice extent increases in the Southern Ocean, the Greenland-Iceland-Norwegian Seas and the north-western Atlantic Ocean from PI to LGM1. The increase in sea-ice extent in the Greenland-Iceland-Norwegian Seas and the North Atlantic Ocean is continued from LGM1 to LGM2, with the sea-ice edge at 40°N in LGM2. This extensive ice cover is accompanied by a southward shift in the sinking branch of the Atlantic Meridional Overturning Circulation (AMOC) and a decrease in the strength of the upper branch of the AMOC. Measured as the maximum of the AMOC stream function in the North Atlantic the annual mean AMOC is 21.0 Sv in the PI climate, 17.3 Sv in the LGM1 climate and 10.0 Sv in the LGM2 climate (not shown). The depth of the AMOC at 45°N is decreased from 3.8 km at PI to 2.3 km at LGM1 and 2.0 km at LGM2. The AMOC is not significantly changed in LGM-v and LGM-vd as compared with LGM2.

The salinity stratification is increased from the PI simulation to the LGM1 simulation, and further the in LGM2, LGM-v and LGM-vd simulations (not shown). The salinity is increased preferentially in high-latitude regions and the deep and bottom water, with the most saline water found on the Antarctic shelf and at the bottom of the Arctic Ocean, suggesting enhanced brine rejection from increased sea-ice formation. Brine rejection during sea-ice formation, which is more vigorous and extensive in the LGM simulation, greatly enhances the salinity of the bottom waters in these basins. This change is accompanied by a decrease in the ocean water temperature which is relatively uniform with depth.

Comparison with proxy data

Simulated SSTs were compared with proxy data for annual mean conditions for the LGM1 quasi-equilibria (Figure 3-18). The simulated SST is colder than the proxy data indicate in the North Atlantic and the North Pacific, implying that the sea ice extent is too far south in the simulation. The simulated tropical and subtropical SST is in good agreement with proxy data (i.e. within $\pm 3^{\circ}\text{C}$) at most locations. An exception is the low temperatures indicated by some proxy data off the western coasts of South America and Africa south of the Gulf of Guinea (coupled to the upwelling of colder water) which is not captured by the model. The explanation for this discrepancy is likely to be found in the coarse resolution of the ocean model.

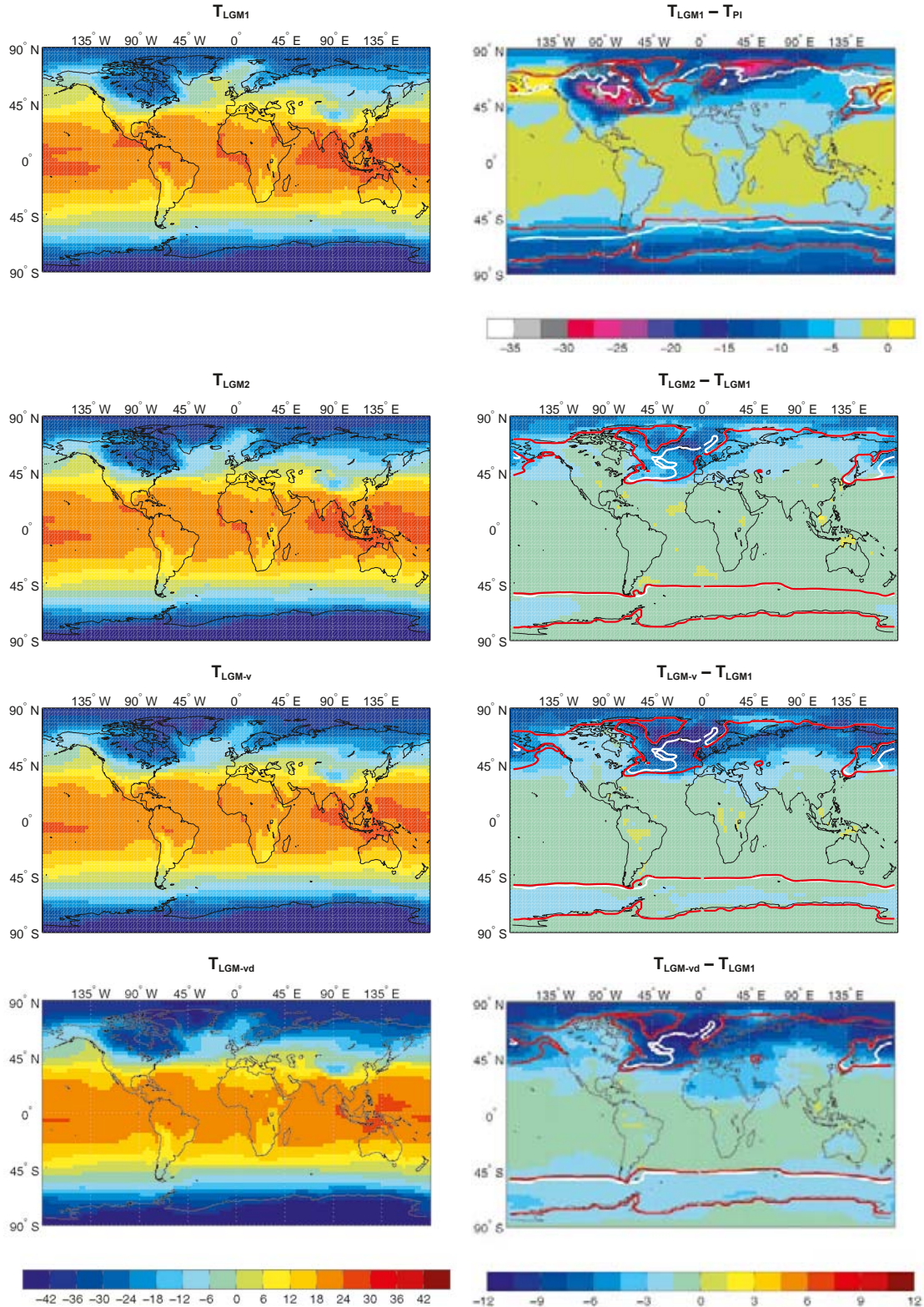


Figure 3-17. Annual mean near-surface temperature (left) in the four LGM simulations (LGMI, LGM2, LGM-v and LGM-vd). To the right are differences in the annual mean surface temperature between the LGMI and the pre-industrial simulation (T_{PI}) and between the LGM2, LGM-v and LGM-vd simulations and LGMI. Units are $^{\circ}\text{C}$. Also shown in the right panels is the annual mean sea-ice edge (defined at 10% areal sea ice cover) for the two simulations where the pre-industrial (LGMI) is denoted by the white line in the upper (lower 3 panels) and the respective other simulation is denoted with a red line.

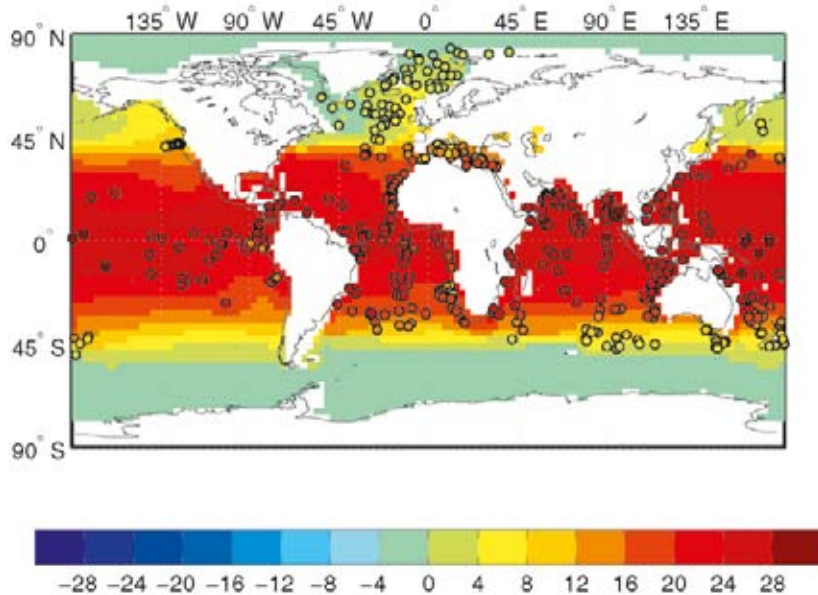


Figure 3-18. The annual mean SST in the LGM1 simulation (shaded) as compared with proxy data for SST (coloured circles). Units are °C.

These results can be compared with those from the LGM2, LGM-v and LGM-vd simulations, which are shown in comparison with annual mean, July–September and January–March proxy SST data (Section 2.4) in Figures 3-19, 3-20 and 3-21, respectively. As described earlier, T_{agm} decreases from LGM1 to LGM2, from LGM2 to LGM-v and from LGM-v to LGM-vd. This leads to increasingly larger discrepancies (up to 6°C) between the simulated SST and the proxy data in central parts of the North Atlantic which are coupled to the increased extent of sea ice. The discrepancies in the North Atlantic are largest in the LGM2-vd simulation in summer, with proxy SST above 0°C and simulated SST below 0°C. The estimated error of the proxy data is up to 3°C which could explain part of the discrepancy. However, unless the proxy errors are systematically giving too high temperatures in high northern latitudes, the errors can not explain the discrepancy between simulated and proxy SST. We therefore conclude that the simulated SSTs are too low in these regions, which is indicative of a simulated sea-ice cover that extends too far south.

We can also compare the simulated temperature climate over land areas with terrestrial proxy data on temperature obtained from pollen data. As mentioned in Section 2.4 these data can have large errors of more than ±10°C, but may still give an indication of the temperatures at the time. Figure 3-22 shows proxy data for near-surface temperature /Wu et al. 2007/ for the coldest month of the year, as compared with temperature two metres above the ground surface (T_{2m}) in the LGM2, LGM-v and LGM-vd simulations. The uncertainty in the pollen data is evident from the figure with widely differing values in nearby locations. The temperatures derived from pollen data are valid in a localized region which can explain this variation, however this also makes it difficult to compare this proxy to a global climate simulation with a resolution that is no way near capturing the local variations in topography and other surface properties that cause the local variations in near-surface temperatures captured by the proxy. The comparison indicates that the simulated LGM climate is colder than the pollen-based climate reconstruction for northern Europe and Siberia. In the case of the northern European sites, this is probably a consequence of dating problems as discussed more in detail when we compare proxy data with results from RCA3 in Section 3.2.4. For southern Europe, the reverse is true, i.e. the simulation is warmer than the pollen-based reconstruction.

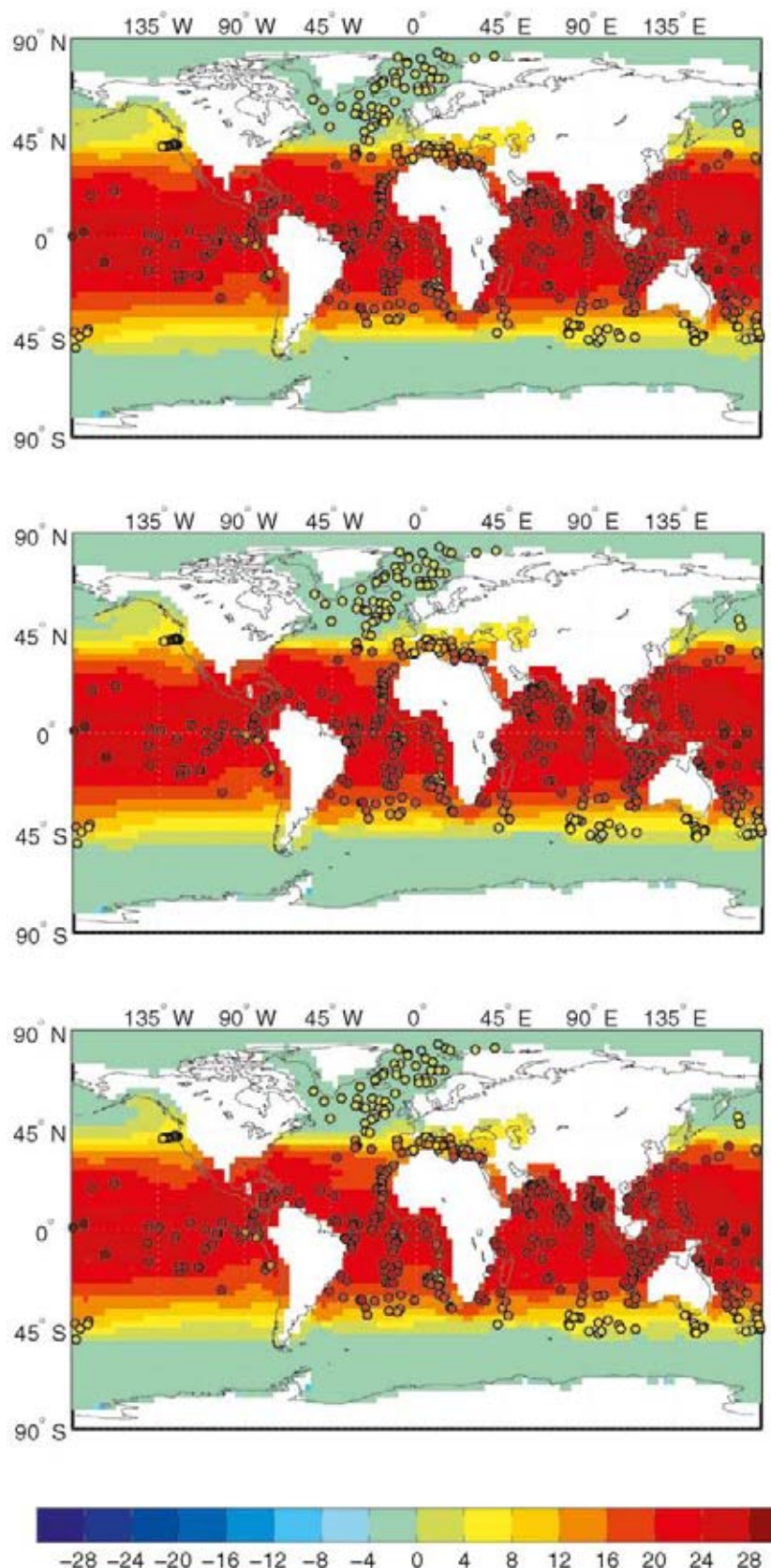


Figure 3-19. The annual mean SST in the LGM2 (upper), LGM-v (middle) and LGM-vd (lower) simulations as compared with proxy data for SST (coloured circles). Units are °C.

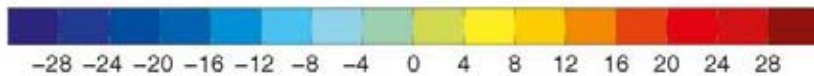
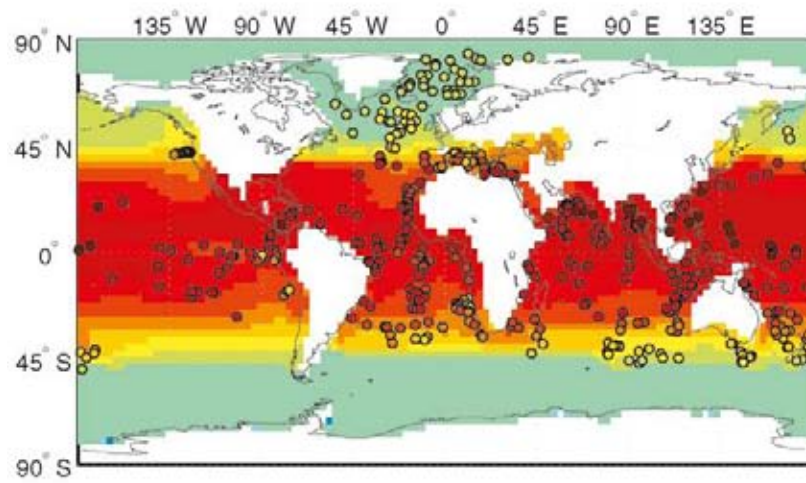
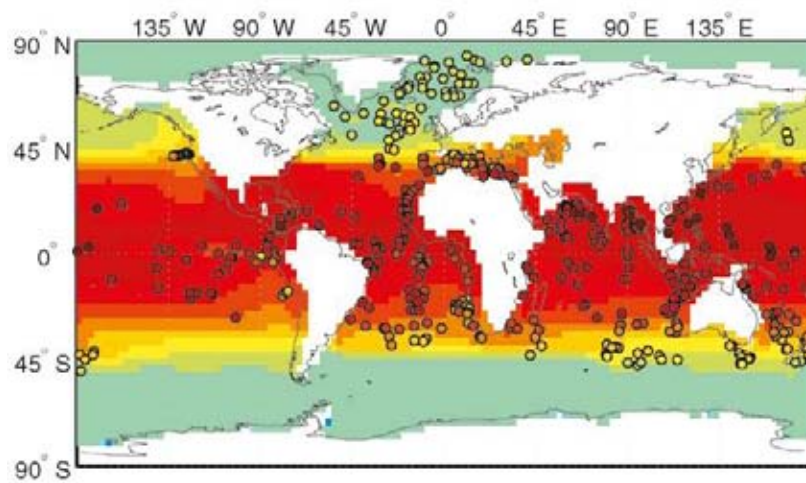
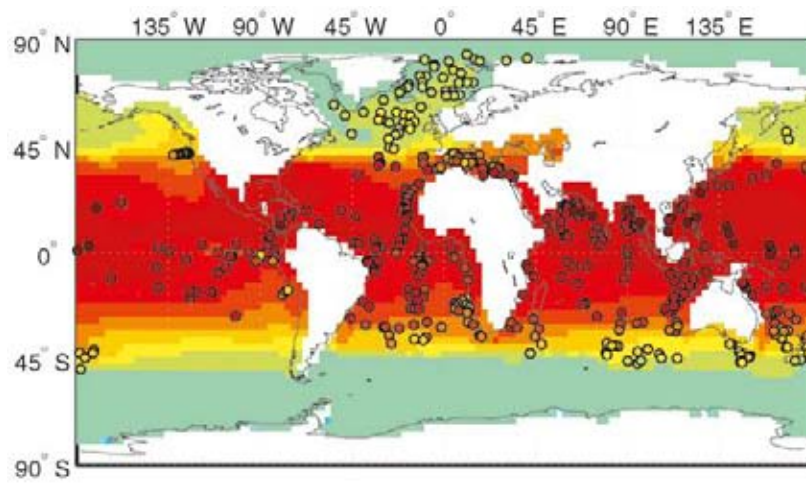


Figure 3-20. The northern hemisphere summer (July–September) mean SST in the LGM2 (upper), LGM-v (middle) and LGM-vd (lower) simulations and proxy data for SST (coloured circles). Units are °C.

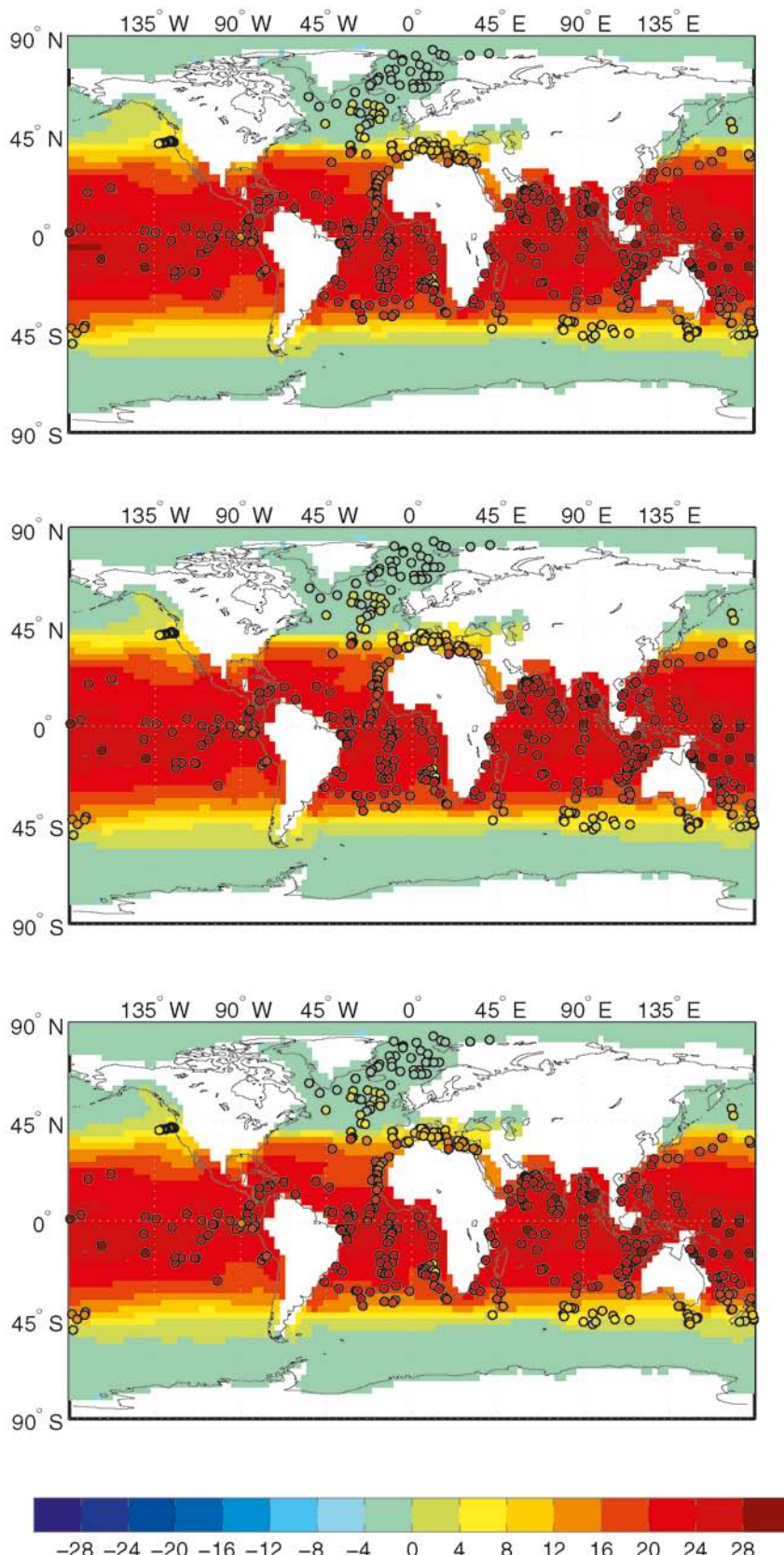


Figure 3-21. The northern hemisphere winter (January–March) mean SST in the LGM2 (upper panel), LGM-v (middle panel) and LGM-vd (lower panel) simulations as compared with proxy data for SST (coloured circles). Units are °C.

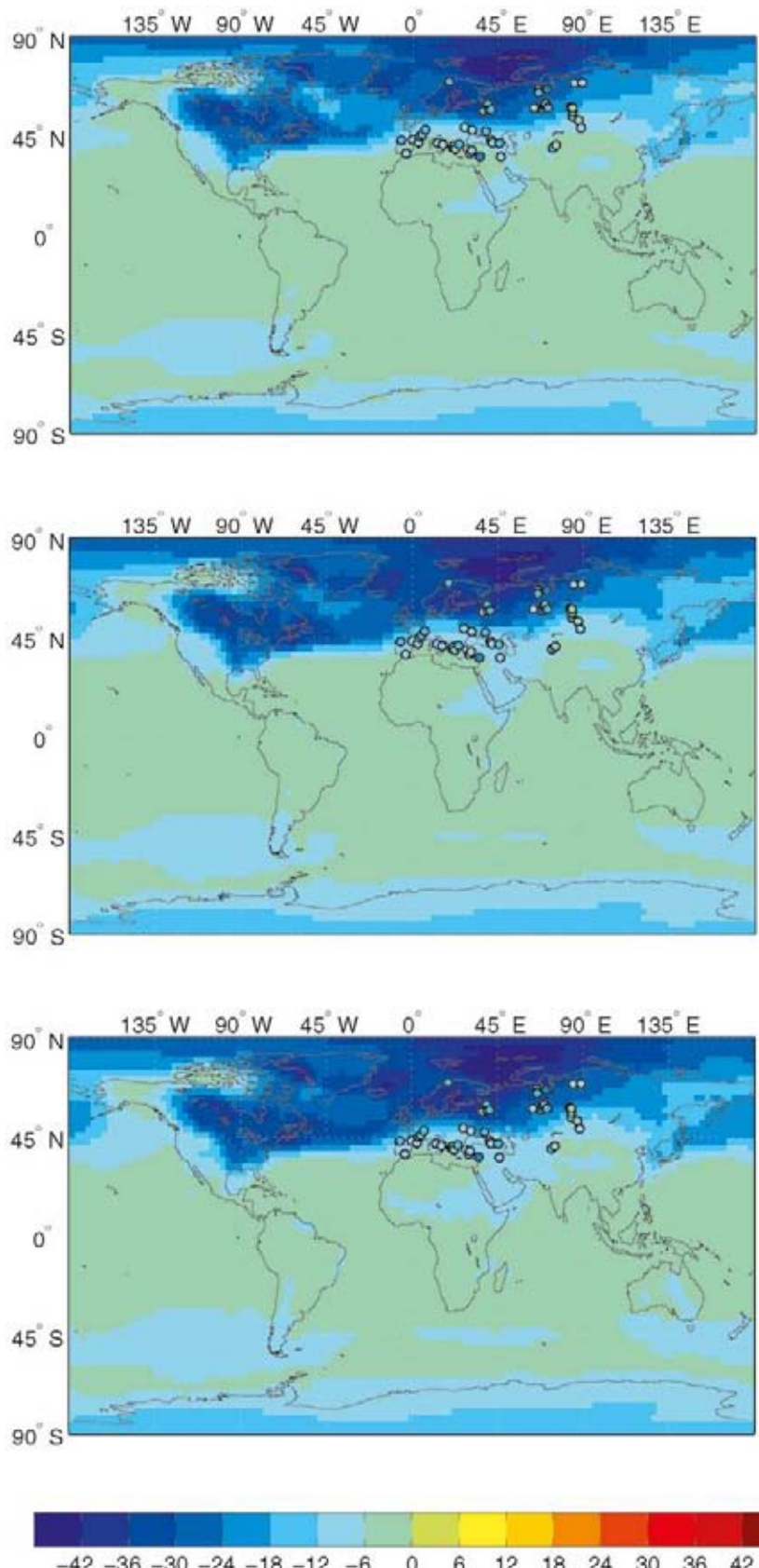


Figure 3-22. February mean near-surface temperature anomalies in the LGM2 (upper panel), LGM-v (middle panel) and LGM-vd (lower panel) simulations compared with the simulation of the pre-industrial climate (PI). Also shown are corresponding anomalies derived from proxy data for the coldest month of the year (coloured circles). Units are °C.

Atmospheric circulation

Annual mean Z300 changes from the PI simulation to the LGM1 simulation are shown in Figure 3-23. The upper-tropospheric circulation changes from the PI to the LGM1 simulation are dominated by an amplification of the topographic wave over the Rocky Mountains and the Laurentide ice sheet. This produces an increased flow of cold Arctic air towards the south west in the Labrador Sea and the North Atlantic which cools the region and helps to increase the sea-ice cover.

Annual mean Z300 changes from the LGM1 simulation to the LGM2, LGM-v and LGM-vd simulations (also shown in Figure 3-23) are not influenced by topographic changes. The changes from the LGM1 to these three cases show the same spatial pattern. Z300 is decreased over the north-eastern Laurentide ice sheet and Greenland and increased over the North Atlantic, the Arctic and large parts of the Northern Hemisphere. These changes are associated with an amplification of the upper-tropospheric waves.

Precipitation

The Atlantic storm track is shifted southwards from the pre-industrial simulation to the LGM1 simulation which results in a decrease in the high latitude precipitation and an increase in that at mid-latitudes (see Figure 3-24). The difference in the annual mean precipitation between the LGM2, LGM-v and LGM-vd and LGM1 simulations is also shown in Figure 3-24. The dominating change in all three is the decrease in precipitation in the Greenland-Iceland-Norwegian Seas that accompanies the increase in sea-ice extent in this region (Figure 3-17). These changes also influences the Fennoscandian precipitation resulting in a net decrease in northern Scandinavia and a net increase in southern Fennoscandia in the annual mean precipitation from the pre-industrial simulation to the LGM2, LGM-v and LGM-vd simulations, respectively.

Variability

The amplitude of the variability in T_{agm} (Figure 3-16) is increased from the LGM1 simulation to LGM2, LGM-v and LGM-vd. The standard deviation of the inter-annual variability is 0.07°C in the LGM1 simulation as compared with 0.1°C in the LGM2 simulation. The corresponding value for the recent past climate is 0.07°C and for the pre-industrial (PI) climate is 0.08°C, showing that the inter-annual variability is higher in the sensitivity experiments LGM2, LGM-v and LGM-vd. To investigate how this variability in the global mean is connected to variability in the atmospheric and oceanic dynamics we looked at a 100 year time period from each simulation (including the 50 year periods used for the discussion above). For this period, we determined the correlation of the time series of T_{agm} with the time series of another variable e.g. surface temperature at each grid point. This gives us a field of correlation coefficients indicating regions that are positively and negatively correlated to the variations in T_{agm} . Using a two-sided Student's t-test with 25 degrees of freedom, we find that correlation coefficients of above (below) 0.4 (-0.4) are statistically significant at the 95% level. The number of degrees of freedom is classically obtained, for time series, by dividing the number of samples by the decorrelation time, i.e. the lag for which the auto-correlation drops below 1 over e. Note, however that the amount of variability explained by the correlation is given by the square of the correlation coefficient, e.g. a correlation coefficient of 0.5 explains not more than 25% of the variability.

The correlation analysis shows that much of the variation in T_{agm} in the LGM2 simulation is associated with variations in temperature, sea ice, precipitation and atmospheric circulation in the North Atlantic and North Pacific regions (Figure 3-25, top). The variability in T_{agm} in the LGM2 simulation is positively correlated with T_s and negatively correlated to sea-ice fraction over the North Atlantic and North Pacific regions (Figure 3-25). Furthermore, the precipitation rate is positively correlated to T_{agm} in the North Atlantic region (also shown in Figure 3-25). The correlation with the MSLP is positive over Greenland and negative over Iceland, indicating a strengthening of the Icelandic low pressure and thus a strengthening of the surface winds in this region (Figure 3-25, bottom). To conclude, the variations in T_{agm} in the LGM2 simulation are primarily associated with variability in the atmosphere and ocean in the North Atlantic and North Pacific with warmer, wetter conditions when T_{agm} is above the mean. Globally warm years are also associated with stronger winds and wind stress in the North Atlantic region which gives a stronger oceanic gyre circulation. Under the assumption that the salinity and temperature of the upper ocean in the subtropics is unchanged, an increased ocean gyre circulation is consistent with an increased transport of warm, saline water to the northern latitudes. Such an increased transport supports melting of sea ice and heating of northern latitudes as seen in the LGM2 simulation.

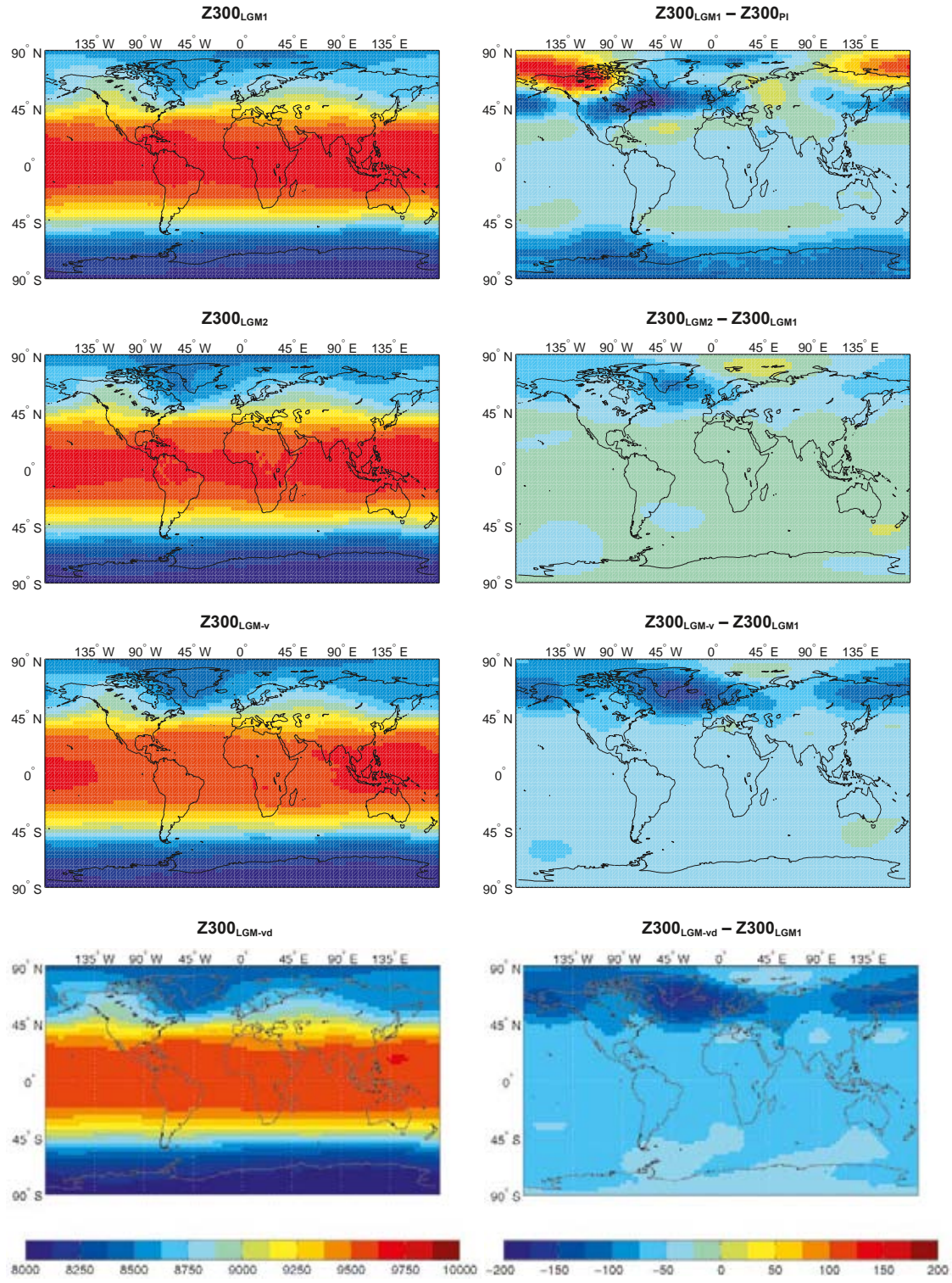


Figure 3-23. Annual mean $Z300$ in the four LGM simulations (left). To the right are differences in the annual mean $Z300$ between the $LGM1$ and the pre-industrial simulations (top) and between the $LGM2$, $LGM-v$ and $LGM-vd$ simulations and the $LGM1$ simulation (lowermost three panels). Units are geopotential metres.

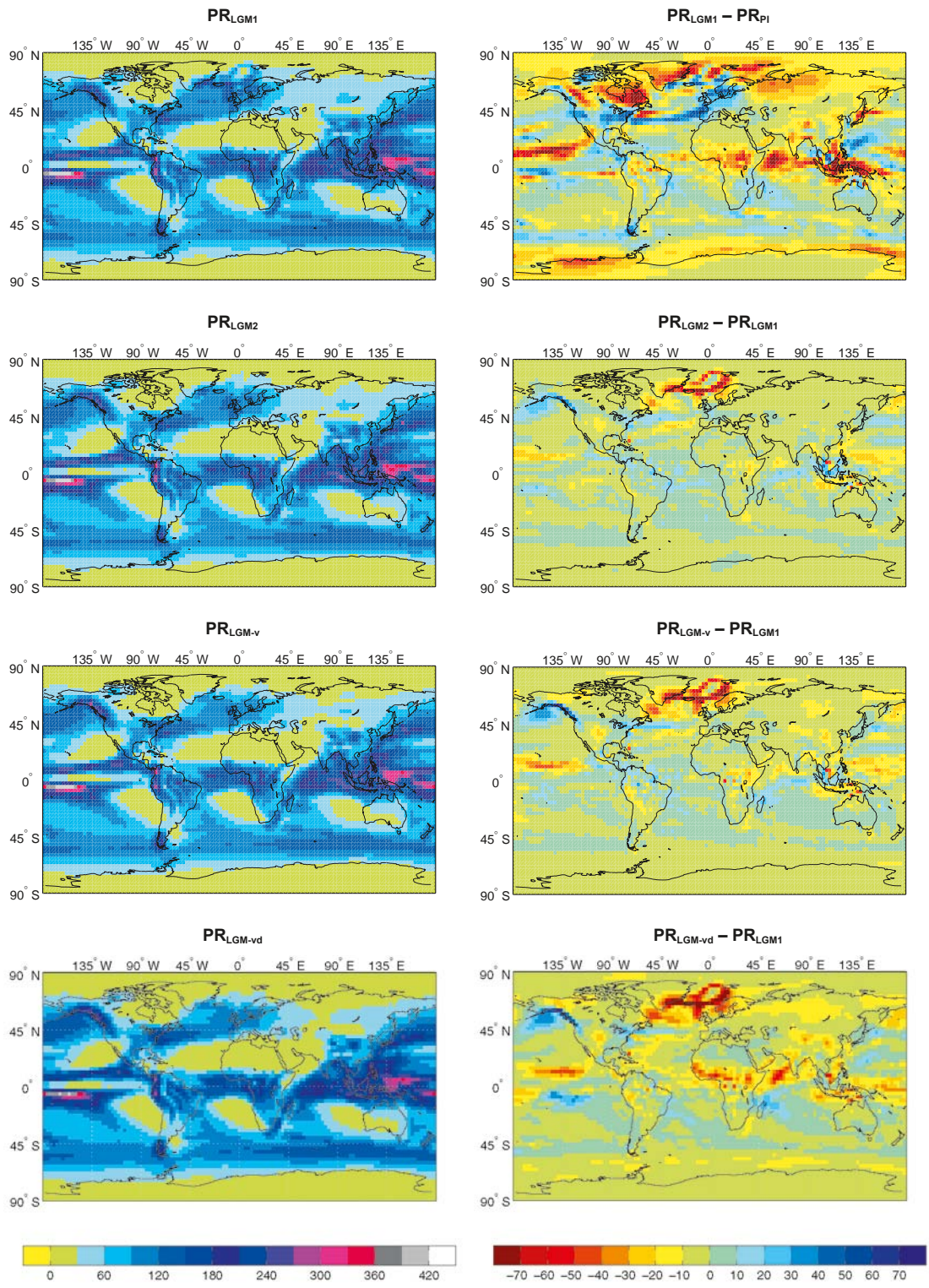


Figure 3-24. Annual mean precipitation (PR) in the four LGM simulations (left). To the right are the difference in the annual mean precipitation between the LGM1 simulation and the pre-industrial (PI) simulation (top) and between the LGM2, LGM-v and LGM-vd simulations and the LGM1 simulation (lowermost three panels). Units are mm/month.

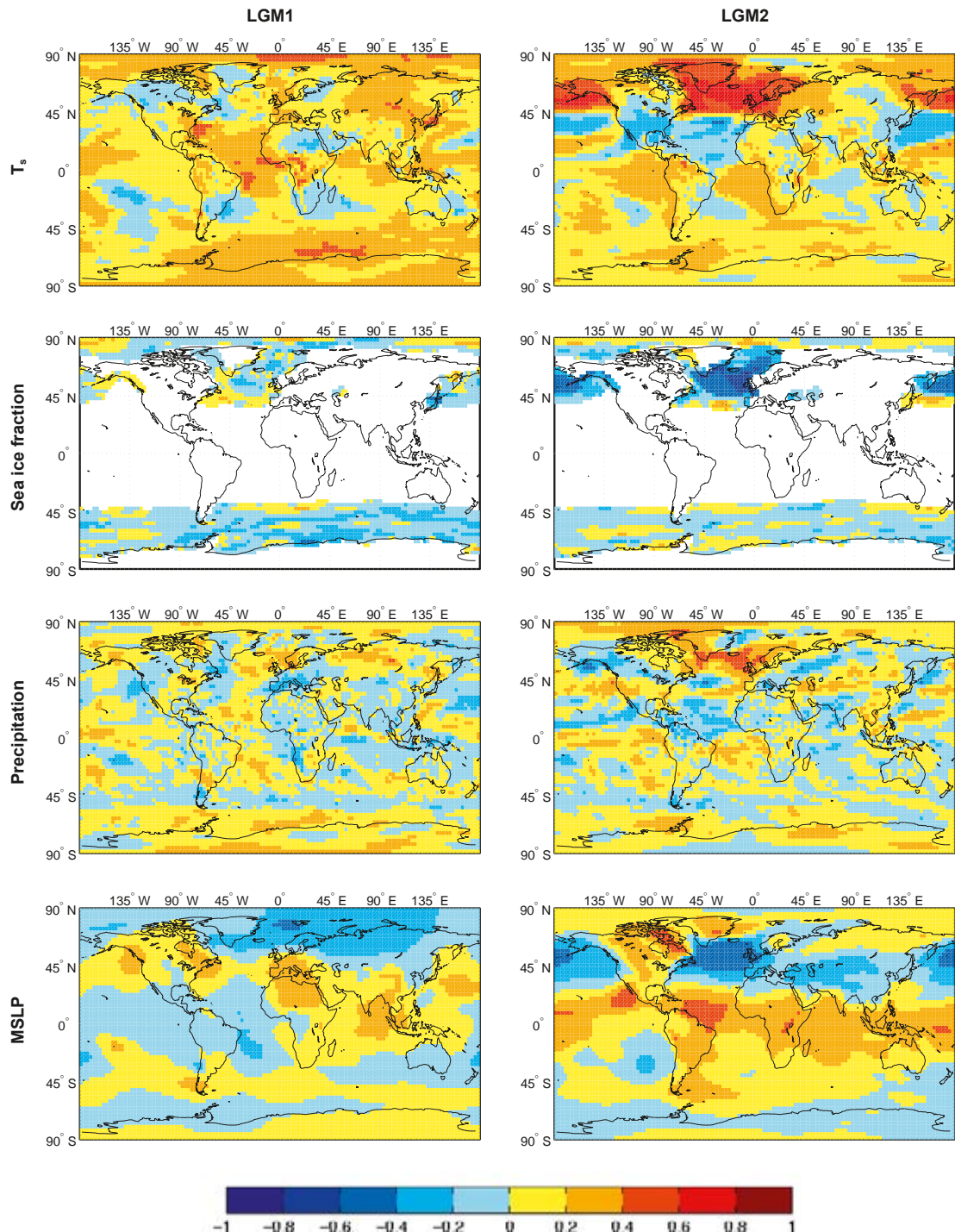


Figure 3-25. The correlation of annual global mean surface temperature (T_{agm}) with the annual mean surface temperature (T_s ; top), sea ice fraction (second row), precipitation (third row) and MSLP (bottom) in the LGM1 (left) and LGM2 (right) simulations. Correlation coefficients above (below) 0.4 (-0.4) are statistically significant at the 95% level.

Alternatively, if the sea ice extent begins to decrease, this produces a heating anomaly in the northern latitudes with a maximum in the region of the sea ice edge. It is difficult to determine if the anomalous atmospheric circulation is forcing the sea-ice anomaly or if the sea-ice anomaly is forcing the large-scale circulation anomaly. /Byrkjedal et al. 2006/ tested the sensitivity of the LGM climate to sea-ice conditions in the Nordic Seas using an atmospheric general circulation model. They found that a reduction in the sea ice in the North Atlantic gives locally increased temperature and precipitation and reduced MSLP. Further, they found that the signal from intensified thermal forcing in the North Atlantic is carried zonally in the atmosphere by upper tropospheric waves and thus generates a non-local response to the changes in sea ice. The reduction in North Atlantic sea ice in their study is greater than between globally warm and cold years in the present study and the response in temperature and precipitation is stronger, but the patterns of decreased MSLP and the changes in the upper tropospheric waves (not shown here) are similar.

Interestingly, the sea ice in the North Atlantic and North Pacific regions is not significantly correlated with the variations in T_{agm} in the LGM1 simulation. The correlation of T_{agm} and T_s for the LGM1 simulation does not clearly point out a specific region as in the LGM2 simulation (Figure 3-25). The correlation coefficient of T_{agm} and the precipitation rate and sea-ice fraction does not exceed 0.4 in any region of the globe. The correlation analysis of the LGM-vd simulation gives quite similar results to LGM2 (not shown).

3.2.2 Regional climate model simulations

In this section we discuss the downscaling of the model years 1125–1174 in the LGM simulation. RCA3 was first run to produce an initial climate (LGM2-r). This climate was then used to produce new vegetation, as outlined in Section 2.2.3 and presented below in Section 3.2.3. Finally, a repeated run (LGM2-r-veg) with RCA3 forced also by the new vegetation was completed to produce the final climate which is discussed here. We also present results from the downscaling of model years 1600–1649 in the sensitivity experiment LGM-vd. In this case, RCA3 was run just once with the same prescribed vegetation as in the global model. This simulation is denoted LGM2-r-vd.

The simulated temperature and precipitation are compared with proxy data as described in Section 2.4. Figure 3-26 shows the location of the sites used. The colours are used to group the data to facilitate interpretation of the scatter plots below. Apart from scatter plots we also show the proxy data in the maps showing results from RCA3 for all of Europe.

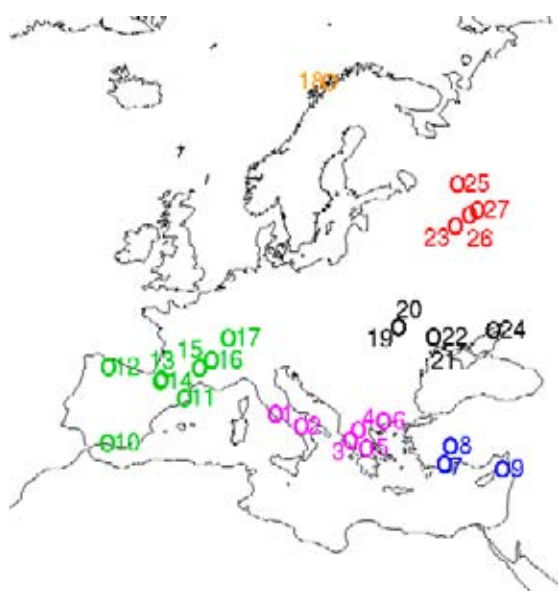


Figure 3-26. Location of the sites used in the comparison of temperature and precipitation proxies with RCA3 results for the glacial case. All sites are not used for all comparisons as all do not contain proxies of both temperature and precipitation. Note that some of the sites are located in close vicinity to each other, so that they may be difficult to discern from each other in the maps.

Temperature

The very cold climate at LGM with annual mean temperatures below 0°C in all of Europe north of about 50°N and also in high-altitude regions in southern Europe is clearly seen in Figure 3-27 (top right). In winter the situation is even more striking with the 0°C line encompassing basically all of continental Europe and monthly mean temperatures below -40°C over the northern parts of the ice sheet. During summer, the area with the lowest temperatures is more confined to the ice sheet, the extent of which is readily visible in Figure 3-27 (top left). In winter when most parts of Europe are snow covered, the gradient is less pronounced as there is no abrupt shift from snow-covered to snow-free conditions. The annual mean temperature in the LGM2-r-veg is 25–30°C lower than in the simulated recent past climate. Over the southern parts of the ice sheet (British Isles, southern Fennoscandia) the annual mean temperature is around 15°C lower than today. At the edge of the ice sheet, there is a strong gradient towards smaller temperature differences. Central Europe is around 8°C colder than today and southern Europe around 6°C colder. In winter the temperature over the Fennoscandian ice sheet is around 40°C colder than today.

The model results from regions outside the ice sheet are compared with pollen-based proxy data of temperature differences with respect to the present climate (Figures 3-27 and 3-28). The uncertainty margins of the proxy data given by /Wu et al. 2007/ are large, as indicated by the vertical bars in Figure 3-28. There exist only a few proxy records for change in annual mean temperature and all are confined to a restricted region in the southwest. Also, most of them are in close vicinity to high-altitude areas like the Alps and the Pyrenees making comparisons with the model results difficult. On the Iberian Peninsula, the simulation gives about the same temperature as one of the proxy records and colder by around 4°C compared with the other two. In the Alpine region, good agreement is seen for one of the records whereas the others are colder than indicated by the model. It should be noted that the model results are within the uncertainty ranges for all proxy records apart from one in the Alps.

For the coldest month large differences, of up to 15°C, between model and proxies are seen in many records (Figure 3-28, middle row). The poorest agreement is seen for the site in northern Norway where RCA3 is colder by some 25°C. We judge this record as not representative of the situation that we are simulating here, with an extended ice sheet in this area. According to /Wu et al. 2007/, that particular site is more representative for the conditions at 18 kyr BP, which is 3,000 years after our period. At that time, large parts of the ice sheet in this region had melted and warmer conditions prevailed /Svendsen et al. 2004/. Also, the very small response in temperature at this site and also at the northernmost one in Russia (number 25 in Figure 3-28) indicate that these may not be suitable as proxies for LGM conditions. The responses in temperature at those two points are more in the range of those in southern Europe where the model indicates a much weaker signal consistent with the absence of an ice sheet in that region. We have decided to keep these northern records in the comparisons even if there are problems with representativity. We believe that it is interesting to show this proxy as it belongs to the data set that /Wu et al. 2007/ presents as representative for LGM conditions. It is worthwhile mentioning the problems that exist with dating and what consequences it can have to use the data as they are. Also, the northernmost Russian site is another example, but maybe not as evident as the Norwegian site. Disregarding these two records there is a relatively clear regional pattern that emerges. It shows that the model tends to simulate a larger decrease in temperature than proxies indicate in the northeast (by at least 7–8°C) and that it shows a fair agreement (mostly within a few degrees) in other areas in the southern half of Europe. There are some notable local exceptions to this with proxy records showing up to 15°C larger change than the model (e.g. in Greece and Cyprus). However, the agreement is fairly good with most sites in the surrounding regions implying that these specific sites may not be representative of the larger regional scale. We also note that as the uncertainty ranges in the proxy data are very large, the model simulated temperatures are within the uncertainty estimates at all but two or three of the sites.

In the warmest month (July) the uncertainty ranges in the proxy records are much smaller than in winter. This means that the comparison between model and proxies has the potential of being more useful than in winter when uncertainties are very large. For summer, the model shows a larger decrease in temperature compared to the recent past climate than the proxies do at a majority of the locations (Figure 3-28, upper row). For most stations in the Mediterranean area, the model simulated temperatures are higher by some 2–5°C. This may be a consequence of the low SSTs in the North Atlantic as simulated by CCSM3. In eastern Europe the picture is ambiguous. At some sites, the model simulates a weaker anomaly than the proxies and in others a stronger anomaly. These differences between model and proxies are in the range of a few up to 10°C. The Norwegian site again shows a weak anomaly more in line with those in the Mediterranean area.

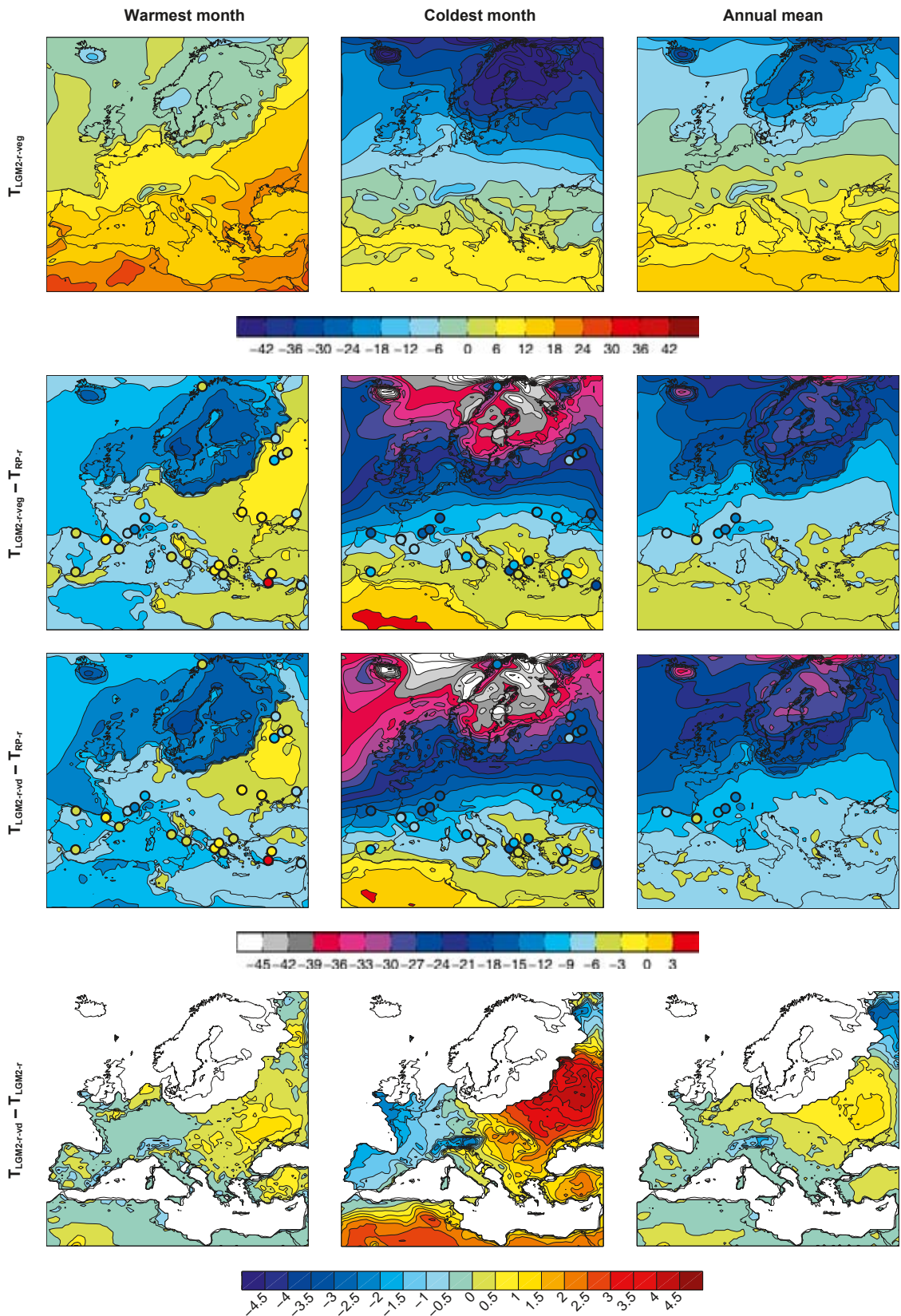


Figure 3-27. Mean temperatures of the warmest and coldest month and annual mean for the LGM2-r-veg simulation. Also shown are differences between LGM2-r-veg and the simulations of the recent past climate (RP-r), and the simulation with the initial vegetation (LGM2-r). Corresponding anomalies as given by proxy based reconstructions are denoted in the filled circles. In the lowest panels, areas without vegetation have been masked out. Units are °C.

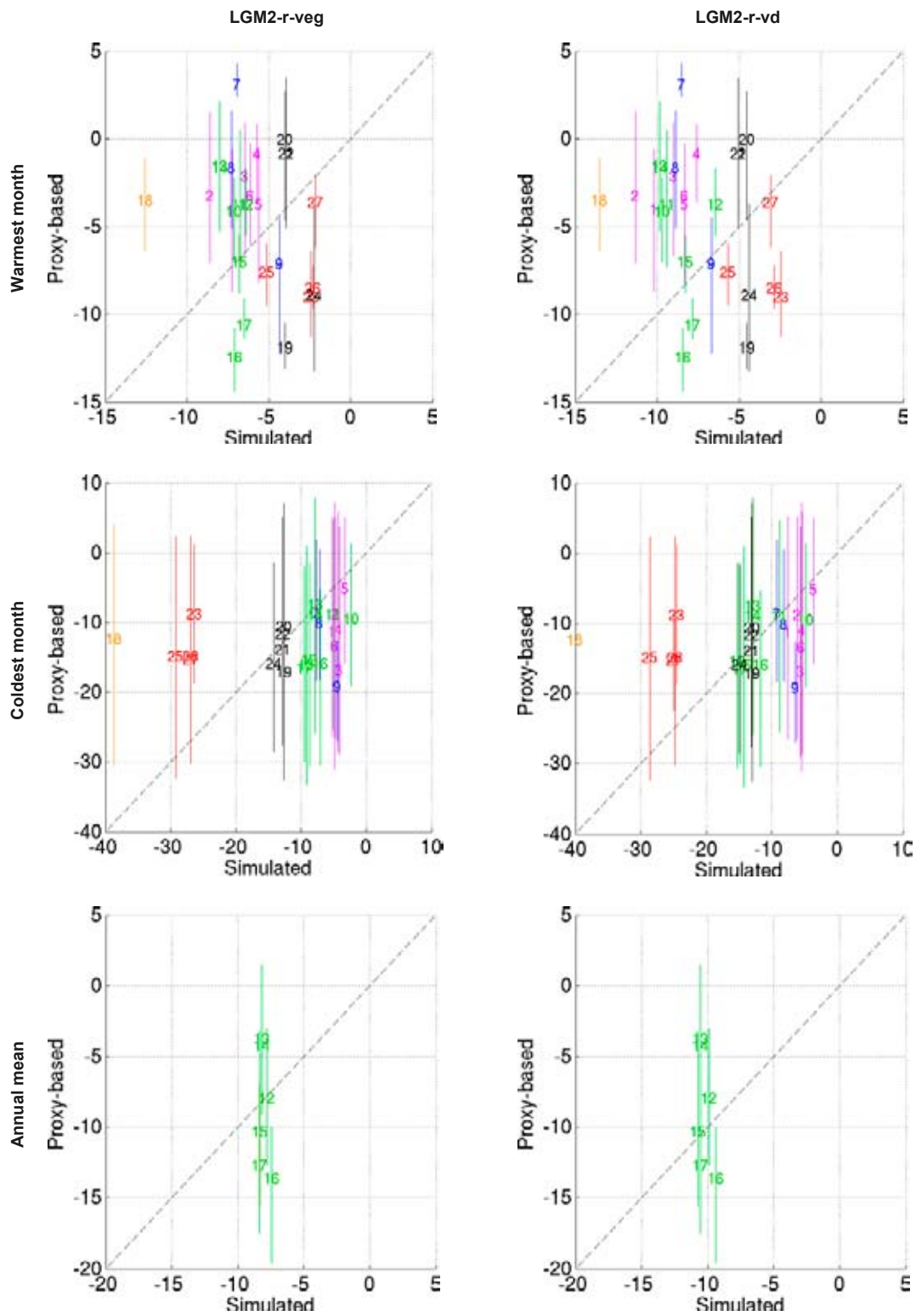


Figure 3-28. Comparison of near-surface temperature in the *LGM2-r-veg* (left) and *LGM2-r-vd* (right) simulations with proxy data for the warmest month of the year (top), the coldest month of the year (middle) and annual mean conditions (bottom). The uncertainty margins for the proxy data are denoted by the vertical lines. The numbers correspond to the specific sites in Figure 3-26. Units are °C.

Compared with the LGM2-r-veg simulation, the LGM2-r simulation (with present-day vegetation) shows only minor differences (Figure 3-27, lowermost panels). Most prominent is a slightly stronger temperature response in the LGM2-r-veg simulation in south-western Europe and slightly weaker response in the northeast. The LGM-r-vd simulation with a stronger radiative forcing from mineral dust shows larger differences compared to LGM2-r-veg. Also, the LGM-r-vd simulation shows a better agreement with proxy data for the coldest month in southern Europe than the LGM2-r-veg simulation (Figure 3-28, middle row). In summer, the stronger forcing in the LGM-r-vd experiment makes the agreement worse in the Mediterranean (Figure 3-28). On the other hand, there is a slight improved agreement on the northern side of the Alps (sites 16 and 17 in Figure 3-28).

In northern Europe, the annual temperature range is much wider than today, ranging between $-40 - 5^\circ\text{C}$ approximately (Figure 3-29). The variability in winter is also much larger with a difference between the coldest and warmest winter of around 20°C . Further south, where the difference between LGM climate and today's climate is less, the annual temperature range and variability are more like today.

The north-south temperature gradient in Europe (comparing Sweden to the Iberian Peninsula) for summer (JJA) is stronger in CCSM3 than in RCA3 (Figure 3-30). The difference is more than 5°C taken as a seasonal average. In winter the north-south temperature gradient is similar albeit with RCA3 in general a few degrees colder than CCSM3 both in the north and the south.

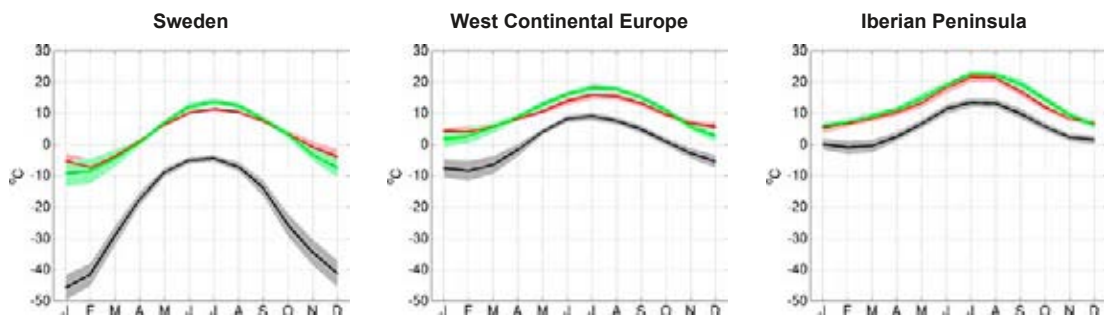


Figure 3-29. Annual temperature range in the glacial case for the LGM-r-veg simulation (black). Also shown is the simulation of the recent past climate (RP-r, red) and according to the CRU observational data (green). Shaded areas in corresponding colours indicate the ± 1 standard deviation range of individual monthly averages in the three data sets.

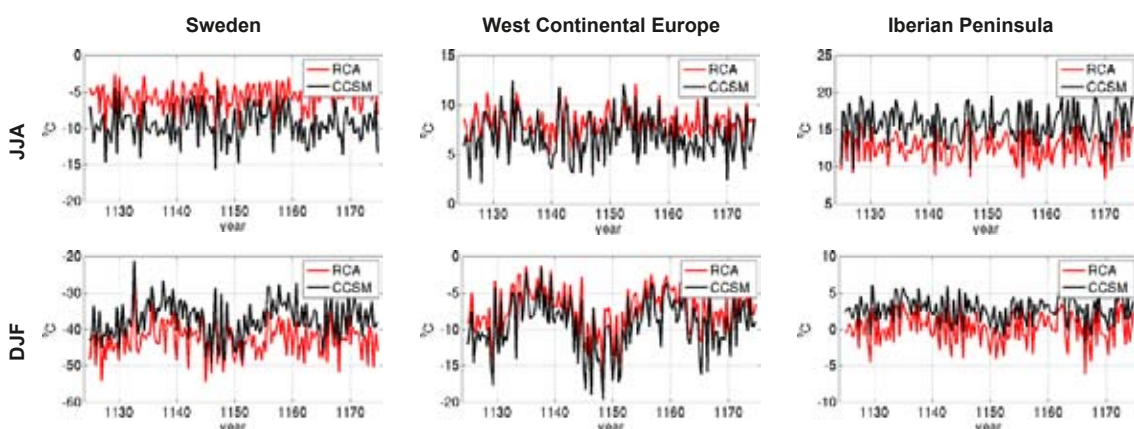


Figure 3-30. Summer (JJA) and winter (DJF) temperatures for the glacial case in RCA3 (LGM2-r-veg, red) and CCSM3 (LGM2, black). Units are $^\circ\text{C}$.

Precipitation

Annual mean precipitation in the model domain has its maximum over the North Atlantic and over parts of western Europe (Figure 3-31, top right). Relatively small amounts of precipitation are simulated in the northern parts of Fennoscandia and over the Mediterranean Sea and North Africa. Compared with the recent past climate, Fennoscandia, the British Isles and Iceland are drier (Figure 3-31, bottom right). More precipitation than in the recent past is seen in southernmost Europe (the Iberian Peninsula, Italy) and northwest Africa. In winter, the differences resemble those in the annual mean but they are more pronounced, notably the Iberian Peninsula and the southern Alps and Italy gets more precipitation than in the recent past climate (Figure 3-31, bottom middle) due to changed atmospheric circulation. Fennoscandia and western Europe receive less precipitation than in the recent past climate. The steep coastlines of western Fennoscandia and Scotland which today are facing the ocean and therefore get a lot of precipitation were, during the LGM, parts of the ice sheet that is extending westward. Without the orographic effect, precipitation is much smaller. In summer, as in winter, precipitation is less than in the recent past climate in most parts of northern Europe. However, more precipitation in LGM2-r-veg is seen on the edge of the ice sheet northwest of Fennoscandia and the British Isles (Figure 3-31, upper and lower left panels). Another area with more precipitation than in the recent past climate is the area of what is today the Baltic Sea. During the LGM this area partly coincided with the most elevated parts of the ice sheet in which RCA3 produces large amounts of precipitation during summer.

All proxy data for precipitation are confined to southernmost Europe (Figure 3-26). A majority of the sites show reduced precipitation at the LGM for both summer and winter, although the uncertainties are large (Figure 3-32). In terms of annual mean precipitation there exist six sites; three in France and the Alpine region, for which model and proxy based data agree fairly well on a decrease of around 300 mm/year, and three in the northern parts of the Iberian Peninsula where the model overestimates

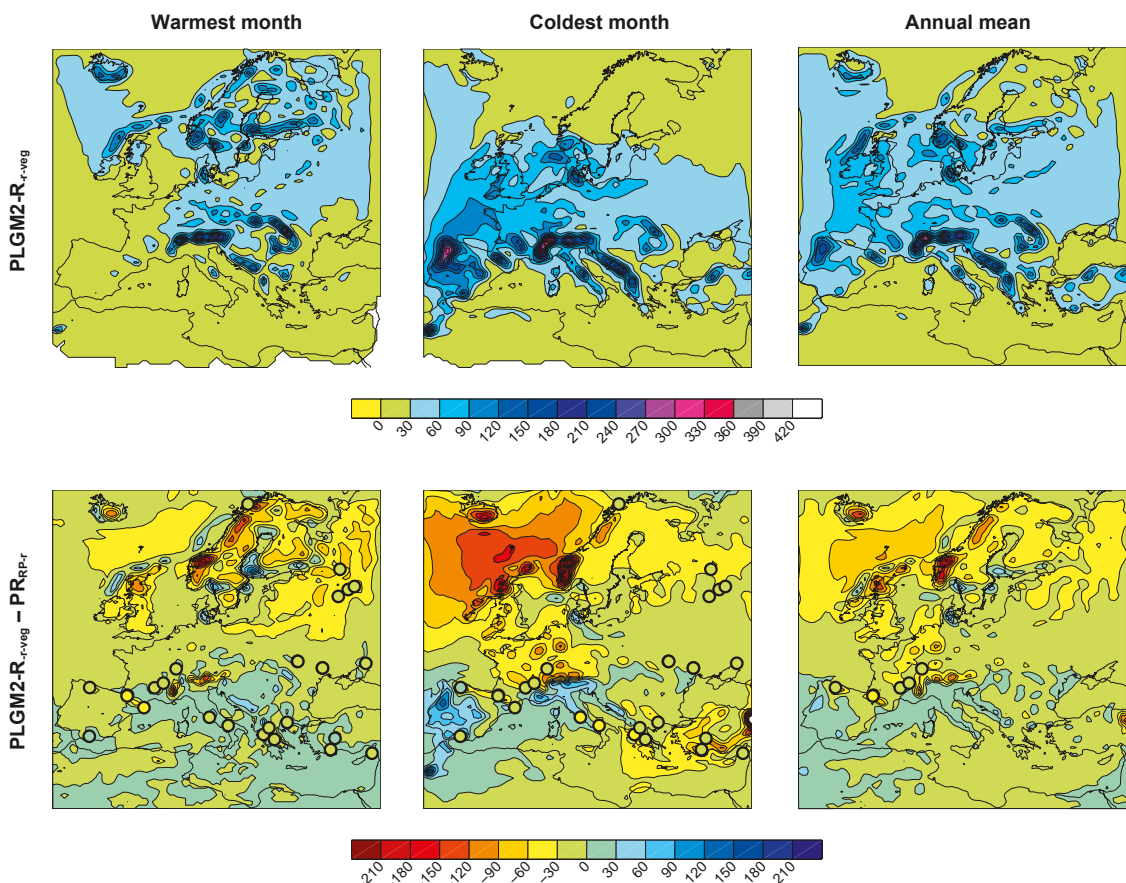


Figure 3-31. Mean precipitation of the warmest month, coldest month and annual mean in the LGM2-r-veg simulation. Also shown are differences between LGM2-r-veg and the simulation of the recent past climate (RP-r). Units are mm/month.

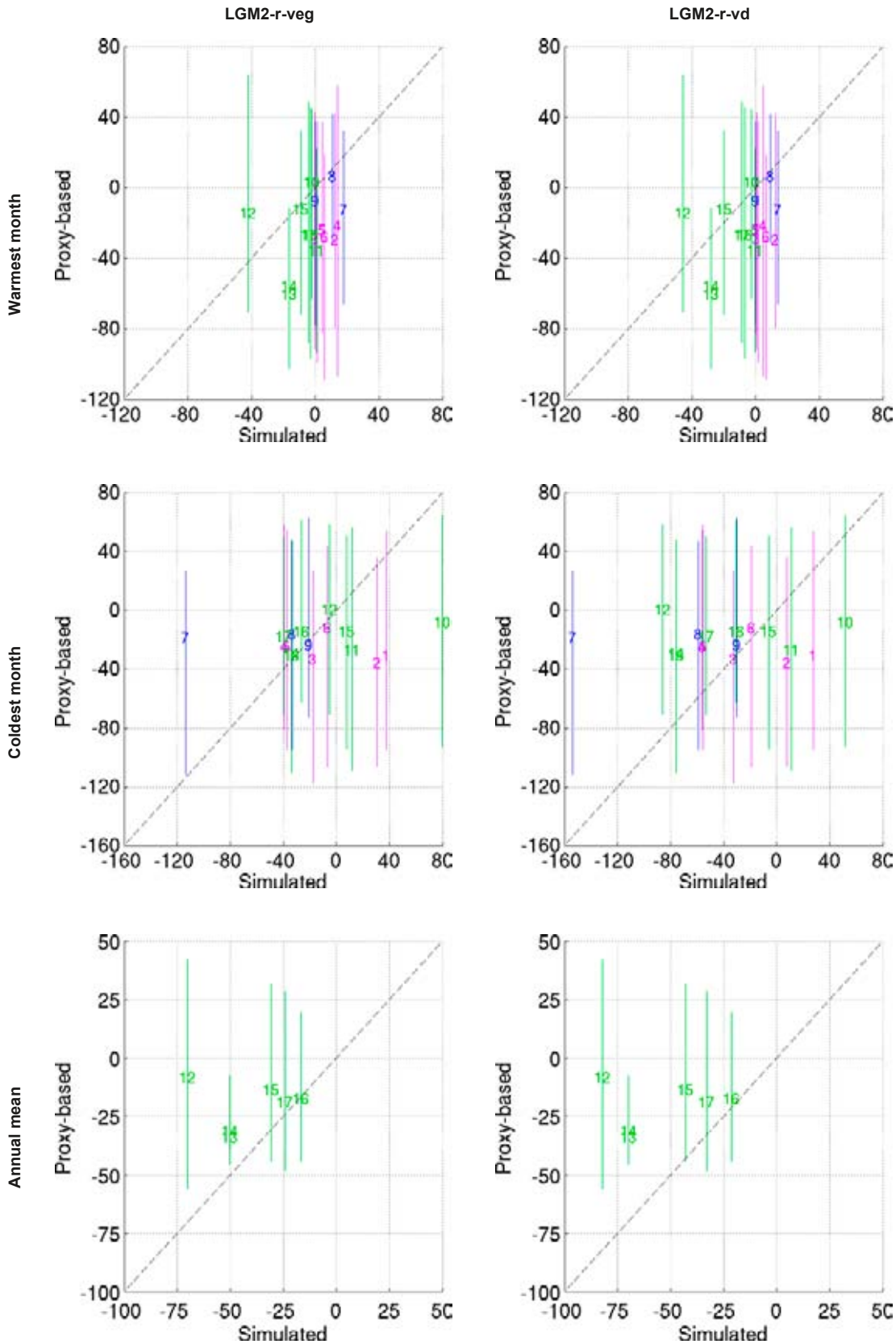


Figure 3-32. Comparison of precipitation anomalies in the *LGM2-r-veg* (left) and *LGM2-r-vd* (right) simulations with proxy data for the warmest month of the year (top), the coldest month of the year (middle) and annual mean conditions (bottom). The uncertainty ranges for the proxy data are denoted by the vertical lines. The numbers corresponds to the specific sites in Figure 3-26. Units are mm/month.

the reduction in precipitation compared to the proxy data. For the coldest month of the year, all proxy based data indicate less precipitation compared with the recent past climate. The model, on the other hand, shows a spread here with increased precipitation at some sites and decreases at others (Figure 3-32). Nevertheless, for most of the sites, the model is within the uncertainty ranges defined for the proxies. This applies to summer, winter and annual mean conditions. An exception to this relatively good agreement is site number 7 in southern Turkey. For this location, there is a large difference in altitude (about 1,000 m) between the actual site and the model grid elevation, as this is an area of a strong gradient in topography. As RCMs at the horizontal resolution we use here may not simulate details of precipitation in mountainous areas, we suspect that the large differences are more of a representativity problem than an actual bias. It can also be noted from Figure 3-31 that the pattern in precipitation change is noisy in its nature and that relatively small horizontal offsets from the sites may alter the correspondence between model and proxies. RCA3 gives a similar amount of precipitation in winter as CCSM3 for most of Europe except south-eastern Europe and west continental Europe where RCA3 gives up to 30% less precipitation (Figure 3-34). In summer, RCA3 gives about 30% more precipitation than CCSM3 in Sweden and up to, or even more than, 100% more in the rest of Europe. Again, the temporal correlation is higher in winter (0.8–0.95 for most regions) than in summer (0.5–0.7 for most regions).

The drier conditions in most of northern Europe are reflected in Figure 3-33 showing less simulated precipitation in Sweden and West Continental Europe for all months of the year. The effect of the southward shift of the storm tracks is clearly seen as the wintertime precipitation decreases in the northern regions whereas it increases in the Iberian Peninsula and western parts of the Mediterranean region.

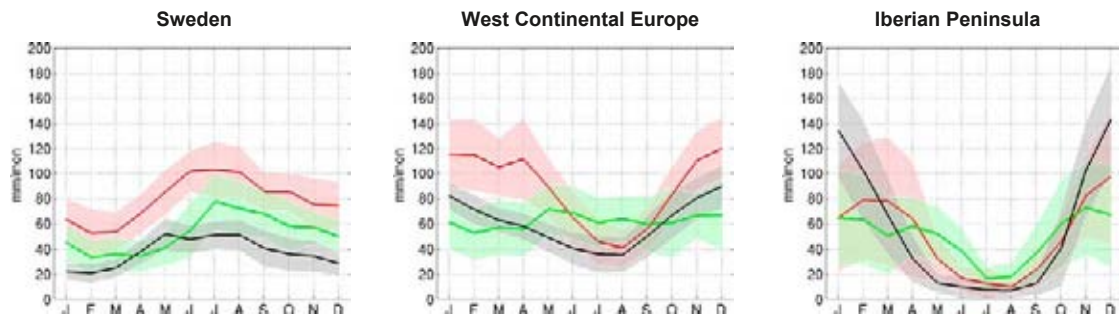


Figure 3-33. Annual precipitation range for the glacial case in the LGM-r-veg simulation (black). Also shown is the simulated recent past climate (RP-r; red) and the CRU observational estimate for 1961–1990 (green). Shaded areas indicate the ± 1 standard deviation range of individual monthly averages in the three data sets. Units are mm/month.

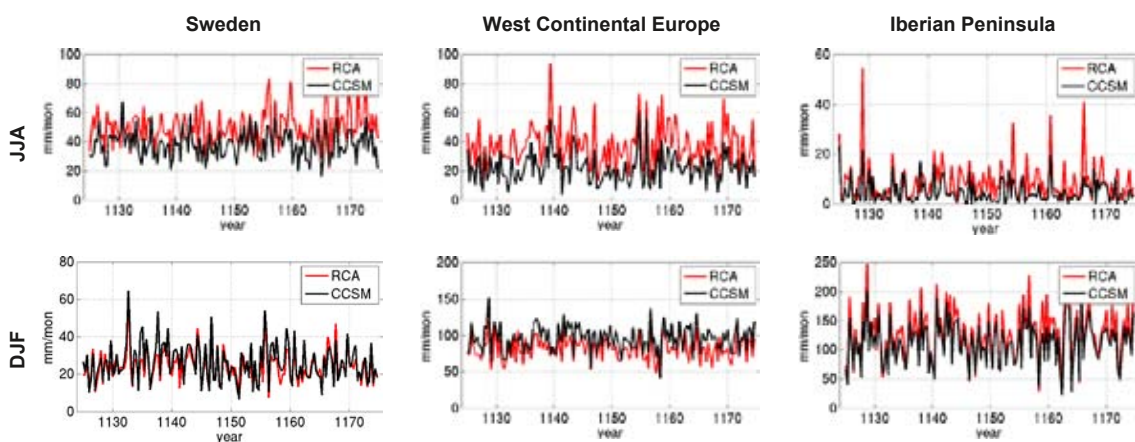


Figure 3-34. Summer (JJA) and winter (DJF) precipitation in RCA3 (LGM2-r-veg, red) and CCSM3 (LGM2, black). Units are mm/month.

The comparison of the simulated precipitation between the two models reveals systematic differences between them. In some regions, RCA3 has a wider, or less wide, annual range than CCSM3. In some regions RCA3 gives systematically more, or less, precipitation than CCSM3. The reasons for this are likely partly due to differences in model physics, but also due to differences in spatial resolution. One thing that is clear is that the differences in temperature and precipitation between RCA3 and CCSM3 are somewhat systematic. Both models nevertheless follow the same variations on decadal and inter-annual time scales.

Mean sea level pressure

The basic pressure patterns are similar to those of today, but with a southward shift of the north-south gradient in MSLP during winter (Figure 3-35). This leads to a less pronounced westerly flow over north-western Europe and an increase in the southwest. The absolute number for the Iceland to Portugal pressure difference decreases from 30 (RP-r) to 10 hPa (LGM2-r-veg).

Regardless of this relatively strong decrease, the inter-annual variability of the westerlies is pronounced, as indicated by the normalised NAO index (Figure 3-35). These changes in NAO index from year to year are similar to those in the simulation of the recent past climate. Again, in this case, there is significant correlation in some areas between temperature, precipitation and MSLP. Correlation coefficients are statistically significant for temperature (0.32 in LGM2-r-veg and 0.43

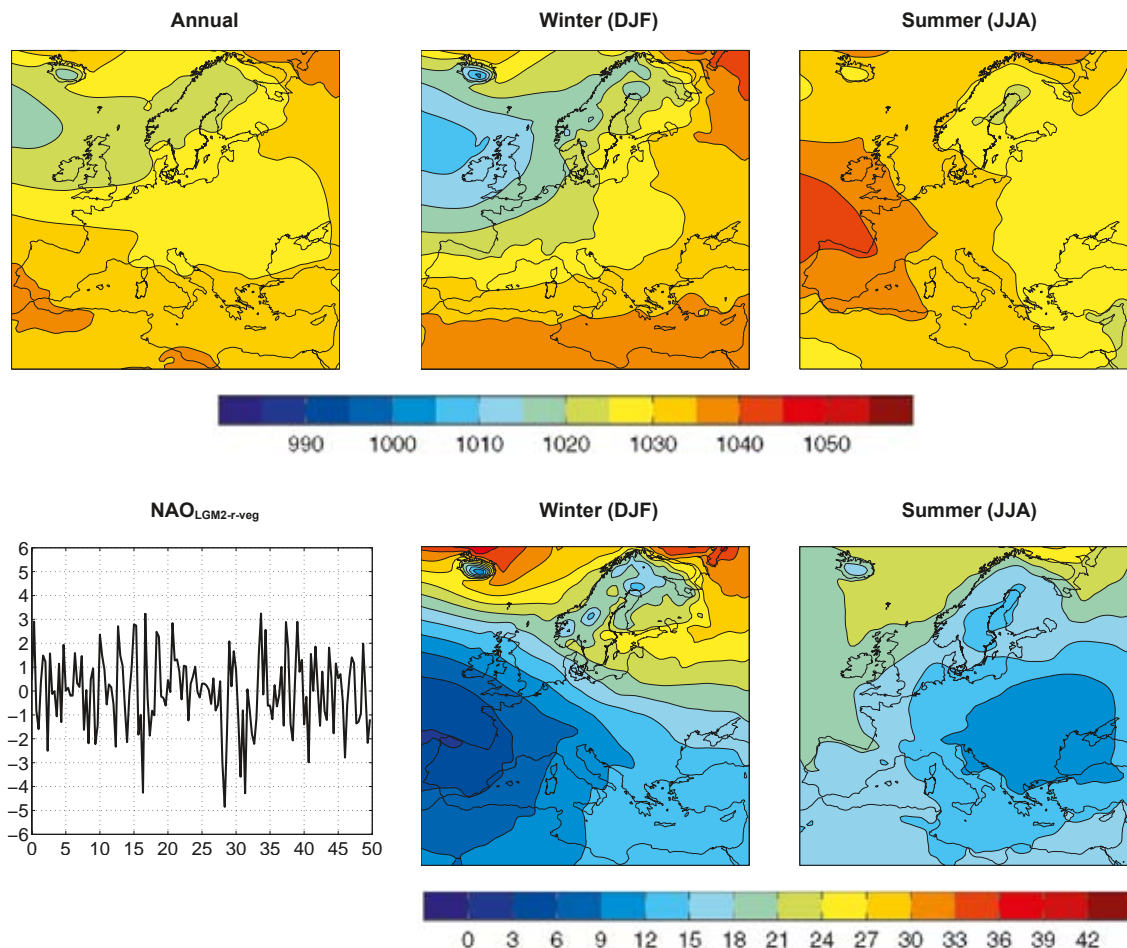


Figure 3-35. Annual and seasonal mean MSLP (top). The lower panels show winter (DJF) normalised NAO index in LGM2-r-veg (left) and MSLP anomalies for LGM2-r-veg compared with the simulation of the recent past climate (right). Unit hPa.

in LGM2-r.vd) and precipitation (-0.40 for LGM2-r-veg and -0.41 in LGM2-r-vd) in the Iberian Peninsula. The positive correlation coefficient for temperature and the NAO-index implies that the winters in the Iberian Peninsula are warm when the westerlies over the North Atlantic are strong (similarly to northern Europe in today's climate). For western continental Europe, the correlation with precipitation is statistically significant (0.28) implying more precipitation when there are more pronounced westerlies. The large high-elevated ice sheet over Fennoscandia leads to disturbances in the MSLP field during winter.

3.2.3 Regional vegetation model simulations

The vegetation model simulates vegetation reminiscent of tundra and/or montane woodland over ice-free parts of central and southern Europe (Figure 3-36). Short, cool summers and low CO₂ concentrations limit primary production and tree growth (Figure 3-27). Boreal needle-leaved trees dominate the tree canopy in the more continental climate of eastern Europe, whereas low growing season heat sums limit establishment to broadleaved deciduous trees of the mountain birch type in western Europe.

The LPJ-GUESS simulated vegetation is, not surprisingly, quite different from the PMIP-2 vegetation map for the same geographical area prescribed in the LGM1 and LGM2 simulations (Figure 2-12, upper panel). Areas not masked out as ice are mainly classified as C₄ grassland and appear to reflect the areal dominance of croplands in the modern European land cover map. In terms of simulated land-atmosphere exchange this may result in some consistency between the CCSM3 and the RCA3 simulation constrained by LPJ-GUESS vegetation (WARM-r-veg), the latter likewise being characterised by an abundance of grassland, though for the very different reason that simulated temperatures are too low in many areas to support tree establishment and/or growth. Compared with the vegetation from /Mahowald et al. 2006a/ used in the LGM-v and LGM-vd simulations (Figure 2-12, lower panel), the agreement is better, with boreal woody vegetation, both needle-leaved trees and broadleaved shrubs/small trees, dominating a few central/eastern European pixels in the Mahowald et al. vegetation map, where LPJ-GUESS likewise predicts needle-leaved and broadleaved 'trees' at low densities.

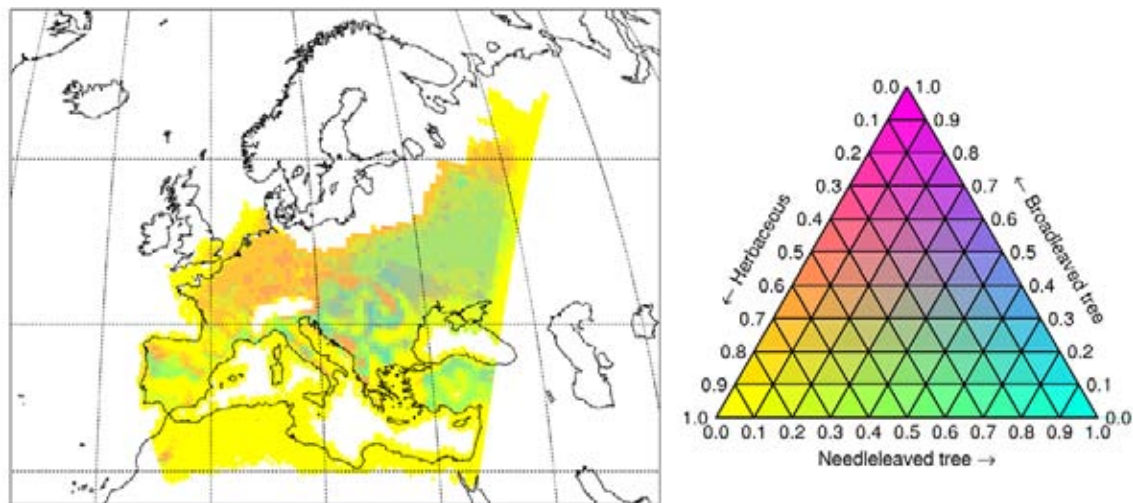


Figure 3-36. Vegetation map resulting from LPJ-GUESS simulation forced by the initial RCA3 climate for LGM2 (LGM2-r).

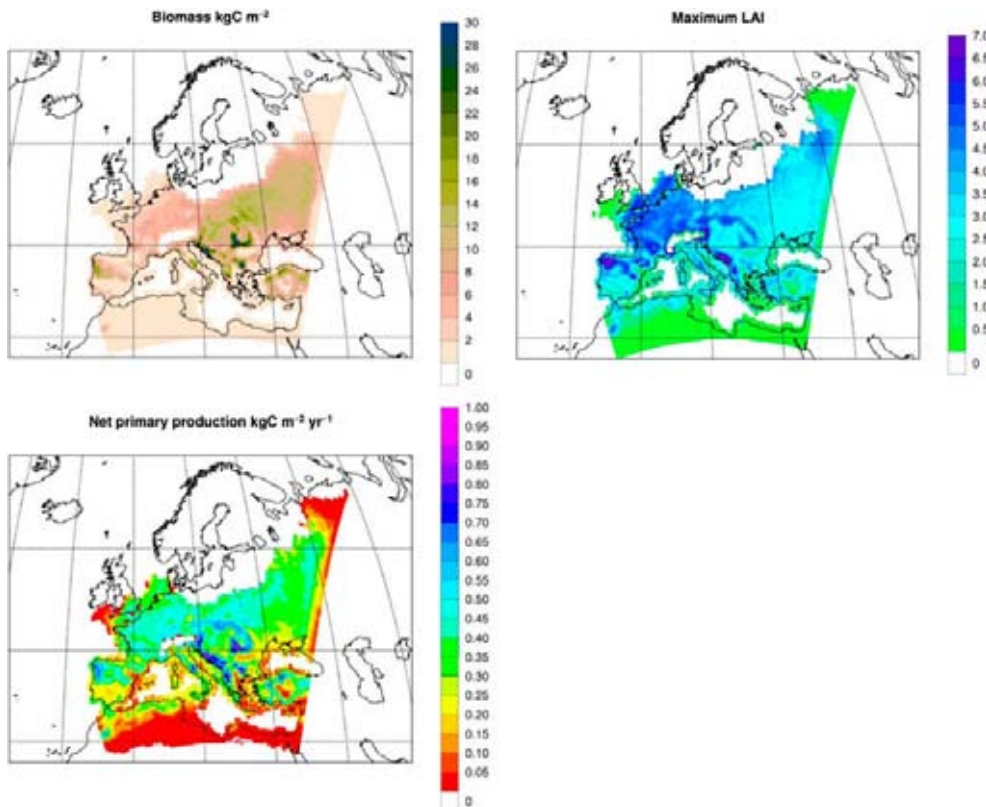


Figure 3-37. Vegetation biomass (kgC m^{-2}), maximal growing season leaf area index (LAI) and net primary productivity (NPP, $\text{kgC m}^{-2} \text{yr}^{-1}$) as simulated by LPJ-GUESS forced by the initial RCA3 climate for LGM2 (LGM2-r).

3.2.4 Synthesis of the glacial case

Comparison to proxy data

The comparison of sea-surface temperature (SST) proxies with the CCSM3 simulated climate reveals a good correspondence to the proxies in the tropics. It also shows a clear indication that the simulated climate is colder in the north Atlantic sector in both summer and winter (Section 3.2.1, Figures 3-19 to 3-21). The low SSTs are related to extensive sea-ice cover in this area. Compared with terrestrial proxy data for temperature of the coldest month of the year, the model tends to be colder than proxies in northern Europe and Siberia (Figure 3-22). In southern Europe, CCSM3 shows an equal or possibly slightly weaker anomaly in temperature compared with that indicated by the proxy data.

Also the regional model is compared with proxy data for temperature (Section 3.2.2). In winter, a clear regional pattern that is inherited from the global model emerges. It shows that the model tends to simulate a larger decrease in temperature than proxies indicate in the northeast (by at least 7–8°C) and that it shows a fair agreement (mostly within a few degrees) in other areas in the southern half of Europe (Figure 3-28). For summer, the model shows a larger decrease in temperature compared with the recent past climate than the proxies do at a majority of the locations (Figure 3-28). For most stations in the Mediterranean area, the model anomalies are larger by some 2–5°C. This may be a consequence of the low SSTs in the North Atlantic as simulated by CCSM3.

A comparison with proxy data on precipitation in southern Europe for LGM conditions shows that the geographical distribution of simulated changes in precipitation is similar to the proxy data. A difference is that most sites show decreased precipitation, whereas the model sometimes shows increases and sometimes decreases compared with the recent past climate. However, the model simulated changes are within the uncertainty limits of the proxy data at most sites, although these uncertainty ranges are wide.

As a summary, we can conclude that the simulated climate in southern Europe agrees with the proxy data although there is a stronger decrease in summer temperatures in the simulation. The comparison with proxy data in Northern Europe is more complicated as there are only very few data points available. Also, some of them are in close vicinity to the ice sheet where the temperature is highly dependent on the exact distribution of the ice sheet. This means that the dating issue is very important for these points, as only small changes in the ice extent may have a profound impact on the temperature climate. Compared to the few available proxies in this area, RCA3 is colder.

Comparison to other model simulations

The simulated annual global mean temperature in the LGM2 simulation (i.e. the second quasi-equilibrium of our reference case) is 6.9°C lower than in the recent past climate. This is a stronger response than in most of the PMIP1 (full range is 1.85–9.17°C colder than in the recent past climate) and PMIP2 simulations (3.4–5.46°C colder than the preindustrial climate) presented by /Kageyama et al. 2006/. Our results indicate that much of the strong cooling is associated with low SSTs (up to 6°C colder than some proxy data indicates) and extensive sea-ice cover in the North Atlantic and North Pacific. These changes in sea-ice extent are a result of the changes in the temperature climate, but they also act to amplify the changes, as increased sea-ice extent leads to a colder climate through the feedback mechanisms involving increased surface albedo and reduced heat fluxes from the ocean to the atmosphere. This connection between low SSTs at high northern latitudes and the global mean temperature as presented here for the LGM2 simulation is in contrast with the LGM1 simulation and the PMIP simulations discussed by /Kageyama et al. 2006/. They find that winter and summer temperature changes over the North Atlantic, Europe and western Siberia do not relate very well to global temperature changes. Another uncertainty relates to the response of the Atlantic Meridional Overturning Circulation (AMOC). This has previously been shown to differ among different PMIP2 models for the LGM; one model gives an unchanged AMOC, whereas two models give an increased AMOC strength /Otto-Bliesner et al. 2007/. Our simulations indicate a relatively severe weakening of the upper branch of the AMOC between the LGM1 and LGM2 periods. The strength of the AMOC is reduced by more than 50% in the LGM2 period compared with the pre-industrial (PI) climate.

Regardless of possible biases in SSTs, the simulated changes in annual mean temperatures over Europe in CCSM3 are similar to those obtained in the high-resolution atmosphere-only CCM3-simulations by /Kim et al. 2008/. They used proxy-based reconstructions of SSTs as a lower boundary condition to their simulation indicating that the possible SST bias we report on here does not have a major influence on the annual mean temperature conditions over Europe. Similarly, /Kageyama et al. 2006/ reported that the relationship between SST anomalies in the North Atlantic and surface temperature anomalies over Europe is not straightforward for the warmest month of the year. They only found significant relationship between anomalies in the western European region and the North Atlantic for temperatures of the coldest month. They showed this for a large range of simulations including those with prescribed SSTs and slab-ocean simulations in PMIP1 and also for fully coupled model simulations in PMIP2. Our results with CCSM3 show a stronger north-south gradient in temperature for the coldest month of the year than do most of the PMIP models. North of 60°N CCSM3 is 10–20°C colder while in the Mediterranean area it is equally warm or warmer than the other models.

In both our global and regional models, the coldest month of the year is warmer than proxy data indicate (Figures 3-22, 3-27 and 3-28). This is a result also shown for the PMIP1 and PMIP2 simulations /Ramstein et al. 2007, Kageyama et al. 2006/. However, even though the models are warmer than the proxy data indicates, /Ramstein et al. 2007/ conclude that they are within the confidence interval of the proxy based reconstructions. The simulated (LGM-r-veg) winter temperatures in southern Europe are only a few °C higher than can be inferred from the proxy based reconstructions. These differences for southern Europe are comparable also to those found by /Jost et al. 2005/ for the HadRM3 regional climate model.

Implications of the sensitivity studies

We note that changing the forcing to be more consistent with LGM conditions (i.e. introducing a different vegetation distribution and including mineral dust) leads to even lower global mean temperatures than in the reference case (cf. Figure 3-16). The changes in the global model indicate

a colder climate in the North Atlantic/European sector in the sensitivity experiments (Figure 3-17). In the regional model we show that changing the vegetation from present-day vegetation to LGM-vegetation as simulated by LPJ-GUESS does not change the results markedly (Figure 3-27, bottom row). On the other hand, the run with increased load of mineral dust in the atmosphere in combination with another vegetation representative for the LGM (LGM-vd) leads to a colder climate more in line with proxy based reconstructions for the coldest month (Figure 3-27, third row).

The trend in global mean temperature in the last 100-year period in the NCAR LGM simulation /Otto-Btiesner et al. 2006a/ was relatively strong. As our continuation of that simulation with a greatly reduced trend is more in balance, this indicates that our simulation is a more consistent simulation of the LGM given the PMIP2 forcing. However, this depends strongly on the rate of transition of the climate system during the LGM. If the real climate system was not in balance we may expect that a balanced state from a simulation is not the best representation of the climate system. The strong global cooling in the LGM2 simulation compared with the recent past climate is in part connected to the regional cooling in the Atlantic sector. As the simulated SSTs in the North Atlantic tend to be lower than indicated by SST proxies, the strong global cooling in this experiment may be exaggerated. Based on our results, we cannot conclude if this is the case and if so how large a possible bias would be. However, the difference between the LGM2 and LGM1 simulations (and also between LGM2 and the other sensitivity experiments for the glacial case) show that this region responds strongly to changes in the climate (Figure 3-17).

Realism of the simulated climate

Given the scarcity of proxy records and their large error bars, the question remains if the simulated climate is realistic. However, some very qualitative statements on the realism of the climate can be made. i) The climate is warm enough in southern Europe to prevent the ice sheet expanding in this direction. ii) The climate in northern Europe, over the ice sheet surface, is cold enough to sustain the ice sheet. Monthly mean temperature seldom rises above 0°C, and over most parts of the ice sheet at least 70% of the precipitation falls as snow. If 60–100% of the precipitation accumulates on the ice sheet it would grow with 0.3–0.5 m/year. iii) The precipitation in the north-eastern part of the Fennoscandian ice sheet is very low, indicating that only limited ice sheet growth was possible in that region. This is in general agreement with the findings of only a small extent of the LGM ice sheet in the Ural region in Russia as presented by /Mangerud et al. 2008/.

3.3 The permafrost case

3.3.1 Global climate model simulations

Stability of the simulated global climate

We do not have access to initial conditions for CCSM3 for a period within MIS 3 (to our knowledge there exist no long-term simulations with a fully coupled AOGCM for this time period). For the *permafrost case* we are interested in simulating a cold climate, possibly warmer than at the LGM, but substantially colder than the pre-industrial climate. Therefore we choose to initialise the *permafrost case* simulation from the LGM simulation (Table 3-1). We start two simulations with identical forcing for the *permafrost case* (Table 2-1) to test the sensitivity to the choice of starting point. One starts at model year 301 (directly after the relatively warm LGM1 period, Figure 3-16) and the other at model year 901 (in the cold LGM2 period, Figure 3-38). Both were run for 105 years. At that time, we noted that the two simulations were converging (not shown) and levelled out. As the initial temperature climate in the two simulations was fairly different we decided to continue only one of them. We decided to use the one starting from model year 901. From model year 901, the simulation was run for, in total, 886 years to allow for a shift to a warmer state followed by an equilibration (Figure 3-38).

The annual global mean surface temperature (T_{agm}) displayed in Figure 3-38, increases from the cold LGM quasi-equilibrium and reaches a new quasi-equilibrium after 600 years. The mean T_{agm} is 9.2°C in the new quasi-equilibrium as compared with 9.0°C and 7.9°C in the first and second LGM quasi-equilibria. The linear trend in T_{agm} over the last 100 years of the PERMAFROST simulation is 0.037°C per century as compared with -0.17°C per century over the last 100 years of the LGM

simulation. The sea-ice covered percentage of the Earth's surface is also shown for the LGM and the PERMAFROST simulations in Figure 3-38. The evolution in T_{agm} is anti-correlated with the evolution of the sea-ice cover in both simulations. The correlation is -0.91 for the annual mean time series of T_{agm} and sea-ice extent.

In the following we discuss the 50-year mean climate for the model years 1420–1469 in the PERMAFROST simulation. This period coincides with the period chosen for the regional simulation. Since the equilibration of the climate in this simulation took much more time to reach than we anticipated, we had to choose a period for the regional simulation before the simulated climate had reached its final quasi-equilibrium. However, the T_{agm} changes by less than 0.1°C from the period 1420–1469 to the end of the simulation and the analysed period still gives a good representation of the climate in the PERMAFROST simulation.

Temperature and sea ice

The annual mean surface cooling in the PERMAFROST simulation as compared with pre-industrial (PI) conditions is most pronounced over the Laurentide and the Fennoscandian ice sheets and over the Greenland-Iceland-Norwegian Sea, with a maximum cooling of 25°C (Figure 3-39). A large portion of the cooling over the Fennoscandian and Laurentide ice sheets is due to the increased

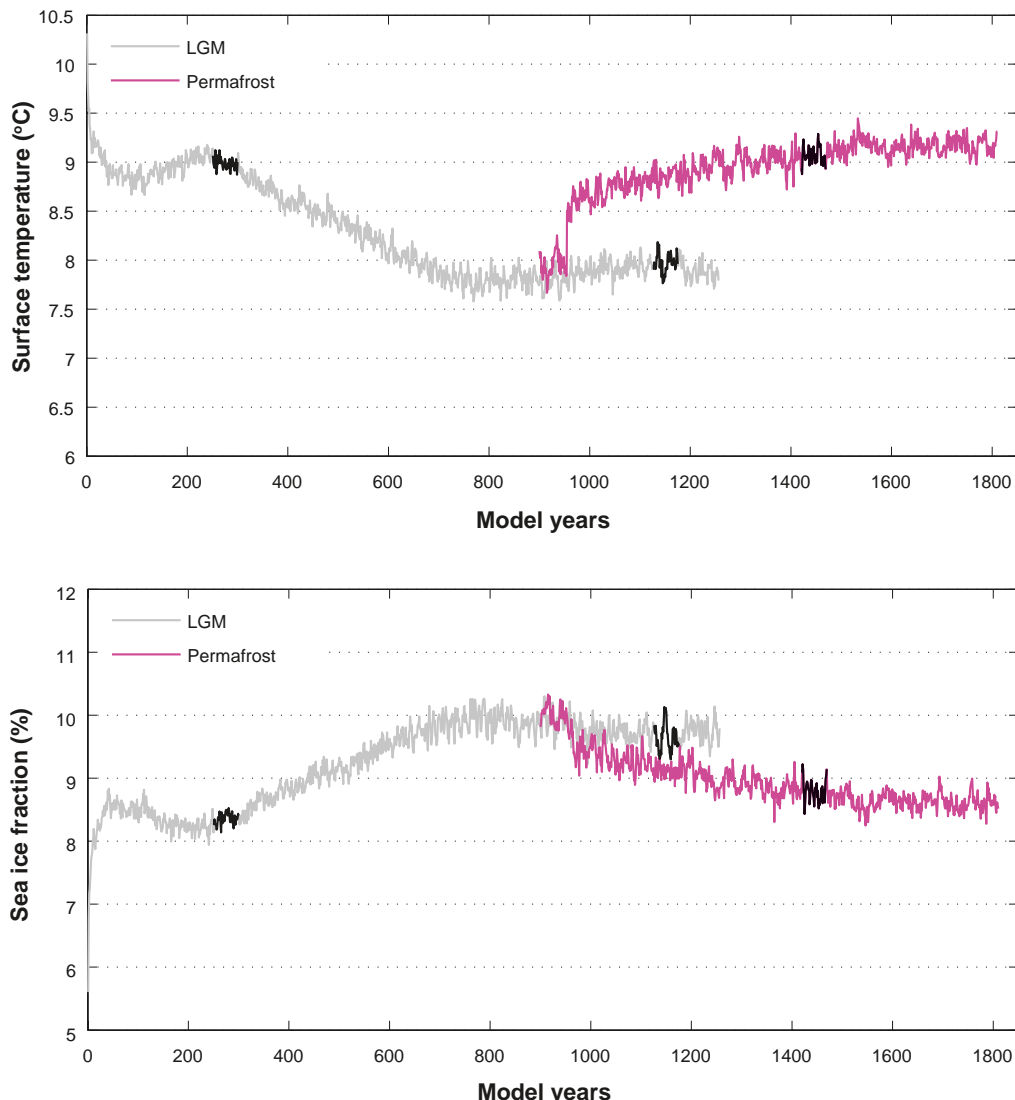


Figure 3-38. Annual mean global mean near-surface temperature (upper panel) and sea ice fraction (lower panel) in the LGM (grey) and PERMAFROST (pink) simulations. Darker parts of the curves marks the 50-year periods analysed here. Units are $^{\circ}\text{C}$ and % of the Earth's surface covered by sea ice.

elevation over the ice sheet. The cooling amounts to 5–10°C north of 40°N in the Atlantic Ocean, the Arctic Ocean and over Antarctica and the Southern Ocean. The annual mean temperature in the PERMAFROST simulation as compared with the LGM2 simulation shows the effect of the relatively smaller and lower Laurentide and Fennoscandian ice sheets in this simulation. These regions are up to 20°C warmer in PERMAFROST than in LGM2 (cf. Figures 3-17 and 3-39). The sea-ice extent is increased in the PERMAFROST simulation in the North Atlantic and north Pacific as compared with the PI simulation (also shown in Figure 3-39). Compared with the LGM2 simulation, the warmer climate in the North Atlantic sector leads to less sea ice off the western European coast in the PERMAFROST simulation. On the other hand, the extent of the sea ice is larger in the north-western Pacific Ocean. This increase is associated with a decrease in the surface temperature over Alaska.

The salinity stratification is increased in the simulated PERMAFROST ocean, as compared with the stratification in the PI simulation. It is similar to the stratification in the LGM1 simulation. This change is accompanied by a decrease in the potential temperature which is relatively uniform with depth. The AMOC is of similar strength in the PERMAFROST simulation as in the LGM2 simulation, i.e. a reduction by around 50% compared to the pre-industrial conditions.

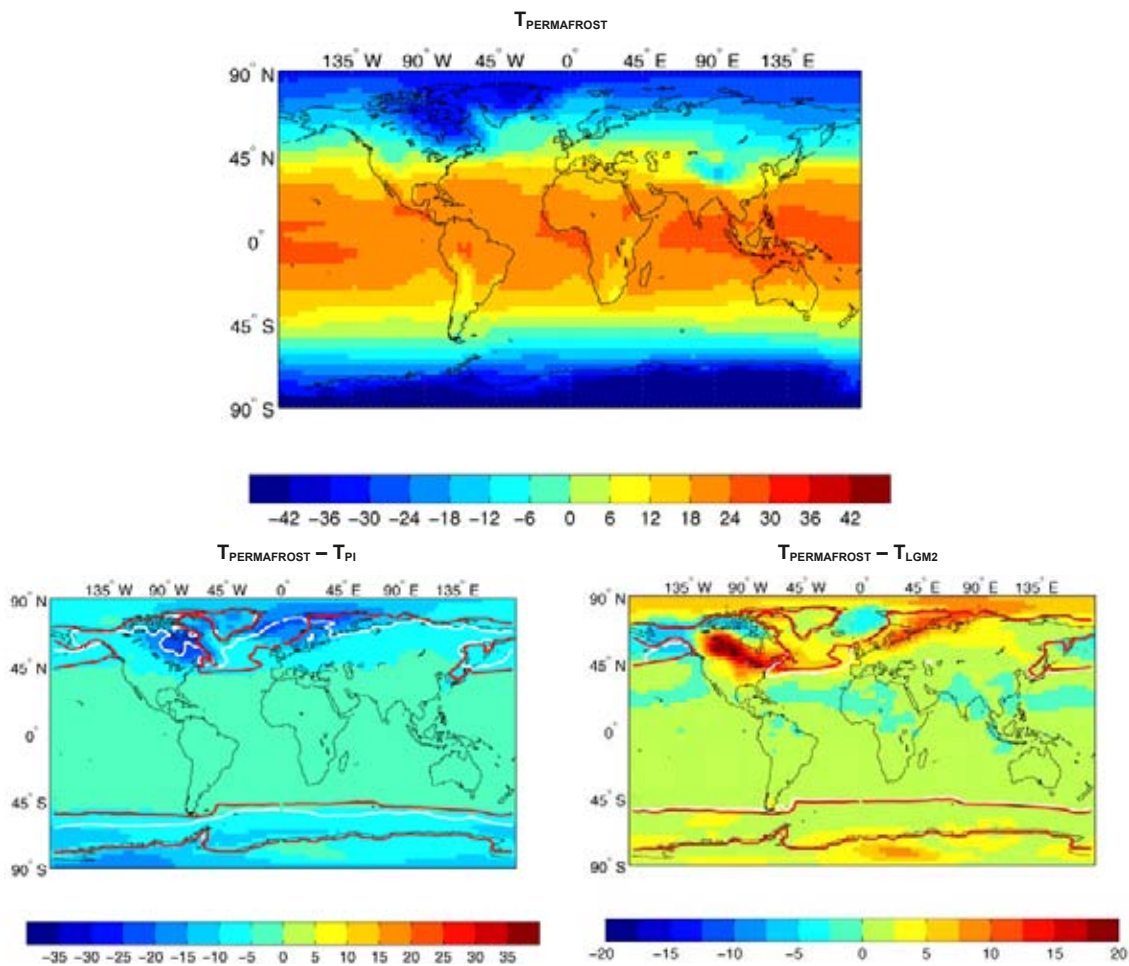


Figure 3-39. Annual mean near-surface temperature in the PERMAFROST simulation (top). The lower panels show the difference in the annual mean near-surface temperature between the PERMAFROST simulation and the pre-industrial (PI) simulation (left) and between the PERMAFROST simulation and the LGM2 simulation (right). Units are °C. Also shown is the annual mean sea ice edge (defined at 10% areal sea ice cover) for the PI simulation (white; left panel) and the LGM2 simulation (white; right panel) and the PERMAFROST simulation (red; both panels).

Comparison with proxy data

Proxy data on temperature are sparse for the period around 44 kyr BP that we simulate. The compilation of proxy-data for the *permafrost* case (see Section 2.4) produced 13, 22 and 22 sites with SST data for this period for annual mean, July–September (JAS) and January–March (JFM), respectively (Appendix F). The comparison with these data is shown in Figures 3-40 (annual mean), 3-41 (JAS) and 3-42 (JFM) respectively. Since the results from the last glacial maximum simulations indicate that the global model may produce too cold conditions in high northern latitudes it is interesting to compare also the *permafrost* case simulation with proxy data in this region. Only three sites are available north of 45°N for Northern Hemisphere winter (JFM) and six sites are available for Northern Hemisphere summer (JAS). The simulated SST is in reasonable agreement with the proxy data for annual mean and JFM and JAS seasons (i.e. within $\pm 4^{\circ}\text{C}$ at most locations). For the locations in the North Atlantic the agreement is also relatively good and better than the corresponding agreement in the LGM simulations although biases of up to and around 5°C are seen at many sites at mid and high latitudes in the North Atlantic during JAS.

Proxy data of air temperature close to the ground surface obtained from continental pollen data are even sparser for this period than SST data. Since the data found covers the domain over which the regional climate model simulations are performed, we choose to do the comparison only for the regional model simulations and not the global simulation (Section 3.3.2).

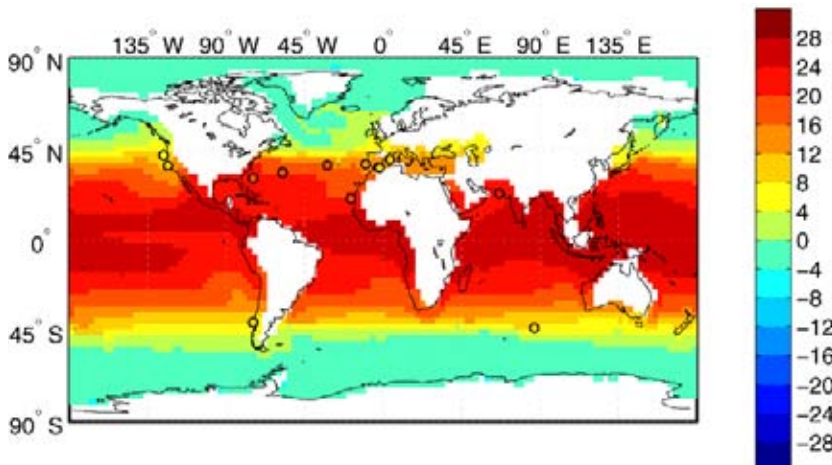


Figure 3-40. The annual mean SST in the PERMAFROST simulation (shaded) and proxy data for SST (coloured circles). Units are $^{\circ}\text{C}$.

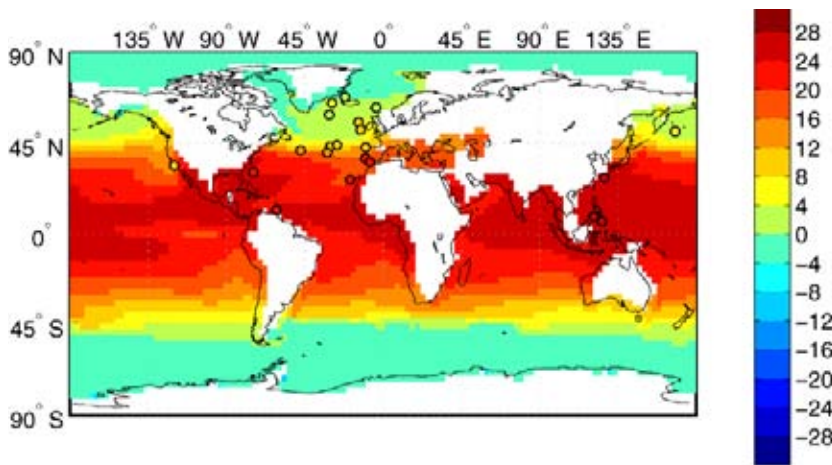


Figure 3-41. The northern hemisphere summer (June–August) mean SST in the PERMAFROST simulation and proxy data for SST (coloured circles). Units are $^{\circ}\text{C}$.

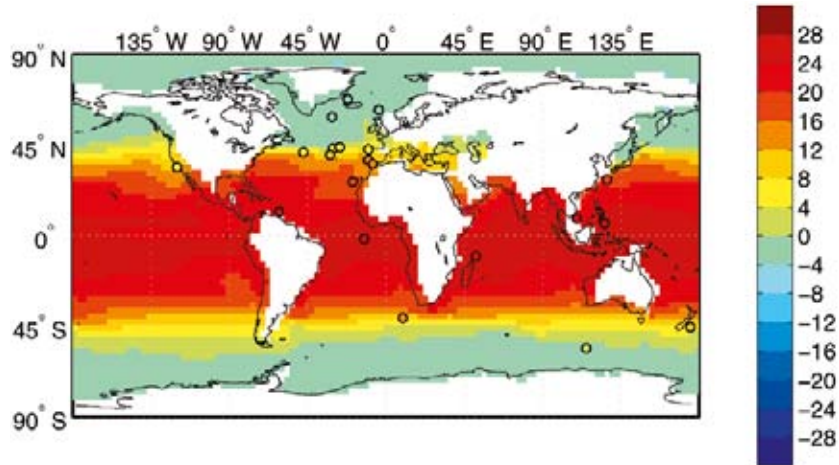


Figure 3-42. The northern hemisphere winter (December–February) mean SST in the PERMAFROST simulation and proxy data for SST (coloured circles). Units are °C.

Atmospheric circulation

The upper-tropospheric circulation changes from the PI to the PERMAFROST simulation are dominated by an amplification of the topographic wave over the Rocky Mountains and the Laurentide ice sheet, similar to that in the LGM1 simulation (Figure 3-43). Due to the reduction in the extent and height of the ice sheets in PERMAFROST as compared with LGM2, the amplification of the topographic wave is only about half of that in LGM1.

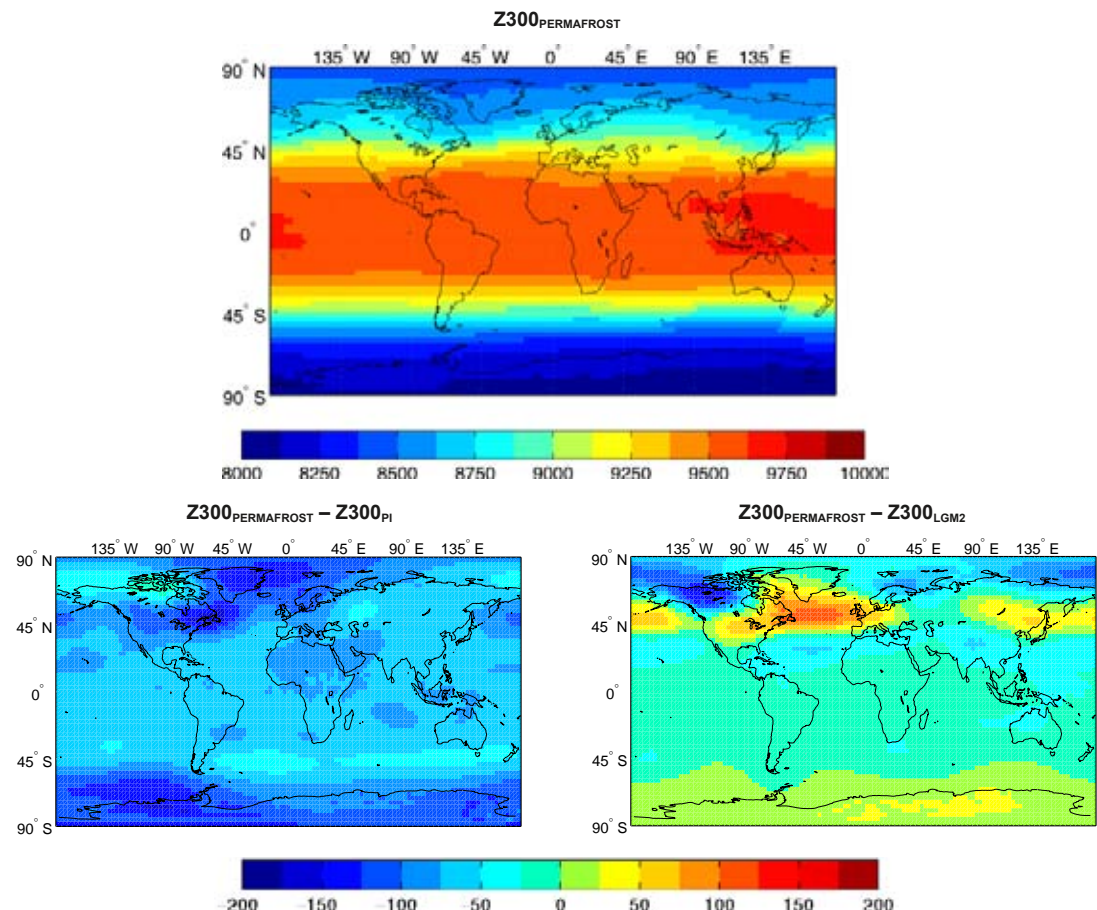


Figure 3-43. Annual mean Z300 in the PERMAFROST simulation (top). The lower panels show differences in the annual mean Z300 between the PERMAFROST simulation and the pre-industrial simulation and between the PERMAFROST simulation and the LGM2 simulation. Units are geopotential metres.

Precipitation

The Atlantic storm track is shifted southwards from the PI simulation to the PERMAFROST simulation, similarly to the situation in the LGM simulations. Therefore, the change from the PI simulation to the PERMAFROST simulation in Fennoscandian precipitation is similar to the change from PI to LGM2. This leads to less precipitation in the northern parts of Fennoscandia and more in the southern parts (see Figure 3-44). The shift is however not as extensive as in the LGM simulations, thus precipitation is shifted northwards in the Atlantic in PERMAFROST as compared with the LGM2 simulation (also shown in Figure 3-44)

Variability

The amplitude of the inter-annual variability in the T_{agm} (Figure 3-38) is similar in the PERMAFROST simulation as compared with the LGM2, LGM-v and LGM-vd simulations. The standard deviation is 0.09°C in the PERMAFROST simulation as compared with 0.1°C in the LGM2 simulation. To investigate how this variability in the global mean is connected to variability in the atmospheric and oceanic dynamics we analysed the correlation of T_{agm} and other variables at each grid point. The method is described in Section 3.2.1.

Similarly to the LGM2 case (Figure 3-25); the correlation analysis of T_{agm} and T_s for the PERMAFROST simulation points out the North Atlantic as the region with the highest positive correlations. However, the region with a correlation coefficient above 0.4 covers a smaller area than in the LGM2 simulation and specifically it does not include the North Pacific. Similarly to the LGM2 simulation, the sea ice and precipitation in the North Atlantic region are significantly correlated to the variations in T_{agm} in the PERMAFROST simulation (Figure 3-45). MSLP, on the other hand, is not significantly correlated in the North Atlantic region.

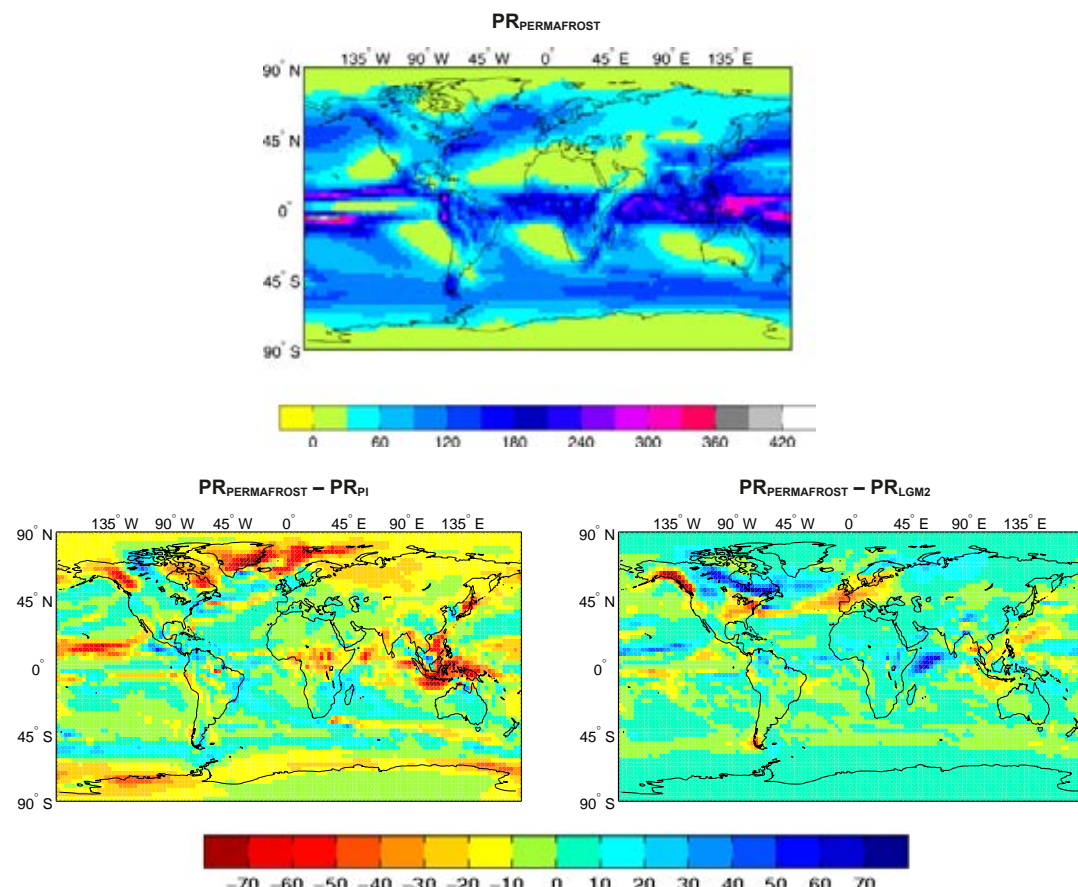


Figure 3-44. Annual mean precipitation in the PERMAFROST simulation (top). The lower panels show differences in the annual mean precipitation between the PERMAFROST simulation and the pre-industrial simulation and between the PERMAFROST simulation and the LGM2 simulation. Units are mm/month.

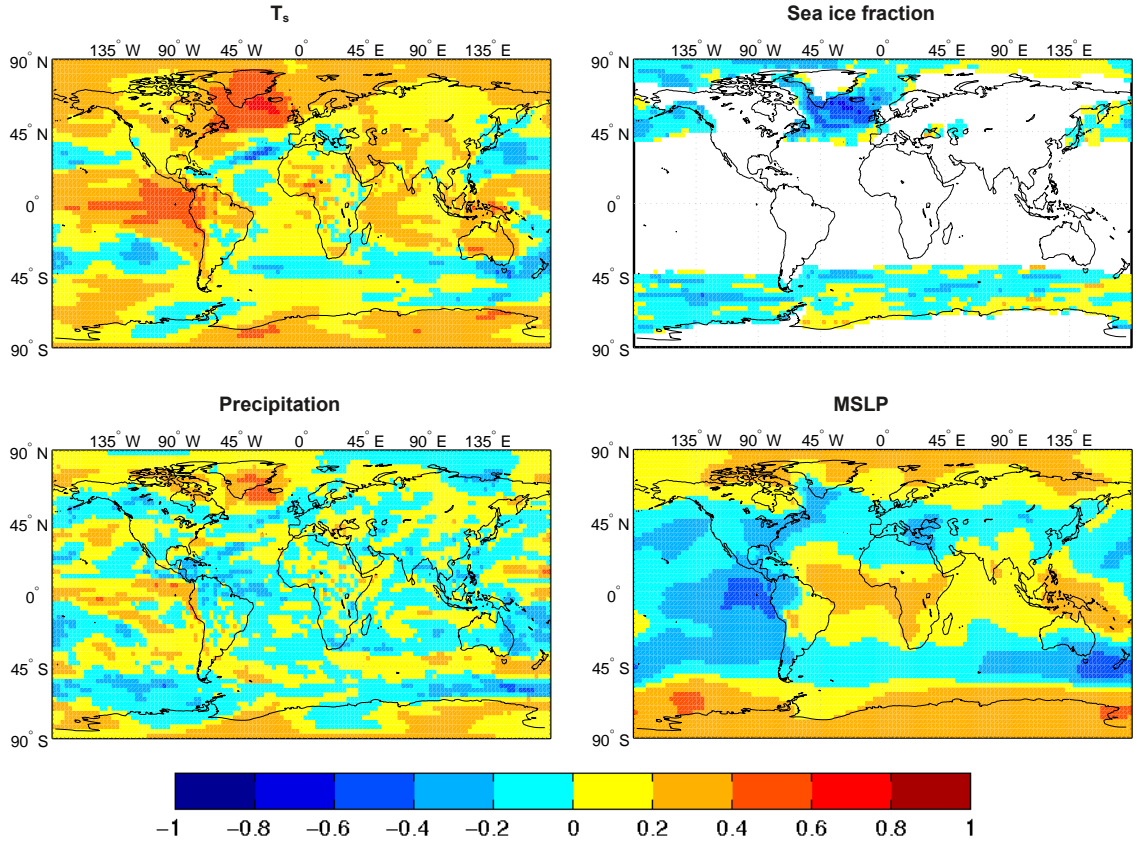


Figure 3-45. The correlation of annual global mean surface temperature (T_{agm}) with the annual mean surface temperature (T_s ; top left), sea ice fraction (top right), precipitation (bottom left and MSLP (bottom right)) in the PERMAFROST simulation. Correlation coefficients above (below) 0.4 (−0.4) are statistically significant at the 95% level.

3.3.2 Regional climate model simulations

In this section we discuss the downscaling of the model years 1420–1469 in the PERMAFROST simulation. RCA3 was first run to produce an initial climate (PERMAFROST-r). This climate was then used to produce a new vegetation distribution, as outlined in Section 2.2.3 and presented below in Section 3.3.3. Finally, a repeated run (PERMAFROST-r-veg) with RCA3 forced also by the new vegetation was completed to produce the final climate which is discussed here.

The simulated temperature and precipitation is compared with MIS 3 proxy data as described in Section 2.4 (see also Appendix E, Table E2). Figure 3-46 shows the location of the sites that are used. The colours are used to group the data to facilitate interpretation of scatter plots below. Apart from scatter plots we also show the proxy data in the maps showing results from RCA3 for all of Europe. We note here that the availability of proxies is highly limited for stadial conditions during MIS 3. We therefore include also data representative of interstadial conditions in the comparison and note that the comparisons presented here are qualitative.



Figure 3-46. Location of the sites used in the comparison of temperature and precipitation proxies with RCA3 results for the permafrost case. All sites are not used for all comparisons as all do not contain proxies of both temperature and precipitation. Note that some of the sites are located in close vicinity to each other, implying that they may be difficult to discern from each other in the maps.

Temperature

As in the *glacial case* (cf. Section 3.2.2), the temperature climate is dominated by a very strong seasonal cycle and a pronounced north-south gradient in the winter (Figure 3-47). In the north, the effect of the ice sheet is clearly seen in the isolines of temperature showing the low temperatures in parts of Fennoscandia (Figure 3-47, upper panels). The isotherm showing 0°C annual mean temperature goes south of Ireland, through England and the southern parts of Denmark, just south of Sweden and then eastwards (Figure 3-47, upper row, right). Compared with the recent past climate, the annual mean temperature in the PERMAFROST-r-veg simulation is around 5°C colder around the Mediterranean, 5–10°C colder in central Europe and more than 8°C colder in the ice-free parts of Fennoscandia (Figure 3-47, second row, right panel). The same values as for difference in annual temperature apply for winter temperature in southern and central Europe. The winter temperature of the British Isles is 10–15°C colder and the southern tip of Fennoscandia around 15°C colder in comparison with the recent past climate (Figure 3-47, second row, middle). Over the ice sheet in northern Fennoscandia, temperatures are at least 30°C colder than in the recent past. On Iceland and over the Norwegian Sea, the difference from the late 20th century is even larger. In summer most of continental Europe is 0–5°C colder than in the late 20th century, western Europe and the British Isles are 5–10°C colder and northern Fennoscandia is 10–15°C colder than in the recent past (Figure 3-47, second row, left). The effect of adding a different vegetation cover is marginal, both in winter and summer (Figure 3-47, lowermost row).

There exist some proxies for temperature in MIS 3 (Sect. 2.4 and map in Figure 3-46). Data are sparse and uncertain, but give a hint about the temperature climate of MIS 3 at some locations in Western Europe (Figure 3-47, upper row and Figure 3-48). We note that most of the proxies are representative of interstadial conditions implying that a comparison with simulated data must be qualitative. The model and proxy data agree fairly well with differences below 5°C at most of the sites both in summer and in winter. In winter, this is within the ranges associated with the proxies at all locations but one. In summer, there is a systematic difference over the British Isles as the proxies indicate higher temperatures (by some 5–10°C) than those predicted by the model (Figure 3-48). Again, we note that many of the proxies, including those in the British Isles, are representative of interstadial conditions implying that the discrepancies do not necessarily imply a model bias.

The colder climate in all of Europe compared with the recent past is seen for all months in the seasonal cycles shown for some regions in Figure 3-49. The amplitude of the seasonal cycle is similar to that of today in western and southern Europe, whereas it is much more pronounced in Sweden due to the cold winters.

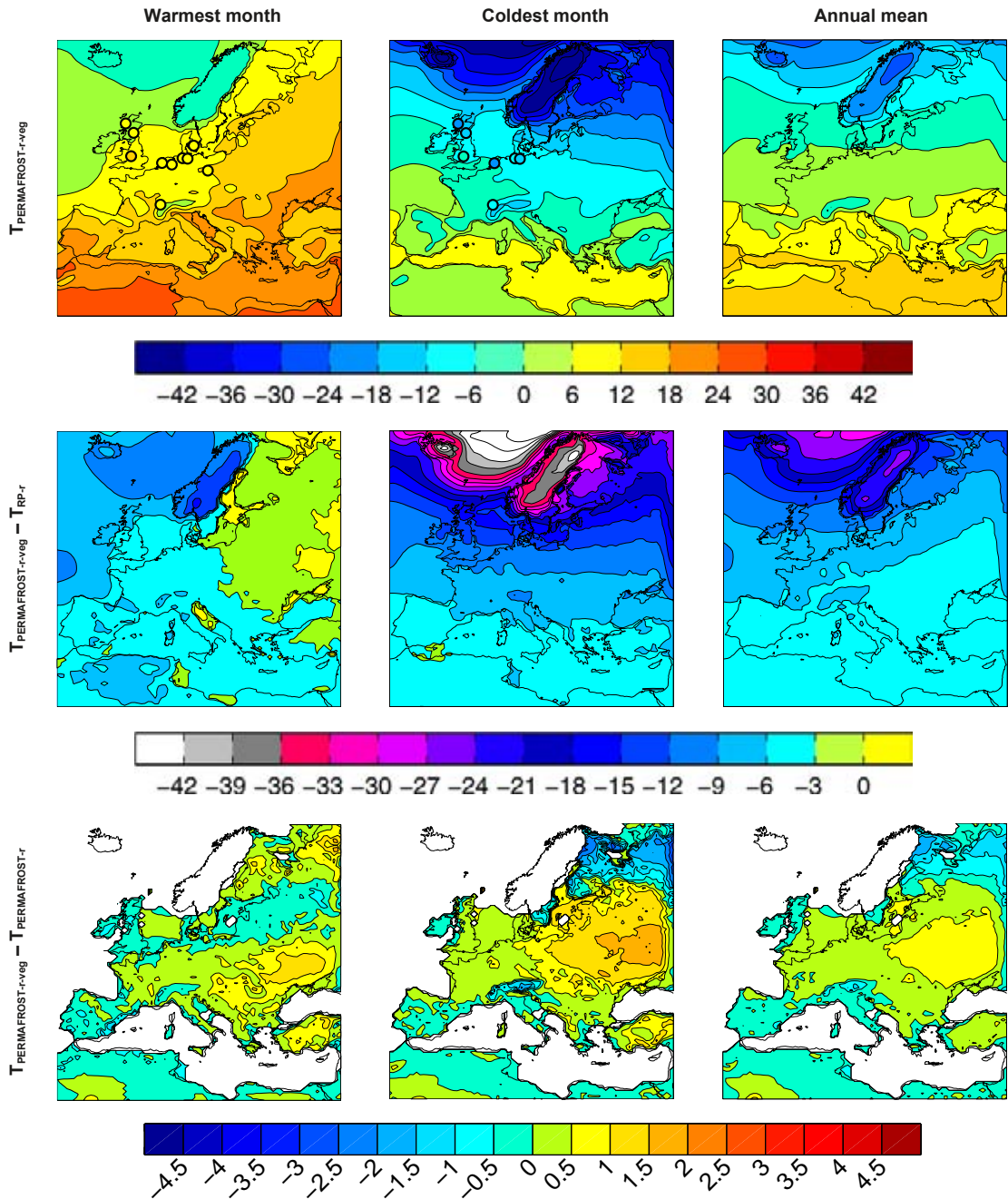


Figure 3-47. Mean temperatures of the warmest month, coldest month and annual mean in the PERMAFROST-r-veg simulation (top). Shown also are temperature estimates based on proxy data as described in Section 2.4 (coloured circles). In the middle row we show differences between PERMAFROST-r-veg and the simulation of the recent past climate (RP-r). The lowermost panels show the impact on the temperature climate by using a new vegetation distribution, by comparing PERMAFROST-r-veg and PERMAFROST-r. Units are $^{\circ}\text{C}$.

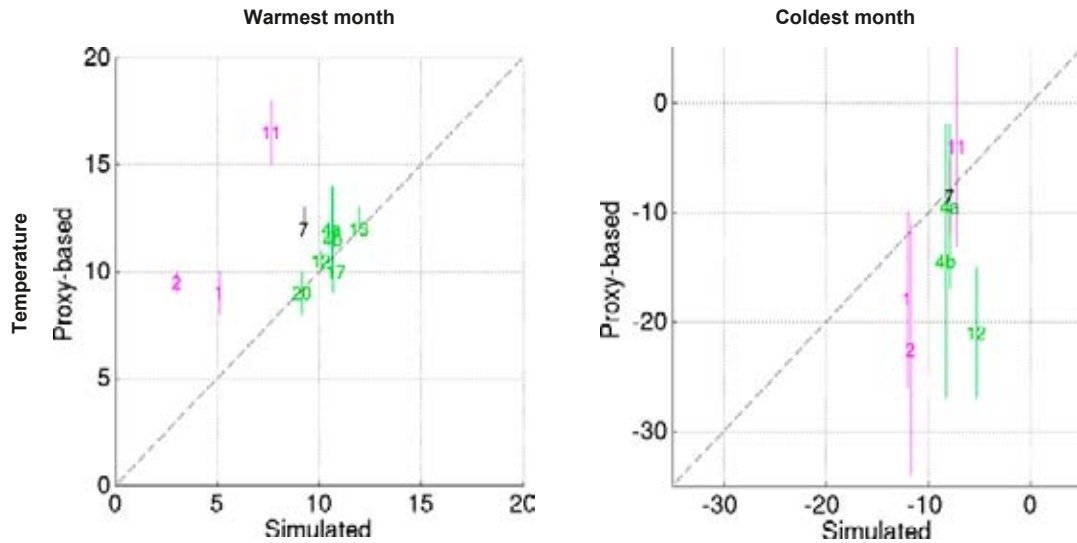


Figure 3-48. Comparison of temperature in the PERMAFROST-r-veg simulation (horizontal axis) with proxy data (vertical axis) for the warmest month of the year (left) and the coldest month of the year (right). The vertical bars illustrated for the proxy data define the intervals given by /Wohlfarth 2009/. The numbers corresponds to the specific sites in Figure 3-46. Units are °C.

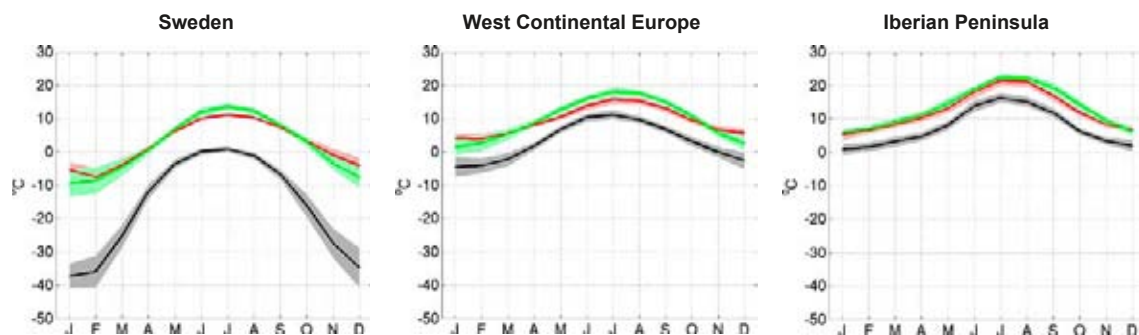


Figure 3-49. Annual temperature range in PERMAFROST-r-veg (black), RP-r (red) and according to the CRU observational data for the time period 1961–1990 (green). Shaded areas in corresponding colours indicate the ± 1 standard deviation range of individual monthly averages in the three data sets.

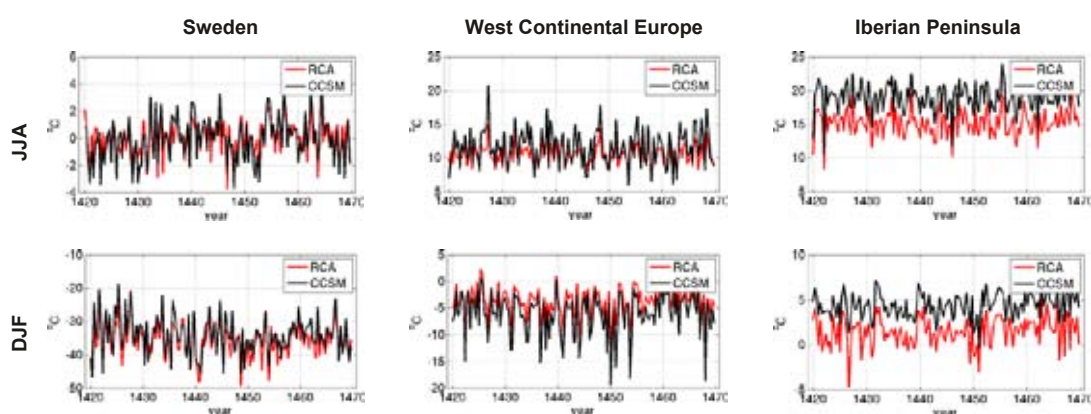


Figure 3-50. Summer (JJA) and winter (DJF) temperatures in RCA3 (PERMAFROST-r-veg, red) and CCSM3 (PERMAFROST, black). Units are °C.

Compared with CCSM3, RCA3 gives lower temperatures on the Iberian Peninsula in both summer and winter as a result of the differences in topography as mentioned before (Figure 3-50). In the remainder of Europe, except north-western Russia, RCA3 give equal, or 1–2 °C warmer temperatures than CCSM3. In north-western Russia, RCA3 is up to 10 °C warmer than CCSM3 (not shown). In summer, the area around the Mediterranean is 2–3 °C colder than in CCSM3. For the rest of Europe, RCA3 gives similar summer temperatures to CCSM3.

Precipitation

The annual mean precipitation in the PERMAFROST-r-veg simulation differs from the recent past, in that it is characterized by drier conditions, by more than 360 mm/year in large parts of Fennoscandia and over the North Atlantic, and by an increase in precipitation of up to 360 mm/year in parts of the southwest (Figure 3-51, upper right). In the rest of the model domain, differences are, with few exceptions, smaller. Around the Mediterranean, precipitation amounts are about the same as in the recent past, although with more precipitation in the southwest. Most of central Europe gets 10–20 mm/month less precipitation than today. The largest difference is over the Norwegian Sea where the sea-ice prevents evaporation and convection, and thereby leads to reduced precipitation. Also in western Fennoscandia there are large differences, as much of the orographic precipitation is eliminated. In summer, the situation is similar: small changes in the south, around 20 mm/month drier in central Europe, and at least 30 mm/month less precipitation over the Norwegian Sea and Fennoscandia. The “Baltic Sea”, which in this case consists mostly of land grid points, gets about equally much precipitation in summer as its surroundings. Compared with the recent past climate, this implies a relatively large increase (Figure 3-51, lower left).

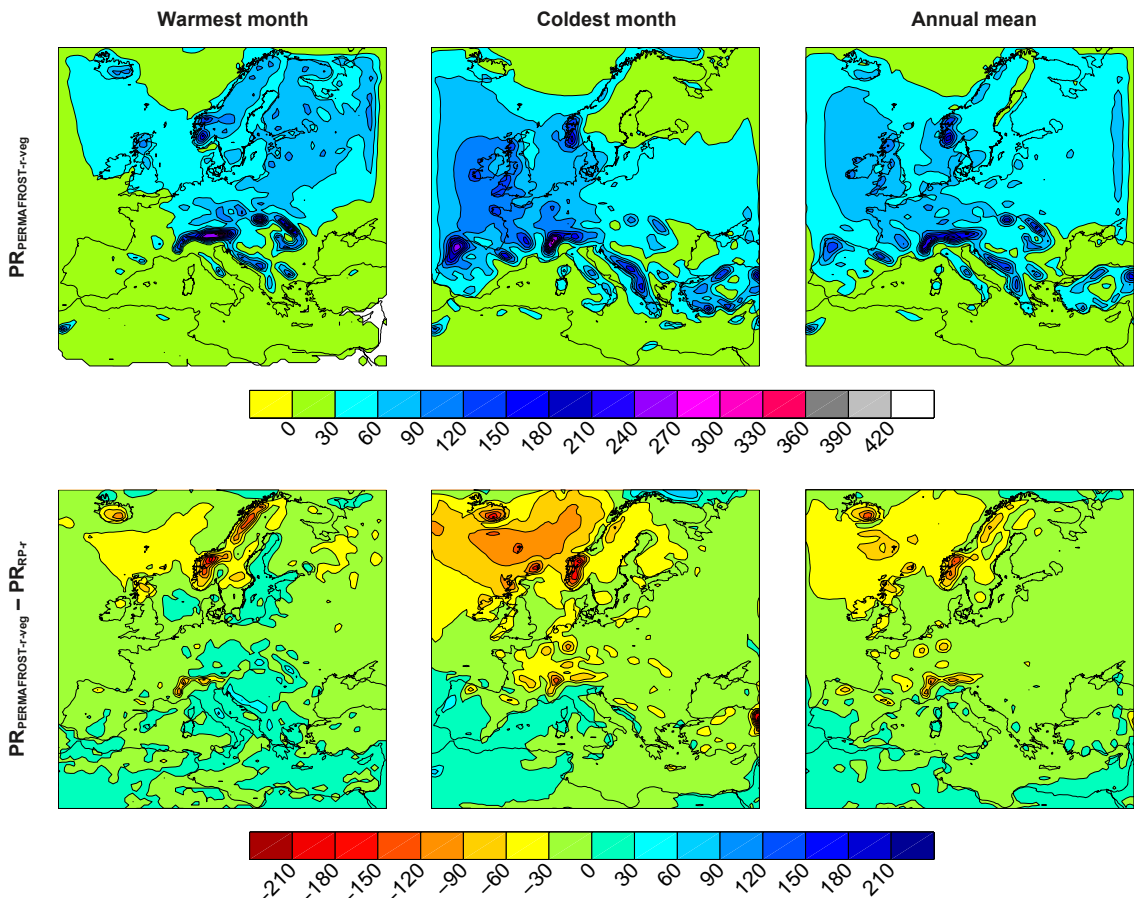


Figure 3-51. Mean precipitation of the warmest month, coldest month and annual mean in the PERMAFROST-r-veg simulation. Also shown are differences between PERMAFROST-r-veg and the simulation of the recent past climate (RP-r). Units are mm/month.

The drier climate in northern Europe is reflected in the seasonal cycle of precipitation as seen in Figure 3-52. For Sweden there is a reduction of more than a factor of two in winter and substantial reduction also during summer. Further south the reduction is most evident in the winter half of the year whereas in southernmost Europe the changes relative to the recent past climate are small for all months.

Precipitation in CCSM3 is more evenly spread over Europe than in RCA3, where the more detailed topography and land-sea distribution affect precipitation on local scale. In winter, RCA3 gives more precipitation in western Europe (Figure 3-53) as a result of topographic effects and less precipitation compared with CCSM3 in south-eastern Europe (not shown). This is also due to topographic effects. Since most precipitation in the area falls on the east coast of the Adriatic Sea, there is less precipitation left for the inner parts of the Balkan Peninsula. In summer, RCA3 gives about 30% more precipitation than CCSM3 in most of Europe, mostly due to topographic effects but also possibly due to differences in the parameterizations of convection in the two models.

Mean sea level pressure

The circulation pattern is about the same as today, but with weaker westerly flow over Europe in winter, and a more pronounced high pressure over the Atlantic outside south-western Europe in summer (Figure 3-54). The north-south pressure gradient between Iceland and Portugal is about 10 hPa lower in the PERMAFROST-r-veg simulation compared with RP-r. The inter-annual variability represented by the normalised NAO-index in Figure 3-54 is about as large as in the recent past climate. There are statistically significant correlations between the NAO index and precipitation and temperature for all three areas shown in Figures 3-50 and 3-53. In the Iberian Peninsula there is a strong negative correlation for precipitation (-0.65), whereas in west continental Europe and Sweden there are positive correlations for temperature (0.40 and 0.38, respectively) implying that winters are milder when the westerlies are stronger.

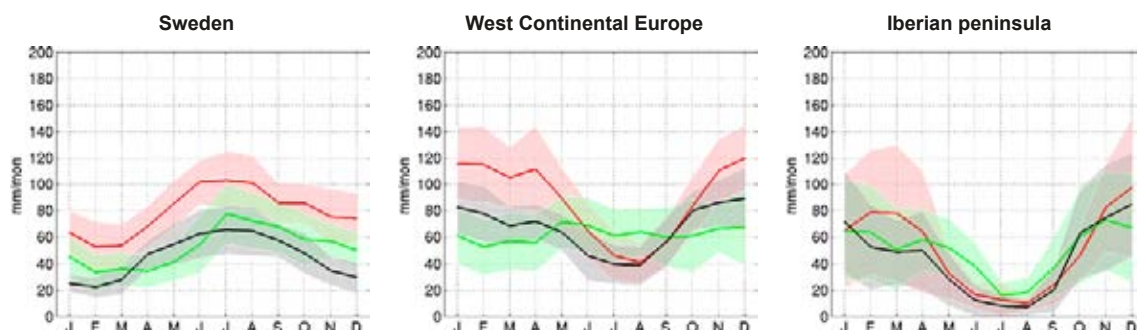


Figure 3-52. Annual precipitation range in PERMAFROST-r-veg (black), RP-r (red) and according to the CRU observational data (green). Shaded areas in corresponding colours indicate the ± 1 standard deviation range of individual monthly averages in the three data sets.

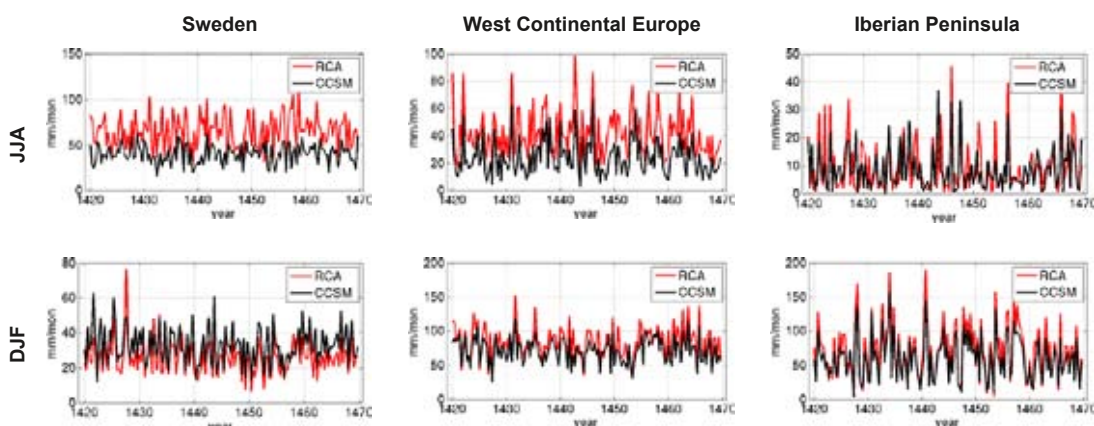


Figure 3-53. Summer (JJA) and winter (DJF) precipitation in RCA3 (PERMAFROST-r-veg, red) and CCSM3 (PERMAFROST, black). Units are mm/month.

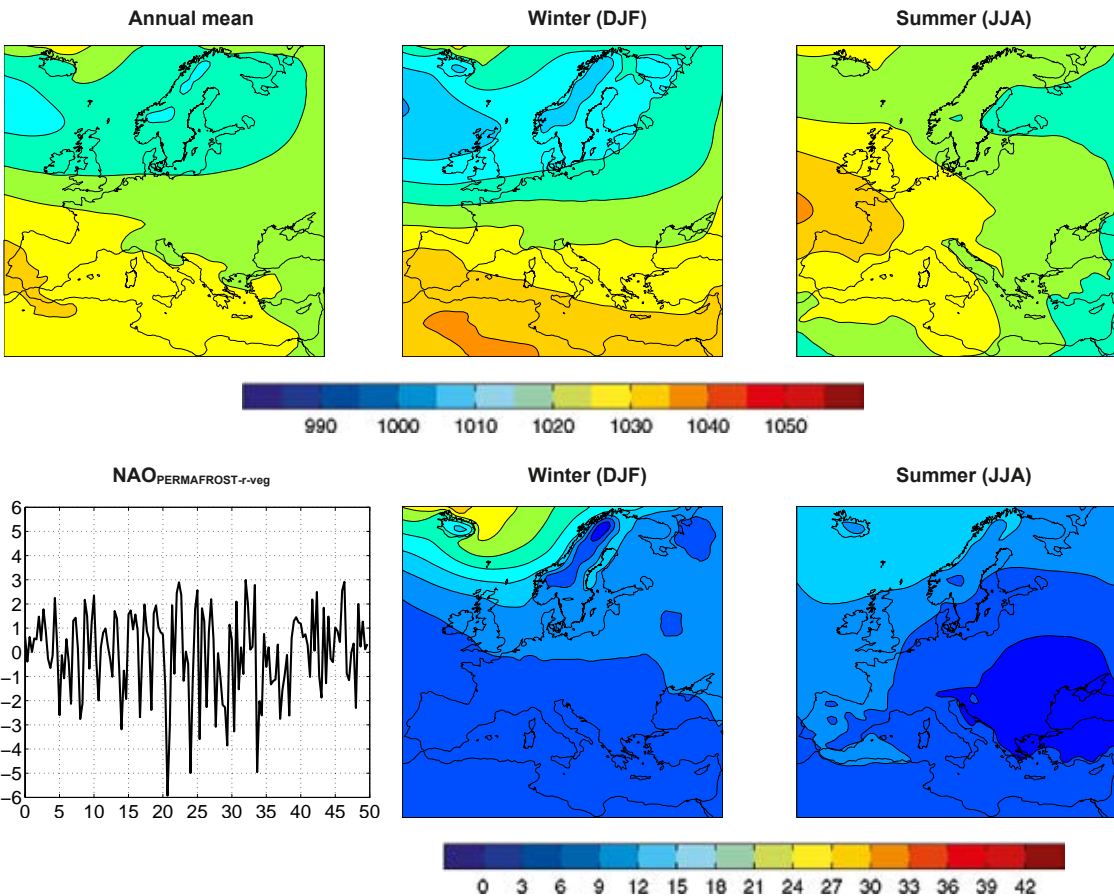


Figure 3-54. Annual and seasonal mean MSLP (top). The lower panels show winter (DJF) normalised NAO index in PERMAFROST-r-veg (left) and MSLP anomalies for differences between PERMAFROST-r-veg and the simulation of the recent past climate (right). Unit hPa.

3.3.3 Regional vegetation model simulations

The simulated vegetation distribution in the *permafrost case* is reminiscent of the LGM situation, but with a more northerly extent of needle-leaved forest, mountain birch type-woodland, and herbaceous vegetation, the latter extending into southern Sweden and central Finland (cf. Figures 3-55 and 3-36). Broadleaved trees and boreal conifers co-dominate the simulated forest in central Europe, whereas ‘Mediterranean’ type evergreen vegetation is restricted to southern coastal areas and northern Africa (Figure 3-55). The overall patterns appear broadly consistent with available reconstructions around MIS 3 based on pollen data, as summarised in Figure 2-15. In both cases, tree cover is mainly restricted to continental Europe and the Mediterranean coast, with treeless tundra (represented in LPJ-GUESS by the herbaceous plant functional type) possibly extending further north into the British Isles and Fennoscandia. The broadleaved birch may extend further northward beyond the boreal conifer forest (pine) limit around central Germany. Forest peters out into steppe or semi-desert vegetation in the Iberian Peninsula and Italy.

The vegetation simulated by LPJ-GUESS for the *permafrost case* bears little resemblance to the vegetation map used in CCSM3, which mainly comprises C₄ grasses over the non-ice areas of Europe (Figure 2-11, upper panel). For further discussion, see Section 3.1.3.

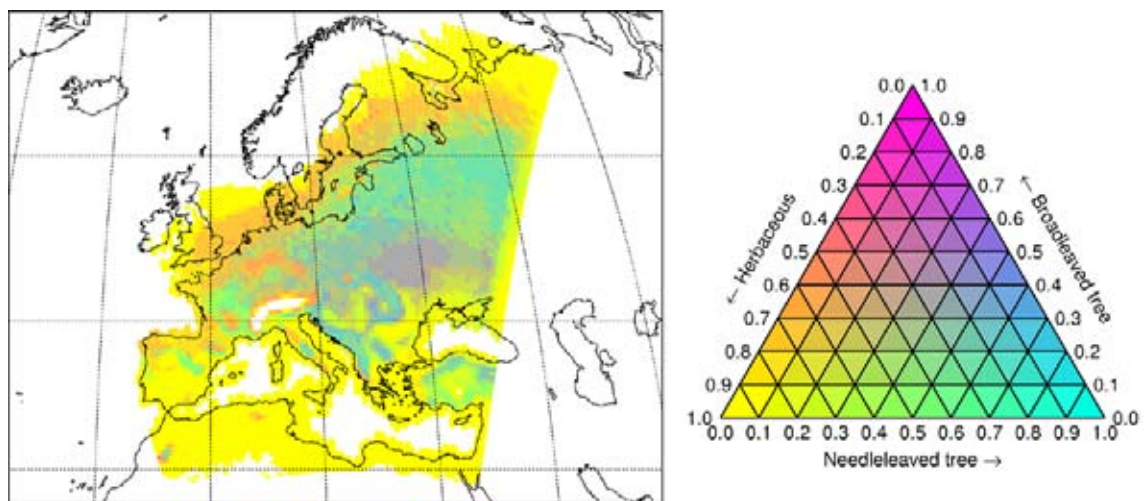


Figure 3-55. Vegetation map resulting from LPJ-GUESS simulation of the permafrost case forced by the initial climate from RCA3 (PERMAFROST-r).

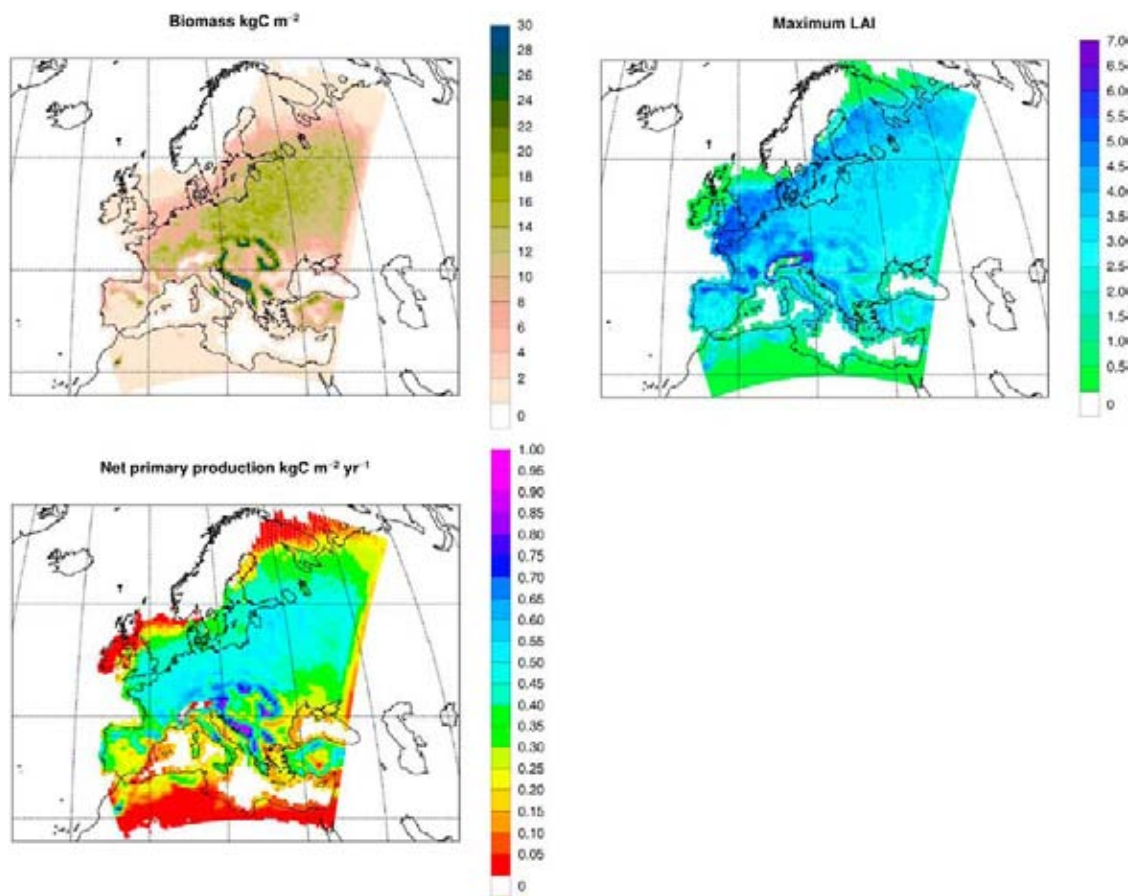


Figure 3-56. Vegetation biomass (kgC m^{-2}), maximal growing season leaf area index (LAI) and net primary productivity (NPP, $\text{kgC m}^{-2} \text{yr}^{-1}$) as simulated by LPJ-GUESS forced by the initial climate from RCA3 (PERMAFROST-r).

3.3.4 Synthesis of the permafrost case

Comparison with proxy data

The limited amount of proxy data restricts any profound evaluation of the model results. The simulated sea surface temperatures (SSTs) are in reasonable agreement with the few existing SST proxies that we have compared with. For the sites at high latitudes in the North Atlantic, the agreement is relatively good at some sites. Others, including two sites close to the British Isles, indicate that there may be a cold bias in the model. The comparison of terrestrial proxies with the regional climate model results shows that RCA3 is colder than the proxies indicated at the three available sites in the British Isles for the warmest month of the year. The differences are between 5 and 10°C for all three sites. This may indicate that summertime SSTs in parts of the North Atlantic are too low but it is highly uncertain as the proxies are representative of interstadial conditions. For all the other locations in western Europe where we have been able to compare RCA3 results with proxy based records, the agreement is reasonable (i.e. within ±5°C) and within the uncertainty ranges assigned to the proxies.

Comparison with other model studies

The regional temperature anomalies as simulated by RCA3 are in a qualitative agreement with the results shown by /Barron and Pollard 2002, van Huissteden et al. 2003/. In both of these studies, a RCM was used to downscale results from global climate model simulations for the MIS 3 period for the European area. The agreement appears to be better compared with their experiment with forcing conditions of a stadial than with those of an interstadial. Further, both Barron and Pollard and van Huissteden et al. show decreased precipitation compared with present-day conditions during summer and in most areas also during winter. A comprehensive comparison with their results is difficult as they have simulated a fairly small area that only encompasses half of the Fennoscandian ice sheet with a different land-sea distribution in the Baltic Sea region. Further, they only simulate a very short period (two times 3 years) which should be problematic as our results indicate a quite considerable inter-annual variability.

Do the results support a cold and dry climate favourable for permafrost growth and a restricted MIS 3 Fennoscandian ice sheet?

The *Permafrost case* was designed to test the hypothesis if a cold and dry climate favourable for permafrost growth would exist in the ice-free regions surrounding a Fennoscandian MIS 3 ice sheet with a restricted ice configuration (Figures 2-7 to 2-10). The temperature and precipitation in the regional climate model were used to make a first coarse analysis of whether the prerequisites for permafrost growth in Fennoscandia were satisfied.

/Heginbottom et al. 1995/ examined the relation between ground temperature and permafrost continuity. An annual ground temperature of between -5 and -2°C is defined as the boundary for extensive discontinuous permafrost (50–90% of landscape covered by permafrost) and -5°C and colder as the boundary for continuous permafrost (90–100%). However, it is also stated that a large part of the area with continuous permafrost has a ground temperature warmer than -5°C. As the ground temperature differs from the near-surface air temperature presented (Figure 3-47) by a few degrees we show simulated annual mean ground temperatures in Figure 3-57. In central and northern Fennoscandia, outside of the ice sheet, the modelled MIS 3 annual average ground temperature is colder than -5°C (Figure 3-57), which suggest that the climate conditions are favourable for development of continuous permafrost. South of this the modelled annual average ground temperature increases, reaching 0°C in the southernmost parts of Fennoscandia. The higher ground temperatures in the southern areas including northernmost Denmark, southern Sweden, Estonia and part of what today is the Baltic Sea and Gulf of Finland do not fulfil the thermal requirements for extensive permafrost. However, it is cold enough for sporadic permafrost (less than 50% of landscape covered), which may exist when the annual mean ground temperature is between 0 and -2°C. The temperature intervals of Heginbottom et al. are rather precise and the uncertainties in the model results lead to difficulties in the interpretation. However, the regional climate model does not show any large systematic biases in annual mean temperatures in the recent past climate, and the results of both the global and regional model are within the proxy-based uncertainty ranges. Based on these measures of the realism of the model simulations we conclude that conditions are favourable for permafrost growth in the suggested ice-free parts of Fennoscandia.

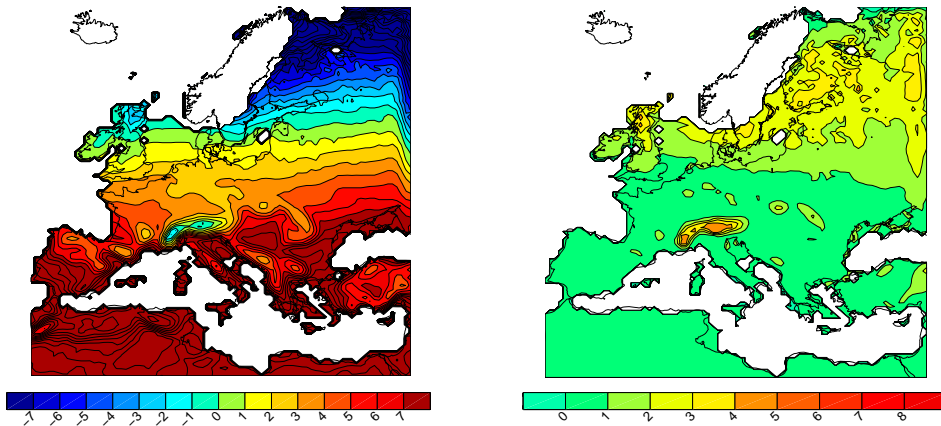


Figure 3-57. Annual mean soil temperature (left) and difference between near-surface temperature and the soil temperature (right) in the PERMAFROST-r-veg simulation. Units are °C.

As previously mentioned, our global and regional models do not include dynamical modelling of ice sheets and thus an ice sheet cannot form in the models, even if the climate conditions are favourable for ice sheet growth. The snow pack is, however, allowed to build up in the model. If the snow depth increases in time in a specific region, we can take this as an indication that an ice sheet would grow in this region if such processes were included in the model. However, the opposite situation, a lack of snow accumulation in front of, or at the margins of, a prescribed ice sheet, does not necessarily mean that the ice sheet would not grow (simply the lowermost part of the ice sheet would have a net mass loss, which is typical for ice sheets ending on land). Growth of the ice sheet could still well be possible if the precipitation over the ice sheet were large enough compared with its mass loss by melting, i.e. if conditions for the common pattern of ice sheet growth were satisfied.

In the PERMAFROST simulation, the snow depth in eastern Sweden and Finland (including the Forsmark, Oskarshamn and Olkiluoto regions) does not increase in time. The annual minimum snow depth (occurring in September) is close to zero (varying from 0–0.02 m equivalent water depth). For the issue of whether the simulated climate is in line with the prescribed restricted ice sheet configuration (Figures 2-7 to 2-10 and 4-1 to 4-2.), we can therefore conclude that 1) an ice sheet would not grow locally from the local precipitation in front of the ice margin, 2) the modelled temperature and precipitation climate in front of the ice sheet is consistent with the assumed ice-free conditions and restricted ice sheet coverage, but it does not exclude the possibility of a larger ice sheet, and 3) given the restricted Fennoscandian ice sheet configuration (Figure 2-7 and 4-1), the simulated periglacial climate would support permafrost growth in the ice-free areas of Sweden and Finland.

4 Extreme climate conditions in Sweden and Finland – synthesis

4.1 General features of the simulated climate for the different cases

Global and Fennoscandian averages

We start this section with a comparison of some of the general features of the climate as simulated in the global and regional climate models for the three cases; *warm*, *glacial* and *permafrost*. The range of experiments performed allows us to discuss the climate under very different forcing conditions. Table 4-1 summarizes some of the results for the different simulations, facilitating comparison over the different cases.

The temperature climate in northern Europe differs substantially between the different cases with the most pronounced differences for wintertime conditions. In Sweden and Finland, winter seasonal mean temperature is more than 40°C higher in the *warm case* compared with the climate over the ice sheet in the *glacial case* for winter and more than 20°C higher for summer. The corresponding range in global annual mean temperatures is about 10°C. Also, the precipitation climate differs between the cases with generally more precipitation the warmer it gets. The sensitivity experiment for LGM with increased dust load and a different vegetation in the global model (LGM-vd) leads to an even colder climate. For temperature in Sweden, this is particularly clear for winter conditions, which are on average 3°C lower in this simulation compared with the reference simulation for the *glacial case* (LGM2).

Geographical differences

The local and regional climate is highly dependent on local forcing conditions such as land-sea distribution, extent and shape of ice sheets, elevation of mountains etc. Figure 4-1 shows in detail the land-sea mask and the extent of ice sheets in the Fennoscandian area for the three cases. Also indicated in Figure 4-1 are the grid boxes closest to, and surrounding, the three geographical locations Forsmark, Oskarshamn and Olkiluoto that are discussed in more detail in Section 4.2. The extent (Figure 4-1) and elevation of the ice sheet (Figure 4-2) differs significantly between the three cases. In the glacial case the Oskarshamn, Forsmark and Olkiluoto sites are situated under the ice sheet, while the grid box locations describe the climatic situation at the ice sheet surface. This implies that the local climate at the grid box locations is determined, in part, by the distribution of climatic conditions over larger parts of the ice sheet. In this particular case the local climate as presented here is a possible climate at the surface of the ice sheet, and not the climate for the three sites in question. There are also differences in the extent of the Baltic Sea in the different cases due to land uplift and sea level changes.

Table 4-1. Differences in global mean temperature (T_{agm}) as well as seasonal mean temperature and precipitation over Sweden for the different simulations compared with the recent past climate (1961–2000). For RCA3, the numbers are from the simulations with the new vegetation from LPJ-GUESS. DJF stands for December–February and JJA for June–August. Units are °C and mm/month.

Simulation	CCSM3	RCA3 – Sweden seasonal mean averages			
		ΔT_{agm}	ΔT_{djf}	ΔT_{jja}	$\Delta \text{PRECIP}_{\text{djf}}$
WARM-v	+2.4	–	–	–	–
WARM	+2.1	+4.0	+3.5	+24 (+37%)	0 (0%)
Recent past	0	0	0	0	0
Pre-industrial	-1.3	–	–	–	–
PERMAFROST	-5.6	-30.2	-10.5	-38 (-60%)	-38 (-38%)
LGM1	-5.8	–	–	–	–
LGM2	-6.9	-37.2	-16.2	-40 (-63%)	-50 (-48%)
LGM-v	-7.5	–	–	–	–
LGM-vd	-8.5	-40.5	-17.4	-43 (-68%)	-53 (-52%)

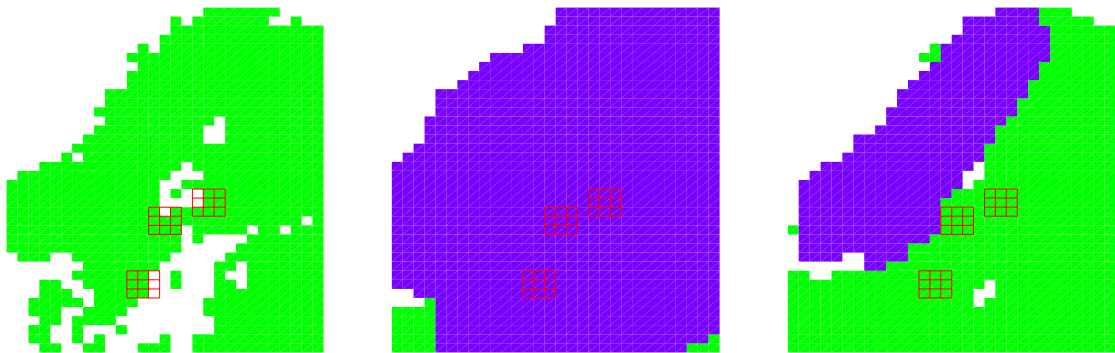


Figure 4-1. Land (green) and ice extent (blue) in RCA3 in the Fennoscandian region in the warm (left), glacial (middle) and the permafrost (right) case. The 3x3-grids marked in red represent the RCA3 grid box covering the three locations (centre box) and the eight surrounding boxes. Grid boxes with a land fraction lower than 20% are not filled.

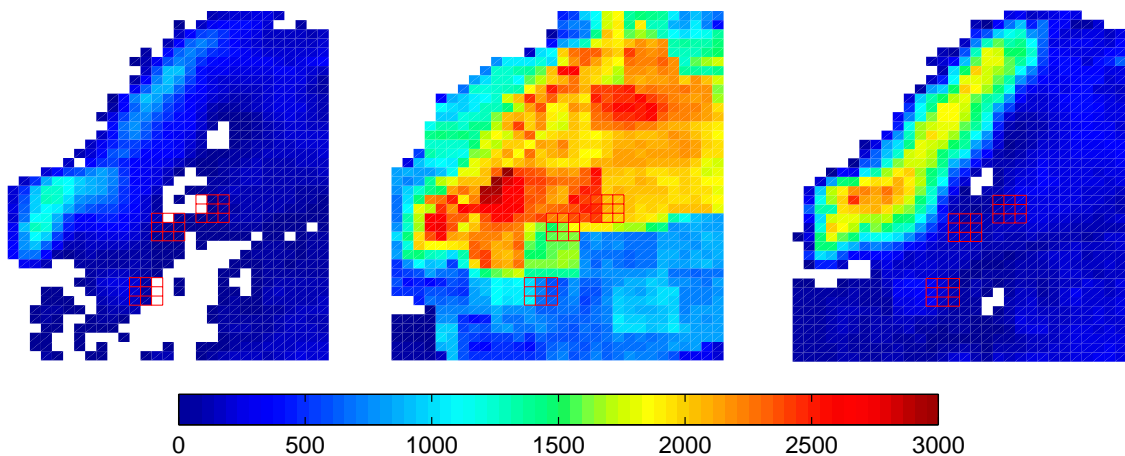


Figure 4-2. The distribution of land areas and elevation (m above the sea-level in each case) in RCA3 in the Fennoscandian region for the warm (left), glacial (middle) and permafrost (right) cases. The 3x3-grids marked in red represent the RCA3 grid box covering the three locations (centre box) and the eight surrounding boxes. Grid boxes with a land fraction lower than 20% are not filled.

Temperature

The highly different temperature climatic conditions in the Fennoscandian region in the three cases are illustrated in Figure 4-3. Maximum differences between coldest and warmest climates exceed 30°C in annual mean temperatures mainly due to the presence of the ice sheet in the *glacial case*. Even larger temperature differences are seen for winter which is the season with the strongest changes relative to the recent past climate (see also Figure 4-4). The spatial patterns are relatively similar in the *warm case* and the recent past climate albeit with higher temperatures in all areas in the *warm case*. The stronger climate change signal for winter compared with summer is seen in the *warm case* for most of the area. An exception is an area of what today are the northern parts of the Baltic Sea but in the future becomes land due to land uplift (see also Section 3.1.2). In that particular area, future forests in the grid boxes promote higher temperatures in summer than over the Baltic Sea in the recent past climate. Also in the *permafrost case* there is a large change in summer temperatures over parts of what is today the Baltic Sea. Again, it has to do with the fact that these land areas were exposed to the atmosphere due to the lower sea level in the *permafrost case*. The spatial pattern of differences between the recent past climate and the two cold climates differ somewhat due to the different extent and altitude of the ice sheet in the two cold cases. In the *permafrost case*, the largest differences are in the northern parts of Fennoscandia, whereas in the *glacial case* differences are more widespread over the ice sheet.

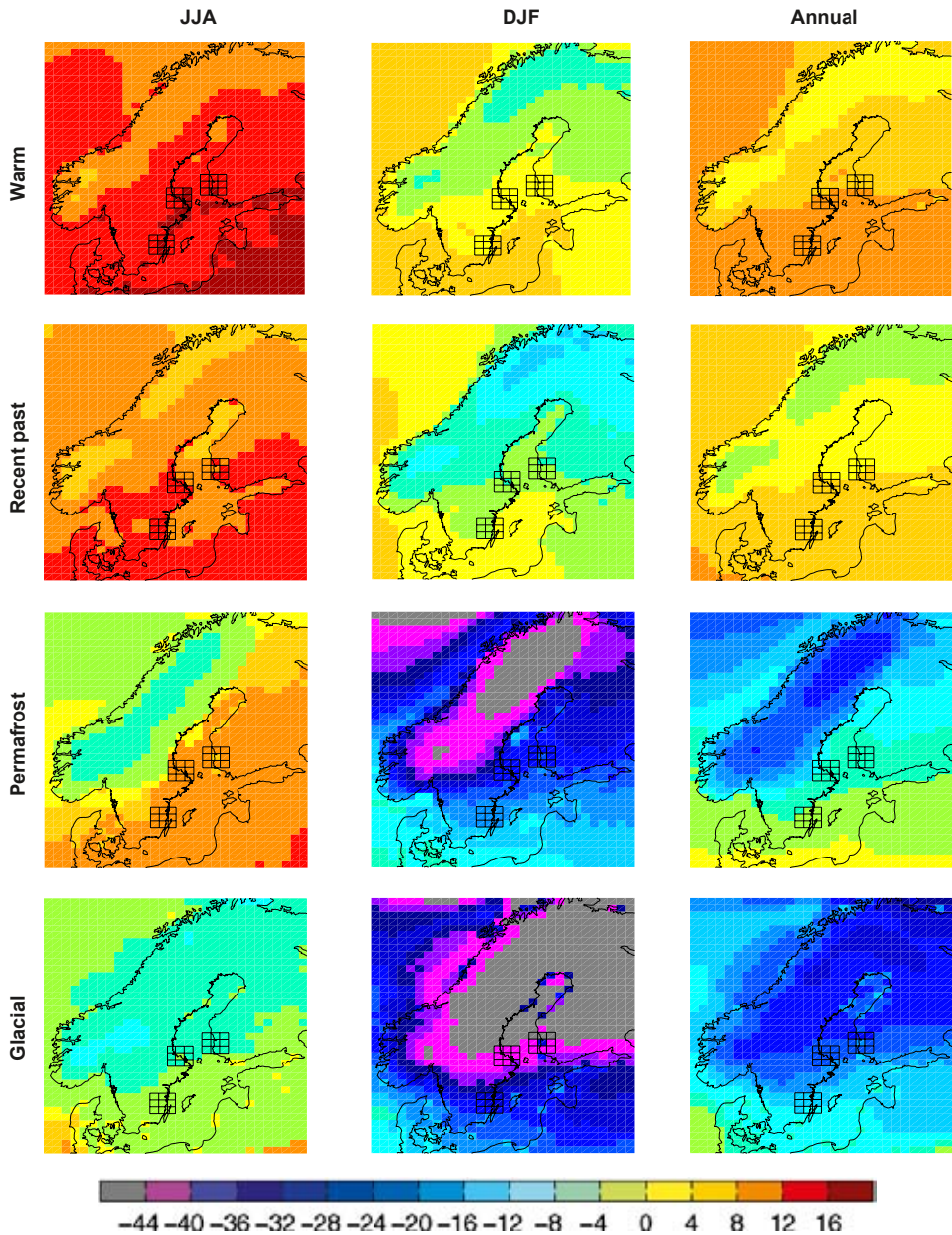


Figure 4-3. Seasonal and annual mean temperature for the three cases and for the recent past (1961–2000). The data are taken from the simulations WARM-r-veg (warm case), RP-r (recent past), PERMAFROST-r-veg (permafrost) and LGM2-r-veg (glacial). Units are °C.

The fact that the glacial climates were indeed very cold can be exemplified by the fact that the summer temperatures in the *glacial case* were as low as the average winter condition temperatures in the recent past climate. This is mostly a regional topographic effect of the ice sheet, south of the ice sheet differences are not that large (cf. Figure 3-27, first row). A similar situation prevails in the *permafrost case*, with low summer temperatures located on the ice sheet and higher temperatures elsewhere. Also, the fact that the North Atlantic was cold in the *glacial* and *permafrost cases* can be seen in the temperatures off the Norwegian coast (off the ice sheet) as these are below 0°C all year round in both cases (Figure 4-3) where there is extensive sea ice cover (cf. Figure 3-39). The comparison of the SSTs in the global model to proxy-based information does not show unduly cold conditions in the *permafrost case* as was found in the *glacial case*. This better agreement with the proxies indicates that such low temperatures were indeed possible in the *permafrost case*.

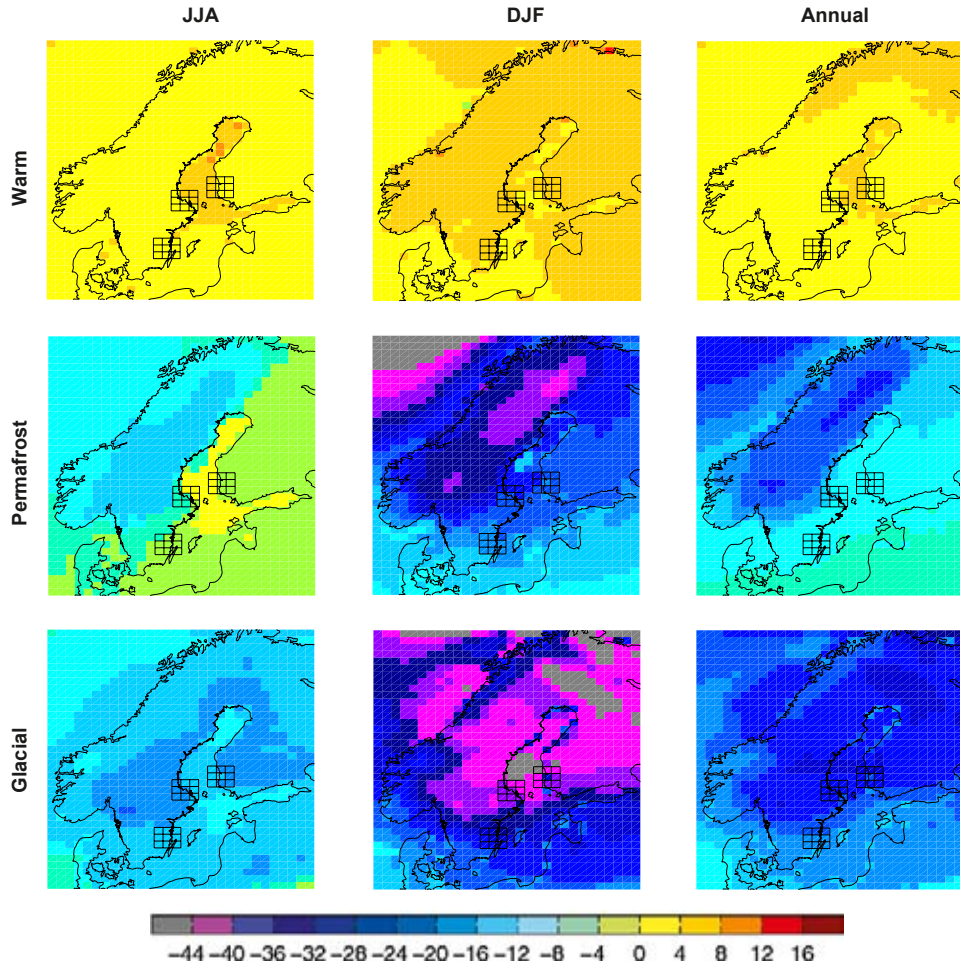


Figure 4-4. Changes in seasonal and annual mean temperature when the three cases are compared with the recent past climate. The data are taken from the simulations WARM-r-veg (warm case), PERMAFROST-r-veg (permafrost) and LGM2-r-veg (glacial). The reference simulation is the RP-r (recent past). Units are °C.

Precipitation

As for temperature, precipitation shows large differences between the different cases (Figure 4-5). The climate in the Fennoscandian region is generally wetter the warmer it gets. Specifically, this is consistent with many other climate change scenarios for the 21st century and also in general agreement with the fact that a warmer atmosphere can hold more water vapour. Increasing precipitation with increasing temperatures as a result of increasing moisture convergence has been shown for the northern mid latitudes by /Held and Soden 2006/. The largest amounts of precipitation are localized to the mountainous areas in the recent past and future warm climates. Also in the colder climates, the elevation plays a role with a precipitation maximum in south-western Norway as can be seen for the *permafrost case* (Figure 4-5, third row). In the *glacial case*, the precipitation maximum was shifted even further to the south in winter. In summer, there is also precipitation over the ice sheet and in this season the local topography plays a role in generating precipitation.

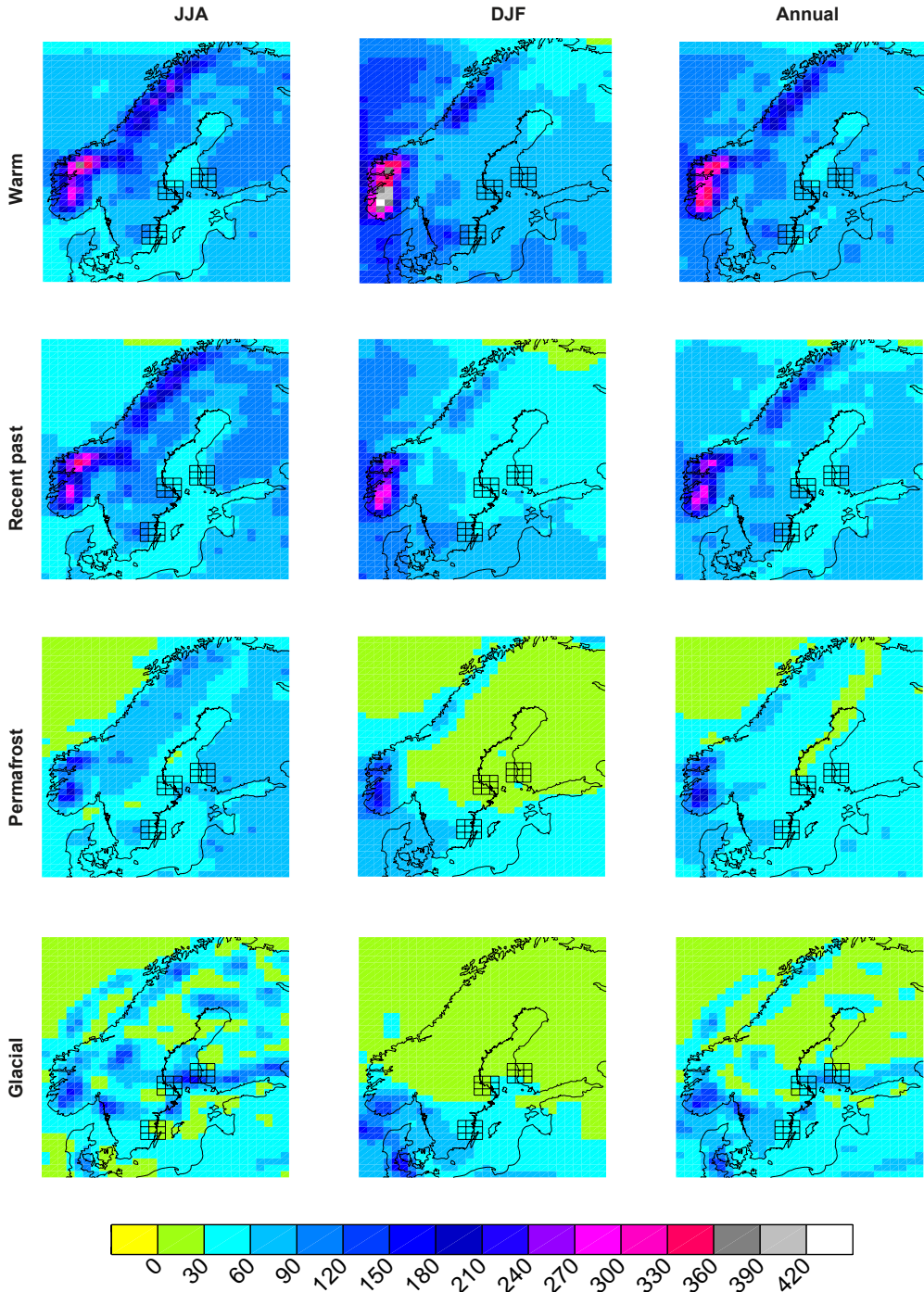


Figure 4-5. Seasonal and annual mean precipitation in the three cases and for the recent past (1961–2000). The data are taken from the simulations WARM-r-veg (warm case), RP-r (recent past), PERMAFROST-r-veg (permafrost) and LGM2-r-veg (glacial). Units are mm/month.

The changes in precipitation between the recent past climate and the three different cases are seen in Figure 4-6. The overall wetter conditions for wintertime conditions in the *warm case* are clear. In summer the differences are smaller, but there is an indication that the precipitation may increase slightly in the north. For the cold climates there is instead a marked decrease in precipitation. This decrease is largest in the *glacial case* and most so during winter in the north over the high-altitude parts of the ice sheet. Also the *permafrost case* shows its largest decreases during winter. The changes in summer seem to be more related to local effects of the elevation and/or extent of the ice sheets.

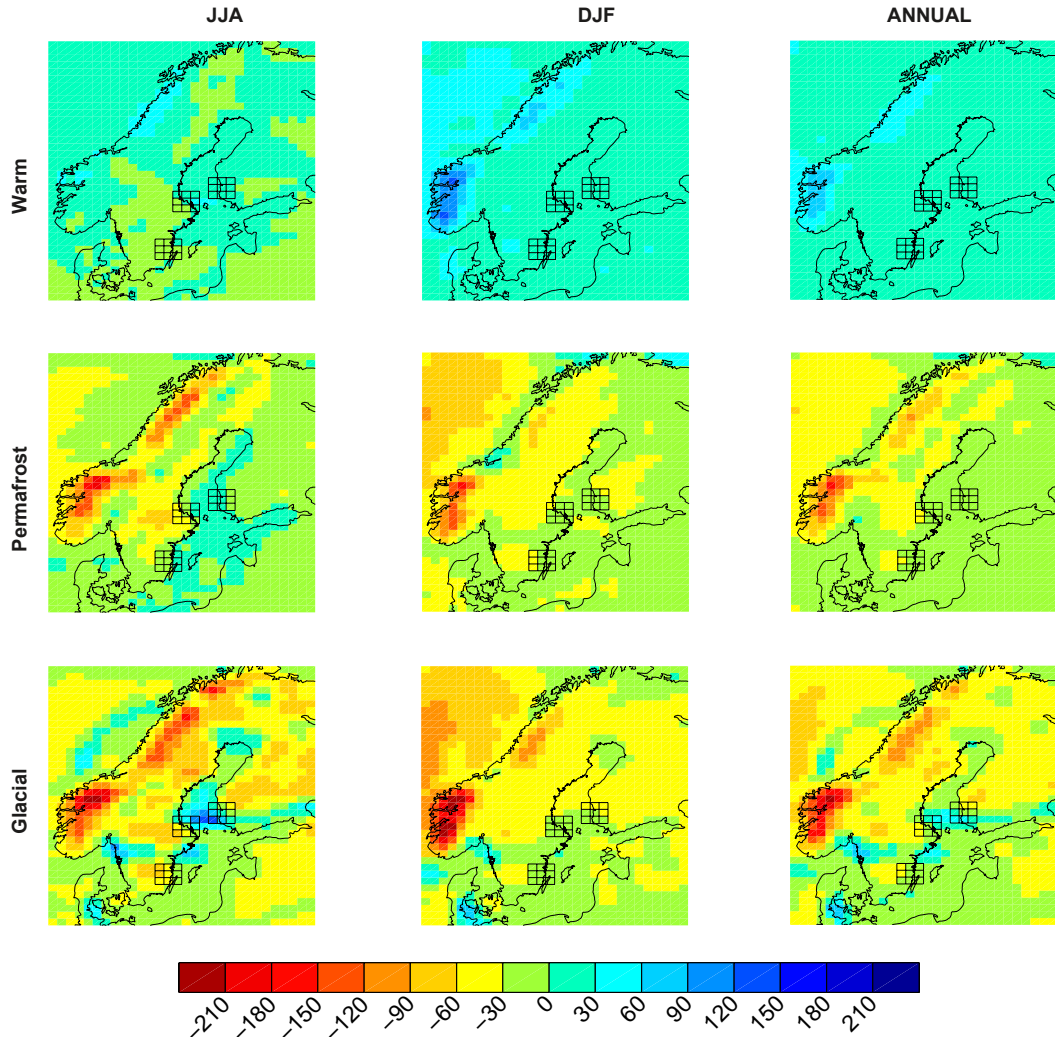


Figure 4-6. Changes in seasonal and annual mean precipitation when the three cases are compared with the recent past climate. The data are taken from the simulations WARM-r-veg (warm case), PERMAFROST-r-veg (permafrost) and LGM2-r-veg (glacial). The reference simulation is the RP-r (recent past). Units are mm/month.

4.2 Climate conditions at three sites in Sweden and Finland

Location of sites and choice of simulations for which a detailed analysis is made

In this section we present and discuss results from the regional climate model specifically for three sites: Forsmark (60.4°N 18.1°E) and Oskarshamn (57.3°N 16.4°E) on the Swedish east coast, and Olkiluoto (61.35°N 21.6°E) on the Finnish west coast (see Figure 3-1 for locations). For these sites, we have extracted and analysed data from the WARM-r-veg, LGM2-r-veg and PERMAFROST-r-veg simulations, respectively. These three simulations are internally consistent in that they have all been forced with regional vegetation as simulated based on preliminary regionalizations with RCA3.

Illustrating uncertainties by looking at more scenarios

In addition to the three selected simulations for the three cases, we also show data from the simulation of the recent past climate (RP-r) and from the CRU observations representing conditions in the late 20th century. In addition to this, we also show results from three other climate-change simulations with RCA3 for the 21st century as described in /Persson et al. 2007/. These simulations follow the A2, A1B and B2 emission scenarios /Nakićenović and Swart 2000/. We recall from Section 3.3.4 that the A1B emission scenario leads to greenhouse gas concentrations close to our *warm case* by

the end of the 21st century. The two other scenarios have more (A2) or less (B2) emissions than the A1B scenario. The boundary data for these three experiments have been taken from the AOGCMs ECHAM4 /Roeckner et al. 1999/ and ECHAM5 /Roeckner et al. 2006/. As these two AOGCMs have different climate sensitivities compared to CCSM3 we sample more of the model uncertainty by comparing to those simulations. The largest difference in climate sensitivity is for the ECHAM5 model that has an equilibrium climate sensitivity of 3.4°C and a transient response of 2.2°C. These numbers could be compared to CCSM3 (2.7°C and 1.5°C respectively). Also, as different AOGCMs simulate different regional response to changes in forcing, the addition of these scenarios can help illustrating some of the inherent uncertainty in using only one AOGCM.

Characteristics of the sites and their surroundings in the regional climate model

We have extracted information from the grid point located closest to the three sites. As there is a high degree of spatial heterogeneity in land-sea distribution and topography, we have also looked at the information from the surrounding eight grid boxes to discuss uncertainties related to these in homogeneities (cf. Figure 4-1).

In the *warm case*, all three sites are located close to the Baltic Sea (Figure 4-1) and the fraction of land ranges between 0 and 95% in all three 3x3 grid box areas. The land parts of these grid boxes are almost entirely dominated by forests. As the seasonal cycle of temperature is lower over sea compared with the grid boxes further inland, this will induce a geographical spread in the data. The elevation of the grid boxes is fairly similar in all three areas surrounding the three sites for the *warm case* (Figure 4-2), the largest difference between two grid boxes is 200 m and it is found in the Oskarshamn area.

In the *glacial case*, all three sites are located below interior parts of the ice sheet. A closer inspection of the topography reveals large horizontal differences, as the Forsmark and Olkiluoto regions are below the outskirts of the most elevated parts of the ice sheet whereas the Oskarshamn site is situated under an area with less thick ice. Differences in altitude between lowest and highest elevated grid boxes, out of the nine extracted for each area, are about 800 m for Forsmark, 450 m for Oskarshamn and 400 m for Olkiluoto. Such large differences in altitude imply large differences in air temperature (the lapse rate in the standard atmosphere is 5°C over 800 m). Also the precipitation climate will be influenced by these altitude differences as these will lead to increased/decreased precipitation depending on the direction of the flow of air in relation to the slopes of the ice sheet.

In the *permafrost case* all three sites are situated outside the prescribed ice sheet configuration, in areas relatively distant (> 200 km) from the ice sheet margin, with the exception of Forsmark where the distance is closer (about 100 km). Also, the altitude range is more modest in this case, with ranges of typically 50–300 m in the three regions. The main difference in the model configuration compared with the recent past climate case is the absence of the Baltic Sea, due to the 70 m lowering of the sea level in this case.

4.2.1 Forsmark

The recent past climate (1961–1990)

The combination of RCA3 downscaling results from CCSM3 shows a fairly good representation of the recent past (1961–1990) temperature climate in the Forsmark region (Figure 4-7, top row, second column). There exists some spatial variability (indicated by the shaded area in Figure 4-7) in the Forsmark area with a maximum in spring. This maximum is a consequence of the proximity to the Baltic Sea that is still relatively cold in this season when land areas are heated more quickly. The low temperatures during winter allow for a fairly extensive snow cover during January and February (Figure 4-7, bottom row, second column). Runoff shows a weak maximum in the early spring associated with the snowmelt (Figure 4-7, third row, second column). The geographical spread in runoff is fairly large, but for partly the wrong reason as some adjacent grid boxes represents the Baltic Sea from which no runoff is calculated in the model. The geographical spread is larger for precipitation (Figure 4-7, second row, second column). Again, as for temperature, this large spread reflects the heterogeneity of the area with the central grid box in close proximity to the Baltic Sea. The phase and amplitude of the seasonal cycle of precipitation differ from the observations. The maximum is reached about one month earlier and the winter precipitation is higher in the model than in the

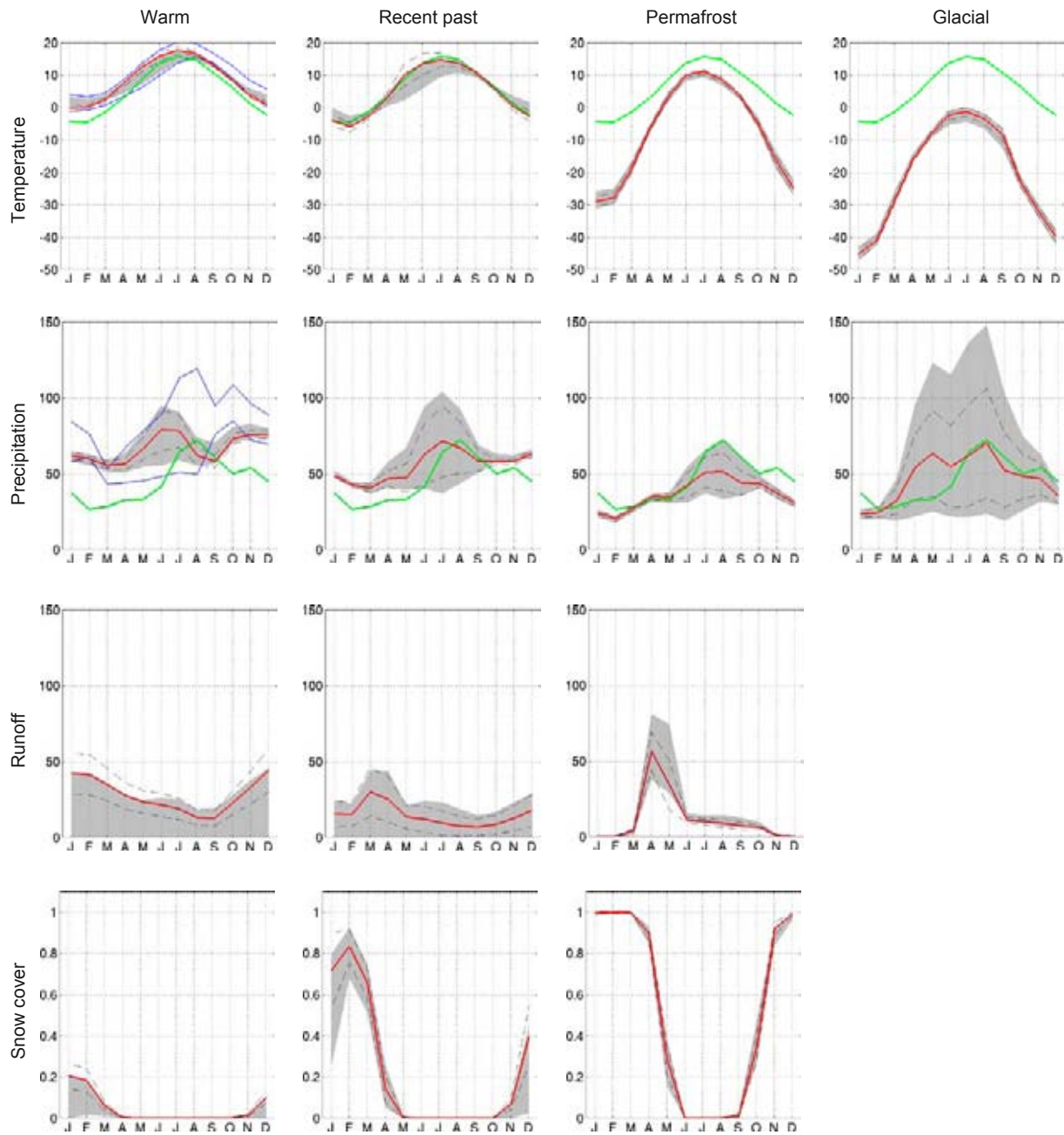


Figure 4-7. Simulated seasonal cycles of temperature ($^{\circ}\text{C}$), precipitation (mm/month), runoff (mm/month) and snow fraction (dimensionless ranging from 0 to 1) at the grid box closest to the Forsmark site (red line). The spatial variability in the 3x3-grids (see Figures 4-1 and 4-2) is displayed with the dashed lines representing ± 1 standard deviation calculated from the 9 grid boxes, and the grey area representing the absolute maximum and minimum of the 9 grid boxes. The green line for temperature and precipitation is the observed seasonal cycle from the CRU data set in the period 1961–1990 (see the text). In the warm case, an additional uncertainty range defined by ± 1 standard deviation of the data calculated from the 9 surrounding grid boxes from three additional simulations for the 21st century with RCA3 is shown with blue full lines.

observations. The fact that there is more precipitation in the model during the winter half of the year is partly attributed to biases in the global model (Section 2.3.1) but may also partly be related to a problem with under-catch in the observations (Section 2.3.2).

The warm case

The fairly small annual temperature range in the recent past climate is even smaller in the future warm climate for the Forsmark area (Figure 4-7, upper row, first column). This reduction in the seasonal cycle of temperature is a consequence of the future warming being stronger in winter than in summer. The snow season is much shorter, or even totally absent, in the warm climate. The seasonality of the runoff is closely connected to the presence or absence of snow. In the warmer future climate, the spring peak in runoff is absent and there is now a more widespread wintertime maximum related to the large amounts of precipitation for that season.

The spread in the presented variables due to differences in geographical location is reduced compared with that in the simulation of the recent past climate. This is partly a result of the land uplift turning two of the Baltic Sea grid boxes to the east of Forsmark into land in the warm case. Thereby, the surrounding area becomes more homogeneous than in the present-day situation.

When including also the uncertainty ranges based on results from the three other climate simulations for the 21st century, also simulated with RCA3 /Persson et al. 2007/, it is seen that the weakening of the annual cycle is a robust trend when going to a warmer climate. (Figure 4-7, upper left). For precipitation, it is obvious that the uncertainty ranges are larger for all months when taking also the three 21st century simulations into consideration (Figure 4-7, second row, left).

The glacial case

For the *glacial case*, the largest differences compared with the recent past temperature climate are seen in winter, as expected yielding a completely different annual cycle due to the presence of the ice sheet (Figure 4-7, upper row, fourth column). The geographical spread close to the Forsmark grid box is smaller than what would be expected from the large differences in altitude of ca 800 m between the 9 grid-boxes in the 3x3 grid surrounding Forsmark. As the monthly mean temperature is always below 0°C there is a permanent snow cover on top of the ice sheet, which means that the Forsmark site is located under the ice sheet accumulation area, upstream of the ice sheet equilibrium line. As the representation of the ice sheet is crude in our study (see Section 2.3.3) we do not show runoff or snow cover for the *glacial case*. The main change in the precipitation climate is that the geographic spread becomes much more pronounced in the *glacial case* compared to the recent past climate. This is probably related to the highly heterogeneous terrain (see also Figure 4-5). In terms of fluxes, precipitation is as large, or larger, than in the recent past climate during summer but notably lower in winter (Figure 4-7, second row, fourth column).

The permafrost case

As for the glacial climate, the largest difference compared with the recent past climate in the seasonal cycle of temperature is seen in winter. The resulting seasonal cycle is almost as strong as in the *glacial case*, albeit with generally higher temperatures (Figure 4-7, upper row, third column). For this case, the surrounding area in RCA3 is fairly homogeneous in terms of altitude and surface characteristics, leading to a small geographical spread in climate characteristics across the area (Figures 4-1 and 4-2). In this permafrost climate, there is a very strong seasonal cycle in snow cover as the temperatures during summer get well above 0°C allowing complete snow melting (Figure 4-7, upper and lower row, third column). The length of the completely snow-free season is three months according to the model and there seems to be a more or less constant snow cover during at least 3 months. In the permafrost climate, there is a clear spring peak in runoff connected to the snow melt which is more extensive than in the recent past climate, since more snow is accumulated on the ground during the winter. During the remaining part of the year, the runoff is fairly small, due to the cold conditions during winter and the relatively small amounts of precipitation during summer. In the permafrost climate, the precipitation is lower than in the recent past climate for most parts of the year. Also the geographical spread is smaller for this case. This is most likely a consequence of the more homogeneous terrain with all surrounding areas being land.

The annual mean ground temperature is about -4°C (Figure 3-57). According to /Heginbottom et al. 1995/ these temperatures indicate that climate conditions are favourable for discontinuous permafrost (covering 50–90% of the landscape). We can also note that the precipitation is low in this case compared with the glacial climate. The cold and dry climate with partially snow-free conditions implies that the climate is very favourable for permafrost growth.

4.2.2 Oskarshamn

The recent past climate (1961–1990)

Also for Oskarshamn, the combination of RCA3 and CCSM3 shows a fairly good representation of the recent past climate (1961–1990), although with a somewhat too weak seasonal cycle in temperature (Figure 4-8). The spatial variability in temperature is small, implying that the underestimate of the amplitude of the seasonal cycle is not related to local geographical features. The temperatures during winter are relatively high, and there is less snow and a shorter snow season at Oskarshamn than at Forsmark and Olkiluoto. The maximum snow cover occurs in February, but the simulated fractional coverage is lower by about 50% compared with that at Forsmark. The snowmelt induces a maximum in runoff in early spring. High temperatures and thereby efficient evaporation leads to only little runoff in summer. The seasonal cycle of precipitation is fairly subdued with a weak maximum in December, which is in contrast to the CRU observations showing a maximum in summer (Figure 4-8, second row, second panel). But, the geographical spread in precipitation is large and some of the adjacent grid boxes receive most precipitation in summer more in line with the observations. Again, as at Forsmark, there is more precipitation than observed during the winter half of the year.

The warm case

The small annual temperature range in the recent past climate is even smaller in the future warm climate for the Oskarshamn area (Figure 4-8, upper row, first column), just as at Forsmark. The snow season is much shorter, or even totally absent, in the warm climate as monthly mean temperatures mostly exceed 0°C . The characteristic snow melt peak in runoff in the recent past climate is absent. Instead, runoff shows a maximum in winter when there is more precipitation. In summer, runoff is low due to high temperatures and related evaporation. Precipitation shows a maximum in summer and a secondary maximum in winter. The geographical spread in the presented variables is reduced compared with that in the simulation of the recent past climate.

When including also the uncertainty ranges based on results from the three other climate simulations for the 21st century /Persson et al. 2007/, it is seen that the weakening of the annual cycle is a robust trend when going to a warmer climate. (Figure 4-8, upper left). For precipitation, it is obvious that the uncertainty ranges are larger for all months when taking also the three 21st century simulations into consideration (Figure 4-8, second row, left).

The glacial case

For the *glacial case* the largest differences compared with the recent past temperature climate is seen in winter, yielding, as expected, a completely different annual cycle due to the presence of the ice sheet (Figure 4-8, upper row, fourth column). The geographical spread in temperature close to the Oskarshamn grid box is small smaller than what would be expected from the large differences in altitude of ca 550 m between the 9 grid-boxes in the 3x3 grid surrounding Oskarshamn. As the monthly mean temperature is always below 0°C there is a permanent snow cover on top of the ice sheet simulated by the model, which means that also the Oskarshamn site is located under the ice sheet accumulation area, upstream of the ice sheet equilibrium line. As the representation of the ice sheet is crude in our study (see Section 2.3.3) we do not show runoff or snow cover for the *glacial case*. The main change in the precipitation climate is that the geographic spread becomes much more pronounced in the *glacial case* compared with the recent past climate. This is probably related to the highly heterogeneous terrain (see also Figure 4-5). In terms of fluxes, precipitation is almost as large as in the recent past climate during winter but notably lower in summer (Figure 4-8, second row, fourth column).

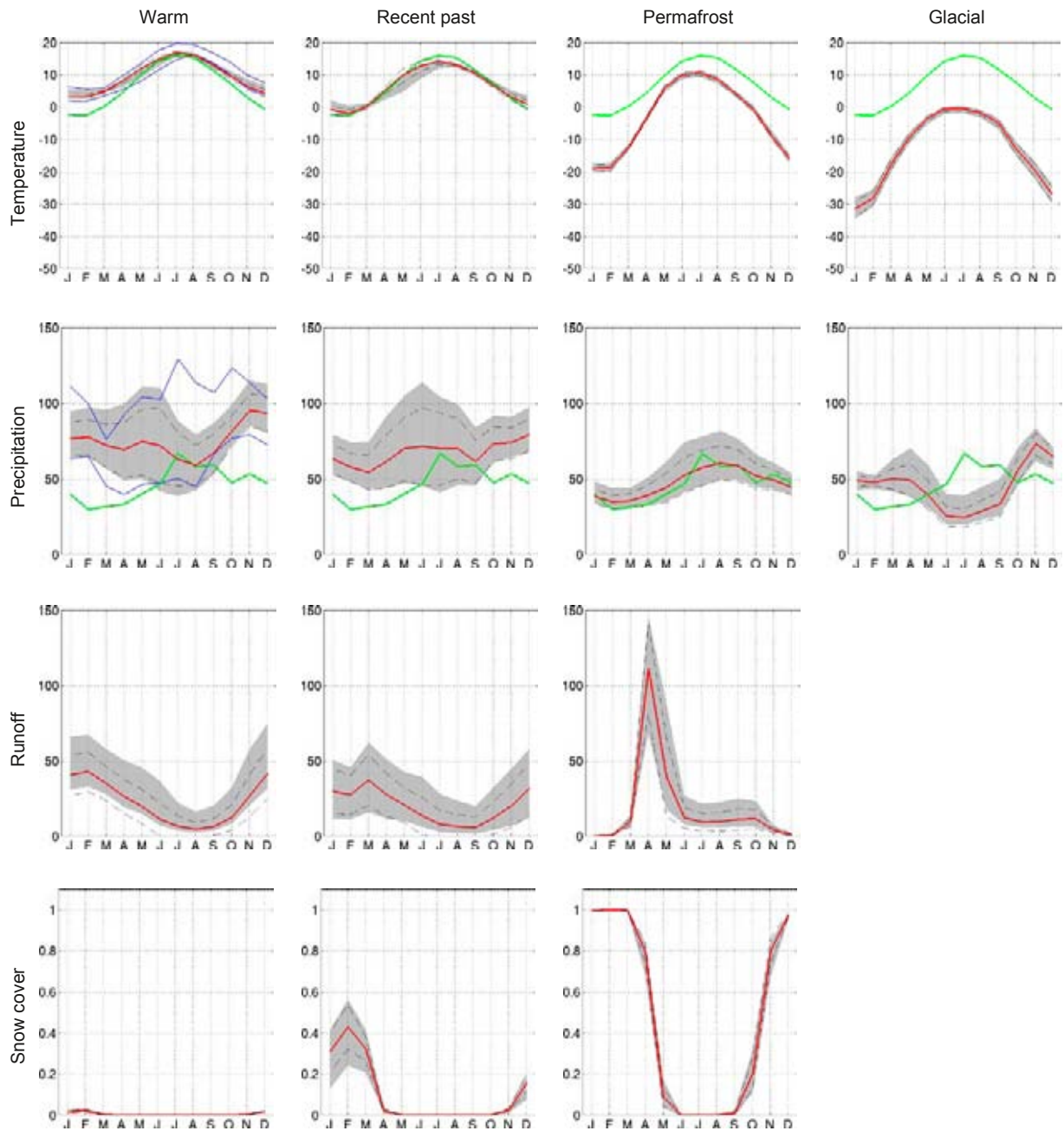


Figure 4-8. Simulated seasonal cycles of temperature ($^{\circ}\text{C}$), precipitation (mm/month), runoff (mm/month) and snow fraction (dimensionless ranging from 0 to 1) at the grid box closest to the Oskarshamn site (red line). The spatial variability in the 3x3-grids (see Figures 4-1 and 4-2) is displayed with the dashed lines representing ± 1 standard deviation calculated from the 9 grid boxes, and the grey area representing the absolute maximum and minimum, of the 9 grid boxes. The green line for temperature and precipitation is the observed seasonal cycle from the CRU data set in the period 1961–1990 (see the text). In the warm case, the uncertainty range (blue lines) is defined by ± 1 standard deviation of the data calculated from the 9 surrounding grid boxes from three additional simulations for the 21st century with RCA3.

The permafrost case

As for the *glacial case*, the largest difference compared to the recent past climate in the seasonal cycle of temperature is seen in winter. The resulting seasonal cycle is almost as strong as in the *glacial case* albeit with year-round higher temperatures (Figure 4-8, upper row, third column). For this case, the surrounding area in RCA3 is fairly homogeneous in terms of altitude and surface characteristics leading to a small geographical spread in the area (Figures 4-1 and 4-2). In the permafrost climate, there is a very strong seasonal cycle in snow cover, as the temperatures during summer get well above 0°C allowing for a complete snow melting (Figure 4-8, upper and lower row, third column). The length of the completely snow-free season is three months according to the model and there seems to be a more or less constant snow cover during at least 3 months. In the permafrost climate, there is a clear spring peak in runoff connected to the snow melt which is more extensive than in the recent past climate, as more snow is accumulated on the ground during the winter. During the remainder of the year the runoff is fairly small, due to the cold conditions during winter and the relatively smaller amounts of precipitation during summer. In the permafrost climate, the precipitation is lower than in the recent past climate for most parts of the year. Also the geographical spread is smaller for this case, most likely as a consequence of the surrounding areas being land.

The annual mean ground temperature is close to -1°C (Figure 3-57). According to /Heginbottom et al. 1995/ such a temperature indicates that sporadic permafrost (covering less than 50% of the landscape) is possible. We can also note that the precipitation is low in this case as in the glacial climate. The cold and dry climate with partially snow free conditions implies that the conditions are very favourable for permafrost growth.

4.2.3 Olkiluoto

The recent past climate (1961–1990)

Also at Olkiluoto, the seasonal cycle in temperature is weaker than the observations (Figure 4-3). The spatial variability is fairly small and, as for the other locations, the maximum occurs in spring which again is a consequence of proximity to the cold Baltic Sea in this season when land areas are heated. The snow cover is similar to that in Forsmark, with about two months of fairly large snow fractions. Also here the snowmelt leads to a maximum in runoff in the early spring. Precipitation at this location is simulated to have its maximum in the fall which is later than observed. But, in some of the adjacent grid points the maximum coincided with the observed maximum in the recent past climate. Also at this site there is too much precipitation during the winter half of the year by approximately 10–20 mm/month.

The warm case

Like at the two Swedish sites, the small annual temperature range in the recent past climate is even smaller in the future warm climate for the Olkiluoto area (Figure 4-9, upper row, first column). The snow season is much shorter, or even totally absent, in the warm climate as monthly mean temperatures mostly exceed 0°C. The characteristic snow melt peak in runoff in the recent past climate is absent. Instead, runoff shows a maximum in winter when there is more precipitation. Precipitation shows a maximum in late fall at about the same time as it is simulated to occur in the recent past climate which, in turn, is about two months later than observed. The spread in the presented variables due to geographical factors is reduced compared with that in the simulation of the recent past climate.

When including also the uncertainty ranges based on results from the three other climate simulations for the 21st century /Persson et al. 2007/, it is seen that the weakening of the annual cycle is a robust trend when going to a warmer climate. (Figure 4-9, upper left). For precipitation, it is obvious that the uncertainty ranges are larger for all months when taking also the three 21st century simulations into consideration (Figure 4-9, second row, left).

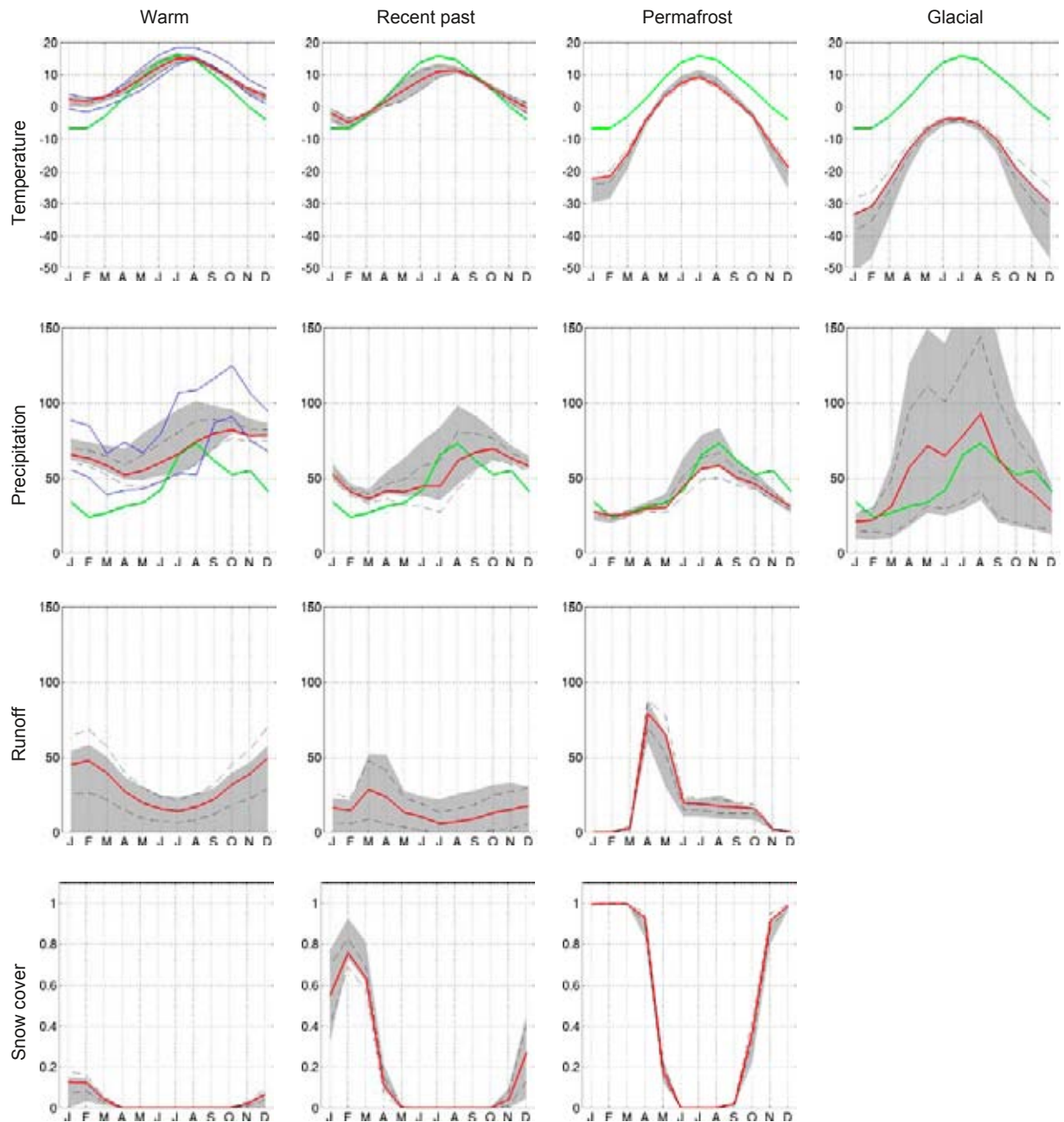


Figure 4-9. Simulated seasonal cycles of temperature ($^{\circ}\text{C}$), precipitation (mm/month), runoff (mm/month) and snow fraction (dimensionless ranging from 0 to 1) at the grid box closest to the Olkiluoto site (red line). The spatial variability in the 3x3-grids (see Figures 4-1 and 4-2) is displayed with the dashed lines representing ± 1 standard deviation calculated from the 9 grid boxes, and the grey area representing the absolute maximum and minimum, of the 9 grid boxes. The green line for temperature and precipitation is the observed seasonal cycle from the CRU data set in the period 1961–1990 (see the text). In the warm case, the uncertainty range (blue lines) is defined by ± 1 standard deviation of the data calculated from the 9 surrounding grid boxes from three additional simulations for the 21st century with RCA3.

The glacial case

For the *glacial case* the largest differences compared with the recent past temperature climate is seen in winter yielding, as expected, a completely different annual cycle due to the presence of the ice sheet (Figure 4-9, upper row, fourth column). The geographical spread in temperature close to the Olkiluoto grid box is large. The fairly large differences in altitude of ca 500 m between the 9 grid-boxes in the 3x3 grid surrounding Olkiluoto can explain temperature differences of about 3°C following the standard lapse rate of the atmosphere (6.5°C/km). As the differences here are up to 5°C, and not always colder for the grid boxes with the highest elevations, also other non-identified factors have to play a role in explaining the large spread. As the monthly mean temperature is mostly below -5°C, Olkiluoto is the coldest of the three sites investigated here. The low temperatures leads to a permanent snow cover on top of the ice sheet which means that also the Olkiluoto site is located under the ice sheet accumulation area, upstream of the ice sheet quasi-equilibrium line. As the representation of the ice sheet is crude in our study (see Section 2.3.3) we do not show runoff for the *glacial case*. The main change in the precipitation climate is that the geographic spread becomes much more pronounced in the *glacial case* compared with the recent past climate. This is probably related to the highly heterogeneous terrain (see also Figure 4-5). In terms of fluxes, precipitation is larger compared with the recent past climate during summer but notably lower in winter (Figure 4-9, second row, fourth column).

The permafrost case

As for the glacial climate, the largest difference compared with the recent past climate in the seasonal cycle of temperature is seen in winter. The resulting seasonal cycle is almost as strong as in the *glacial case* albeit with year-round higher temperatures (Figure 4-9, upper row, third column). As for the *glacial case* there is a relatively large geographical spread in landscape characteristics in the area (Figures 4-1 and 4-2). During the permafrost climate there is a very strong seasonal cycle in snow cover as the temperatures during summer get well above 0°C allowing for complete snow melting (Figure 4-9, upper and lower row, third column). The length of the completely snow-free season is three months according to the model and there seems to be a more or less constant snow cover during at least 3 months. There is a clear spring peak in runoff connected with the snow melt which is more extensive than in the recent past climate as more snow is accumulated on the ground during the winter. During the remainder of the year, the runoff is fairly small, due to the cold conditions during winter and the relatively smaller amounts of precipitation during summer. The precipitation is lower than in the recent past climate for most parts of the year. Also the geographical spread smaller for this case, most likely as a consequence of the surrounding areas being land.

The annual mean ground temperature is close to -5°C (Figure 3-57). According to /Heginbottom et al. 1995/ this low temperature indicates that continuous permafrost covering more than 90% of the land area is possible. We can also note that the precipitation is low in this case even compared with the glacial climate. However, this difference in the precipitation climate in these two cases is of a local nature, on larger scales the glacial climate is somewhat drier (cf. Figure 4-6). The cold and dry climate with partially snow-free conditions implies that the conditions are very favourable for permafrost growth.

4.2.4 Summary and comparison of the climate at the three sites

All three locations show similar changes in the climate parameters discussed in the previous sections, although with some differences (cf. Figures 4-7 to 4-9). Table 4-2 summarizes the climate at the three sites in all simulations in terms of 50-year annual mean temperature and precipitation. It can be seen that Oskarshamn is the warmest site in all simulations by 1–4°C compared with the second warmest site. In the *warm case* and in the simulation of the recent past climate, Olkiluoto sticks out as the coldest site whereas Forsmark is the coldest in the *permafrost case* due to the vicinity of the ice sheet. The latter is also the case for the *glacial case* when the sites are covered by the ice sheet. Table 4-2 also illustrates the geographical spread in the near vicinity of the sites by showing the standard deviation of the nine closest grid boxes. It is clearly seen that the variability in the climate of the regional climate model is larger in the colder climates than in the warm climate. It is particularly high at the high-altitude sites in the *glacial case*. But, also during the *permafrost case* there is a large variability in the Forsmark area, as this site is closest to the ice sheet in the northwest.

Table 4-2. 50-year averages of annual mean temperature (T), precipitation (PR) and runoff (R) for the three sites Forsmark, Oskarshamn and Olkiluoto in the regional climate model simulations (Table 3-1). Runoff is not given for the glacial case. In parenthesis is the standard deviation of the nine grid boxes closest to the location (Figure 4-1).

Simulation	T (°C)	PR (mm/year)	R (mm/year)
Forsmark			
WARM-r-veg	8.3 (0.4)	804 (54)	337 (114)
WARM-r	8.0 (0.3)	852 (66)	249 (102)
RP-r	4.7 (0.6)	666 (93)	175 (113)
PERMAFROST-r	-7.8 (0.9)	438 (53)	170 (40)
PERMAFROST-r-veg	-7.6 (1.0)	441 (51)	139 (20)
LGM2-r	-20.3 (1.0)	564 (161)	—
LGM2-r-veg	-20.8 (1.2)	567 (83)	—
LGM-r-vd	-22.9 (1.4)	512 (206)	—
Oskarshamn			
WARM-r-veg	9.4 (0.4)	901 (186)	275 (135)
WARM-r	9.2 (0.5)	929 (196)	283 (168)
RP-r	6.2 (0.3)	806 (192)	242 (158)
PERMAFROST-r	-3.2 (0.5)	582 (117)	218 (80)
PERMAFROST-r-veg	-3.4 (0.7)	569 (100)	221 (96)
LGM2-r	-13.2 (1.0)	581 (71)	—
LGM2-r-veg	-13.1 (1.4)	542 (84)	—
LGM-r-vd	-15.1 (1.4)	468 (77)	—
Olkiluoto			
WARM-r-veg	7.8 (0.4)	813 (100)	369 (174)
WARM-r	7.6 (0.4)	827 (107)	255 (168)
RP-r	3.8 (0.4)	621 (102)	174 (142)
PERMAFROST-r	-5.3 (0.7)	465 (53)	179 (48)
PERMAFROST-r-veg	-5.6 (0.6)	464 (40)	238 (40)
LGM2-r	-17.0 (1.9)	621 (286)	—
LGM2-r-veg	-17.0 (2.6)	617 (356)	—
LGM-r-vd	-18.8 (2.7)	583 (340)	—

The annual precipitation is largest in the *warm case* simulations. Compared with the recent past climate it is 20–30% wetter at Forsmark, 15–20% wetter at Oskarshamn and around 30% wetter at Olkiluoto. The *permafrost case* is driest, with reductions in precipitation compared with the recent past climate of 25–35% at the three sites. Oskarshamn is the wettest site in all simulations apart from the *glacial case*. Annual integrated runoff is largest in the *warm case* simulations and generally smallest in the *permafrost case* except for Olkiluoto which has the smallest runoff in the recent past climate.

5 Summary and conclusions

In this chapter we discuss limitations and uncertainties in the project before summarizing the main results and drawing conclusions. We also mention a number of additional experiments and analyses that could be worth pursuing to reduce some of the uncertainties.

5.1 Summary of limitations and uncertainties in the methodology

The major uncertainties in the assessment of simulated climate change for different periods are related to uncertainties in forcing, model formulation and natural variability. Here, we have chosen an experimental setup with a limited number of simulations, as we could not sample the uncertainty ranges. Additional simulations that would help to better address the uncertainties would be model integrations with i) different AOGCMs, ii) more sensitivity studies and iii) integrations sampling the natural variability. The issue of natural variability pertains to the simulations with the regional climate model as we have chosen to downscale relatively short periods (50 years). Downscaling of *other* 50-year periods from the simulations with the global model would not give identical results. However, we believe that the 50-year periods chosen from the quasi-equilibria of the global model are long enough to exclude any major differences due to decadal natural variability in the sought representations of long-term climate conditions.

A large number of simulations are recommendable in order to address uncertainties. As these kinds of integrations are highly time consuming we have, as previously mentioned, opted to complement with a number of sensitivity experiments. In particular, the simulations with the global model have clearly shown that a very long time is required to get the climate system into quasi-equilibrium. Long-term drift occurs even at long times after initialization with what were initially thought to be quasi-equilibrium conditions. The results presented in this report show that the simulations finally reach at least quasi-equilibrium first after several hundreds of years. However, we cannot rule out further drift in our simulations if the integrations were continued. As the long-term tendency in the LGM simulation was towards colder climates, this means that the resulting final climate might be even colder than what we have obtained here. Prolongation of the LGM, LGM-vd and PERMAFROST simulations has been conducted outside of this project with about 300 years without encountering any further drift. Finally, we note that there is an uncertainty as to whether the real climate ever has been in quasi-equilibrium as simulated here or not. If the real climate system was not in balance at LGM we may expect that a balanced state from a simulation is not the best representation of the climate system.

The prescribed forcing conditions contain a large number of uncertainties. The sensitivity experiments with the global model indicate that the uncertainties related to vegetation and aerosols needs to be taken into account in studies of past and future climates. In the *warm case* and the *glacial case*, the associated feedbacks from changing to a vegetation consistent with the climate leads to a stronger climate response (i.e. a larger deviation from the pre-industrial climate). These differences in climate response between the sensitivity experiments are large for some regions but relatively small for the Fennoscandian region. The use of higher mineral dust aerosol concentrations further enhances the climate response in the glacial domain. The sensitivity experiment with increased dust load in the atmosphere (i.e. a globally uniform increase of aerosol concentrations by a factor of three) is of course a very simplistic one. A more realistic experiment would include a horizontally varying dust load that would imply a higher degree of variability in the local/regional response. In particular, the temperature response at high northern latitudes would be expected to be even stronger as these are areas where the atmospheric aerosol loads were presumably much higher /Mahowald et al. 2006b/. The ice sheet configuration is another uncertainty in the forcing conditions as the extent and altitude of the ice sheets may have a strong influence on the atmospheric circulation and thereby on the temperature and precipitation climate. A number of sensitivity experiments with different configurations of the ice sheets could elucidate this. In particular, tests with a different extent and altitude of the Laurentide ice sheet could be pursued in the global model to test the influence on the atmospheric circulation. Also, sensitivity to changes in the configuration of the Fennoscandian ice sheet could be studied in the regional model to test the influence on the regional climate.

In the simulations with the regional climate model, a difficulty has been related to the fact that we do not have a module for simulating ice sheets coupled to the model. This lack has reduced our ability to explicitly simulate the coupling between ice sheets and the atmosphere. Probably this has no profound influence on the results for the simulated climate, since we perform only relatively short simulations. In long-term integrations such a module could have produced more detailed results on the mass balance of the ice sheets. A complication with the prescribed forcing conditions has been that they have not been treated identically in the global and regional climate models. As stated above, we have tried to mimic conditions in CCSM3 to a high degree in RCA3, but some discrepancies still remain. These include; different descriptions of the astronomical forcing and different treatment of greenhouse gases and aerosols. For future palaeoclimatic studies, development of the regional climate model to include better description of relevant processes is recommendable.

The regional climate simulations with different vegetation indicate that the regional response in Fennoscandia is only slightly dependent on the feedback from vegetation. The initial simulations with present-day vegetation differ from the ones with vegetation simulated by the dynamical vegetation model for each case. But, it can be noted that the differences are mostly relatively small. However, in some regions and seasons, larger discrepancies have been identified. Maximum differences are obtained for wintertime conditions in parts of eastern Europe for the *glacial case*. In RCA3 this is an area that in today's situation is dominated by open land (agricultural areas) whereas it is converted into semi-open areas in the glacial simulation, which leads to higher winter temperatures. Consequently, this experiment shows that not only changes in potential (natural) vegetation play a role. Human-induced changes of the vegetation may also be relevant in some areas and some seasons. An additional simulation of the pre-industrial climate with potential (natural) vegetation could be used here to act as a reference. In the *warm case*, the feedback from changing vegetation leads to a stronger regional response both in winter and summer.

One important outcome of this project is the production of a range of climate scenarios for which there exist large amounts of data that could be further analysed or used for studies of climate impacts on repository safety in Sweden and Finland. A consequence of the long time for production runs is that the time for analysis and evaluation of the model simulated climate in the three climate domains has been somewhat shorter than initially planned. In particular, we believe that a more thorough analysis of the global model in regions other than the North Atlantic and European sectors would be helpful for the overall evaluation of our results. For the North Atlantic and European sectors, differences in the large-scale atmospheric circulation including synoptic-scale variability could be scrutinized. Finally, a more detailed investigation of aspects of the regional anomalies over Europe as simulated by RCA3 could be undertaken.

5.2 Summary of results and conclusions

Global and regional details of the simulations

The simulations for the *warm*, *permafrost* and *glacial cases* illustrate a large span in both global and regional climate. The global mean temperature differs by 11°C between our most extreme cases (Table 5-1). Compared with the recent past climate, the *warm case* is 2.4°C warmer on a global scale, which is similar to what is found for many scenarios for the 21st century with increased greenhouse-gas forcing /Meehl et al. 2007/. In the global simulations, the cold *permafrost* and *glacial cases* are between 5.6 and 8.5°C colder than the recent past climate. The Atlantic Meridional Overturning Circulation (AMOC) also differs between the different cases. It is at its maximum in the pre-industrial climate and is reduced both for the warmer climates of the recent past and the future *warm case*, as well as in the colder climates of the *permafrost* and *glacial cases* (Table 5-1). It can be noted, however, that even if the AMOC is substantially reduced in the colder climates, it is not completely shut off, and it does not result in a regional cooling in Fennoscandia.

The climate in Fennoscandia as simulated by the regional climate model is significantly different in the different cases. The simulated changes in many climate variables are largest during winter in northern Europe. Differences in annual mean temperature and precipitation at the three sites in Sweden and Finland are shown in Table 5-1. The temperature span at these locations is in the range

Table 5-1. Summary of results for annual mean conditions in all simulations. The change in the global annual mean temperature (ΔT_{agm}) and the maximum of the Atlantic Meridional Overturning Circulation (AMOC) below 500 m depth are both taken from the global model as discussed in Sections 3.1.1, 3.2.1 and 3.3.1. We also present a summary of the local changes in temperature and precipitation at the three sites in Sweden and Finland when compared to the simulation of recent past climate (1961–2000) (see further Table 4-2).

Simulation	CCSM3		RCA3 – Annual means for three sites in Fennoscandia		
	ΔT_{agm} (°C)	AMOC (Sv)	Forsmark $\Delta T/\Delta PR$ (°C/%)	Oskarshamn $\Delta T/\Delta PR$ (°C/%)	Olkiluoto $\Delta T/\Delta PR$ (°C/%)
WARM-v	+2.4	15.1	–	–	–
WARM	+2.1	18.2	+3.6/+21	+3.2/+12	+4.0/+31
Recent past	0	19.4	0	0	0
Pre-industrial	-1.3	21.0	–	–	–
PERMAFROST	-5.6	10.2	-12.5/-34	-9.4/-29	-9.1/-25
LGM1	-5.8	17.4	–	–	–
LGM2	-6.9	11.6	-25.0/-15	-19.3/-33	-20.8/-1
LGM-v	-7.5	11.1	–	–	–
LGM-vd	-8.5	11.2	-27.6/-33	-21.3/-42	-22.6/-6

25–30°C between the most extreme cases (when including temperatures on the ice sheet surface in the *glacial case*). Increased temperature in the *warm case* is associated with increased precipitation, whereas the reverse is true for the colder climates in the *permafrost case* and the *glacial case*, i.e. decreased temperatures are associated with decreased precipitation. The regional climate model simulations illustrate that the proximity to the ice sheet has a significant impact on local climate conditions. When comparing extreme climates for ice-free conditions, the difference in annual mean temperature is about 15°C between the *warm case* and the *permafrost case* (Table 5-1). When compared against the recent past climate (1961–2000), summertime temperatures do not differ by more than 5–8°C for the warmest month of the year whereas wintertime differences are 20–25°C for the coldest month of the year with the largest differences at Forsmark, which is closest to the ice sheet (Figures 4-7 to 4-9). When compared against the recent past climate, precipitation changes over the range between the drier *permafrost case* climate with a 25–35% reduction in precipitation to the wet *warm case* climate with a 10–30% increase in precipitation.

Comparison with proxy data

As mentioned before, the comparison of model simulations to proxy-based reconstructions are complicated by the relatively sparse proxy data and the large uncertainties related to these both in terms of quality and representativity in time and space. We have compared sea-surface temperature and near-surface temperature from the global model and near-surface temperature and precipitation from the regional model to proxies. These comparisons show that the model results generally fall within the uncertainty ranges defined for the proxies.

The main identified systematic difference compared with proxy data in the global model simulations pertains to the fact that for the *glacial case* the global model is colder compared with proxy-based reconstructions of sea-surface temperatures at high northern latitudes. The uncertainties in the proxy-based reconstructions are large and for many stations the model results fall within the specified uncertainty ranges. Nevertheless, the model is mostly on the cold side of the central proxy data value, and there are also sites for which the model is clearly outside the uncertainty ranges. Therefore, over the North Atlantic, these differences indicate too much sea-ice in the model and thereby possibly a too cold climate in northern Europe. As proxy data are not available from Northern Europe for the period of the LGM, we can not investigate if this is indeed the case. Also for the *permafrost case*, there is an indication that the simulated SSTs over the North Atlantic is too low at some sites while others show a good agreement.

In southern Europe, the regional model produces a somewhat colder (i.e. 2–5°C) climate for the warmest month in summer and a fair agreement in winter and for annual mean conditions in the *glacial case*. For winter, the small number of available proxies in north-eastern Europe show a weaker response than the model does (by at least 7–8°C). The comparison of precipitation with proxies for the *glacial case* is inconclusive, partly due to the very large uncertainty ranges associated with the proxies, but also because there is no clear regional pattern that emerges. For the *permafrost case*, there is an indication that the model is colder by 5–10°C than the proxies in the British Isles during summer. At the same time the agreement between model and proxies is relatively good (i.e. within ±5°C) for all other available sites in western continental Europe indicating that a possible cold bias in parts of the North Atlantic does not have any major influence on the results for the climate in western Europe.

Comparison with other model simulations

For the *warm case* we compare our results with those from a number of transient simulations for the 21st century under a range of emission scenarios, of which some have about equal concentrations of CO₂ as assumed here. Even if these simulations differ from ours in some aspects, as how the Greenland ice sheet is handled and that these are transient experiments instead of equilibrium ones, the overall message is that our *warm case* falls within the range defined by those scenarios for the end of the 21st century. The climate sensitivity in CCSM3 is in the range of other AOGCMs. Therefore, a higher climate sensitivity in CCSM3 would most likely lead to a stronger climate change signal also for the Fennoscandian region. For this region, judging from the combined ranges of climate sensitivity and regional response in the CMIP3 AOGCMs, the uncertainty may well be a factor of two.

For the *glacial case* we compare our results with those from the PMIP1 and PMIP2 projects /e.g. Kageyama et al. 2006/. Our LGM2 simulation is colder than most of the PMIP simulations taken as a global average and also for the high northern latitudes. We find a strong correlation between SSTs and sea-ice in the North Atlantic and the global mean temperature. This is in contrast to what has been reported for the PMIP simulations. Further, our LGM2 simulation show a stronger north-south temperature gradient over Europe than most of the PMIP simulations does. Further, the sensitivity studies, that presumably have a more realistic forcing for LGM conditions are even colder in the north leading to an even stronger gradient.

The main conclusions from the study are that:

- i) Given forcing conditions based on theory, other independent models, and proxy data the climate models produce reasonable climates for the three climate cases; *warm*, *permafrost* and *glacial*. In this context, *reasonable* means that the results are in broad agreement with available proxy data and other climate model simulations.
- ii) The resulting climates are in qualitative agreement with the imposed extent of ice sheets for the respective climate case. In particular, we show that the results for the cold *permafrost case* have some impact on the interpretation and understanding of the Weichselian glacial history. Given the prescribed restricted MIS 3 ice sheet, the GCM and RCM model simulations produce a cold and dry climate which is in line with such an ice sheet configuration during MIS 3/GS12. Such restricted ice sheet coverage is in line with most, but not all, recent results from glacial geological studies /Wohlfarth 2009, Wohlfarth and Näslund (eds.) in prep./. Even if the results do not exclude the possibility of a large MIS 3/GS12 ice sheet configuration, the results are consistent with restricted ice sheet coverage, and thus a dynamic Middle Weichselian ice sheet behaviour.
- iii) The *warm case* simulations shows that there is no possibility of regrowth of the Greenland ice sheet once it has melted if forcing conditions are not altered.
- iv) The results of our sensitivity experiments show that changing the vegetation and increasing dust load in the *glacial case*, and changing the vegetation in the *warm case* increases the response in the global climate model.
- v) The results of the iterative simulations with the regional climate model and the dynamic vegetation model show that this is indeed a viable approach as the resulting vegetation is close to the vegetation in the *glacial case* as estimated by other models and to the vegetation in the

permafrost case as deduced from palaeo data. Different from the initial, present-day, vegetation used in the regional climate model the resulting vegetation for the two cold cases includes extended areas with tundra-like vegetation in northern Europe outside of the ice sheet. In southern Europe forested areas appears only in restricted parts of continental Europe and along parts of the Mediterranean coast.

- vi) The strong correlation between inter-annual variability in the North Atlantic Oscillation (NAO) index and the wintertime temperatures in Sweden shows that there is a strong influence from the atmospheric circulation over the North Atlantic on the temperature climate. This is, however, not applicable in the *glacial case* and indicates that the temperature climate over the central parts of the ice sheet is governed by processes other than the atmospheric circulation over the North Atlantic.
- vii) The simulated temperatures for the *permafrost case*, with prescribed ice-free conditions in south-central Fennoscandia, are favourable for permafrost growth at the Forsmark and Oskarshamn sites.
- ix) In the *warm* case there is a reduction of the Atlantic Meridional Overturning Circulation by 6% in the reference simulation and by 22% in the simulation with altered vegetation. However, these changes are not large enough to produce regionally colder conditions over Fennoscandia. Instead the simulated case with increased concentrations of greenhouse gases yields a warmer climate than at present, including Forsmark, Oskarshamn and Olkiluoto.
- x) There is a large range in possible climates for the Forsmark, Oskarshamn, and Olkiluoto sites in a 100,000 year time perspective, as summarized above. This range needs to be included in analyses of long-term safety of repositories for spent nuclear fuel.

Acknowledgements

This project was initiated by Jens-Ove Näslund and Lena Morén at Svensk Kärnbränslehantering AB (SKB). Anders Moberg at the Stockholm University, Markku Rummukainen at SMHI and Antje Voelker at INETI, Portugal, are acknowledged for valuable inputs to the project.

Without the help from a large number of people this project would not have been feasible. We have received help with initial conditions for the CCSM3 simulations from NCAR. In particular we are grateful to Jeff Kiehl and Yoshida Yoshikatsu for providing restart data for the *warm case*. Marko Scholze, Zav Kothavala, Nathalie Mahowald and Nan Rosenbloom are acknowledged for providing vegetation data. Antje Voelker is acknowledged for compiling and providing proxy data for sea-surface temperature for both the *glacial* and *permafrost cases*. Masa Kageyama and Joel Guiot provided terrestrial proxy data. Andrey Ganopolski and Stefan Rahmstorf provided us with ice sheet data from CLIMBER-2. We would also like to thank all participants of the workshop “Fennoscandian paleo-environment and ice sheet dynamics during Marine Isotope Stage (MIS) 3 /see Näslund et al. 2008/ for their input on environmental conditions for the MIS 3 simulations.

This research study used data provided by the Community Climate System Model project supported by the Directorate for Geosciences of the National Science Foundation and the Office of Biological and Environmental Research of the U.S. Department of Energy. All model simulations with the global and regional climate models were performed on the climate computing resource Tornado operated by the National Supercomputer Centre at Linköping University. Tornado is funded with a grant from the Knut and Alice Wallenberg foundation.

Further we acknowledge the modelling groups, the Program for Climate Model Diagnosis and Intercomparison (PCMDI) and the WCRP’s Working Group on Coupled Modelling (WGCM) for their roles in making available the WCRP CMIP3 multi-model dataset. Support of this dataset is provided by the Office of Science, U.S. Department of Energy.

Pippa Whitehouse (University of Durham, UK) provided data on topography, while Mike Thorne (Mike Thorne and Associated Limited, UK), Markku Rummukainen (Swedish Meteorological and Hydrological Institute), and Natalia Pimenoff (Finnish Meteorological Institute) made valuable comments on the manuscript.

References

- Adler R F, Huffman G J, Chang A, Ferraro R, Xie P-P, Janowiak J, Rudolf B, Schneider U, Curtis S, Bolvin D, Gruber A, Susskind J, Arkin P, Nelkin E, 2003.** The version-2 Global Precipitation Climatology Project (GPCP) monthly precipitation analysis (1979–present). *Journal of Hydrometeorology* 4: 1147–1167.
- Allen J R M, Brandt U, Brauer A, Hubberten H W, Huntley B, Keller J, Kraml M, Mackensen A, Mingram J, Negendank J F W, Nowaczyk N R, Oberhansli H, Watts W A, Wulf S, Zolitschka B, 1999.** Rapid environmental changes in southern Europe during the last glacial period. *Nature* 400: 740–743.
- Allen J R M, Huntley B, 2000.** Weichselian palynological records from southern Europe: correlation and chronology. *Quaternary International* 73/74: 111–125.
- Antic S, Laprise R, Denis B, de Elia R, 2004.** Testing the downscaling ability of a one-way nested regional climate model in regions of complex topography. *Climate Dynamics* 23: 473–493.
- Archer D, Ganopolski A, 2005.** A movable trigger: Fossil fuel CO₂ and the onset of the next glaciation. *Geochemistry Geophysics Geosystems* 6: Q05003, doi:10.1029/2004GC000891.
- Barron E, Pollard D, 2002.** High-resolution climate simulations of oxygen isotope stage 3 in Europe. *Quaternary Research* 58: 296–309.
- Behre K E, 1989.** Biostratigraphy of the Last Glacial Period in Europe. *Quaternary Science Reviews* 8: 24–44.
- Behre K E, van der Plicht J, 1992.** Towards an absolute chronology for the last glacial period in Europe: radiocarbon dates from Oerel, northern Germany. *Vegetation History and Archaeobotany* 1: 111–117.
- Berger A, 1978.** Long-term variation of daily insolation and Quaternary climatic changes. *Journal of Atmospheric Sciences* 35: 2362–2367.
- Berger A, Loutre M F, 2002.** An exceptionally long interglacial ahead? *Science* 297: 1287–1288.
- BIOCLIM, 2001.** Deliverable D3: Global Climatic Features over the Next Million Years and Recommendation for Specific Situations to be Considered, ANDRA, Parc de la Croix Blanche, 1/7 rue Jean Monnet, 92298 Châtenay-Malabry, France. 27 p.
- Bitz C M, Chiang J C H, Cheng W, Barsugli J J, 2007.** Rates of thermohaline recovery from freshwater pulses in Modern, Last Glacial Maximum and Greenhouse Warming Climates. *Geophysical Research Letters* 34: L07708.
- Bonan G B, Levis S, Kergoat L, Oleson K W, 2002.** Landscapes as patches of plant functional types: An integrating concept for climate and ecosystem models. *Global Biogeochemical Cycles* 16: 1021, doi:10.1029/2000GB001360.
- Bonan G B, Levis S, 2006.** Evaluating aspects of the Community Land and atmosphere Models (CLM3 and CAM) using a dynamic global vegetation model. *Journal of Climate* 19: 2290–2301.
- Brandefelt J, Otto-Bliesner B, in prep.** Quasi-equilibria and variability in a Last Glacial Maximum climate simulation with CCSM3.
- Byrkjedal Ø, Kvamstø N G, Meland M, Jansen E, 2006.** Sensitivity of last glacial maximum climate to sea ice conditions in the Nordic Seas. *Climate Dynamics* 26: 473–487.
- Calov R, Ganopolski A, Claussen M, Petoukhov V, Greve R, 2005.** Transient simulation of the last glacial inception. Part 1: glacial inception as a bifurcation in the climate system. *Climate Dynamics* 24: 545–561.
- Cochelin A-S, Mysak L A, Wang Z, 2006.** Simulation of long-term future climate changes with the green McGill paleoclimate model: the next glacial inception. *Climatic Change* 79: 381–401.

- Collins W D, Bitz C M, Blackmon M L, Bonan G B, Bretherton C S, Carton J A, Chang S, Doney C, Hack J J, Henderson T B, Kiehl J T, Large W G, McKenna D S, Santer B D, Smith R D, 2006.** The Community Climate System Model (CCSM3), *Journal of Climate* 19: 2122–2143.
- Cramer W, Bondeau A, Woodward F I, Prentice I C, Betts R A, Brovkin V, Cox P M, Fisher V, Foley J A, Friend A D, Kucharik C, Lomas M R, Ramankutty N, Sitch S, Smith B, White A, Young-Molling C, 2001.** Global response of terrestrial ecosystem structure and function to CO₂ and climate change: results from six dynamic global vegetation models. *Global Change Biology* 7: 357–373.
- Dansgaard W, Johnsen S J, Clausen H B, Dahl-Jensen D, Gundestrup N S, Hammer C U, Hvidberg C S, Steffensen J P, Sveinbjörnsdóttir A E, Jouzel J, Bond G, 1993.** Evidence for general instability of past climate from a 250-kyr ice-core record. *Nature* 364: 218–220.
- Déqué M, Jones R G, Wild M, Giorgi F, Christensen J H, Hassell D C, Vidale P L, Rockel B, Jacob D, Kjellström E, de Castro M, Kucharski F, van den Hurk B, 2005.** Global high resolution versus Limited Area Model climate change projections over Europe: quantifying confidence level from PRUDENCE results. *Climatic Dynamics* 25: 653–670.
- EPICA members, Augustin L, Barbante C, Barnes P R F, Barnola J M, Bigler M, Castellano E, Cattani O, Chappellaz J, Dahl-Jensen D, Delmonte B, Dreyfus G, Durand G, Falourd S, Fischer H, Flückiger J, Hansson M E, Huybrechts P, Jugie G, Johnsen S J, Jouzel J, Kaufmann P, Kipfstuhl J, Lambert F, Lipenkov V Y, Littot G C, Longinelli A, Lorrain R, Maggi V, Masson-Delmotte V, Miller H, Mulvaney R, Oerlemans J, Oerter H, Orombelli G, Parrenin F, Peel D A, Petit J-R, Raynaud D, Ritz C, Ruth U, Schwander J, Siegenthaler U, Souchez R, Stauffer B, Steffensen J P, Stenni B, Stocker T F, Tabacco I E, Udisti R, Van De Wal R S W, Van Den Broeke M, Weiss J, Wilhelms F, Winther J-G, Wolff E W, Zucchielli M, 2004.** Eight glacial cycles from an Antarctic ice core. *Nature* 429: 623–628.
- FAO, 1991.** The Digitized Soil Map of the World (Release 1.0). *World Soil Resources Report 67/1*. Food and Agriculture Organization of the United Nations, Rome.
- Forster P, Ramaswamy V, Artaxo P, Berntsen T, Betts R, Fahey D W, Haywood J, Lean J, Lowe D C, Myhre G, Nganga J, Prinn R, Raga G, Schulz M, Van Dorland R, 2007.** Changes in Atmospheric Constituents and in Radiative Forcing. In: *Climate Change 2007: The Physical Science Basis. Contribution of Working Group I to the Fourth Assessment Report of the Intergovernmental Panel on Climate Change* [Solomon S, Qin D, Manning M, Chen Z, Marquis M, Averyt K B, Tignor M, Miller H L, (eds.)]. Cambridge University Press, Cambridge, United Kingdom and New York, NY, USA.
- Graham L P, Chen D, Christensen O B, Kjellström E, Krysanova V, Meier H E M, Radziejewski M, Rockel B, Ruosteenoja K, Räisänen J, 2008.** Projections of future climate change. In *Assessment of Climate Change for the Baltic Sea Basin*. The BACC Author Team. 2008, XXI, 473 p., ISBN: 978-3-540-72785-9.
- Gregory J M, Huybrechts P, Raper S C B, 2004.** Threatened loss of the Greenland ice sheet. *Nature* 428: 616.
- Gregory J M, Huybrechts P, 2006.** Ice sheet contributions to future sea-level change. *Philosophical Transactions of the Royal Society A* 364: 1709–1731.
- Gritti E S, Smith B, Sykes M T, 2006.** Vulnerability of Mediterranean basin ecosystems to climate change and invasion by exotic plant species. *Journal of Biogeography* 33: 145–157.
- Harrison S P, Braconnot P, Joussaume S, Hewitt C, Stouffer R J, 2002.** Comparison of palaeoclimate simulations enhances confidence in models. *EOS* 83: 447.
- Heginbottom J A, Dubreuil M A, Harker P A, 1995.** Canada – Permafrost, in: *National Atlas of Canada, 5th Edition*, National Atlas Information Service, Natural Resources Canada, MCR 4177.
- Held I, Soden B, 2006.** Robust response of the hydrological cycle to global warming. *Journal of Climate* 19: 5686–5699.
- Hély C, Bremond L, Alleaume S, Smith B, Sykes M T, Guiot J, 2006.** Sensitivity of African biomes to changes in the precipitation regime. *Global Ecology and Biogeography* 15: 258–270.

- Hickler T, Smith B, Sykes M T, Davis M B, Sugita S, Walker K, 2004.** Using a generalized vegetation model to simulate vegetation dynamics in the western Great Lakes region, USA, under alternative disturbance regimes. *Ecology* 85: 519–530.
- Hughen K, Southon J, Lehman C, Betrand C, Turnbull J, 2006.** Marine-derived ^{14}C calibration and activity record for the past 50,000 years updated from the Cariaco Basin. *Quaternary Science Reviews* 25: 3216–3227.
- Huijzer B, Vandenberghe J, 1998.** Climatic reconstructions of the Weichselian Pleniglacial in northwestern and central Europe. *Journal of Quaternary Science* 13: 391–417.
- Hurrell J W, 1995.** Decadal trends in the North Atlantic Oscillation: Regional Temperatures and Precipitation. *Science* 269: 676–679.
- IPCC, 2001.** Climate Change 2001. The Scientific Basis. Contribution of Working Group I to the Third Assessment Report of the Intergovernmental Panel on Climate Change [Houghton J T, Ding Y, Griggs D J, Noguer M, van der Linden P J, Dai X, Maskell K, Johnson C A (eds.)]. Cambridge University Press, Cambridge, United Kingdom and New York, NY, USA, 881pp.
- Jones C G, Ullerstig A, Willén U, Hansson U, 2004.** The Rossby Centre regional atmospheric climate model (RCA). Part I: Model climatology and performance characteristics for present climate over Europe. *Ambio* 33: 199–210.
- Jost A, Lunt D, Kageyama M, Abe-Ouchi A, Peyron O, Valdes P J, Ramstein G, 2005.** High-resolution simulations of the last glacial maximum climate over Europe: a solution to discrepancies with continental palaeoclimatic reconstructions? *Climate Dynamics* 24: 577–590.
- Joussaume S, Taylor K E, 2000.** The paleoclimate modeling intercomparison project. In PMIP, Paleoclimate Modeling Intercomparison Project (PMIP): proceedings of the third PMIP workshop, Canada, 4–8 October 1999, in WCRP-111, WMO/TD-1007, edited by P. Braconnot, pp. 271.
- Jouzel J, Stiévenard M, Johnsen S J, Landais A, Masson-Delmotte V, Sveinbjörnsdóttir A, Vimeux F, von Grafenstein U, White J W C, 2007.** The GRIP deuterium-excess record. *Quaternary Science Reviews* 26: 1–17.
- Kageyama M, Lainé A, Abe-Ouchi A, Braconnot P, Cortijo E, Crucifix M, de Vernal A, Guiot J, Hexitt C D, Kitoh A, Kucera M, Martí O, Ohgaito R, Otto-Bliesner B, Peltier W R, Rosell-Melé A, Vettoretti G, Weber S L, Yu Y, MARGO project members, 2006.** Last Glacial Maximum temperatures over the North Atlantic, Europe and western Siberia: a comparison between PMIP models, MARGO sea-surface temperatures and pollen-based reconstructions. *Quaternary Science Reviews* 25: 2082–2102.
- Kalnay E, Kanamitsu M, Kistler R, Collins W, Deaven D, Gandin L, Iredell M, Saha S, White G, Woollen J, Zhu Y, Leetmaa A, Reynolds R, Chelliah M, Ebisuzaki W, Higgins W, Janowiak J, Mo K, Ropelewski C, Wang J, Jenne R, Joseph D, 1996.** The NCEP/NCAR 40-Year Reanalysis Project. *Bulletin of the American Meteorological Society* 77: 437–471.
- Kiehl J T, Shields C A, Hack J J, Collins W D, 2006.** The Climate Sensitivity of the Community Climate System Model Version 3 (CCSM3). *Journal of Climate* 19: 2584–2596.
- Kim S-J, Crowley T J, Erickson D J, Govindasamy B, Duffy P B, Lee BY, 2008.** High-resolution climate simulation of the last glacial maximum. *Climate Dynamics* 31: 1–16.
- Kjellström E, Bärring L, Gollvik S, Hansson U, Jones C, Samuelsson P, Rummukainen M, Ullerstig A, Willén U, Wyser K, 2005.** A 140-year simulation of European climate with the new version of the Rossby Centre regional atmospheric climate model (RCA3). *Reports Meteorology and Climatology*, 108, SMHI, SE-60176 Norrköping, Sweden, 54 pp.
- Kjellström E, Lind P, 2009.** Changes in the water budget in the Baltic Sea drainage basin in future warmer climates as simulated by the regional climate model RCA3. *Boreal Environment Research* 14: 114–124.
- Koca D, Smith B, Sykes M T, 2006.** Modelling regional climate change effects on Swedish ecosystems. *Climatic Change* 78: 381–406.

Krogh Andersen K, Svensson A, Olander Rasmussen S, Steffensen J P, Johnsen S, Bigler M, Röhlisberger R, Ruth U, Siggaard-Andersen M L, Dahl-Jensen D, Vinther B M, Clausen H B, 2006. The Greenland Ice Core Chronology 2005, 15–42 kyr. Part 1: Constructing the time scale. *Quaternary Science Reviews* 25: 3246–3257.

Kucera M, Rosell-Melé A, Schneider R, Waelbroeck C, Weinelt M, 2005. Multiproxy approach for the reconstruction of the glacial ocean surface. *Quaternary Science Review* 24: 813–819.

Lambeck K, 2004. Sea-level change through the last glacial cycle: geophysical, glaciological and palaeogeographic consequences. *Comptes Rendus Geoscience* 336: 677–689.

Lenton T, Wilkinson P, Edwards N, Marsh R, Price J, Ridgwell A, Shepherd J, Cox S J, The GENIE team, 2006. Millennial timescale carbon cycle and climate change in an efficient Earth system model. *Climate Dynamics* 26: 687–711

Lenton T M, Held H, Kriegler E, Hall J W, Lucht W, Rahmstorf S, Schellnhuber H J, 2008. Tipping Elements in the Earth System, *Proceedings of the National Academy of Sciences USA* 105: 1786–1793.

Lind P, Kjellström E, 2008. Temperature and precipitation changes in Sweden; a wide range of model-based projections for the 21st century. *Reports Meteorology and Climatology*, 113, SMHI, SE-60176 Norrköping, Sweden.

Lüthi D, Le Floch M, Bereiter B, Blunier T, Barnola J-M, Siegenthaler U, Raynaud D, Jouzel J, Fischer H, Kawamura K, Stocker T F, 2008. High-resolution carbon dioxide concentration record 650,000–800,000 years before present. *Nature* 453: 379–382.

Mahowald N M, Muhs D R, Levis S, Rasch P J, Yoshioka M, Zender C S, Luo C, 2006a. Change in atmospheric mineral aerosols in response to climate: Last glacial period, preindustrial, modern, and doubled carbon dioxide climates, *Journal of Geophysical Research* 111: D10202.

Mahowald N M, Yoshioka M, Collins W D, Conley A D, Fillmore D W, Coleman D B, 2006b. Climate response and radiative forcing from mineral aerosols during the last glacial maximum, pre-industrial, current and doubled-carbon dioxide climates, *Geophysical Research Letters* 33: L20705.

Mangerud J, Gosse J, Matiouchkov A, Dolvik T, 2008. Glaciers in the polar Urals, Russia, were not much larger during the last global glacial maximum than today. *Quaternary Science Reviews*: 1047–1057.

Meehl G A, Stocker T F, Collins W D, Friedlingstein P, Gaye A T, Gregory J M, Kitoh A, Knutti R, Murphy J M, Noda A, Raper S C B, Watterson I G, Weaver A J, Zhao Z-C, 2007. Global Climate Projections. In: *Climate Change 2007: The Physical Science Basis. Contribution of Working Group I to the Fourth Assessment Report of the Intergovernmental Panel on Climate Change* [Solomon S, Qin D, Manning M, Chen Z, Marquis M, Averyt K B, Tignor M, Miller H L (eds.)]. Cambridge University Press, Cambridge, United Kingdom and New York, NY, USA.

Miller P A, Giesecke T, Hickler T, Bradshaw R H W, Smith B, Seppä H, Valdes P J, Sykes M T, 2008. Exploring climatic and biotic controls on Holocene vegetation change in Fennoscandia. *Journal of Ecology* 96: 247–259.

Mitchell T D, Jones P D, 2005. An improved method of constructing a database of monthly climate observations and associated high-resolution grids. *International Journal of Climatology* 25: 693–712.

Moberg A, Gouirand I, Wohlfarth B, Schonning K, Kjellström E, Rummukainen M, de Jong R, Linderholm H, Zorita E, 2006. Climate in Sweden during the past millennium – Evidence from proxy data, instrumental data and model simulations. Report TR-06-35, Svensk Kärnbränslehantering AB. 87 pp.

Morales P, Sykes M T, Prentice I C, Smith P, Smith B, Bugmann H, Zierl B, Friedlingstein P, Viovy N, Sabate S, Sanchez A, Pla E, Gracia C A, Sitch S, Arneth A, Ogee, J, 2005. Comparing and evaluating process-based ecosystem model predictions of carbon and water fluxes in major European forest biomes. *Global Change Biology* 11: 2211–2233.

Morales P, Hickler T, Rowell D P, Smith B, Sykes M T, 2007. Changes in European ecosystem productivity and carbon balance driven by Regional Climate Model output. *Global Change Biology* 13: 108–122.

Nakićenović N, Swart R (eds.), 2000. Special Report on Emissions Scenarios. A Special Report of Working Group III of the Intergovernmental Panel on Climate Change. Cambridge University Press, Cambridge, United Kingdom and New York, NY, USA, 599 pp.

NGRIP Members, Andersen K K, Azuma N, Barnola J-M, Bigler M, Biscaye P, Caillon N, Chappellaz J, Clausen H B, Dahl-Jensen D, Fischer H, Flückiger J, Fritzsche D, Fujii Y, Goto-Azuma K, Grønvald K, Gundestrup N S, Hansson M, Huber C, Hvidberg C S, Johnsen S J, Jonsell U, Jouzel J, Kipfahl S, Landais A, Leuenberger M, Lorrain R, Masson-Delmotte V, Miller H, Motoyama H, Narita H, Popp T, Rasmussen S O, Raynaud D, Rothlisberger R, Ruth U, Samyn D, Schwander J, Shoji H, Siggard-Andersen M-L, Steffensen J P, Stocker T, Sveinbjörnsdóttir A E, Svensson A, Takata M, Tison J –L, Thorsteinsson T, Watanabe O, Wilhelms F, White J W C, 2004. High-resolution record of Northern Hemisphere climate extending into the last interglacial period. *Nature* 431: 147–151.

Näslund J O, Wohlfarth B, Alexanderson H, Helmens K, Hättestrand M, Jansson P, Kleman J, Lundqvist J, Brandefelt J, Houmark-Nielsen M, Kjellström E, Strandberg G, Knudsen K L, Krog Larsen N, Ukkonen P, Mangerud J, 2008. Fennoscandian paleo-environment and ice sheet dynamics during Marine Isotope Stage (MIS) 3. Report of a workshop held September 20–21, 2007 in Stockholm, Sweden. SKB R-08-79, Svensk Kärnbränslehantering AB, 52 pp.

Otto-Bliesner B L, Brady E C, Clauzet G, Thomas R, Levis S, Kothavala Z, 2006a. Last glacial maximum and Holocene climate in CCSM3. *Journal of Climate* 19: 2526–2544.

Otto-Bliesner B L, Thomas R, Brady E C, Ammann C, Kothavala Z, Clauzet G, 2006b. Climate sensitivity of moderate and low-resolution versions of CCSM3 to pre-industrial forcings. *Journal of Climate* 19: 2567–2583.

Otto-Bliesner B L, Hewitt C D, Marchitto T M, Brady E, Abe-Ouchi A, Crucifix M, Murakami S, Weber S L, 2007. Last Glacial Maximum ocean thermohaline circulation: PMIP2 model intercomparisons and data constraints. *Geophysical Research Letters* 34: L12706.

Overpeck J T, Otto-Bliesner B L, Miller G H, Muhs D H, Alley R B, Kiehl J T, 2006. Paleoclimatic evidence for future ice sheet instability and rapid sea-level rise. *Science* 24: 1747–1750.

Peltier W R, 2004. Global glacial isostasy and the surface of the ice-age circulation. *Earth: The ICE-5G (VM2) model and GRACE, Annual Review of Earth Planet. Sciences*, 32: 111–149.

Persson G, Bärring L, Kjellström E, Strandberg G, Rummukainen M, 2007. Climate indices for vulnerability assessments. *Reports Meteorology and Climatology* 111, SMHI, Norrköping, Sweden.

Preusser F, 2004. Towards a chronology of the Late Pleistocene in the northern Alpine Foreland. *Boreas* 33: 195–210.

Ramstein G, Kageyama M, Guiot J, Wu H, Hély C, Krinner G, Brewer S, 2007. How cold was Europe at the Last Glacial Maximum? A synthesis of the progress achieved since the first PMIP model-data comparison. *Climate of the Past* 3: 331–339.

Randall D A, Wood R A, Bony S, Colman R, Fichefet T, Fyfe J, Kattsov V, Pitman A, Shukla J, Srinivasan J, Stouffer R J, Sumi A, Taylor K E, 2007. Climate Models and Their Evaluation. In: *Climate Change 2007: The Physical Science Basis. Contribution of Working Group I to the Fourth Assessment Report of the Intergovernmental Panel on Climate Change* [Solomon, S., D. Qin, M. Manning, Z. Chen, M. Marquis, K.B. Averyt, M.Tignor and H.L. Miller (eds.)]. Cambridge University Press, Cambridge, United Kingdom and New York, NY, USA.

Ridley J K, Huybrechts P, Gregory J M, Lowe J A, 2005. Elimination of the Greenland Ice Sheet in a high CO₂ climate. *Journal of Climate* 18: 3409–3427.

Roeckner E, Bengtsson L, Feichter J, Lelieveld J, Rodhe H, 1999. Transient climate change simulations with a coupled atmosphere–ocean GCM including the tropospheric sulfur cycle. *Journal of Climate* 12: 3004–3032.

Roeckner E, Brokopf R, Esch M, Giorgieta M, Hagemann S, Kornblueh L, Manzini E, Schlese U, Schulzweida U, 2006. Sensitivity of simulated climate to horizontal and vertical resolution in the ECHAM5 atmosphere model. *Journal of Climate* 19: 3771–3791.

- Rubel F, Hantel M, 2001.** BALTEX 1/6-degree daily precipitation climatology. *Meteorology and Atmospheric Physics* 77: 155–166.
- Rummukainen M, Räisänen J, Ullerstig A, Bringfelt B, Hansson U, Graham P, Willén U, 1998.** RCA – Rossby Centre regional Atmospheric climate model: model description and results from the first multi-year simulation. *Reports Meteorology and Climatology* 83, Swedish Meteorological and Hydrological Institute, SE-601 76 Norrköping, Sweden, 76 pp.
- Rummukainen M, Räisänen J, Bringfelt B, Ullerstig A, Omstedt A, Willén U, Hansson U, Jones C, 2001.** A regional climate model for northern Europe: model description and results from the downscaling of two GCM control simulations. *Climate Dynamics* 17: 339–359.
- Räisänen J, Hansson U, Ullerstig A, Döscher R, Graham L P, Jones C, Meier M, Samuelsson P, Willén U, 2003.** GCM driven simulations of recent and future climate with the Rossby Centre coupled atmosphere – Baltic Sea regional climate model RCAO. *Reports Meteorology and Climatology* 101, Swedish Meteorological and Hydrological Institute, SE-601 76 Norrköping, Sweden, 61 pp.
- Räisänen J, Hansson U, Ullerstig A, Döscher R, Graham L P, Jones C, Meier H E M, Samuelsson P, Willén U, 2004.** European climate in the late twenty-first century: regional simulations with two driving global models and two forcing scenarios. *Climate Dynamics* 22: 13–31.
- Shin S-I, Liu Z, Otto-Bliesner B, Brady E C, Kutzbach J E, Harrison S P, 2003.** A simulation of the Last Glacial Maximum climate using the NCAR CSM, *Climate Dynamics* 20: 127–151.
- Sholze M, Knorr W, Arnell N W, Prentice I C, 2006.** A climate-change risk analysis for world ecosystems. *Proceedings of the National Academy of Sciences of the United States of America*, 103: 13116–13120.
- Siegenthaler U, Stocker T, Monnin E, Luthi D, Schwander J, Stauffer B, Raynaud D, Barnola J-M, Fischer H, Masson-Delmotte V, Jouzel J, 2005.** Stable carbon cycle-climate relationship during the late Pleistocene. *Science* 310: 1313–1317.
- Sitch S, Smith B, Prentice I C, Arneth A, Bondeau A, Cramer W, Kaplan J, Levis S, Lucht W, Sykes M, Thonicke K, Venevsky S, 2003.** Evaluation of ecosystem dynamics, plant geography and terrestrial carbon cycling in the LPJ Dynamic Global Vegetation Model. *Global Change Biology* 9: 161–185.
- Sitch S, Brovkin V, von Bloh W, van Vuuren D, Eickhout B, Ganopolski A, 2005.** Impacts of future land cover changes on atmospheric CO₂ and climate. *Global Biogeochemical Cycles* 19: GB2013.
- Sitch S, Huntingford C, Gedney N, Levy P E, Lomas M, Piao S L, Betts R, Ciais P, Cox P, Friedlingstein P, Jones C D, Prentice I C, Woodward F I, 2008.** Evaluation of the terrestrial carbon cycle, future plant geography and climate-carbon cycle feedbacks using five Dynamic Global Vegetation Models (DGVMs). *Global Change Biology* 14: 2015–2039.
- SKB, 2006.** Climate and climate related issues for the safety assessment SR-Can. SKB TR-06-23, Svensk Kärnbränslehantering AB, 186pp.
- Smith B, Prentice I C, Sykes M T, 2001.** Representation of vegetation dynamics in modelling of terrestrial ecosystems: comparing two contrasting approaches within European climate space. *Global Ecology and Biogeography* 10: 621–637.
- Smith B, Knorr W, Widlowski J L, Pinty B, Gobron N, 2008.** Combining remote sensing data with process modelling to monitor boreal conifer forest carbon balances. *Forest Ecology & Management* 255: 3985–3994.
- Spahni R, Chappellaz J, Stocker T F, Loulergue L, Hausmann G, Kawamura K, Fluckiger J, Schwander J, Raynaud D, Masson-Delmotte V, Jouzel J, 2005.** Atmospheric methane and nitrous oxide of the late Pleistocene from Antarctic ice cores. *Science* 310: 1317–1321.
- Stouffer R J, Yin J, Gregory J M, Dixon K W, Spelman M J, Hurlin W, Weaver A J, Eby M, Glato G M, Hasumi H, Hu A, Jungclaus J-H, Kamenkovich I V, Levermann A, Montoya M, Murakami S, Nawrath S, Oka A, Peltier W R, Robitaile D Y, Sokolov A, Vettoretti G, Weber S L, 2006.** Investigating the causes of the response of the thermohaline circulation to past and future climate changes, *Journal of Climate* 19: 13651387.

- Svendsen J I, Alexanderson H, Astakhov V I, Demidov I, Dowdeswell J A, Funder S, Gataullin V, Henriksen M, Hjort C, Houmark-Nielsen M, Hubberten H W, Ingólfsson Ó, Jakobsson M, Kjær K H, Larsen E, Lokrantz H, Lunkka J P, Lyså A, Mangerud J, Matoushkov A, Murray A, Möller P, Niessen F, Nikolskaya O, Polyak L, Saarnisto M, Siegert C, Siegert M J, Spielhagen R F, Stein R, 2004.** Late Quaternary ice sheet history of northern Eurasia. *Quaternary Science Reviews* 23: 1229–1271.
- Sykes M T, Prentice I C, 1995.** Boreal forest futures: modelling the controls on tree species range limits and transient responses to climate change. *Water, Air and Soil Pollution* 82: 415–428.
- Tarasov P E, Peyron O, Guiot J, Brewer S, Volkova V S, Bezusko L G, Dorofeyuk N I, Kvavadze E V, Osipova I M, Panova N K, 1999.** Last Glacial Maximum climate of the former Soviet Union and Mongolia reconstructed from pollen and macrofossil data. *Climate Dynamics* 15: 227–240.
- Texier D, Degnan P, Loutre M F, Paillard D, Thorne M, 2003.** Modelling BIOsphere systems under CLIMATE change for radioactive waste disposal. Proceedings of the International High-Level Waste Management Conference March 30–April 2, 2003, Las Vegas, USA.
- Tonizazzo T, Gregory J M, Huybrechts P, 2004.** Climatic impact of a Greenland deglaciation and its possible irreversibility. *Journal of Climate* 17: 21–33.
- van Huissteden K, Vandenberghe J, Pollard D, 2003.** Palaeotemperature reconstructions of the European permafrost zone during Oxygen Isotope Stage 3 compared with climate models. *Journal of Quaternary Science* 18: 453–464.
- Voelker A H L and workshop participants, 2002.** Global distribution of centennial-scale records for Marine Isotope Stage (MIS) 3: a database. *Quaternary Science Review* 21: 1185–1212.
- Whittington G, Hall A M, 2002.** The Tolsta Interstadial, Scotland: correlation with D-O cycles GI-8 to GI 5? *Quaternary Science Reviews* 21: 901–915.
- Wohlfarth B, 2009.** Ice-free conditions in Scandinavia during Marine Oxygen Isotope Stage 3? SKB TR-09-12, in press. Svensk Kärnbränslehantering AB.
- Wohlfarth B, Näslund J O (eds.), in prep.** Bores thematic volume on MIS 3.
- Wolf, A, Callaghan, T. V., and Larson, K., 2008.** Future changes in vegetation and ecosystem function of the Barents Region. *Climatic Change* 87: 51–73.
- Wramneby A, Smith B, Zaehle S, Sykes M T, 2008.** Parameter uncertainties in the modelling of vegetation dynamics – effects on tree community structure and ecosystem functioning in European forest biomes. *Ecological Modelling* 216: 277–290.
- Wu H, Guiot J, Brewer S, Guo Z, 2007.** Climatic changes in Eurasia and Africa at the last glacial maximum and mid-Holocene: reconstruction from pollen data using inverse vegetation modeling. *Climate Dynamics* 29: 211–229.
- Yurova A Y, Lankreijer H, 2007.** Carbon storage in the organic layers of boreal forest soils under various moisture conditions: A model study for Northern Sweden sites. *Ecological Modelling* 204: 475–484.
- Zaehle S, Sitch S, Prentice I C, Liski J, Cramer W, Erhard M, Hickler T, Smith B, 2006.** The importance of representing age-related decline in forest NPP for modeling regional carbon balances. *Ecological Applications* 16: 1555–1574.
- Zobler L, 1986.** A world soil file for global climate modelling. NASA Technical Memorandum 87802. NASA Goddard Institute for Space Studies, New York.

ERRATUM

This erratum contains corrections and minor updates to the report TR-09-04. The updates are based on extended global climate model simulations performed after the project was finalised, but do not affect the regional climate model simulations. Furthermore, none of the corrections and updates change the main conclusions of the project. Therefore, no changes are made in Chapter 4 and 5.

Stockholm, February 2010

Jens-Ove Näslund
Person in charge of the SKB climate program

Precipitation

An error was made in the figures of the precipitation rate in the global climate model simulation in that precipitation falling as snow was counted twice. Figures 2-3, 3-4, 3-24 and 3-44 should therefore be replaced by the new figures included below. Since the error was made for all simulations, the total error in differences between two simulated climates is sometimes small and the general features of the differences unchanged when the error is corrected. Paragraphs that should be replaced due to this error are given below (the Section in TR-09-04 is indicated in parenthesis).

The global climate model (Section 2.2.1)

Pages 15-16 (last paragraph, page 15, first lines of page 16)

The simulated climate of the recent past is compared with the National Centre for Environmental Protection (NCEP) re-analysis /Kalnay et al. 1996/ of surface temperature (T_s) for summer (June–August) and winter (December–February). The re-analysis data set consists of data from a numerical weather prediction model that is forced by a very large number of observations of the state of the atmosphere. This implies that the re-analysis closely follows the actual evolution of the climate system and that it is a physically consistent data set. The simulated climate shows a reasonable agreement to observations although regionally large differences of up to 10°C occur (Figure 2-2). The simulated summer near-surface temperature is 1°C too warm in western Fennoscandia and 4°C too cold in eastern Fennoscandia. Fennoscandian winter near-surface temperature is 1–4°C too warm as compared with the re-analysis. The simulated present-day total surface precipitation is shown in comparison to observed precipitation in Figure 2-3. Rather large errors are found in the tropics similar to the results reported by /Collins et al. 2006/ for their simulation with CCSM3 of the recent past climate with higher atmospheric resolution. The simulated climate is 20–30% (5–15 mm/month) too dry around the Scandinavian coast in summer. The simulated climate is 40–50% (15–45 mm/month) too dry at the Norwegian west coast and up to 50% (45 mm/month) too wet in eastern Scandinavia in winter. This west to east distribution of the error across the Scandinavian mountain range is mainly explained by the coarse representation of the Scandinavian mountain range in the CCSM3 model domain. Only small errors in summer and winter precipitation are found over eastern Fennoscandia, the simulated climate is 10–15% too dry corresponding to 5–10 mm/month.

Page 17 (last paragraph)

Figure 2-4 shows a comparison between the RP-r simulation and climatological data from observations from the Climatic Research Centre (CRU, version TS2.1) /Mitchell and Jones 2005/ for the years 1961–1990. The CRU gridded data are interpolated into the RCA3 grid without any adjustment of altitude. In locations where the altitude of the model grid and the CRU grid differs significantly this can result in biases as there is a strong altitude dependence in temperature (6.5°C per 1,000 m in the standard atmosphere). As large differences in altitude are restricted to a few grid boxes in

mountainous areas this will only have a local effect and even there it does not introduce any large-scale systematic differences. The comparison between RCA3 and CRU is made for monthly mean conditions for July and January. These specific months are the coldest and warmest in Europe in the *glacial case* and are consequently used for the RCM comparison to proxy data (see Section 3.2.2). Large-scale features inherited from CCSM3 are seen also in RCA3. Examples of this are; a warm bias in winter particularly over eastern Europe (Figure 2-4, upper right panel), and a cold bias in most of northern Europe in summer (Figure 2-4, upper left), implying too weak a seasonal cycle in large areas. Likewise, for precipitation, large-scale features from CCSM3 can also be identified, like a dry bias in summer in south-eastern central Europe (Figure 2-4, lower left) and a wet bias in central Europe in winter (Figure 2-4, lower right). Also notable differences between RCA3 and CCSM3 can be seen. Due to the higher horizontal resolution, RCA3 shows, as expected, more details in many areas including mountainous areas and coastal regions. The geographical distribution of precipitation across the Scandinavian mountain range in RCA3 and CCSM3 during winter in comparison to observations is similar (i.e. a smaller dry bias along the Norwegian west coast and a smaller wet bias in Sweden) (Figure 2-4, lower right). Some biases still exist, these may include excessive precipitation in mountainous regions, although part of this potential bias may in fact be related to the observations, as there are known problems with under-catch of precipitation /Rubel and Hantel 2001/. Some more results showing how RCA3 simulates the recent past climate are given when we present results for the *warm case* (Section 3.1.2). A limited comparison with observations for the combination RCA3 and CCSM3 for the recent past climate can be found in Chapter 4, where we present results for a few specific locations in Sweden and Finland.

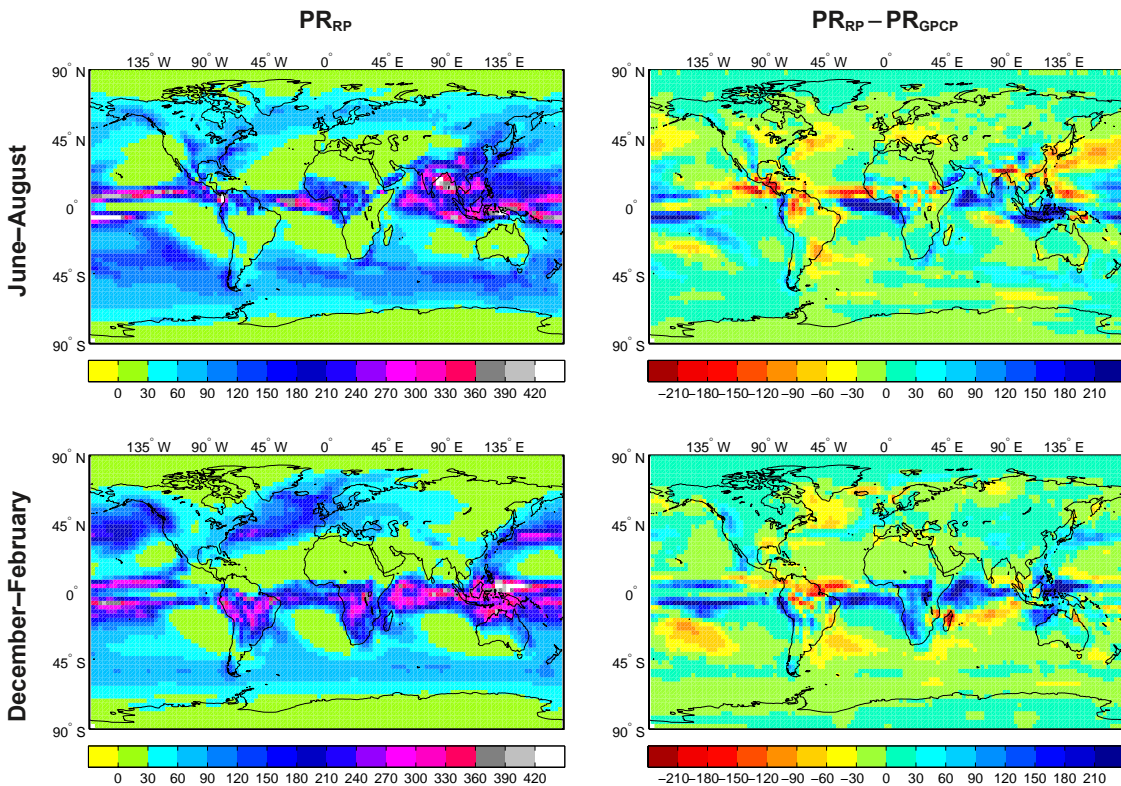


Figure 2-3. The simulated recent past (RP) precipitation (PR_{RP}) and the difference between simulated recent past climate and observed data as shown by the GPCP dataset (PR_{GPCP} , /Adler et al. 2003/). Units are mm/month.

The warm case; Global climate model simulations (Section 3.3.1)

Precipitation paragraph, page 39

No text changes are needed.

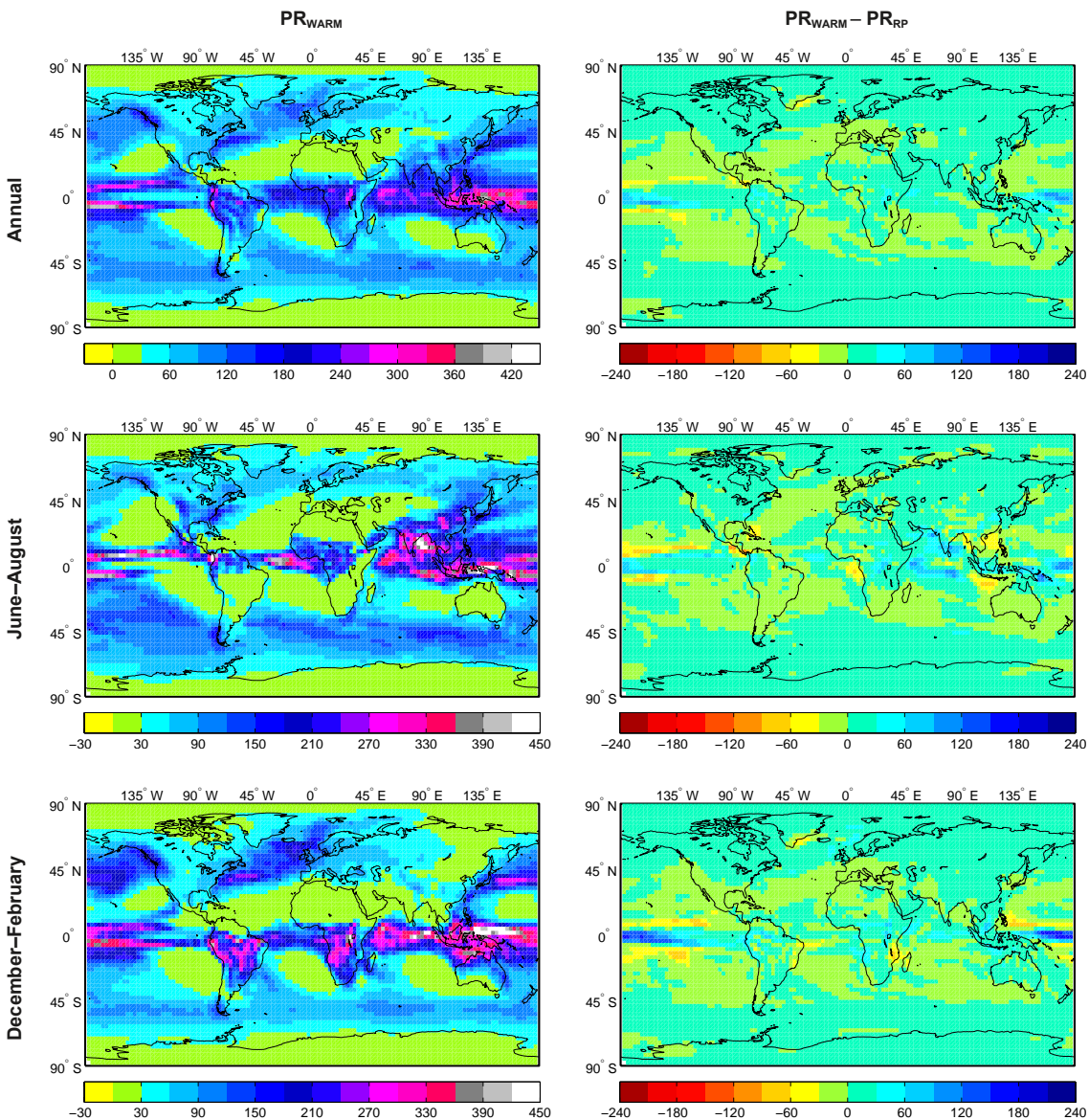


Figure 3-4. The simulated precipitation in the WARM simulation (PR_{WARM}) and the difference compared with the simulated recent past climate (PR_{RP}). Units are mm/month.

The glacial case; Global climate model simulations (Section 3.2.1)

Precipitation paragraph, page 59

The Atlantic storm track is shifted southwards from the pre-industrial simulation to the LGM1 simulation which results in a decrease in the high latitude precipitation and an increase in that at mid-latitudes (see Figure 3-24). The difference in the annual mean precipitation between the LGM2, LGM-v and LGM-vd and LGM1 simulations is also shown in Figure 3-24. The dominating change in all three is the decrease in precipitation in the Greenland-Iceland-Norwegian Seas that accompanies the increase in sea-ice extent in this region (Figure 3-17). These changes also influence the Fennoscandian precipitation resulting in a net decrease in the annual mean precipitation from the pre-industrial simulation to the LGM2, LGM-v and LGM-vd simulations, respectively.

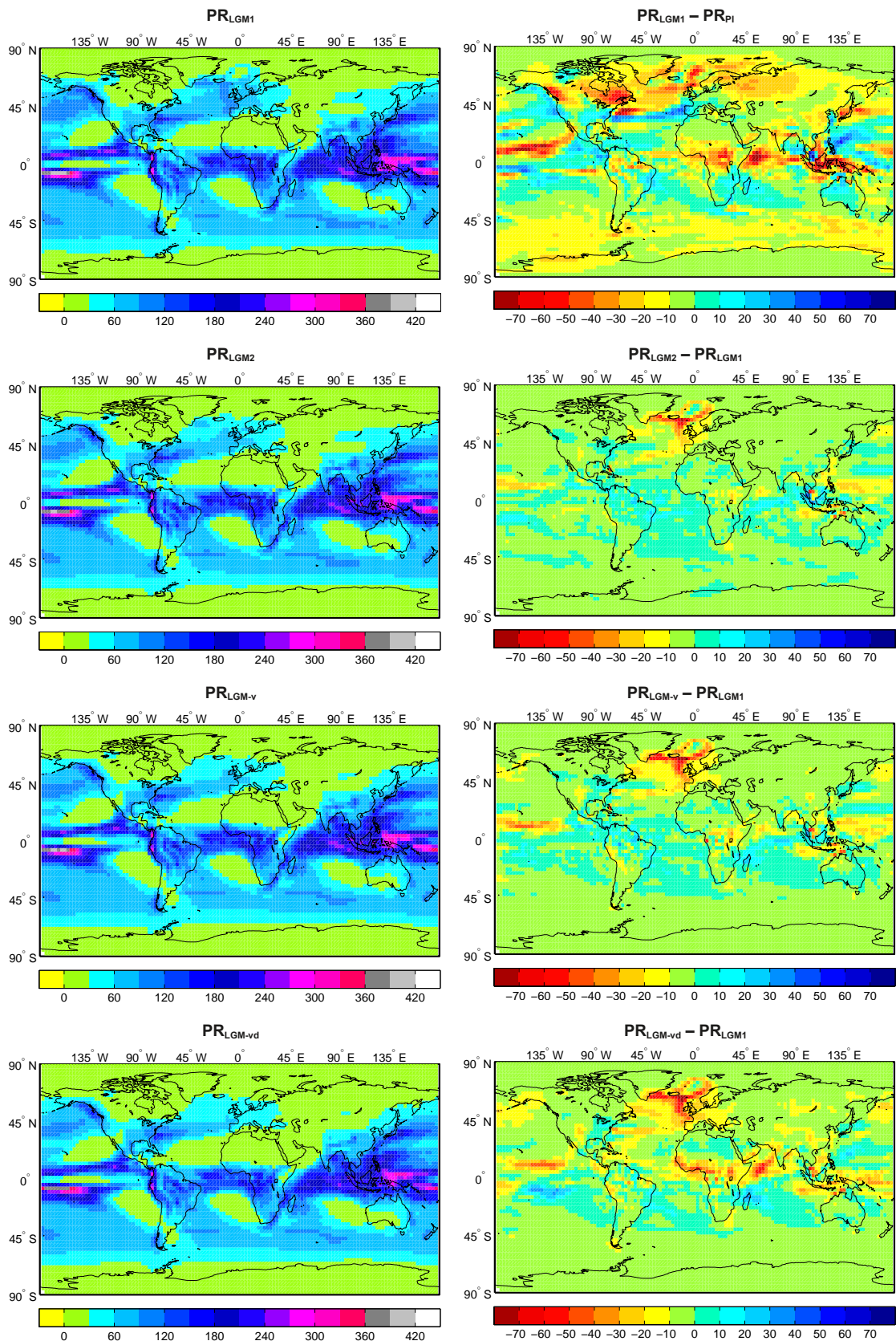


Figure 3-24. Annual mean precipitation (PR) in the four LGM simulations (left). To the right are the difference in the annual mean precipitation between the LGM1 simulation and the pre-industrial (PI) simulation (top) and between the LGM2, LGM-v and LGM-vd simulations and the LGM1 simulation (lowermost three panels). Units are mm/month.

The permafrost case; Global climate model simulations (Section 3.3.1)

Precipitation paragraph, page 80

The Atlantic storm track is shifted southwards from the PI simulation to the PERMAFROST simulation, similar to the situation in the LGM simulations. This shift leads to less precipitation in Fennoscandia (see Figure 3-44). The shift is however not as extensive as in the LGM simulations. Compared with the LGM2 simulation (also shown in Figure 3-44), the precipitation is thus shifted northwards in the Atlantic in the PERMAFROST simulation.

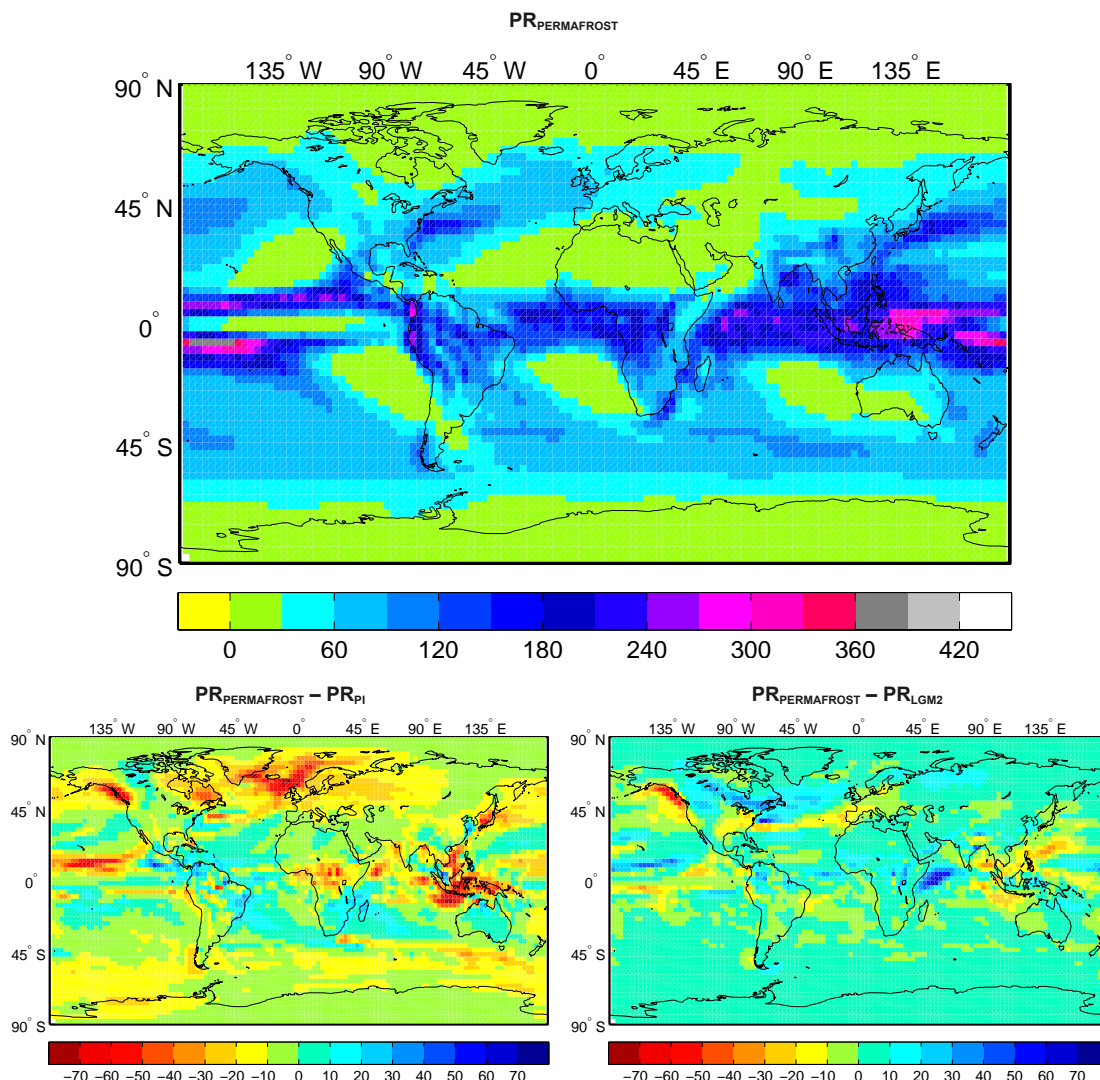


Figure 3-44. Annual mean precipitation in the PERMAFROST simulation (top). The lower panels show differences in the annual mean precipitation between the PERMAFROST simulation and the pre-industrial simulation and between the PERMAFROST simulation and the LGM2 simulation. Units are mm/month.

Variability in the annual global mean surface temperature

The variability in the annual global mean surface temperature is analysed for the *glacial* and *permafrost* cases. This analysis was intended to give an understanding of the dynamics of the variations in the annual global mean surface temperature. We have realised that the method used is very sensitive to trends in the timeseries and in principal the method picks up the trend rather than the variations around the mean. Since the climate is not in an equilibrium state in the first period of the *glacial*

case that we analyse (LGM1), it is not possible to get statistically significant results in an analysis of the variability for this period /Brandefelt and Otto-Bliesner 2009/. For the second period of the *glacial* case (LGM2), which is an equilibrium state, statistically significant results are obtained. The *permafrost* case was not in complete equilibrium when it was stopped after 886 years. Therefore, the simulation has been continued, after the project was finalised, to a total length of 1,538 years. The complete timeseries is shown in Figure 3-38. The *glacial* case simulation was also continued after the project was finalised to a total length of 1,862 years. This was done to confirm that LGM2 is a true equilibrium. The complete timeseries is shown in Figure 3-16. Here, we present the results of analysis of the variability in the last 450 years of the extended glacial case simulation and the last 300 years of the extended permafrost simulation. The analysis follows /Brandefelt and Otto-Bliesner 2009/.

Figures 3-16, 3-25, 3-38 and 3-45 should be replaced by the new figures below. Paragraphs that should be replaced are given below.

The glacial case; Global climate model simulations (Section 3.2.1)

Variability paragraph, pages 59–63

The amplitude of the inter-annual variability in T_{agm} and the sea ice fraction (Figure 3-16) is increased from LGM1 to LGM2, LGM-v and LGM-vd. The standard deviation of T_{agm} (sea ice fraction) is 0.064°C (0.094%) in LGM1 as compared to 0.095°C (0.16%) in LGM2. To investigate how this variability in the global mean is connected to variability in the atmospheric and oceanic dynamics, anomalies from the mean climate are studied. The anomalies are determined as an average over all years with T_{agm} more than (and less than) 1.5 standard deviations above (and below) the average. The difference between anomalies associated with high and low T_{agm} is analyzed. A two-sided students t-test is utilized to test the statistical significance of the difference. We only discuss differences that are statistically significant at the 95% level. Due to the short period of the first quasi steady state (LGM1) the analysis of anomalies from the mean climate does not yield statistically significant results for this period. We therefore concentrate on the results for LGM2.

The difference between globally warm and cold years in LGM2 is focused over oceans in the Northern Hemisphere extra tropics (Figure 3-25). The largest difference is found over Greenland and Northern Europe with a maximum of 6.8°C in T_s and 28% in the fraction of sea ice in the North Atlantic. The mean sea level pressure (MSLP) is up to 2.8 hPa lower and the total amount of precipitation is up to 32% higher over the North Atlantic and the North Pacific region in warm years than in cold years. The difference in the stationary wave component (i.e., the deviation from the zonal mean) of the geopotential height at 300 hPa (not shown) between globally warm and cold years is a wave pattern with five lows and highs (i.e. zonal wavenumber five) encompassing a latitude circle and extending around the Northern Hemisphere. This wave pattern is similar to that found by /Byrkjedal et al. 2006/ in an investigation of the sensitivity of the LGM climate to a reduction in sea ice conditions in the Nordic Seas. They use an atmospheric model forced by prescribed sea surface temperature and sea ice extent. The reduction in North Atlantic sea ice used by /Byrkjedal et al. 2006/ is greater than the difference between globally warm and cold years in the present study and the response in temperature and precipitation is stronger, but the change in stationary waves show a similar wave number five pattern as here. The difference between globally warm and cold years in the MSLP is associated with differences in the surface winds and the surface wind forcing of the oceanic circulation. The forcing of the oceanic circulation (zonal wind stress curl) and the northward oceanic heat transport in the extra-tropical North Atlantic is greater during globally warm than cold years (Figure 3-25). Further, the sinking branch of the AMOC is shifted further north in globally warm years as compared to cold years (not shown). This difference in the ocean circulation is also seen in a 200–400 meters thicker oceanic mixed layer (Figure 3-25) and a $100\text{--}180 \text{ W m}^{-2}$ stronger surface heat flux from the ocean to the atmosphere (not shown) south of Greenland and Iceland and in the Greenland Iceland Norwegian Seas.

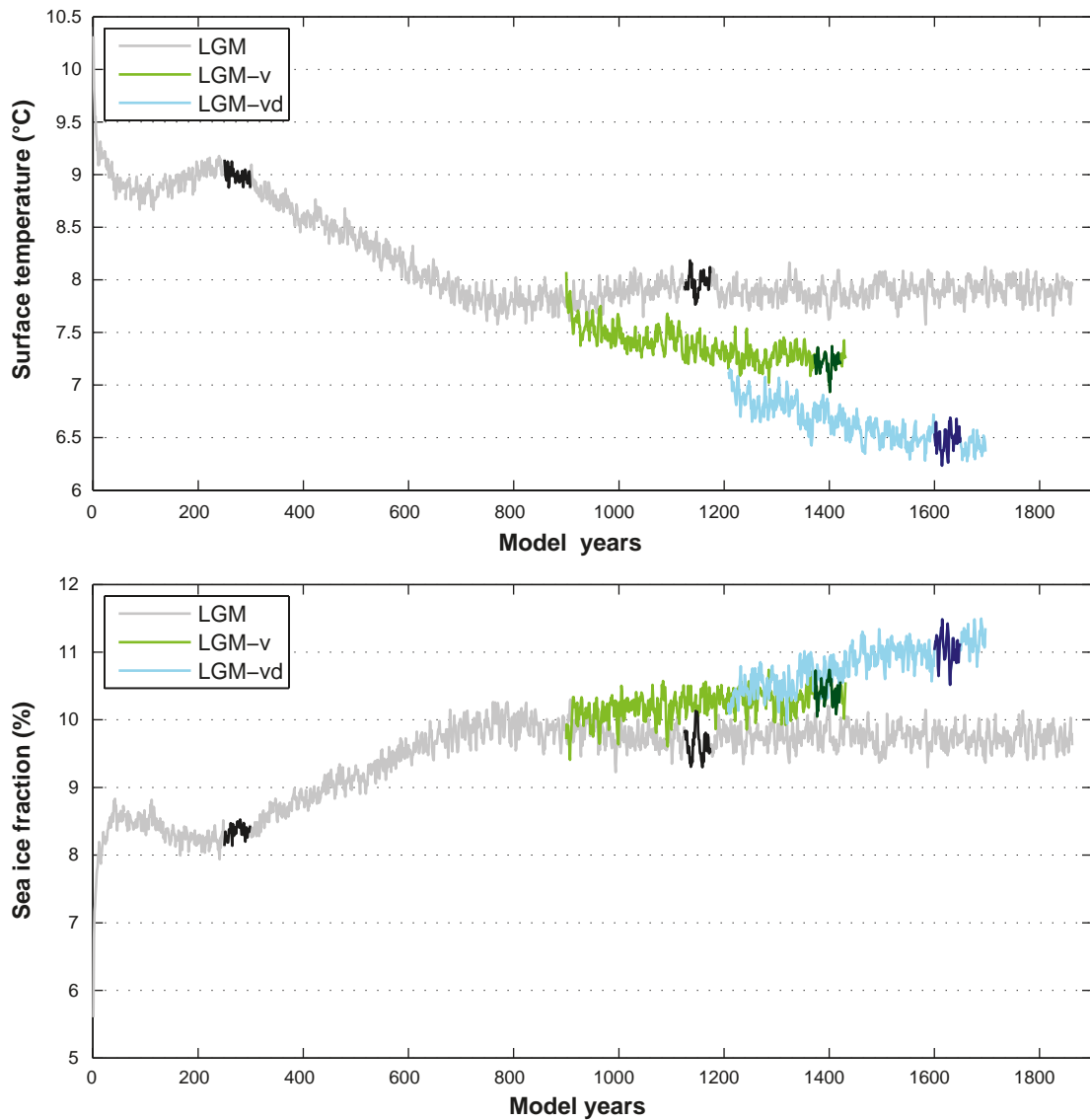


Figure 3-16. Annual global mean near-surface temperature (upper panel) and sea-ice fraction (lower panel) for the glacial case in the LGM (grey), LGM-v (green) and the LGM-vd simulation (blue). Darker parts of the curves mark the 50-year periods analysed here (in the LGM simulation the first 50-year period is referred to as LGM-1 in the text and the second as LGM-2). Units are °C and % of the surface covered by sea ice.

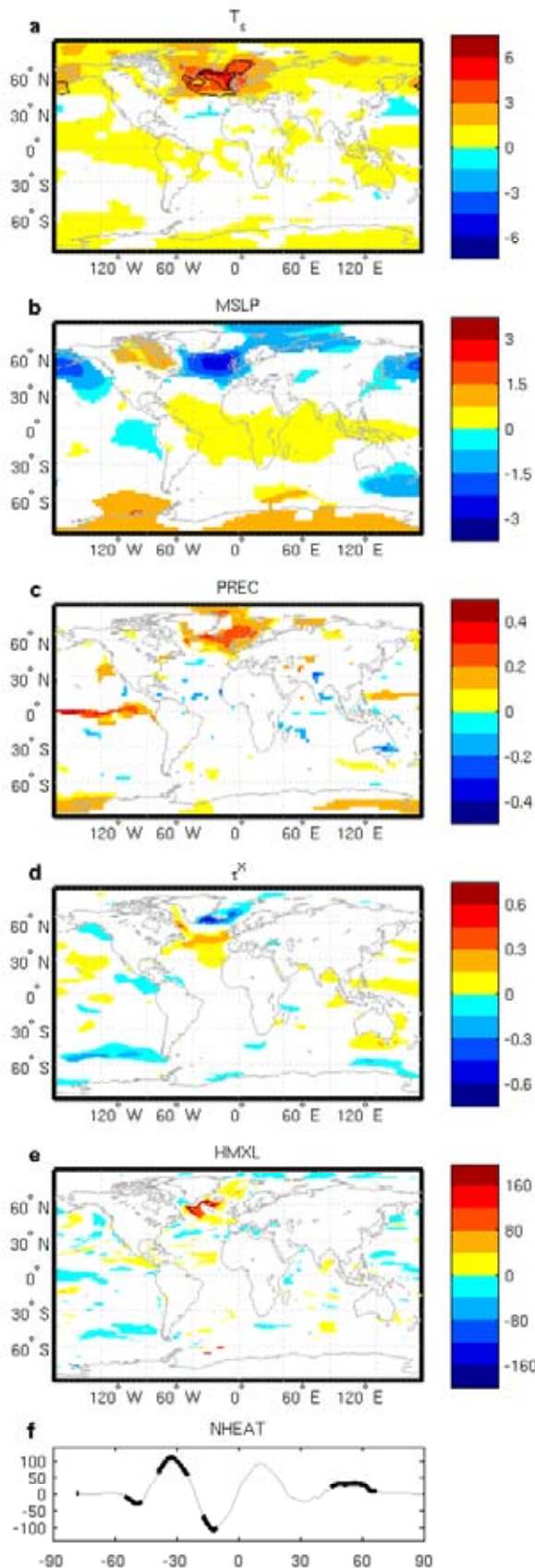


Figure 3-25. Annual mean difference between globally warm and cold years in the LGM2 simulation (model years 1413–1862) in (a) surface temperature (C; shading) and fraction of sea ice (contours at 20% and 10%), (b) mean sea level pressure (hPa), (c) relative precipitation (%), (d) zonal wind stress (Nm^2), (e) oceanic mixed layer depth (m), and (f) oceanic northward heat transport (TW). Only statistically significant (95% level) differences are shown.

The permafrost case; Global climate model simulations (Section 3.3.1)

Variability paragraph, page 80

The amplitude of the inter-annual variability in T_{agm} and the sea ice fraction (Figure 3-38) in the PERMAFROST simulation is higher than in the LGM1 simulation but lower than in the LGM2, LGM-v and LGM-vd simulations. The standard deviation of T_{agm} (sea ice fraction) is 0.081°C (0.10%) in the PERMAFROST simulation as compared to 0.095°C (0.16%) in LGM2. To investigate how this variability in the global mean is connected to variability in the atmospheric and oceanic dynamics, anomalies from the mean climate are studied. The same method is used as for the glacial case.

The difference between globally warm and cold years is not as strong and spatially focused in the PERMAFROST case as in the LGM2 period (Figure 3-45). The largest differences are found in T_s over Alaska with a maximum of 1°C . This heating is associated with a deepening of the Aleutian low in the Northern Pacific by up to 2 hPa and increased precipitation in the tropical Pacific Ocean.

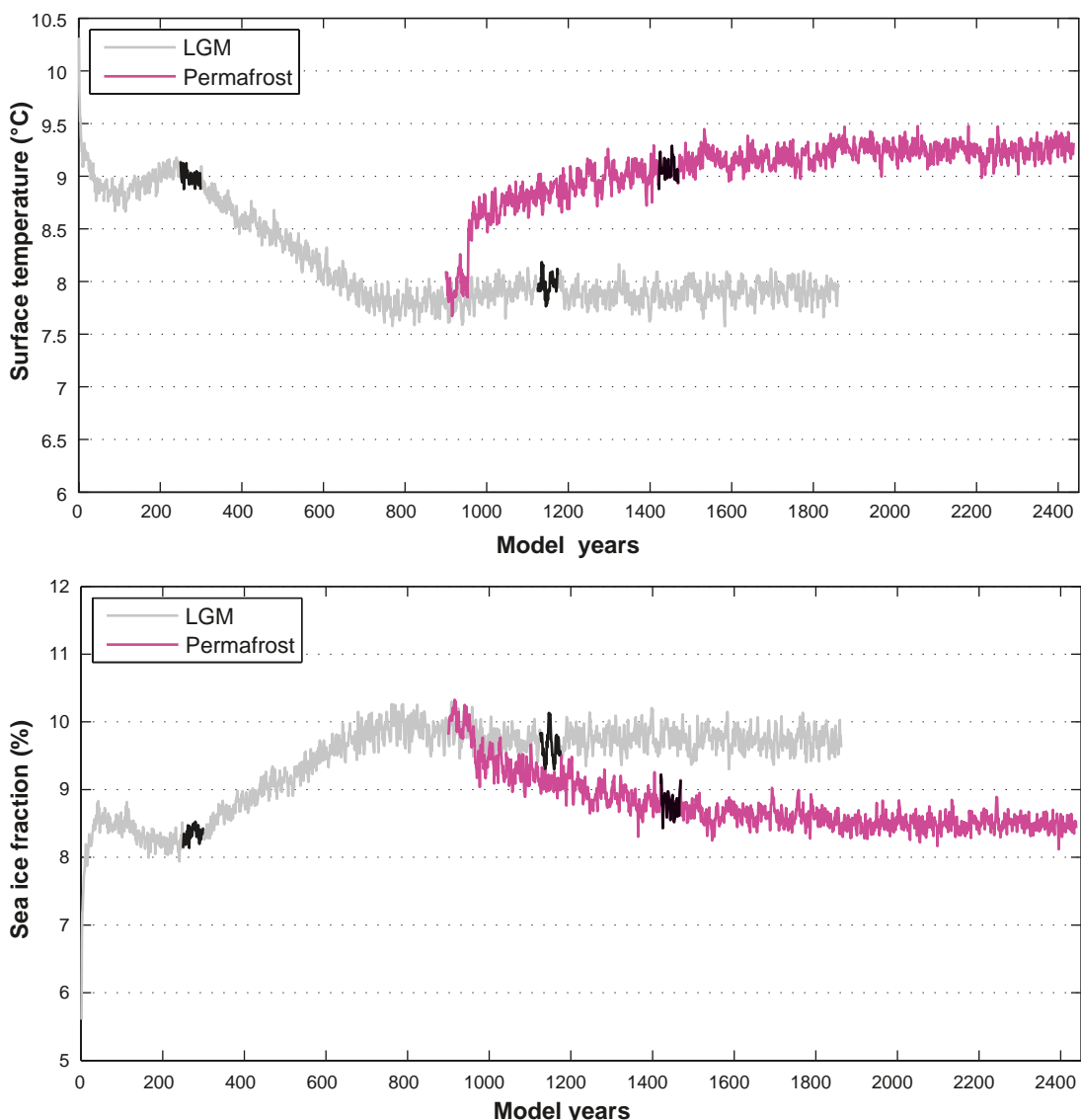


Figure 3-38. Annual mean global mean near-surface temperature (upper panel) and sea ice fraction (lower panel) in the LGM (grey) and PERMAFROST (pink) simulations. Darker parts of the curves marks the 50-year periods analysed here. Units are $^{\circ}\text{C}$ and % of the Earth's surface covered by sea ice.

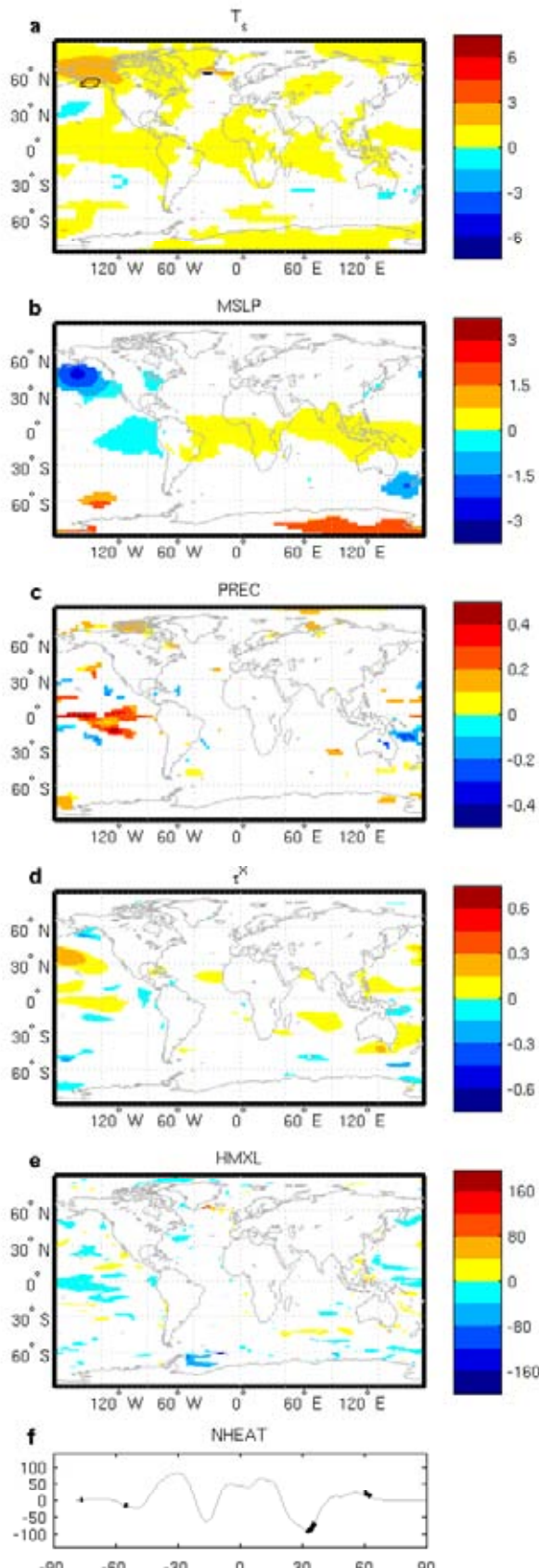


Figure 3-45. Annual mean difference between globally warm and cold years in the PERMAFROST simulation (model years 2139–2438) in (a) surface temperature (C; shading) and fraction of sea ice (contours at 20% and 10%), (b) mean sea level pressure (hPa), (c) relative precipitation (%), (d) zonal wind stress (Nm^2), (e) oceanic mixed layer depth (m), and (f) oceanic northward heat transport (TW). Only statistically significant (95% level) differences are shown.

Extended global simulation of the Permafrost case

The PERMAFROST simulation has been continued after the project was finalised to a total length of 1,538 years in order to allow the ocean to reach equilibrium. The extended simulation used a total of 16 calendar months to run on the computing facility Tornado. This time was not available within the project and we therefore chose to downscale a period after approximately 500 years of simulation. As seen from the timeseries of global annual mean T_s and sea ice fraction (Figure 3-38), the simulated climate slowly adjusts to the imposed changes in forcing and boundary conditions. The annual global mean T_s only changes by 0.10°C from the period analysed and downscaled within the project (model years 1420–1469) to the last 50 years of the simulation (model years 2389–2438). Nevertheless, significant regional differences in the simulated climate between these two periods exist.

The difference between these two periods is significant in Northern Hemisphere winter (December–February) in the Arctic and the northern North Atlantic region. The air temperature at 2 meters height (T_{2m}) is more than 2°C warmer in the northern North Atlantic region with a maximum of 8°C located in south-eastern Greenland in the last century of the simulation than in model years 1400–1499 (Figure E-1). Further, the precipitation rate is increased by more than 20% in this region with a maximum of 65% located in south-eastern Greenland (Figure E-1). These differences are associated with a decrease of 20–30% of the fraction of the surface covered by sea ice also displayed in Figure E-1. The cause of these differences is found in the slow adjustment of the ocean, which only reaches equilibrium after more than 1,000 years of model simulation. After 1,000 years of integration, the trends in the temperature and sea ice fraction in the Greenland – North Atlantic region are small (not shown).

These results are in agreement with /Brandefelt and Otto-Bliesner 2009/ who show that the evolution of the global mean T_s (even if it co-varies with other climate variables such as the strength of the AMOC) is not always a good indicator of when a simulated climate has reached a true equilibrium. Even relatively small trends in the state of the abyssal ocean must be taken into account.

Fortunately, the regional differences between the period that was downscaled within the project (model years 1420–1469) and the last 50 years of the extended simulation are less significant in Fennoscandia (Figure E-1). For Fennoscandia, the only significant differences are found in part summer and amount to 0.5–1°C in T_{2m} in the western part and 4–6 mm/month in precipitation in the southern part. These differences indicate that the simulated regional climate would have been up to 1°C warmer and 10% wetter if the last 50 years of the extended simulation had been downscaled. This difference is small as compared to the difference between the PERMAFROST case and the RP simulation, which amounts to more than –35°C and almost 100% in precipitation in northern Fennoscandia. We therefore conclude that the difference is insignificant for the conclusions drawn from the downscaling in the report regarding Fennoscandian climate. It should however be noted that the heating of the Greenland – North Atlantic region in the last 50 years as compared to the downscaled period makes the agreement with proxy data of SST in this region better.

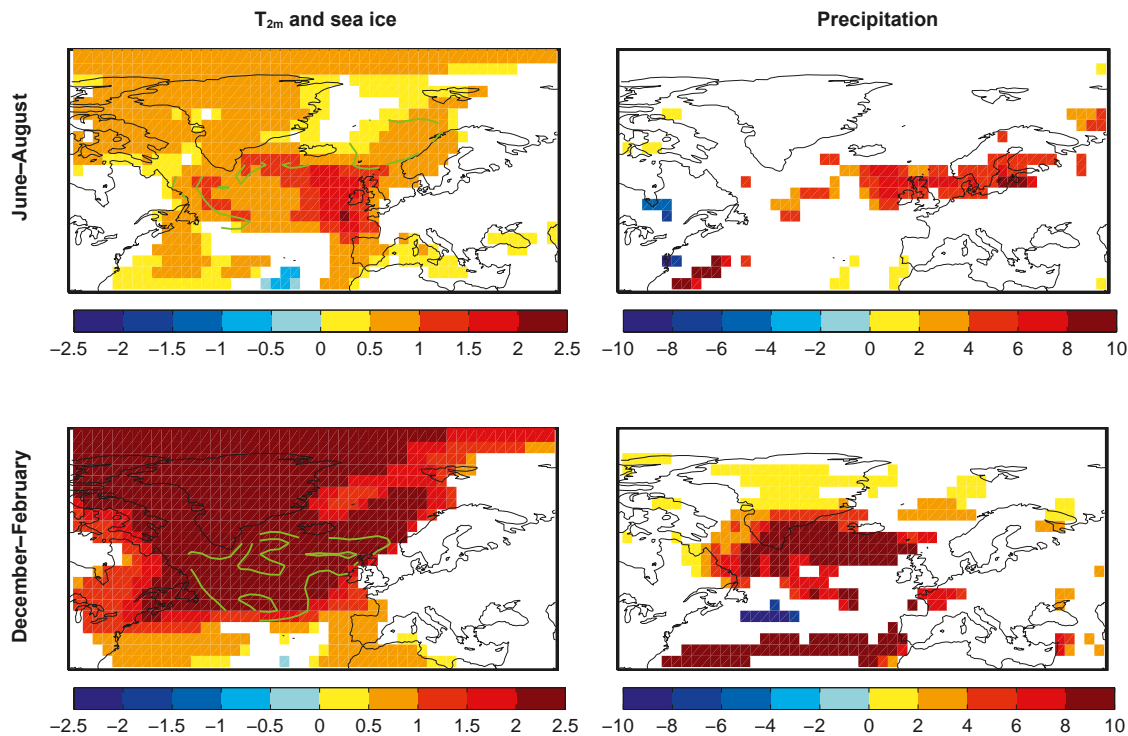


Figure E-1. Difference between the last 50 years of the extended global permafrost simulation (model years 2389–2438) and the downscaled period (model years 1420–1469). Summer (June–August, upper panels) and winter (December–February, lower panels) T_{2m} (shading) and fraction of the surface covered by sea ice (contours at -30% and -10%) (left panels) and precipitation (right panels). Units are °C, % and mm/month, respectively. Only differences that are statistically significant at the 95% level are shown.

References

- Adler R F, Huffman G J, Chang A, Ferraro R, Xie P-P, Janowiak J, Rudolf B, Schneider U, Curtis S, Bolvin D, Gruber A, Susskind J, Arkin P, Nelkin E, 2003. The version-2 Global Precipitation Climatology Project (GPCP) monthly precipitation analysis (1979–present). *Journal of Hydrometeorology* 4: 1147–1167.
- Brandefelt J, Otto-Bliesner B L, 2009. Equilibration and variability in a Last Glacial Maximum climate simulation with CCSM3. *Geophysical Research Letters* 36: L19712, doi:10.1029/2009GL040364.
- Byrkjedal Ø, Kvamstø N G, Meland M, Jansen E, 2006. Sensitivity of last glacial maximum climate to sea ice conditions in the Nordic Seas. *Climate Dynamics* 26: 473–487.
- Collins W D, Bitz C M, Blackmon M L, Bonan G B, Bretherton C S, Carton J A, Chang S, Doney C, Hack J J, Henderson T B, Kiehl J T, Large W G, McKenna D S, Santer B D, Smith R D, 2006. The Community Climate System Model (CCSM3). *Journal of Climate* 19: 2122–2143.
- Kalnay E, Kanamitsu M, Kistler R, Collins W, Deaven D, Gandin L, Iredell M, Saha S, White G, Woollen J, Zhu Y, Leetmaa A, Reynolds R, Chelliah M, Ebisuzaki W, Higgins W, Janowiak J, Mo K, Ropelewski C, Wang J, Jenne R, Joseph D, 1996. The NCEP/NCAR 40-Year Reanalysis Project. *Bulletin of the American Meteorological Society* 77: 437–471.
- Mitchell T D, Jones P D, 2005. An improved method of constructing a database of monthly climate observations and associated high-resolution grids. *International Journal of Climatology* 25: 693–712.
- Rubel F, Hantel M, 2001. BALTEX 1/6-degree daily precipitation climatology. *Meteorology and Atmospheric Physics* 77: 155–166.

Appendix A

Publications resulting from the project¹

Peer-reviewed papers, reports and manuscripts

Näslund J O, Wohlfarth B, Alexanderson H, Helmens K, Hättestrand M, Jansson P, Kleman J, Lundqvist J, Brandefelt J, Houmark-Nielsen M, Kjellström E, Strandberg G, Knudsen K L, Krog Larsen N, Ukkonen P, Mangerud J, 2008. Fennoscandian paleo-environment and ice sheet dynamics during Marine Isotope Stage (MIS) 3. Report of a workshop held September 20–21, 2007 in Stockholm, Sweden. Report R-08-79, Svensk Kärnbränslehantering AB, 52 pp.

Wohlfarth B, 2009. Ice-free conditions in Scandinavia during Marine Oxygen Isotope Stage 3? TR-09-12. Svensk Kärnbränslehantering. *In press.*

Brandefelt J, Otto-Bliesner B, *in prep.* Quasi-equilibria and variability in a Last Glacial Maximum climate simulation with CCSM3.

Kjellström E, Brandefelt J, Näslund J O, Smith B, Strandberg G, Voelker A, Wohlfarth B, *in prep.* Global and regional climate model simulations of a cold stadial within Marine Isotope Stage 3. Manuscript in prep. for Boreas.

Wohlfarth B, *in prep.* Manuscript on MIS 3 palaeodata in preparation for Boreas.

Strandberg G, Brandefelt J, Kjellström E, Smith B, *in prep.* High resolution simulation of Last Glacial Maximum climate and vegetation in Europe.

Conference abstracts

Brandefelt J, Strandberg G, 2007. Simulating extreme climate conditions in Sweden in a 100,000 year perspective. ICESM2007-A-00035, CESM Abstracts, 2007 Second International Conference on Earth System Modelling (ICESM).

Kjellström E, Brandefelt J, Strandberg G, Smith B, Wohlfarth B, Näslund J O, 2008. Global and regional climate model simulations of extreme climate conditions in Sweden in a 100,000 year perspective. EGU2008-A-02249. Abstracts of the contributions of the EGU General Assembly 2008. Geophysical Research Abstracts, 10. ISSN: 1029-7006.

Strandberg G, Brandefelt J, Kjellström E, 2008. Modelling last glacial maximum climate variability with a high resolution regional climate model. EGU2008-A-03244. Abstracts of the contributions of the EGU General Assembly 2008. Geophysical Research Abstracts, 10. ISSN: 1029-7006.

Kjellström E, Brandefelt J, Strandberg G, Smith B, Wohlfarth B, Näslund J O, 2009. Global and regional climate model simulations of extreme climate conditions in Sweden in a 100,000 year perspective. UN Climate Change Conference March 2009, Copenhagen. Theme 1: Exploring the Risks: Understanding Climate Change. Session: Informing the Future by Understanding the Past. Abstract accepted for poster presentation.

Strandberg G, Brandefelt J, Kjellström E, 2009. High-resolution regional climate model simulations for a 50-year period under Last Glacial Maximum conditions. EGU2009-9258. Abstracts of the contributions of the EGU General Assembly 2009. Geophysical Research Abstracts, 11.

Strandberg G, Brandefelt J, Kjellström E, Smith B, 2009. Simulating cold palaeo climate conditions in Europe with a regional climate model. 2nd Lund Regional-scale Climate Modelling Workshop: 21st Century Challenges in Regional-scale Climate Modelling.

¹ as of March 2009

Appendix B

Deliverables and data format for input- and output data stored in data base at SKB

Project: Climate conditions in Sweden in a 100,000 year time Perspective

Delivered: 20090325

From: Gustav Strandberg, SMHI

To: Jens-Ove Näslund, SKB

This data was delivered within the project Climate conditions in Sweden in a 100,000 year time perspective. The project is described in the following report: Kjellström E, Brandefelt J, Näslund J-O, Smith B, Strandberg G, Wohlfart B, Climate conditions in Sweden in a 100,000-year time perspective, Svensk Kärnbränslehantering AB, *report TR-09-04*.

Models

We used the Community Climate System Model version 3 (CCSM3) /Collins et al. 2006/ as Atmosphere-Ocean General Circulation Model (AOGCM). The Rossby Centre regional climate model RCA3 /e.g. Kjellström et al. 2005/ was the Regional Climate Model (RCM) applied for the downscaling of results from CCSM3 to a higher resolution for Europe. We used the Dynamic Vegetation Model (DVM) LPJGUESS /Smith et al. 2001/ to generate fields of potential vegetation (*i.e.* the vegetation that would exist if it were not for human intervention) for land areas covered by the RCM domain (Europe and northern Africa). See /Kjellström et al. 2009/ Chapter 2.2.

Cases

Four cases were modelled: A stadial at 44 kyr BP during Marine Isotope Stage 3 (PERMAFROST), the Last Glacial Maximum (LGM2) at 20 kyr BP, the Recent Past (RP) and a warm period a few thousand years into the future (WARM). RCM output get the suffix “-r”. RCM output where vegetation from the DVM was used get the suffix “-r-veg”. See /Kjellström et al. 2009/ Chapter 2.1.

Time periods

The AOGCM was run for several hundreds of model years to get a climate in equilibrium. 50-year periods were then selected to be down-scaled. The time periods which were down-scaled by the RCM were (in model years): PERMAFROST: 1420-1469, LGM2: 1125-1174, RP:1961-1990, WARM:1151-1200.

Data needed to reproduce results

CCSM3 data

The data needed to restart or rerun the CCSM3 simulations are saved as NetCDF in ccsm3/.

LPJ-GUESS data

The data needed to run LPJ-GUESS is saved as plain text files in lpj_guess/. The files are explained further in the document readme.doc saved with the data.

RCA3 data

The data needed to run RCA3 is saved. They are listed in below.

Resulting data

All variables are saved for the grid box closest to the three locations Forsmark, Oskarshamn and Olkiluoto as NetCDF (.nc) files (rca3/\$CASE/netcdf) and text (.txt) files (rca3/\$CASE/txt). Some variables are saved as fields for the whole model domain. European fields with 3h resolution are for LGM2, PERMAFROST and WARM split into two files of 25 years each, pt1 and pt2. They are marked with “*” in the list below. This is because there was a problem to write large files to the hard drive. All variables are listed below. See /Kjellström *et al.* 2009/ Ch. 4 for information on the three locations.

Figures

All figures in the report “Climate conditions in Sweden in a 100,000 year time perspective” are saved as image files in figures/. Specific fields, time series etc from CCSM3 and RCA3 used to make the figures are also saved in figure_data/.

References

- Collins W D, Bitz C M, Blackmon M L, Bonan G B, Bretherton C S, Carton J A, Chang S, Doney C, Hack J J, Henderson T B, Kiehl J T, Large W G, McKenna D S, Santer B D, Smith R D, 2006.** The Community Climate System Model (CCSM3), *Journal of Climate* 19: 2122–2143.
- Kjellström E, Bärring L, Gollvik S, Hansson U, Jones C, Samuelsson P, Rummukainen M, Ullerstig A, Willén U, Wyser K, 2005.** A 140-year simulation of European climate with the new version of the Rossby Centre regional atmospheric climate model (RCA3). *Reports Meteorology and Climatology*, 108, SMHI, SE-60176 Norrköping, Sweden, 54 pp.
- Smith B, Prentice I C, Sykes M T, 2001.** Representation of vegetation dynamics in modelling of terrestrial ecosystems: comparing two contrasting approaches within European climate space. *Global Ecology and Biogeography* 10: 621– 637.

Variable	Name	Unit	Resolution	Field (Europe)
Convective precipitation	CPrecip	mm	3h	Yes*
Convective snow precipitation	snowconvprc	mm	6h	No
Deep soil temperature	tsoild	K	24h	No
Evaporation	evap_a	mm	6h	Yes
Geopotential height 850	gpot850	m2/s2	6h	Yes
Geopotential height 500	gpot500	m2/s2	6h	Yes
Geopotential height 300	gpot300	m2/s2	24h	Yes
Ground temperature 1	tsland1	K	24h	No
Ground temperature 2	tsland2	K	24h	No
Ground temperature 3	tsland3	K	24h	No
Ground temperature 4	tsland4	K	24h	No
Ground temperature 5	tsland5	K	24h	No
Humidity	q2m	kg/kg	3h	No
Lake ice thickness	Lakelce	m	24h	Yes
Large scale precipitation	LPrecip	mm	3h	Yes*
Large scale snow precipitation	snowlsprc	mm	6h	No
Leaf area index	lwai	–	24h	No
Long wave net. radiation on surface	LnetRad	W/m2	6h	Yes
Maximum surface temperature	tsmax	K	24h	No
Maximum 2 m temperature	t2max	K	24h	No
Minimum surface temperature	tsmin	K	24h	No
Minimum 2 m temperature	t2min	K	24h	No
Potential evapotranspiration	latfp1	mm/day	3h	No
Relative humidity 850	rh850	–	6h	Yes
Relative humidity 500	rh500	–	6h	Yes
Relative 2m humidity, grid average	rh2	–	3h	Yes*
Runoff	runoff	mm	6h	No
Sea ice or lake ice concentration	SLiceConc	–	24h	Yes
Sea level pressure	slp	Pa	3h	No
Sea surface temperature	sst	K	6h	Yes
Short wave net. radiation on surface	SnetRad	W/m2	6h	Yes
Snow cover	snowcov	–	24h	No
Snow fall	snowprc	mm	30min	No
Surface pressure	surfp	Pa	3h	Yes*
Temperature 2m	t2m	K	3h	Yes*
Temperature 850	t850	K	6h	Yes
Temperature 500	t500	K	6h	Yes
Temperature 300	t300	K	24h	Yes
Total cloud cover	cov2d	–	3h	Yes*
U 10m	U10	m/s	3h	No
V 10m	V10	m/s	3h	No

Appendix C

Glossary

This appendix contains a glossary of abbreviations used in the report.

AMOC	Atlantic Meridional Overturning Circulation.
AOGCM	coupled Atmosphere Ocean General Circulation Model.
CCSM3	Community Climate System Model version 3 (http://www.ccsm.ucar.edu/).
CMIP3	Climate Model Intercomparison Project No3 (http://www-pcmdi.llnl.gov/projects/cmip/index.php).
DVM	Dynamic Vegetation Model.
EMIC	Earth system Model of Intermediate Complexity.
IPCC	Intergovernmental Panel on Climate Change (http://www.ipcc.ch/).
GCM	General Circulation Model or Global Climate Model.
GHG	Greenhouse gas.
GIA	Global Isostatic Adjustment or Glacial Isostatic Adjustment.
GIS	Greenland InterStadial. Relatively warm period during glacial, recorded in Greenland ice cores.
GS	Greenland Stadial. Relatively cold period during glacial, recorded in Greenland ice cores.
LGM	Last Glacial Maximum.
LPJ-Guess	DVM used at the Department of Physical Geography and Ecosystems Analysis, Lund University (http://www.nateko.lu.se/lpj-guess/lpj_guess_main.html).
MIS3	Marine Isotope Stage 3.
MSLP	Mean Sea Level Pressure (Surface pressure reduced to the mean level of the sea surface under assumption of an air temperature following the standard atmosphere).
NCAR	National Centre for Atmospheric Research (http://www.ncar.ucar.edu/).
NAO	North Atlantic Oscillation.
PFT	Plant Functional Type. (The concept of PFTs is used to obtain the leaf physiological and whole-plant parameters for biomes consisting of mixed species. A PFT is assumed to have measurable properties of stomatal conductance, root depth, etc. In climate and vegetation modelling the landscape can be represented as patches of PFTs that are combined to yield information about the larger grid box of the model).
PMIP	Paleoclimate Model Intercomparison Project (http://pmip.lsce.ipsl.fr/).
ppm/ppb	Unit for concentration of e.g. gases in air (1 ppm = 1 part per million/billion).
RCA3	RCM at the Rossby Centre, SMHI (http://www.smhi.se/sgn0106/if/re/rca.htm).
RCM	Regional Climate Model.
SRES	Special Report on Emission Scenarios (by the IPCC).
SST	Sea Surface Temperature.
Sv	Sverdrup (unit for flux of water, 1Sv = 1 km ³ /s).
T _{agm}	Annual mean global mean temperature.
Z300	Geopotential height of the 300hPa pressure level.

Appendix D

Terrestrial proxy data for the glacial case (LGM)

Table D1. Sites for which proxy data on temperature and precipitation are available for the glacial case (LGM). Data are from /Wu et al. 2007/.

Site	Long	Latı	Alti	Modern precipi- tation	Lower estimate (95% interval)		Central estimate		Upper estimate														
					Tjan1	Tjan	Tjan2	Tjul1	Tjul	Tjul2	Pjan1	Pjan	Pjan2	Pjul1	Pjul	Pjul2	Precipi- tation	AnnT1	AnnT	AnnT2	AnnP1	AnnP	AnnP2
Castigl	12.75	41.89	44	811.7	-26.5	-11.2	5.3	-8.7	-4	-0.6	-94.7	-30.7	53.4	-99	-25.9	37.9							
Monticc	15.6	40.94	530	863.2	-26.5	-8.7	5.2	-7.1	-3.2	1.5	-106.1	-35.5	36.2	-79.8	-29.4	42.1							
Ioannin	20.73	39.76	469	1,400.2	-29	-16.8	3.6	-6.7	-2.1	0.9	-117.5	-33.1	27.5	-91.3	-28.7	42.9							
Khimadi	21.58	40.61	560	858.8	-28.4	-10.9	5.9	-3.6	-0.8	0.8	-80.6	-24.5	57.9	-106.7	-21.3	57.5							
Xiniax	22.26	39.05	500	766.3	-15.7	-5.1	5	-8.2	-3.7	-0.7	-94.9	-24.9	54.8	-82.2	-24.1	36.8							
TenaghP	24.3	41.17	50	607.9	-31.1	-13.3	7.2	-6	-3.2	-0.3	-106.6	-12	44.1	-108.2	-27.7	18.8							
SutG	29.88	37.05	1,400	722.5	-18.3	-8.6	1.8	2.4	3.1	4.3	-111.4	-18.4	26.6	-66.1	-12.6	31.9							
Karamik	30.8	38.42	1,000	488.6	-18.2	-10	0.6	-5.1	-1.6	1.6	-94.7	-16.1	46.9	-31.4	6.5	41.8							
Ghab	35.3	35.68	300	501	-26.9	-19.1	-12.6	-12.2	-7.1	-4.5	-72.3	-23.6	63.1	-77.5	-7.3	37.5							
Zeribar	46.11	35.53	1,300	564.3	-15.3	-10.1	-5.7	-5.4	-4.4	-3.4	-99.3	-2.5	64.9	-46.4	2.6	39.8							
Padul	-3.67	37	785	496	-19	-9.4	1.4	-7	-4.1	-2.2	-92.5	-8	64.4	-63	3.2	44.3							
Banyols	2.75	42.13	173	737.5	-25.5	-8.8	4.7	-7.3	-3.7	0.5	-109	-27	55.9	-93.5	-35.4	22.2							
Ajo	-6.15	43.05	1,570	1,386.1	-30.7	-15.3	-1.5	-5.5	-3.7	-1.7	-70.7	0.8	58.4	-70.5	-14.3	63.7	1,386.1	-12.7	-7.9	-3	-672.4	-91.5	504.3
Biscaye	-0.17	43.27	410	803.5	-25.9	-7.4	4.7	-5.3	-1.5	2.1	-89.5	-30.7	47.3	-84.4	-60.2	-15.9	803.5	-8.9	-3.7	1.1	-542.1	-398.7	-133.9
Lourdes	-0.17	43.17	430	788.5	-24.8	-8.8	7.9	-5.2	-1.6	1.7	-110.4	-29.5	48.1	-102.3	-55.7	-11.8	788.5	-9.1	-4.2	1.5	-547.3	-365.2	-90.3
Bouchet	3.67	44.89	1,200	1,207.6	-33.3	-15.9	1	-8.8	-7	-5.5	-94.4	-14.2	50.7	-71.9	-12.1	32.7	1,207.6	-15.6	-10.3	-3.2	-532.9	-155.4	379.3
Echets	4.89	45.67	267	880.7	-30.5	-15.8	-5.3	-14.4	-12.4	-10.8	-62.8	-14.3	61.5	-96.7	-26.6	45.4	880.7	-19.6	-13.6	-10	-531.2	-197.6	232.6
GrandeP	6.5	47.73	330	911.6	-30	-16.4	-2	-11.4	-10.6	-9.1	-70.9	-17.5	50.3	-87.4	-26.7	48.7	911.6	-17.5	-12.7	-7	-580.8	-216	340.1
R053	19.08	69.73	35		-30.6	-12.3	4	-6.4	-3.5	-1.1													
R054	27.08	48.92	100		-32.6	-17	-0.6	-13.1	-11.9	-10.5													
R056	27.17	48.92	100		-27.9	-10.5	7.1	-4.6	0	2.7													
R057	31.1	47.65	100		-27.6	-13.8	5.1	-4	-0.8	1.7													
R058	31.11	47.65	100		-23.1	-11.6	3	-5.1	-0.8	3.5													
R003	37.19	56.37	128		-18.6	-8.7	1.2	-11.3	-9	-6.4													
R001	38.35	47.16	38		-28.5	-15.8	-1.5	-13.2	-8.9	-3.7													
R045	39.33	59.7	125		-32.4	-14.8	2.3	-9.5	-7.6	-6													
R002	39.58	56.92	136.8		-30.2	-14.8	2.4	-9.7	-8.5	-7.2													
R046	41	57.08	150		-22.4	-15.2	-8.1	-6.2	-3.6	-2.1													

Terrestrial proxy data for the permafrost case (MIS 3)

Table E1. All MIS3 climate proxy data compiled in /Wohlfarth 2009/.

Site #	Site name	Age range 14C	Age range cal yr BP acc to Cariaco-Hulu	Stratigraphy	MTCM	MTWM	Min summer temp	MAAT	Precipitation	Fossil indicators	Interstadial	GIS/GS	Environment	Author/s	Comments/BW	
1	Balglass Burn/Scotland	34,480-28,050	39,500-32,500		-26 to -10	8-10	13		low	coleoptera, plants	Denekamp	GIS 8-5	Open tundra, low floral diversity periglacial, discontinuous permafrost	/Brown et al 2007/		
2	Sourlie/Scotland	29,000-33,500	34,000-38,500	Layer 1			7		low	plants	Denekamp	GIS 8-5	Treeless, open ground, possibly permafrost	/Bos et al. 2004/		
				Layers 2-4	-34 to -11	6-9	9-10		low	coleoptera, plants						
				Layer 5			7-8		low	plants						
3	Tolsta Head, Lewis/Scotland	32,300-26,000	36,000-31,000				12-13			Nymphaea pollen	Denekamp/Tolsta	GIS 8-5	Rich herbaceous flora	/Whittington and Hall 2002/		
4	Oerel/Germany															
	Oerel	58,000-53,000	>60,000-57,500		-17 to -2	10-14	4- >10			Empetrum, Calluna; coleoptera	Oerel	GIS 15-16	Tree-less shrub tundra, alpine, subalpine	/Behre et al. 2005/		
	Glinde	48,000-52,000	52,000-57,000		-27 to -2	9-14	>4 - 14			S. selaginoides, coleoptera	Glinde	GIS 14	Shrub tundra, tree less	/Behre et al. 2005/		
5	Scheibe/Germany	28,000-32,000	32,500-36,000	OC I								GIS 5-7	Open landscape, locally sparse forests	/Hiller et al. 2004/		
		26,000-24,000	29,000-31,000									GIS 3-4				
		>37,000	>42,000	OC II								GIS 12-10	Open tundra landscape	/Hiller et al. 2004/		
			56,000	OC III								? GIS 14?	forest	/Hiller et al. 2004/	attributed to Early Weichselian	
6	Füramoos/Germany															
	47 59 N 9 53 E															
		50,500-53,700	56,000-58,000	Bellamont 1		6-14			pollen	Bellamont 1		GIS 13-14	Trees	/Müller et al. 2003/		
		43,000-44,000	45,500-46,500	Bellamont 2		6-14			pollen	Bellamont 2		GIS 12	Trees	/Müller et al. 2003/		
		>40,000	>44,000	Bellamont 3		6-14			pollen	Bellamont 3		GIS 11	Trees	/Müller et al. 2003/		
7	Niederweningen/Switzerland	44,400-46,400	47,000-49,000	Upper peat	-12 to -5	12-13				coleoptera		GIS 14-12	Open vegetation, low AP%	/Furrer et al. 2007/		
		43,400-46,800	46,000-49,000	Middle peat			4.3 +/-2.1			d18O tooth enamel		GIS 14-12	Picea, Larix, Betula; forest tundra	/Furrer et al. 2007/		
8	Dzguta River section	48,000-44,000	52,000-46,500	Pollenzone 1						coleoptera		?GIS 14	Low AP%	/Furrer et al. 2007/		
		44,000-42,000	46,500-45,000	Pollenzone 2						pollen		GIS 14-13	Fagus, Abies	/Arslanov et al. 2007/		
		42,000-39,000	45,000-43,000	Pollenzone 3						colder		GS 13	Conifers	/Arslanov et al. 2007/		
		39,000-38,000	43,000	Pollenzone 4						mild		GS 12	Broad-leaved species	/Arslanov et al. 2007/		
		39,000-21,000	42,500-26,000	Pollenzone 5						wet		Bryanzk/Denekamp	GS 12	Conifers & herbs	/Arslanov et al. 2007/	
										moder-		GIS 8-3	Some broad-leaved species followed by coniferous	/Arslanov et al. 2007/		
										ately mild						
9	Gossau/Switzerland	28,000-30,000	32,500-34,500	PZ 7								GIS 5-6	Pinus	/Preusser 2004, Schluechter et al. 1987/		
		33,000-34,000	38,000-39,000	PZ 5								GIS 8	Pinus	/Preusser 2004, Schluechter et al. 1987/		
		40,000	44,000	PZ 4								Picea Interstadial	GIS 12	Picea-Pinus	/Preusser 2004, Schluechter et al. 1987/	
		45,000-48,000	48,000-52,000	PZ3									Pinus	/Preusser 2004, Schluechter et al. 1987/		
		50,000-57,000	55,500- >60,000	PZ 2								Duernten Interst	GIS 14/13	Picea-Pinus	/Preusser 2004, Schluechter et al. 1987/	
10	Sokli/Finland		53,000			10-14						?GIS 14	Shrub tundra	/Helmens et al. 2007, Engels et al. 2008/		
11	England	42,000	40,000		-10 to -20	ca 10				coleoptera						
	England	43,000-42,000	45,500-44,000		-13 to 5	15-18				coleoptera	Upton Warren	GIS 12	Tree less, summer temp as warm as today in S Britain	/Huijzer and Vandenberghe 1998, Coope 2002/		
		44,000	46,000		-10 to -20	ca 10				coleoptera						

Site #	Site name	Age range 14C	Age range cal yr BP acc to Cariaco-Hulu	Stratigraphy	MTCM	MTWM	Min summer temp	MAAT	Precipitation	Fossil indicators	Interstadial	GIS/GS	Environment	Author/s	Comments/ BW
12	Netherlands	43,000-39,000	45,5000-43,000	-27 to -15	10-11	-4 to -10		arid	coleoptera	Hasselo stadial	GS 12			/Huijzer and Vandenberghe 1998/	
			44,000-43,000	-27 to -20	10-11				plants, insects	Hasselo stadial	GS 12			/van Huissteden et al. 2003/	
	Netherlands	39,000-37,000	43,000-42,000		10-15; 13-15; <10; 10-12	0			plant indicators	Hengelo Interstadial	GIS 11-9	Tree less		/Caspers and Freund 2001/	
		41,000-38,000	45,000-41,000	<-20	10-11				plant indicators	Hengelo Interstadial	GIS 11-9			/Caspers and Freund 2001/	
		43,000-40,000		>13	>0				pollen	Hengelo Interstadial	GIS 11-9			/van Huissteden et al. 2003/	
	Netherlands	45,000-48,000	48,000-52,000	??-11,5 to -13	7-11				coleoptera	Riel Interstadial	GIS 13/14			/Huijzer and Vandenberghe 1998/	
	Netherlands	50,000-43,000	55,500-45,500		5-8				plant indicators	Moershoofd Interstadial	GIS 14/13			/Caspers and Freund 2001/	
	Netherlands	36,000-26,000	41,000-31,000	<-12	10	<-1			coleoptera	Denekamp/ Huneborg	GIS 5-8	Warm interval		/Huijzer and Vandenberghe 1998/	
	Netherlands	36,000-26,000	41,000-31,000	-26 to -18	10	-8 to -4			coleoptera	Denekamp/ Huneborg	GIS 5-8	Cold interval		/Huijzer and Vandenberghe 1998/	
		32,000-28,000	36,000-32,500		10					Denekamp/ Huneborg	GIS 5-7			/Caspers and Freund 2001/	
13	Niederlausitz	25,000-34,000	30,000-39,000		8-10				plant indicators		GIS 5-8			/Bos et al. 2001/	
	Niederlausitz	34,000-38,000	39,000-42,500		13-15				plant indicators		GIS 9-10			/Bos et al. 2001/	
	Niederlausitz	38,000-40,000	42,500-45,000						plant indicators		GIS 11			/Bos et al. 2001/	
	Niederlausitz	40,000-42,000	44,000-45,000		12-13				plant indicators		GIS 12			/Bos et al. 2001/	
	Niederlausitz	48,000-50,000	52,000-55,500		8-10				plant indicators		GIS 14			/Bos et al. 2001/	
14	Greece														
	Ioannina		ca 44,000						pollen		GS 12	Decrease in temperate tree pollen		/Tzedakis 2005/	
	Kopais								pollen		GS 12	Decrease in temperate tree pollen		/Tzedakis 2005/	
	Tenaghi Philippon		ca 44,000						pollen		GS 12	Decrease in temperate tree pollen		/Tzedakis 2005/	
15	Italy														
	Monticchio PAZ-11		ca 50,000-42,300	very cold				arid-moist	pollen		GIS 11-13	Wooded steppe/cool mixed woodlands		/Allen and Huntley 2000/	
				moderate seasonality											
				-15											
16	Iberian margin		ca 44,000						charcoal, pollen		GS 12	Low charcoal counts		/Daniau et al. 2007/	
	MD95-2042											Semi desert vegetation		/Sánchez-Goñi et al 2002/	
	SU-8118											Dry conditions			
	38 degreesN, -10 degrees W														
17	Tilligte/German-Holland border	42,000	45,000		10				paleobotany, fauna		GIS 12			/Caspers and Freund 2001/	
18	Nussloch											Paleosols during interstadials,		/Rousseau et al. 2007/	
			44,000									Eolian dust transport during stadials			
				300-500 mm/yr											
19	Vrøgum/Denmark	46,000-52,000	49,000-57,000	warm					macrofossils		GIS 14	Birch, pine vegetation and warmth-requiring plants		/Kolstrup 1991/	
20	Sejerø/Denmark	35,000-38,000	40,000-42,500		8-10				macrofossils		GIS 10-9				
21	Lønstrup Klint/Denmark	ca 30,000	34,000		ca 11				macrofossils		GIS 6	Tree less, warmth demanding herbs mesic tundra environment		/Houmark-Nielsen et al. 1996/	
22	Kobbegård/Denmark	32,000-24,000	36,000-29,000		ca 11				macrofossils		GIS 5-7	Treeless, arctic environment		/Bennike et al. 2004/	

Table E2. Subset of MIS3 proxy records from Table C1 used for the comparisons with regional climate model data in Section 3.3.2.

Site name	Lon	Lat	MTCM1	MTCM2	MTCM	MTWM1	MTWM2	MTWM
1Balglass Burn/Scotland	-3	55.95	-26	-10	-17.9	8	10	9
2Sourlie/Scotland	-5.5	57	-34	-11	-22.5	9	10	9.5
4Oerel	9.1	53.5	-17	-2	-9.5	10	14	12
4Glinde	10.2	53.5	-27	-2	-14.5	9	14	11.5
7Geneve	6.2	46.2	-12	-5	-8.5	12	13	12.5
11England	-1.9	52.5	-13	1	-6	15	18	16.5
12Netherlands	4.9	52.4	-27	-15	-21	10	11	10.5
13Niederlausitz	14.77	51.91	NaN	NaN	NaN	12	13	12.5
17Tilligte	7.03	52.36	NaN	NaN	NaN	10	10	10
20Sejerö/Denmark	11.25	55.51	NaN	NaN	NaN	8	10	9

MTCM is mean of MTCM1 and MTCM2. MTWM is mean of MTWM1 and MTWM2.

References

- Allen J R M, Huntley B, 2000.** Weichselian palynological records from southern Europe: correlation and chronology. *Quaternary International* 73/74:111–125.
- Arslanov K A, Dolukhanov P M, Gei N A, 2007.** Climate, Black Sea levels and human settlements in Caucasus Littoral 50,000–9000 BP. *Quaternary International* 167–168:121–127.
- Behre K-E, Hölzer A, Lemdahl G, 2005.** Botanical macro-remains and insects from the Eemian and Weichselian site of Oerel (northwest Germany) and their evidence for the history of climate. *Vegetation History and Archaeobotany* 14:31–53.
- Bennike O, Jensen J B, Lemke W, Kuijpers A, Lomholt S, 2004.** Late- and postglacial history of the Great Belt, Denmark. *Boreas* 33:18–33.
- Bos J A A, Bohncke S J P, Kasse C, Vandenberghhe J, 2001.** Vegetation and climate during the Weichselian early glacial and pleniglacial in the Niederlausitz, eastern Germany – macrofossil and pollen evidence. *Journal of Quaternary Science* 16/3: 269–289.
- Bos J A A, Dickson J H, Coope G R, Jardine W G, 2004.** Flora, fauna and climate of Scotland during the Weichselian Middle Pleniglacial – palynological, macrofossil and coleopteran investigations. *Palaeogeography, Palaeoclimatology, Palaeoecology* 204:65–100.
- Brown E J, Rose J, Coope R G, Lowe J J, 2007.** An MIS 3 age organic deposit from Balglass Burn, central Scotland: palaeoenvironmental significance and implications for the timing of the onset of the LGM ice sheet in the vicinity of the British Isles. *Journal of Quaternary Science* 22: 295–308.
- Caspers G, Freund H, 2001.** Vegetation and climate in the Early and Pleni-Weichselian in northern Central Europe. *Journal of Quaternary Science* 16:31–48.
- Coope G R, 2002.** Changes in the thermal climate in northwestern Europe during Marine Oxygen Isotope Stage 3, estimated from fossil insect assemblages. *Quaternary Research* 57:401–408.
- Daniau A-L, Sánchez-Goñi M F, Beaufort L, Laggoun-Défarge F, Loutre M-F, Duprat J, 2007.** Dansgaard-Oeschger climatic variability revealed by fire emissions in southwestern Iberia. *Quaternary Science Reviews* 26:1369–1383.
- Engels S, Bohncke S J P, Bos J A A, Brooks S J, Heiri O, Helmens K F, 2008.** Chironomid-based palaeotemperature estimates for northeast Finland during Oxygen Isotope Stage 3. *Journal of Paleolimnology* 40:49–61
- Furrer H, Graf H R, Mäder A, 2007.** The mammoth site of Niederweningen, Switzerland. *Quaternary International* 164–165:85–97.
- Hatté C, Guiot J, 2005.** Palaeoprecipitation reconstruction by inverse modelling using the isotopic signal of loess organic matter: application to the Nusslock loess sequence (Rhine Valley, Germany). *Climate Dynamics* 25: 315–327.

- Helmens K F, Bos J A A, Engels S, van Meerbeeck C J, Bohncke S J P, Renssen H, Heiri O, Brooks S J, Seppä H, Birks H J B, Wohlfarth B, 2007.** Present-day temperatures in northern Scandinavia during the Last Glaciation. *Geology* 35:987-990.
- Hiller A, Junge F W, Geyh M A, Kröbtschek M, Kremenetski C, 2004.** Characterising and dating Weichselian organogenic sediments: a case study from the Lusatian ice marginal valley (Scheibe opencast mine, eastern Germany). *Palaeogeography, Palaeoclimatology, Palaeoecology* 205:273-294.
- Houmark-Nielsen M, Bennike O, Björck S, 1996.** Terrestrial biotas and environmental changes during the late Weichselian in north Jylland, Denmark. *Bulletin of the Geological Society of Denmark* 43:169-176.
- Huijzer B, Vandenberghe J, 1998.** Climatic reconstructions of the Weichselian Pleniglacial in northwestern and central Europe. *Journal of Quaternary Science* 13: 391-417.
- Kolstrup E, Houmark-Nielsen M, 1991.** Weichselian paleoenvironments at Kobbelgård, Mön, Denmark. *Boreas* 20:169-182.
- Müller U C, Pross J, Bibus E, 2003.** Vegetation response to rapid climate change in Central Europe during the past 140,000 yr based on evidence from the Fueramoos pollen record. *Quaternary Research* 59:235-245.
- Preusser F, 2004.** Towards a chronology of the Late Pleistocene in the northern Alpine Foreland. *Boreas* 33:195-210.
- Rousseau D-D, Sima A, Antoine P, Hatté C, Lang A, Zöller L, 2007.** Link between European and North Atlantic abrupt climate changes over the last glaciation. *Geophysical Research Letters* 34:L22713.
- Sánchez Goni M F, Cacho I, Turon J L, Guiot J, Sierro F J, Peypouquet J-P, Grimalt J O, Shackleton N J, 2002.** Synchronicity between marine and terrestrial responses to millennial scale climatic variability during the last glacial period in the Mediterranean region. *Climate Dynamics* 19:95-105.
- Schluechter C, Maisch M, Suter J, Fitze P, Keller W A, Burga C A, Wynistorf E, 1987.** Das Schieferkohlenprofil von Gossau Kanton Zuerich und seine stratigraphische Stellung innerhalb der letzten Eiszeit. *Vierteljahrsschrift der Naturforschenden Gesellschaft Zuerich* 132:135-174.
- Tzedakis P C, 2005.** Towards an understanding of the response of southern European vegetation to orbital and suborbital climate variability. *Quaternary Science Reviews* 24:1585-1599.
- van Huissteden K, Vandenberghe J, Pollard D, 2003.** Palaeotemperature reconstructions of the European permafrost zone during marine isotope Stage 3 compared with climate models. *Journal of Quaternary Science* 18:453-464.
- Whittington G, Hall A M, 2002.** The Tolsta Interstadial, Scotland: correlation with D-O cycles GI-8 to GI 5? *Quaternary Science Reviews* 21:901-915.
- Wohlfarth B, 2009.** Ice-free conditions in Scandinavia during Marine Oxygen Isotope Stage 3? Report TR-09-12, Svensk Kärnbränslehantering AB. *In press*.

Appendix F

SST proxy data for the permafrost case (MIS 3)

This appendix holds the proxy records for SSTs used for comparison with CCSM3 results for the *permafrost case*. The proxy data originates from a compilation of data based on an extended version of the /Voelker et al. 2002/. The data are described in section 2.4.

Table F1. Proxy records for annual mean SSTs. The different columns correspond to different types of proxies. Unit: °C.

Site	Latitude	Longitude	Planktonic foraminifera	Alkenones	Radiolaria
MD01-2444	37° 45'N	10°W		13.3	
MD95-2043	36° 8.598'N	2° 37.27'W		ca. 12.5	
ODP977	36° 01.91'N	1° 57.32'W		12	
MD99-2343	40° 1.69'N	4° 1.69'E	10–10.5		
MD95-2037	37.09°N	32.03°W		17.2	
MD95-2036	33° 41.4'N	57° 34.5'W		18–18.6	
ODP site 1060	30° 46'N	74° 28'W		around 18	
ODP site 658C	20°44.95'N	18°34.85'W		19	
SO90-136KL	23.12°N	66.5°E		23.5	
EW9504-13PC	36.99°N	123.27°W			ca. 10.5
EW9504-17PC	42.24°N	125.89°W			ca. 7.5
MD94-103	43° 32'S	86° 32'E		8.5–9	
ODP1233	41°S	74° 27'W		11.2–11.8	

Table F2. Proxy records for northern hemisphere winter (JFM) SSTs. The different columns correspond to different types of proxies. Unit: °C. The Mg/Ca data are biased towards spring and summer in each hemisphere. Here we have used these data to complement the planktonic foraminifera and radiolaria data for July–September.

Site	Latitude	Longitude	Planktonic foraminifera	Mg/Ca	Radiolaria
PS2644-5	67° 52.02'N	21° 45.92'W	-0.14		
SO82-5	59° 11.3'N	30° 54.5'W	-0.4 ± 0.4		
ENAM93-21	62° 44.3'N	3° 59.9'W	0		
CH69-K09	41°45.4'N	47°21'W	7.4–7.9		
SU90-08	43° 31'N	30° 24'W	6.55–7.23		
GIK15612	44° 21.6'N	26° 32.6'W	4.4		
MD95-2040	37.8°N	10.17°W	11.8		
MD01-2444	37° 45'N	10°W	15.2		
MD99-2339	35.883°N	7.528°W	15.5		
SU92-03	43° 11.75'N	10° 6.78'W	6.8		
SU90-03	40.51°N	32.05°W	10		
GIK15637	27.005°N	18.987°W	17.6		
GeoB1105-4	1.665°S	12.4283°W		22	
ODP site 1089	40° 56.19'S	9° 53.64'E			14.2–15.5
MD97-2120	45° 32.06'S	174° 55.85'E		9.2	
MD98-2181	6.3°N	125.82°E		24–24.5	
WIND 28K	10° 9.23'S	51° 46.15'E			19.6–20.5
MD97-2151	8.728°N	109.869°E	around 24		
M35003	12.083°N	61.233°W	24.5		
ODP site 893	34° 17.25'N	120° 02.20'W	4–5		
E11-2	56° 04'S	115° 05'E			ca. 4
DGKS9603	28° 08.869'N	127° 16.238'E	ca. 19.8		

Table F3. Proxy records for northern hemisphere summer (JAS) SSTs. The different columns correspond to different types of proxies. Unit: °C. The Mg/Ca data are biased towards spring and summer in each hemisphere. Here we have used these data to complement the planktonic foraminifera and radiolaria data for July–September.

Site	Latitude	Longitude	Planktonic foraminifera	Mg/Ca
PS2644-5	67° 52.02'N	21° 45.92'W	3.68	
JM96-1225/1+2	64° 54.3'N	29° 17.4'W	4.5–5	
SO82-5	59° 11.3'N	30° 54.5'W	3.4–4.5	
ENAM93-21	62° 44.3'N	3° 59.9'W	4	
NA87-22	55° 29.8'N	14° 14.7'W	around 8.5°C	
MD01-2461	51° 45'N	12° 55'W		9.2
CH69-K09	41° 45.4'N	47° 21'W	11–13.3	
SU90-08	43° 31'N	30° 24'W	11.65–12.33	
GIK15612	44° 21.6'N	26° 32.6'W	8.8	
MD95-2040	37.8°N	10.17°W	16.5	
MD01-2444	37° 45'N	10°W	20.1	
MD99-2339	35.883°N	7.528°W	20.5	
SU92-03	43° 11.75'N	10° 6.78'W	11.2	
ODP site 1060	30° 46'N	74° 28'W	22–24	
SU90-03	40.51°N	32.05°W	14.5–15	
GIK15637	27.005°N	18.987°W	22.6	
M35003	12.083°N	61.233°W	21.5	
MD98-2181	6.3°N	125.82°E		27–28
ODP site 883	50°55'N	167°50'E	8	
MD97-2141	8.79°N	121.3°E		26.5
ODP site 893	34° 17.25'N	120° 02.20'W	7.5–10	
DGKS9603	28° 08.869'N	127° 16.238'E	ca. 25.3	

References

Voelker A H L and workshop participants, 2002. Global distribution of centennial-scale records for Marine Isotope Stage (MIS) 3: a database. Quaternary Science Review 21: 1185–1212.

ISSN 1404-0344
CM Gruppen AB, Bromma, 2009